



# ENVIRONMENTAL MINERALOGY

## HONOURS SHORTCOURSE

*Presented by:*

*Mehrooz Aspandiar, Tony Eggleton and Ulrike Troitzsch*

**CRC LEME OPEN FILE REPORT 206**

**18 - 22 June 2007**  
**Department of Earth and Marine Sciences, ANU**

CRCLEME

FOR THE MINERALS TERTIARY EDUCATION COUNCIL

CRC LEME is an unincorporated joint venture between CSIRO-Exploration & Mining, and Land & Water, The Australian National University, Curtin University of Technology, University of Adelaide, Geoscience Australia, Primary Industries and Resources SA, NSW Department of Primary Industries and Minerals Council of Australia, established and supported under the Australian Government's Cooperative Research Centres Program.





# **ENVIRONMENTAL MINERALOGY**

## **HONOURS SHORTCOURSE**

*Presented by:*

*Mehrooz Aspandiar, Tony Eggleton and Ulrike Troitzsch*

**CRC LEME OPEN FILE REPORT 206**

18 - 22 June 2007  
Department of Earth and Marine Sciences, ANU

FOR THE MINERALS TERTIARY EDUCATION COUNCIL

© Cooperative Research Centre for Landscape Environments and Mineral Exploration 2007.  
This book is copyright. Apart from any fair dealing for the purpose of private study, research, criticism or review, as permitted under the Copyright Act, no part may be reproduced by any process without written permission. Enquiries should be addressed to the publisher.

---

CRC LEME is an unincorporated joint venture between CSIRO-Exploration & Mining, and Land & Water, The Australian National University, Curtin University of Technology, University of Adelaide, Geoscience Australia, Primary Industries and Resources SA, NSW Department of Primary Industries and Minerals Council of Australia.

*Headquarters:* CRC LEME c/o CSIRO Exploration and Mining, PO Box 1130, Bentley WA 6102, Australia

Electronic copies of the publication in PDF format can be downloaded from the CRC LEME website: <http://crcleme.org.au/Pubs/OFRIndex.html>. Information on this or other LEME publications can be obtained from <http://crcleme.org.au>

Hard copies will be retained in the Australian National Library, the Western Australian State Reference Library, and Libraries at The Australian National University and Geoscience Australia, Canberra, The University of Adelaide and Australian Resources Research Centre, Kensington, Western Australia.

**Reference:**

Eggleton RA, Aspandiar M, 2007. Environmental Mineralogy: Honours Shortcourse, 18-22 June 2007. *CRC LEME Open File Report 206*. 159pp.

**Keywords:**

1. Environmental mineralogy 2. Regolith environment . 3. X-ray diffraction. 4. XRD of clays. 5. Electron microscopy. 6. Rietveld XRD analysis.

ISSN 1329 4768

ISBN 1 921039 76 0

**Authors addresses and affiliations:**

Professor Richard A (Tony) Eggleton  
CRC LEME Honorary Fellow  
The Australian National University  
Acton ACT 0200.  
[tony.eggleton@anu.edu.au](mailto:tony.eggleton@anu.edu.au)

Dr Mehrooz Aspandiar  
CRC LEME  
Curtin University of Technology  
PO Box U 1987, Perth WA 6001  
[m.f.aspandiar@curtin.edu.au](mailto:m.f.aspandiar@curtin.edu.au)

**Publisher:**

CRC LEME  
c/o CSIRO Exploration and Mining  
PO Box 1130  
Bentley, Western Australia 6102

**Disclaimer**

The user accepts all risks and responsibility for losses, damages, costs and other consequences resulting directly or indirectly from using any information or material contained in this report. To the maximum permitted by law, CRC LEME excludes all liability to any person arising directly or indirectly from using any information or material contained in this report.

© **This report is Copyright of the** Cooperative Research Centre for Landscape Environments and Mineral Exploration, (year of publication), which resides with its Core Participants: CSIRO Exploration and Mining and Land and Water, The Australian National University, Curtin University of Technology, The University of Adelaide, Geoscience Australia, Primary Industry and Resources SA, NSW Department of Primary Industries and Minerals Council of Australia.

Apart from any fair dealing for the purposes of private study, research, criticism or review, as permitted under Copyright Act, no part may be reproduced or reused by any process whatsoever, without prior written approval from the Core Participants mentioned above.

# ENVIRONMENTAL MINERALOGY

Written by:

**Professor Richard A (Tony) Eggleton**  
Australian National University  
Tony.Eggleton@anu.edu.au

**Dr Mehrooz Aspandiar**  
Curtin University of Technology  
M.F.Aspandiar@curtin.edu.au

18-22 June 2007





## **ENVIRONMENTAL MINERALOGY**

### **MTEC Honours shortcourse**

#### **Course history**

The following course notes are compiled from a series of annual 5-day shortcourses taught at the Australian National University between 2003 and 2007.

The courses were presented by staff from the Cooperative Research Centre for Landscape Environments and Mineral Exploration (CRC LEME-2) partially based on earlier material taught by staff from the Cooperative Research Centre for Landscape Evolution and Mineral Exploration (CRC LEME-1), the Centre for Australian Regolith Studies (CARS), and undergraduate courses at the ANU. Staff involved in developing and delivering these courses include (in alphabetical order with affiliations and years involved in teaching this course):

- Professor R.A. (Tony) Eggleton, CRC LEME-1 & -2 (2003-2007);
- Dr Ulrike Troitzsch, CRC LEME-2, ANU (2003-2007);
- Dr Mehrooz Aspandiar, CRC LEME-2, Curtin University of Technology (2006-2007).

This course was offered as part of the Minerals Council of Australia's Minerals Tertiary Education Council (MTEC) initiative. The MTEC initiative commenced in 2001 as a partnership between the Minerals Council of Australia and universities or research organisations (including CRC LEME) involved in the earth sciences, mining engineering and metallurgy disciplines.

Dr Ian Roach

CRC LEME Education and Training Program Leader  
MTEC Lecturer in Regolith Geoscience, CRC LEME, ANU  
April 2007

## TABLE of CONTENTS

1. Regolith mineralogy	1
2. The regolith environment	28
3. X-ray Diffraction 1.	44
4. Sample preparation	65
5. Crystal symmetry	72
6. X-ray diffraction 2.	85
7. XRD of clays	98
8. Other methods	
XRF	110
Electron microscopy	113
Adsorption and ion exchange	117
Thermal	121
Infra-red	122
9. Rietveld XRD analysis	133
10. References	155

# PROGRAM

18-22 June 2007

## Monday 18

9:00 -10:30	Clays and iron oxides	Tony
10:30 - 11:00	Morning tea	
11:00 - 12:30	Clays and iron oxides	Tony
12:30 - 1:30	lunch	
1:30 - 3:00	<i>Lab 1 Clays and iron oxides</i>	All
3:00 - 3:30	Afternoon tea	
3:30 - 5:00	<i>Lab 1 cont</i>	All

## Tuesday 19

9:00-10:30	Environments	Mehrooz
10:30-11:00	Morning tea	
11:00 - 12:30	X-ray diffraction basics	Tony
12:30 - 1:30	lunch	
1:30 - 3:00	<i>Sample preparation for XRD – bulk and clay</i>	Ulli
3:00 - 3:30	Afternoon tea	
3:30 - 5:00	<i>Lab 2. XRD identification of unknowns.</i>	All

## Wednesday 20

9:00-10:00	Crystallography: lattices	Tony
10:00 -10:30	<i>Lab 3. Unit cell exercise</i>	Tony & Mehrooz
10:30 - 11:00	Morning tea	
11:00 - 12:30	Diffraction theory	Tony
12:30 - 1:30	lunch	
1:30 - 3:00	Identification of clays by XRD	Tony
3:00 - 3:30	Afternoon tea	
3:30 - 5:00	<i>Lab 4. Clay identification</i>	All

## Thursday 21

9:00 – 10:30	<i>XRD Identification of unknowns –computer</i>	Ulli
10:30 - 11:00	Morning tea	
11:00 - 12:30	Cation exchange, thermal methods Infra-red (PIMA), SEM and X-ray fluorescence analysis	Tony Mehrooz
12:30 - 1:30	lunch	
1:30 - 3:00	Rietveld quantification	Tony
3:00 - 3:30	Afternoon tea	
3:30 - 5:00	<i>Project work</i>	Ulli & Tony

## Friday 22

9:00 -10:30	Combining the techniques	Tony & Mehrooz
10:30 - 11:00	Morning tea	
11:00 - 12:30	<i>Lab 5. followed by Project work</i>	All
12:30 - 1:30	lunch	
1:30 - 3:00	<i>Project works</i>	All
3:00 - 3:30	Afternoon tea	
END		

---

---

# INTRODUCTION

---

---

## Presumed knowledge

Crystallography: 7 crystal systems, crystal symmetry, crystallographic axes, Miller indices. (Preliminary reading on this available on request)  
Mineralogy: major rock-forming minerals.

## Course outline

Crystallography: Bravais lattices, lattice symmetry, unit cell, atoms in the cell.

X-ray diffraction: Diffraction principles, scattering by a lattice, scattering by a crystal.

Clay mineralogy: structure and composition of silicate clays and iron oxyhydroxides.

Other techniques and properties: Cation exchange capacity, water loss on heating, infra-red spectra, SEM imaging and XFA analysis by microprobe.

Interpretation of a regolith sample by combining experimental results.

## Knowledge outcomes

Ability to select the appropriate techniques to identify and quantify the mineral components of the earth surface environment - the regolith: weathered rock and soil. Ability to assess the validity of such an analysis, and coupled with further individual study, to carry out such analyses.

## Work to be done

Class exercises involving calculation of diffraction data and interpretation of "unknown" minerals, both clay and non-clay.

Project work on a single (provided) regolith sample, to result in the identification of the components and a semi-quantitative or quantitative mineral analysis, with discussion of the basis for your interpretation. Most of this work can be completed during the 5 days of the course, with the final report submitted by 20 July 2007.

## Assessment:

In-class exercises 25%, Project 75%.

## Useful materials:

Calculator or lap-top.

---

---

## PROJECT

---

---

**Date due: July 20 2007.**

The Project work will be on a single (provided) regolith sample, which will be one of a suite taken from various depths by drill core from the CRC LEME Gilmore Project. Drill hole number and depth will be provided for your interest, but the course is about materials and methods of their analysis, not the interpretation of the origin or history of regolith materials. The provided data for each sample are:

For the bulk sample:

Cation exchange capacity (cmol(+)/kg = meq/100g)

Water loss on heating over the following temperature ranges:

20-110°C                      adsorbed

110-400°C                     goethite

400-560°C                    kaolinite

>700°                         2:1 clays

Full major element chemical analysis

X-ray diffraction scan

PIMA spectrum

For the clay (<2 µm) fraction:

XRD scan Mg-saturated

XRD scan glycolated

XRD scan after heating to 350°C

From these data you are asked to make a quantitative analysis of the mineral components of the bulk sample, through a series of steps developed during the course.

In brief, these steps are:

1. qualitative non-clay mineralogy using the bulk XRD scan;
2. qualitative clay mineralogy of the <2 µm size fraction using the three clay scans;
3. quantitative non-clay mineralogy by Rietveld (Siroquant) analysis of the bulk XRD scan;
4. quantitative clay mineralogy of the bulk sample based on the bulk XRD scan, CEC, PIMA and water loss determinations, coupled with use of the full major element chemistry and from consideration of the clay fraction XRD.

In your report, each conclusion should be documented and justified or explained, but it is not necessary to repeat any of the theory covered in the course. Normal scientific reporting should include all the data (from your one sample). You should include print-outs of the XRD traces with each peak clearly labelled with the mineral producing it (quite commonly the computer print-outs from the commercial software you will use are too cluttered to be legible. It is better in this case to make an expanded print and label the peaks by hand. The XRD data is readily processed by spread-sheet applications such as Excel, and you can extract significant regions for clearer presentation.

# 1. REGOLITH MINERALOGY

Tony Eggleton

---

---

## INTRODUCTION

---

---

The minerals of the regolith result either from the weathering of rock-forming minerals or are unweathered fragments of primary minerals. Igneous and metamorphic rocks form at high temperatures, under reducing conditions and at low water availability. By contrast, regolith minerals form at low temperatures under either reducing or oxidizing conditions, and in the presence of much water. Their mode of formation may be by hydration and the transformation of a primary mineral or by simple precipitation from solution. Where a primary mineral weathers by hydration, the process is essentially the replacement of a cation by hydrogen. Where oxidation is involved, the main element to be affected is iron, which is ferrous in primary minerals but becomes ferric through oxidation.

The minerals of the regolith can be divided into three groups:

1. Hydrated aluminosilicates formed by weathering primary silicates; the clay minerals;
2. Precipitated minerals composed of the elements leached from primary minerals during the first process, minerals such as gypsum or halite or the iron oxyhydroxides goethite and hematite;
3. Primary unweathered minerals such as quartz or zircon.

There are so many encyclopaedic data sources available on mineralogy today that it is unnecessary to describe the fundamental properties of the minerals of the regolith here. Detailed, constantly updated species-by-species data can be obtained at internet databases such as <http://www.mindat.org> and <http://www.webmineral.com>. It should be borne in mind that regolith minerals depart somewhat from the ideal or classical minerals of basic textbooks. The latter tend to have fixed crystal structures and compositions that vary within strict limits, and may be nearly constant. In contrast, many regolith minerals show considerable disorder of crystal structure, and extreme compositional variability. Most of the clay minerals, the iron oxyhydroxides, and the silica minerals depart so far from ideality that in some instances they become difficult to identify unambiguously. The current International Mineralogical Association definition of a “mineral species” has been carefully worded to include such complex materials, cf. Nickel (1995): “a mineral is an element or chemical compound that is normally crystalline and that has been formed as a result of geological processes”, and this definition is followed by considerable discussion of “crystallinity” and exceptions!

Rock-forming minerals are mostly identifiable quickly by hand specimen examination or by thin section optical microscopy. Electron microprobe analysis (EMPA) adds chemical

confirmation of an identity made optically, and X-ray diffraction (XRD) is commonly used for further characterization or to identify unusual species. But because most regolith-formed minerals occur as grains smaller than about 2  $\mu\text{m}$ , neither optical microscopy nor EMPA are adequate unless the minerals are present as relatively large ( $>10 \mu\text{m}$ ) pure aggregates. Identification of the fine-grained minerals of regolith almost always has to be made by using a technique requiring some interpretation of its results. Most commonly clays and iron oxyhydroxides are identified from their XRD pattern or their infra-red spectrum (IR). Scanning electron microscopy and EMPA provide a more detailed, but more expensive, approach to identification.

Identification by XRD or IR requires the existence of a data bank of previously characterized minerals. Typically these are drawn from beautifully crystallized museum specimens of high purity. Unfortunately, most “real” regolith minerals are less crystallographically and chemically “perfect” than the standards, so their response to XRD or IR does not always conform to the text book response. In this chapter the general properties of the regolith minerals will be described, but the emphasis will be on how they differ from the ideal and what effect this has on identification.

---

## SILICATES

---

The silicates have crystal structures in which every cation is surrounded by oxygens in such a way that the cations are prevented from close approach. The number of oxygens around a cation is the coordination number for that cation, and it depends on the cation size.

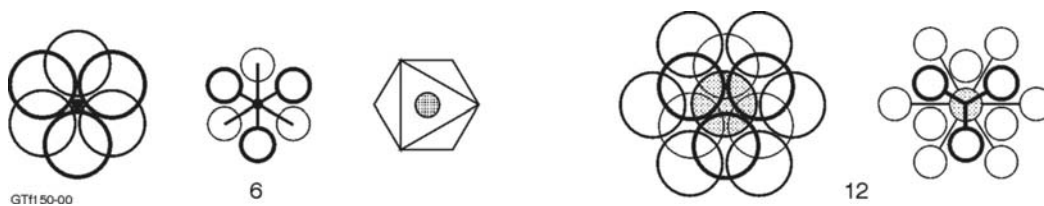


**Figure 1.1:** Six- and 12-coordination represented as packing models, ball and spoke models and for 6-coordination, a polyhedral model.

All silicates (except a few high-pressure phases formed in the mantle or by meteorite impact, such as stishovite, the rutile-structure polymorph of quartz) have silicon in four-fold coordination to oxygen so that the oxygens are at the corners of a tetrahedron. Magnesium and iron are dominantly in 6-fold or octahedral coordination to silicon, and Al, being a little larger than Si but smaller than Mg, may be found in either tetrahedral or octahedral coordination (Figure 1.1). Ca and Na may be squashed into 6-coordination, but are most commonly in 8-fold. K, the largest common ion, is in 12-fold coordination in silicates (Figure 1.1).

The silicate structures are generally classified on the basis of the polymerization of the silica tetrahedra

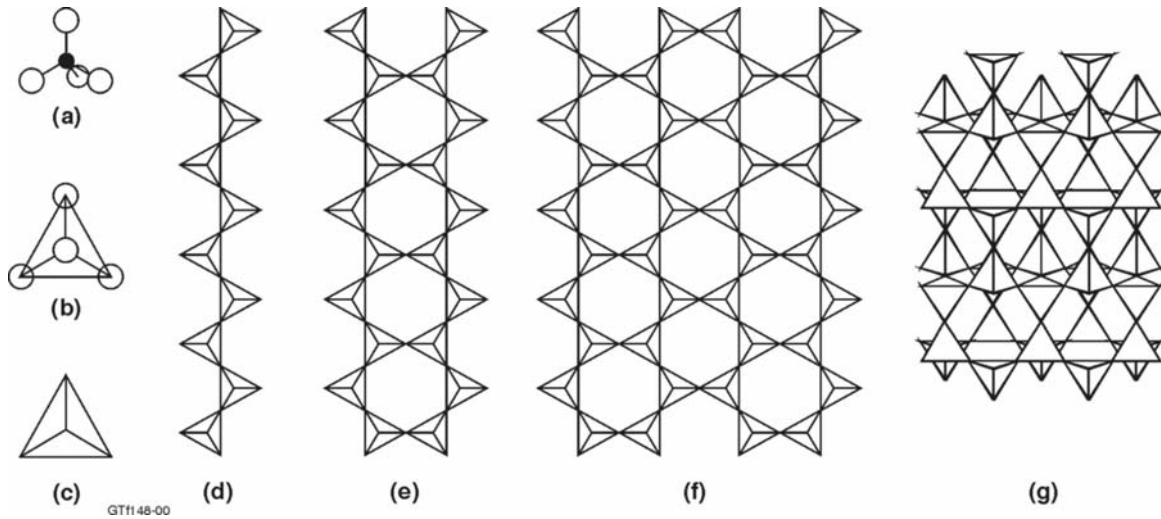


**Figure 1.2:** Classification of silicates according to tetrahedral polymerization.

a. Silica tetrahedron viewed as four oxygens coordinated to a central silicon. b. Tetrahedron viewed as a coordination tetrahedron with the oxygens at the apices. c. Silica tetrahedron simplified. d. single chain polymer. e. double chain. f. tetrahedral sheet. g. tetrahedral framework.

For weathering studies, however, the extent of polymerization of octahedra becomes significant, because some silicates pass whole structural elements on to their weathered products (e.g. mica sheets to kaolinite sheets). It is therefore useful to consider silicates from the perspective of their octahedral cation linkages.

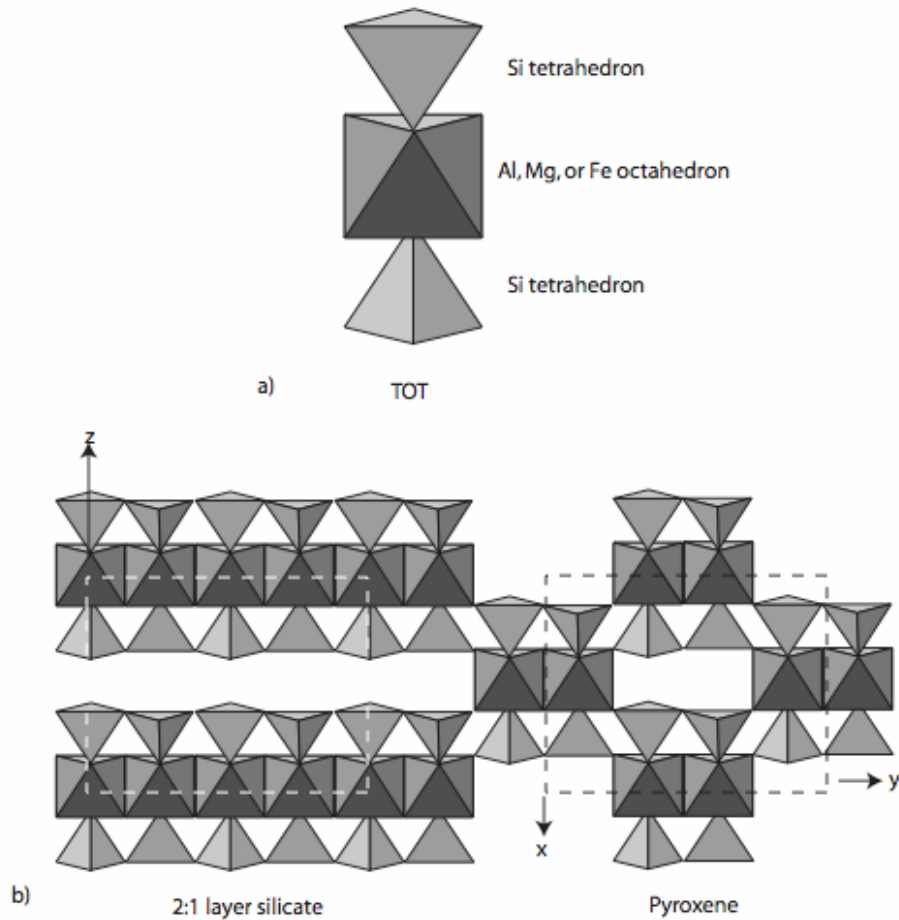


**Figure 1.3a:** Tetrahedron-Octahedron-Tetrahedron Unit (TOT) as in pyroxenes, amphiboles and micas.

**Figure 1.3b:** TOTs linked as in pyroxenes and 2:1 layer silicates such as biotite.

**Framework silicates: (quartz, feldspars, feldspathoids and zeolites)**

None of the framework silicates have cations in octahedral coordination, Al occurs in tetrahedral sites and the other cations, mostly Ca, Na or K, occur in 8 to 12-fold coordination to oxygen.

**Orthosilicates (olivine, garnet, alumino-silicates)**

Mg, Fe, Al in octahedral coordination (Mg, Fe in garnet in 8-fold), tetrahedral cations almost exclusively Si in the tetrahedra, little tetrahedral Al. Oxygens are densely packed (hexagonal close-packing in olivine, cubic close-packing in kyanite).

## Amphiboles and pyroxenes

The amphiboles and pyroxenes have strips of octahedra containing {Mg,Fe,Al}, coordinated above and below by strips of tetrahedra with some Al substituting for Si in amphiboles.

## **Layer silicates: Micas, chlorite, kaolinite and halloysite, smectites.**

The basic crystal structure of the common layer silicates was elucidated in the 1930's (Pauling 1930), and it is now recognised that all the minerals of the group have closely related structures. All have two structural units; an octahedral sheet and a tetrahedral sheet. The octahedral sheet comprises a plane of cations in octahedral coordination with planes of anions on either side. The tetrahedral sheet is formed of one plane of anions from the octahedral sheet, a plane of silicon-aluminium cations, and a third anion plane of oxygens completing the tetrahedra (Fig. 6.4). In all the layer silicates, the small silicon cations occur in tetrahedral coordination to oxygen, the tetrahedra being linked laterally at three of their corners to other tetrahedra in the form of a continuous hexagonal sheet (Fig. 6.1f). The sheet-linking oxygens are referred to as the *basal oxygens*. These two planes of oxygen and cations are completed as polyhedra by oxygens of the adjacent octahedral sheet which provide the fourth, or apical oxygen of the tetrahedra (Fig. 6.4).

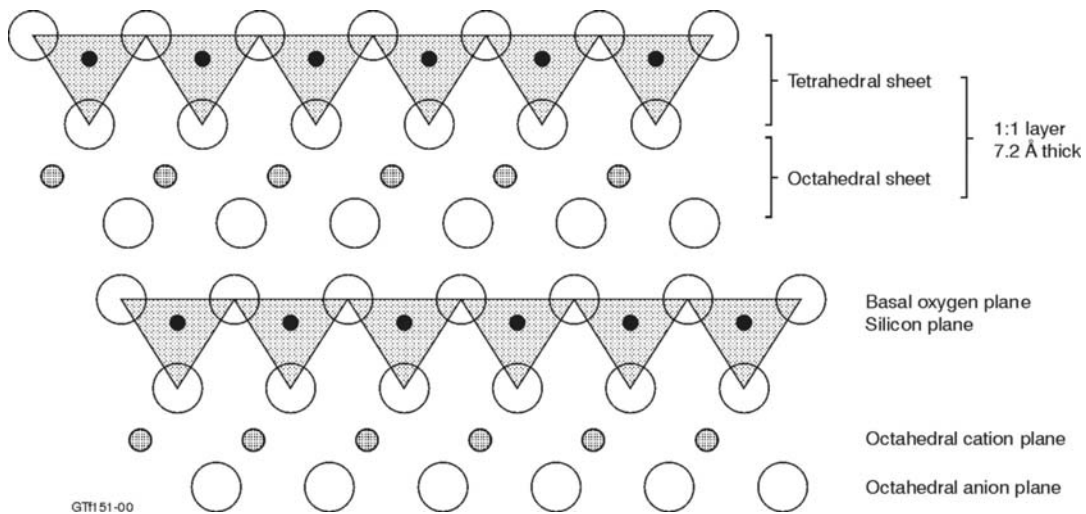


**Figure 1.4:** Structure of kaolinite, a 1:1 dioctahedral layer silicate

A terminology for describing layer silicates has arisen from the work of the Clay Mineral Nomenclature Committee (Bailey *et al.* 1971). All components of the structure are planar. Note that all the early texts on mineralogy report crystallographic dimensions in Ångström units (1 Å = 0.1 nm) and clay minerals are commonly referred to in terms of the basal (001) X-ray diffraction spacing measured in Ångströms. In this chapter nanometres are used except when specifically referring to a clay mineral using the basal spacing terminology, e.g., “mica is a 10-Å layer silicate”.

- atoms are referred to as lying in *planes*

- two planes of anions with a plane of cations coordinated between them to form linked polyhedra are referred to as *sheets*
- sheets linked by common anion planes are referred to as *layers*.

Layer silicates are classified on two criteria. The first identifies the occupancy of the octahedral sheet. An isolated octahedral sheet, such as in the mineral brucite ( $\text{Mg}_3(\text{OH})_6$ ), has trigonal symmetry, and a unit cell containing three  $\text{Mg}_3(\text{OH})_6$  octahedra. By contrast, the mineral gibbsite ( $\text{Al}_2(\text{OH})_6$ ), while also having trigonal symmetry and three octahedra in its unit cell, has one of these vacant. Octahedral sheets having all three octahedra occupied are called *trioctahedral*; those with only two occupied are *dioctahedral*. (Fig. 6.5).

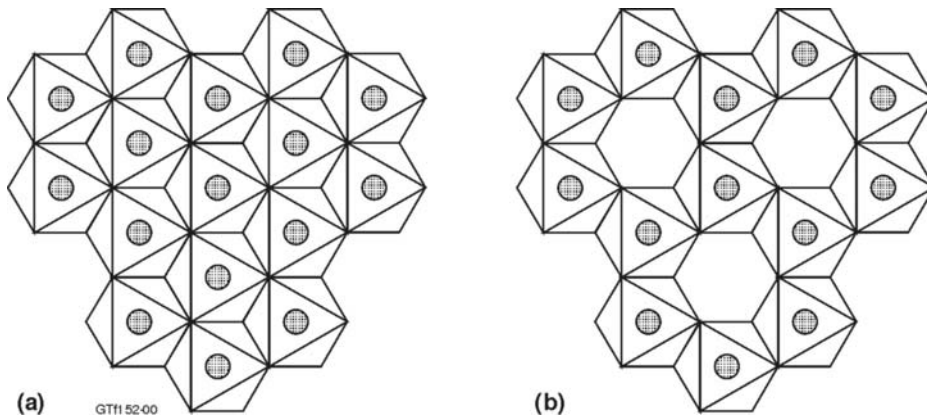


**Figure 1.5:** a) trioctahedral sheet. b) dioctahedral sheet.  
Octahedra are represented as in Figure 1.1.

The second classification criterion refers to the sequence of octahedral sheets and their flanking sheets of [SiAl] tetrahedra.

Known configurations for octahedral and tetrahedral sheet sequences are only three:

- one octahedral sheet with one flanking tetrahedral sheet (1:1 layer silicates) (Fig. 6.4);
- one octahedral sheet with two flanking tetrahedral sheets (2:1 layer silicates), Fig. 6.6a; and,
- 2:1 layers with octahedral sheets between (2:2 layer silicates), Fig. 6.6b.

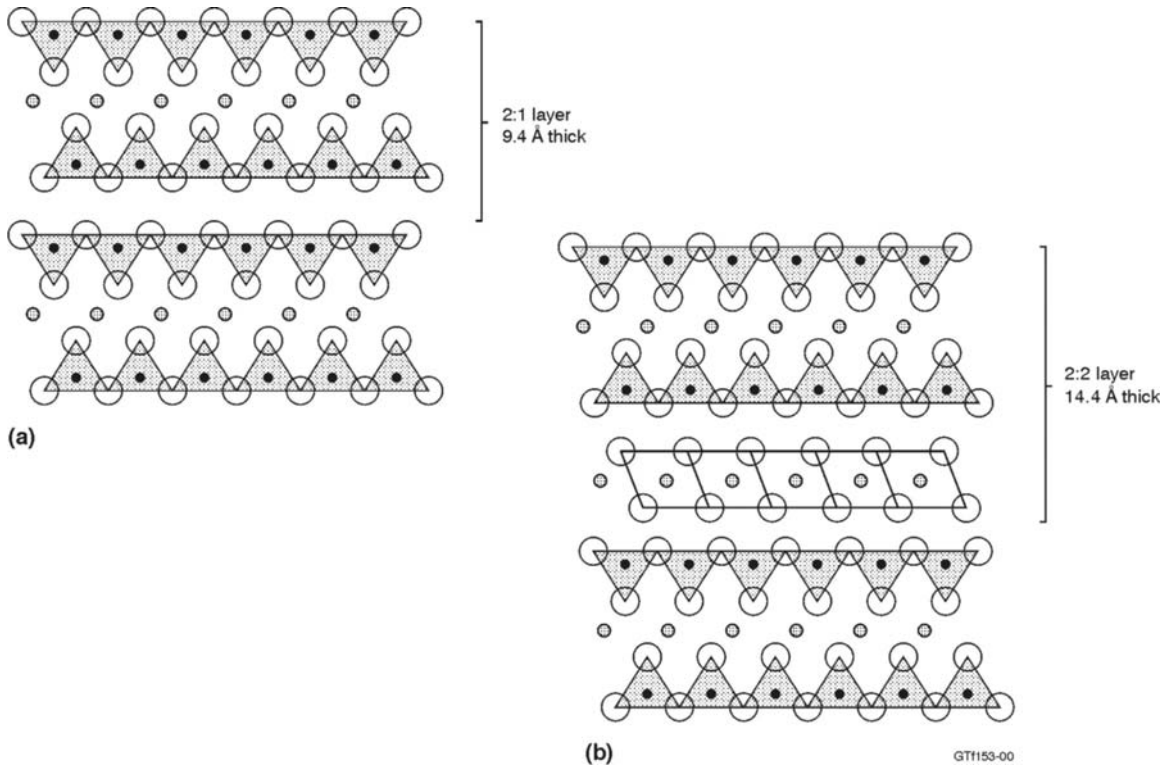


**Figure 1.6:** (a) 2:1 layer silicate. (b) 2:2 layer silicate. Symbols are as in Fig. 3.3.

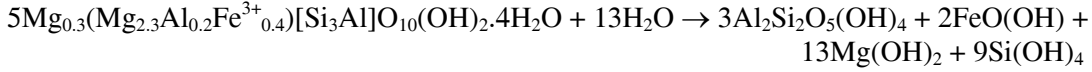
A single plane of oxygens has a thickness of about 0.26 nm. An overlying anion plane fits into hollows in the first, so that the effective thickness of each plane reduces to approximately 0.23 nm. 1:1 layer silicates have three anion planes, and so are about 0.7 nm thick; 2:1 layer silicates with 4 anion planes are about 0.94 nm thick (talc) or 1.0 nm if there is an alkali cation in the interlayer (micas). 2:2 layer silicates are 1.44 nm to 1.54 nm thick. These measurements, and other names applied from time to time, have led to multiple terminologies for clays (recalling that 1 nm = 10 Å):

1:1 layer silicate	7-Å layer silicate	kaolinite, 7-Å halloysite
2:1 layer silicate	10-Å layer silicate	pyrophyllite, talc, mica, illite
2:2 layer silicate	14-Å layer silicate	chlorite, smectite (formerly montmorillonite group), vermiculite

Variations available to each layer type are:

- the nature of the octahedral cation, dominantly Al or Fe<sup>3+</sup> in dioctahedral sheets, and Mg or Fe<sup>2+</sup> in trioctahedral sheets. Mn<sup>2+</sup>, Zn<sup>2+</sup>, Mn<sup>3+</sup>, Cr<sup>3+</sup>, Ti<sup>4+</sup> are common minor components in the octahedral sheet; and,
- substitution in the tetrahedral site of Si by Al, leading to a positive charge deficiency compensated by either a large low-charged cation between 2:1 layers (micas), or by positive charge generated in the octahedral sheet by substitution of a trivalent cation for a divalent, e.g. Al<sup>3+</sup> ↔ Mg<sup>2+</sup>.





In both of these examples, the first weathering product mineral has a 2:1 layer with a hydrated interlayer. Millot (1970) called the process ‘bisiallization’, since the new clay mineral has 2 silica sheets. The second silicate weathering product is kaolinite, which has a single silica sheet. Millot called this step ‘monosiallization’.

The regolith is generally oxidising, and ferrous iron is rare. Among the clays, only early formed vermiculite may carry  $\text{Fe}^{2+}$  and Mg varieties are restricted to weathered mafic rocks. The clay silicates of the regolith can be classified simply according to whether Al,  $\text{Fe}^{3+}$  or Mg is in the octahedral sheet, and by layer type, Table 3.1.

Because the interlayer region is important in the properties of smectite, this family of layer silicates is here included in the 2:2 group (Table 6.1) even though the interlayer cations are transitory.

**Table 6.1:** Classification of regolith layer silicates.

Layer type	Al	$\text{Fe}^{3+}$	Mg
	dioctahedral	dioctahedral	trioctahedral
1:1	kaolinite $\text{Al}_2\text{Si}_2\text{O}_5(\text{OH})_4$ halloysite $\text{Al}_2\text{Si}_2\text{O}_5(\text{OH})_4 \cdot 2\text{H}_2\text{O}$	hisingerite $\text{Fe}_2\text{Si}_2\text{O}_5(\text{OH})_4$	serpentine $\text{Mg}_3\text{Si}_2\text{O}_5(\text{OH})_4$
2:1	illite $\text{K}_{0.9}\text{Al}_2[\text{Si}_{3.1}\text{Al}_{0.9}]\text{O}_{10}(\text{OH})_2$	-	talc $\text{Mg}_3\text{Si}_4\text{O}_{10}(\text{OH})_2$
2:2	montmorillonite $\text{Ca}_{0.3}\text{Al}_{1.8}[\text{Si}_4]\text{O}_{10}(\text{OH})_2 \cdot 2\text{H}_2\text{O}$  beidellite $\text{Ca}_{0.2}\text{Al}_2[\text{Si}_{3.6}\text{Al}_{0.4}]\text{O}_{10}(\text{OH})_2 \cdot 2\text{H}_2\text{O}$	nontronite $\text{Ca}_{0.2}\text{Fe}_2[\text{Si}_{3.6}\text{Al}_{0.4}]\text{O}_{10}(\text{OH})_2 \cdot 2\text{H}_2\text{O}$	saponite $\text{Ca}_{0.2}\text{Mg}_3[\text{Si}_{3.6}\text{Al}_{0.4}]\text{O}_{10}(\text{OH})_2 \cdot 2\text{H}_2\text{O}$  vermiculite $\text{Mg}_{0.3}(\text{Mg}_{2.4}\text{Al}_{0.2}\text{Fe}_{0.4})[\text{Si}_{2.8}\text{Al}_{1.2}]\text{O}_{10}(\text{OH})_2 \cdot n\text{H}_2\text{O}$

Many clay minerals when first formed in the regolith are not very well organized in terms of their atomic structure, hence their crystalline character is difficult to characterize using traditional concepts. Because of this, terms have arisen to describe departure from ideality, such as “disordered”, “poorly ordered”, “of low crystallinity”, “poorly crystalline”, “having short-range order” and so on. Any or all of these terms may be applied to clays and iron oxyhydroxides, but it is rarely clear just what is meant when the words are used.

“Disordered” may properly be used to refer to the distribution of atoms of different type in a specific structural site, randomly over all those sites in a crystal, such as Al-Si disorder over the tetrahedral sites in high sanidine, or the irregular stacking sequence of carbon layers in some graphite crystals. “Poorly ordered” suggests some degree of order, perhaps such as the Al-Si distribution in low sanidine or orthoclase, but it may also refer to sequences of regular layer stacking in a generally randomly stacked layer crystal.

“Of low crystallinity” is more difficult to interpret. It may be used to mean “such small crystals that the X-ray diffraction peaks are broadened”, or “made up of large crystals but with numerous defects”. “Poorly crystalline” commonly means much the same as “of low crystallinity”, but just how the structure departs from perfect crystallinity is unclear. In the case of a clay silicate, the layer sequence might be irregular, the layer type may vary within a packet of layers, or the distribution of atoms or vacant sites in any sheet might be random.

A perfect crystal has its atoms repeating regularly in three dimensions with no breaks in the pattern and no irregularities. Absolute perfection is never observed in nature, but most real crystals, such as quartz or salt, conform very closely to this ideal. While all have defects, they are generally sufficiently few in number and so widely spaced that for most methods of examination (optical, X-ray diffraction, infra-red) their structure is indistinguishable from the ideal. It is only when the departure from ideality is sufficiently marked that it affects the observations that terms such as “poorly crystalline” are used.

The crystal structure of a clay mineral can be thought of in two parts. Firstly there is the layer type: essentially the gibbsite-type layer or the interlayer, the 1:1 layer as in kaolinite or the 2:1 layer as in mica. How the layers stack upon each other in the *z*-direction of a classical crystal lattice determines one aspect of the degree of order. If the layers stack regularly, that is if the arrangement *does* conform to that of an ideal crystal, then the X-ray diffraction pattern, like that of any well-organized crystal, will show sharp, discrete Bragg peaks (Figure 1.7a).

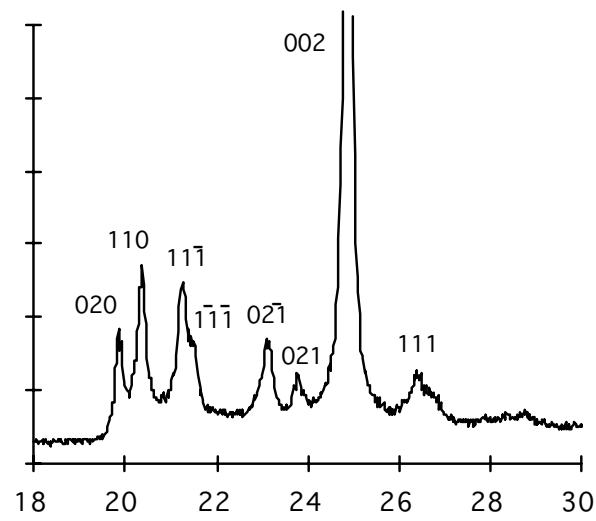


**Figure 1.7a):** XRD pattern of the 02l, 11l region of a well-ordered kaolinite. (Cu K $\alpha$ )

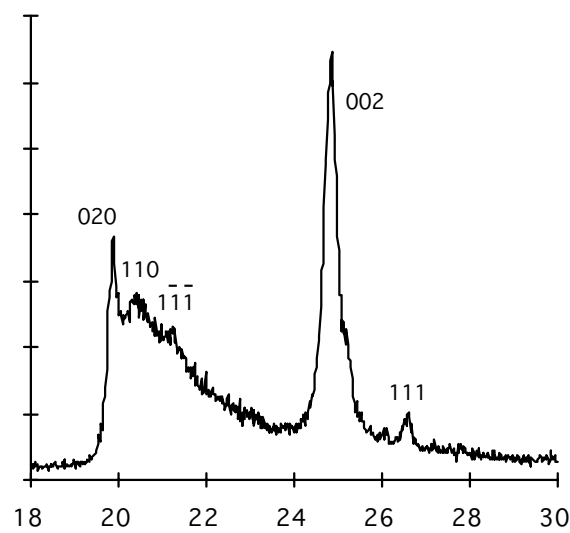


**Figure 1.7b):** XRD scan of the 02, 11 region of a poorly ordered kaolinite. Patterns like this are typical of many soil and transported kaolinites. (Cu K $\alpha$ )

If the layers are NOT regularly stacked, strictly speaking the arrangement is not a crystal, since there is no regularity of arrangement in the  $z$ -direction. Hence there is no direction that can be chosen as the  $z$ -axis, and hence there is no  $c$ -repeat. The arrangement would be referred to as “layer disordered”. Such disorder leads to a merging and a successive diminution in intensity of the XRD Bragg maxima for reflections such as  $hk0$ ,  $hk1$ ,  $hk2$  etc. which gives rise to a saw-tooth pattern (Figure 1.7b).

Structures such as this are commonly referred to as one-layer disordered. If the parent structure has, for example, monoclinic symmetry it may be labeled  $1M_d$  (1 layer, monoclinic, disordered) though strictly, since monoclinic refers to a 3-dimensional ordered arrangement, the word is inappropriate for a layer disordered structure. Similarly the word “crystal” may be inappropriate for such a layer disordered mineral, and the word “tactoid” is sometimes used to refer to an individual layer silicate particle. All smectites have layer disorder, as do many regolith kaolinites and some illites.

Secondly there is the layer itself. The tetrahedral sheet of a clay layer is, as far as has been determined, disordered in the disposition of Al and Si in tetrahedral sites. In illite, the Al-Si distribution is assumed to be the same as in muscovite; that is, disordered. Kaolinite has no tetrahedral Al so the issue does not arise. Smectites yield insufficiently good XRD patterns for Si-Al order to be assessed.

The location of the vacant site in the octahedral sheet of dioctahedral micas is known to be well-ordered, as is the location of octahedral Al<sup>3+</sup> in trioctahedral micas (Brigatti et al., 2000). Conversely, Mg-Fe ordering between octahedral sites is at most a subtle effect which may be steered in either direction by other factors (cf. Holland and Powell, 2006).

Vacant site ordering is also well developed in kaolinites, and indeed it is through the regularity of repeat of the octahedral vacant site in the *z*-direction that layer-ordered kaolinites are defined. So as far as has been determined, each individual layer of a clay mineral maintains 2-dimensional regularity within itself, and for a given simple species (as opposed to interstratifications of more than one layer type), all the layers have this regularity.

In short, the vast majority of disorder in clay minerals arises from random displacements between layers.

Although the sharpness of the *hkl* reflections from clays may be affected by layer disorder, it is the thickness of the layer packets or “tactoids” (i.e, the number of layers accurately positioned on top of each other) which affects the breadth of the 001 reflections. Clay packets may be as thin as one layer – in which case no 001 reflections will be seen at all by XRD, or be several micrometres thick yielding narrow, sharp 001 peaks. In between lie most of the regolith clays, having crystals which are less than 0.1  $\mu\text{m}$  in thickness which introduces broadening of the 001 reflections (Figure 1.8). It is possible to estimate the mean tactoid thickness from the width of a clay mineral peak (see for example Moore and Reynolds 1989 or Brindley & Brown 1980)

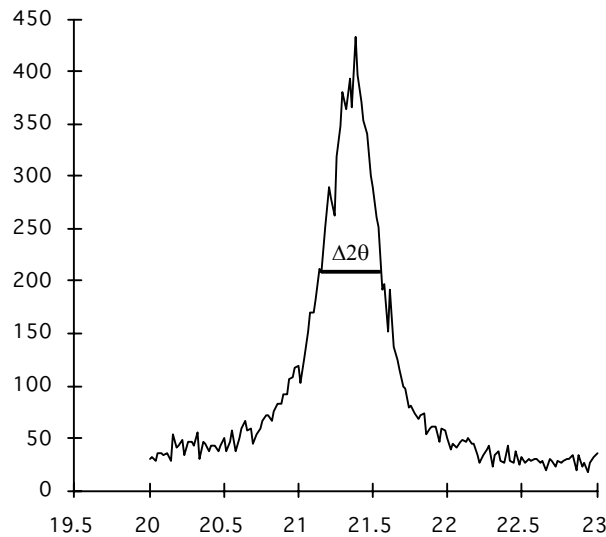


**Figure 1.8:** X-ray diffraction peak broadened by small crystal size (ca 25 nm thick). In this case the full width at half maximum (FWHM) ( $\Delta 2\theta$ ) is approximately  $0.5^\circ$   $2\theta$ , at least 10 times broader than a well-crystallized 2  $\mu\text{m}$  crystal would yield.

## Smectite

Smectites were in the older literature referred to as “montmorillonite”, but that name is now restricted to a particular species in the smectite group. The detailed structure of smectites is not well known, because they yield such broad and indistinct X-ray diffraction peaks. There is general agreement that they have normal 2:1 layers with hydrated cations in the interlayer region. It is assumed that the layers are regular in their atomic arrangement, just like those of micas. Scanning electron micrographs and

transmission electron microscopy show that Na-smectite layers have no apparent rigidity indicating little strength in the inter-particle forces linking one layer to the next. Indeed when placed in water, Na-smectites are thought to completely separate into individual 2:1 layers (Norrish 1954, Foster 1955). This characteristic has important implications for the stability of sodic soils, i.e. soils containing appreciable amounts of exchangeable sodium. The complete separation of Na-smectites into individual 2:1 layers is known as dispersion, and can cause problems of soil crusting (Rengasamy and Olsson 1991). The dispersed clay particles can also block pores and hence decrease soil permeability (Turner et al 2007).

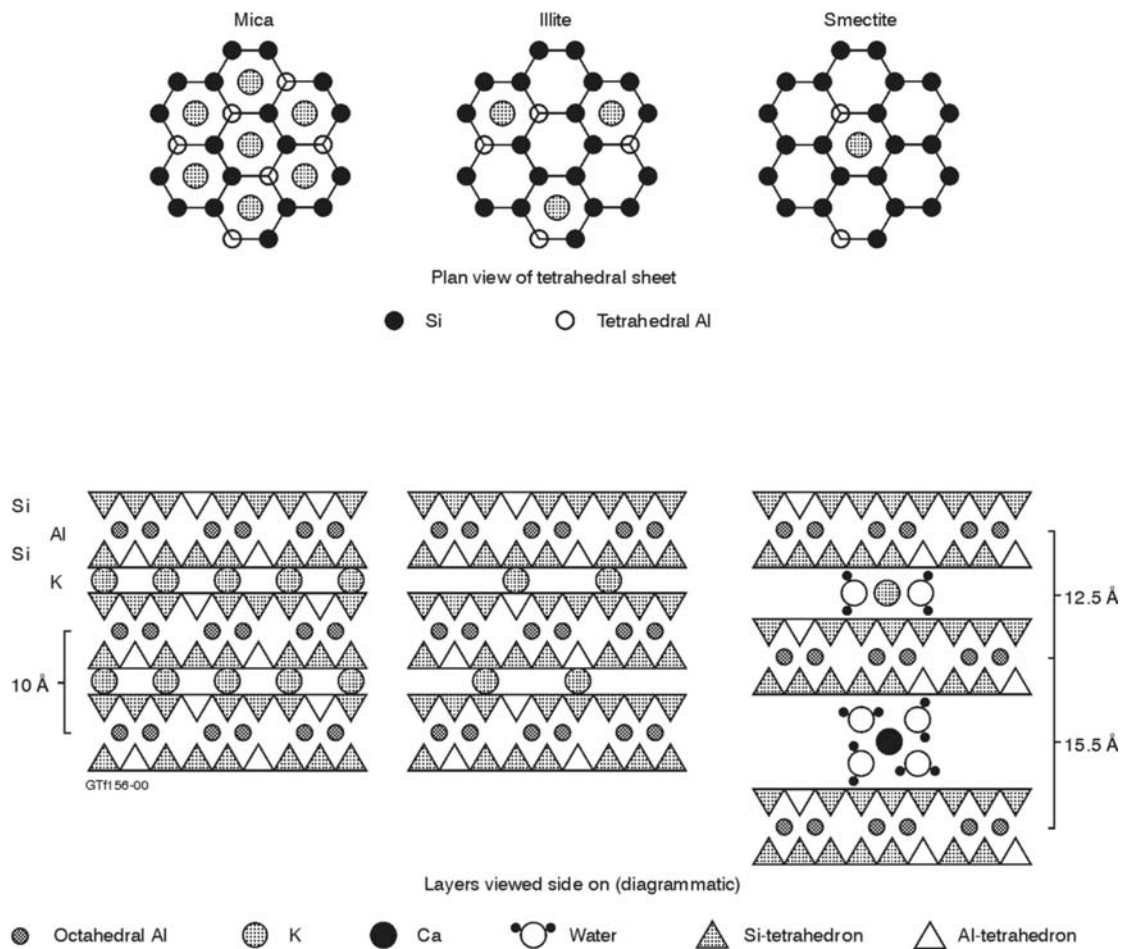


**Figure 1.9:** Diagrammatic plan (upper) and side(lower) views of the structures of muscovite, illite and smectite. When the interlayer charge is less than about 0.5 per 4SiAl, hydrated cations enter the interlayer causing the layers to separate to accommodate the water.

The singly charged ions K<sup>+</sup> and Na<sup>+</sup> attract water relatively weakly, Ca<sup>2+</sup> attracts water more strongly. Na<sup>+</sup> smectites absorb one water layer at humidities above 5% and below about 50%, adding a second above 50% relative humidity. Ca<sup>2+</sup> smectites keep one layer unless completely dried, and add the second water layer at about 20% humidity. The thickness of a smectite unit is 0.94 nm without water, expanding to 1.25 nm with one water layer, and to 1.55 nm with two. Immersed totally in water, some smectites add a

third layer, others expand indefinitely (the layers separate). The water in the interlayer can be replaced by molecules that are more strongly attracted to the interlayer cation such as alcohol, glycerol, urea, and many other organic molecules. Natural and synthetic organics such as pesticides and herbicides may also enter the interlayer region of smectites. Most smectites as collected are well hydrated, and so yield a 1.5 nm 001 reflection. On full dehydration, this spacing collapses to 1.0 nm.

Smectites typically form the finest particles in a soil. They may be no more than two or three layers thick (3.0-4.5 nm), and 0.1  $\mu\text{m}$  across. They have very high cation exchange capacity (800-1200  $\text{mmol}^{+ve}/\text{kg}$ ), largely derived from exchange sites in the interlayer. Their small size also gives them a high edge exchange capacity. A small amount of smectite in a soil therefore has a considerable effect on its properties.

Of the several varieties of smectite listed in Table 3.1, beidellite is the most common, being a product of feldspar and mica weathering. In beidellite, as in most smectites, the interlayer charge arises from the Al/Si substitution in the tetrahedral sheet. Montmorillonite is an aluminous smectite with its net charge arising from reduced cation charge in the octahedral sheet instead. The ferric iron smectite nontronite is found in weathered ultramafic rocks, such as the nickel laterites of Western Australia (Murrin Murrin, Bulong) and east-central Queensland (Marlborough, Greenvale). Saponite (Mg-smectite) forms in weathered basalts and in regolith over high-Mg rocks such as talc schists and ultramafics (for example those at Marlborough, Queensland, and the Ni-laterites of Mt Keith, Western Australia).

Detailed studies of rock weathering have shown that individual parent minerals can give rise to different smectites. On bulk sampling all these phases would be lumped together. Caillaud et al (2006) found saponite and two different Fe-smectites as alteration products of serpentine depending on the micro-site examined, as well as nontronite and a dioctahedral smectite as an alteration product of adjacent chlorite.

## **Chlorite**

Most chlorite is trioctahedral, having talc-like 2:1 layers with brucite-like layers between. The layers have a spacing of about 1.42 nm, and the X-ray pattern is usually quite sharp and clear. Chlorite does not swell with hydration or organics, and is little affected by heating. Chlorite in the regolith is generally residual from bedrock, however aluminous chlorites occur in some soils. Wilson (2004) summarizes the weathering of chlorite in which the first step is the formation of vermiculite by a sequence in which individual brucite-like layers lose  $\text{Mg}^{2+}$  and gain  $\text{H}^+$  until the interlayer is occupied by hydrated  $\text{Mg}^{2+}$  rather than a  $\text{Mg}(\text{OH})_2$  octahedral sheet. In some instances the alteration leads to a regular alternation of chlorite and vermiculite (the species *corrensites*; Figure 1.10). With further weathering random-vermiculite chlorite precedes the full conversion to vermiculite.

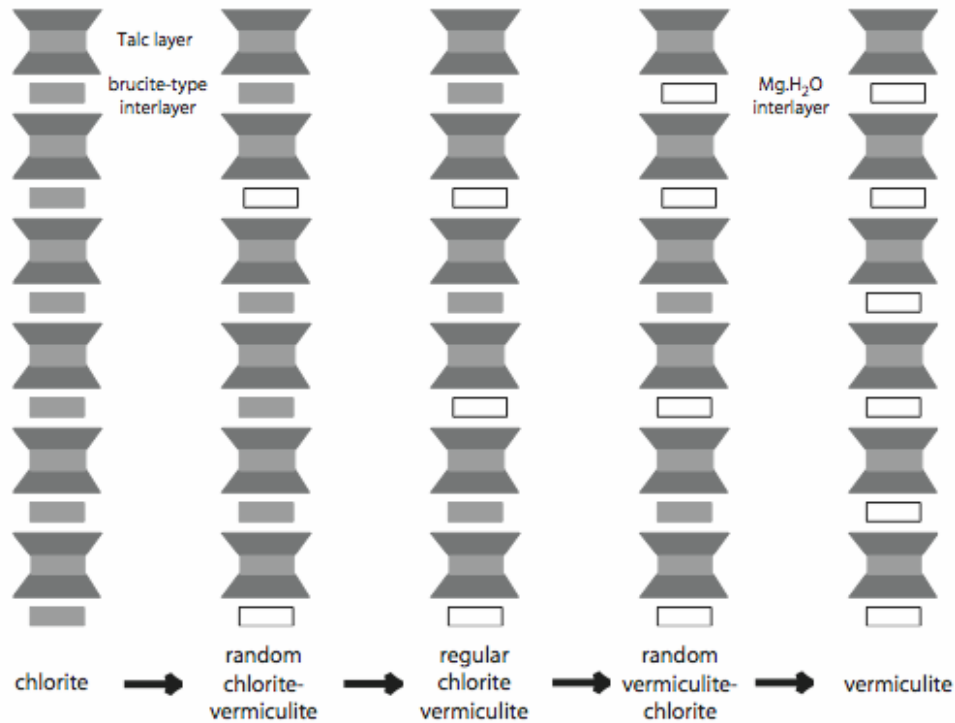


**Figure 1.10:** Diagrammatic representation of the conversion of chlorite to vermiculite. The “cotton reels” represent a single unit cell (*yz* section) of the TOT unit of talc-like layers, the shaded rectangles represent brucite-like interlayers, and the outline rectangles represent hydrated-Mg interlayers.

## Vermiculite

Vermiculite is structurally mid-way between biotite mica and chlorite. It has a trioctahedral 2:1 layer, and an interlayer of  $\text{Mg}^{2+} \cdot n\text{H}_2\text{O}$  or  $\text{Al}^{3+} \cdot n\text{H}_2\text{O}$ . Vermiculite has a higher layer charge than smectite and a high cation exchange capacity (100-150 meq/100g). Both  $\text{Mg}^{2+}$  and  $\text{Al}^{3+}$  are able to hold two layers of water molecules in the interlayer. The layers are more strongly held together than are those of smectite, so the basal spacing is smaller (1.4 nm, cf 1.5 nm for smectite). On heating the water can be expelled, collapsing the structure to 1.25 nm and then to 1.0 nm. If a large vermiculite crystal is rapidly heated, the steam physically blows some of the layers apart, and accordion-like "worms" are formed, from whence its name. These have use as an absorbent for potting soils, kitty litter, and industrial clean-up. The structural spacings, nonetheless, collapse to 1.0 nm.

Vermiculite is formed during the weathering of biotite in a manner similar to its formation during chlorite weathering.  $\text{K}^+$  from the biotite interlayer is leached and replaced by hydrated  $\text{Mg}^{2+}$  derived from elsewhere in the weathering crystal or further away in the profile (See Wilson 2004 for a detailed summary). Vermiculite is also produced by the weathering of pyroxenes and amphiboles. Figure 1.3b shows diagrammatically the way in which TOT chains of pyroxene may coalesce to produce a 2:1 layer, which in turn may evolve to vermiculite.

## Illite

Illite is the term used for clay-sized layer silicate very similar to muscovite. The name 'illite' is commonly attributed to any clay-sized mineral with 1.0 nm layer spacing, and it is important to appreciate that there is much compositional and mineralogical variation possible for a clay mineral identified only by particle size and basal spacing. The literature on illite is large, and permits no simple interpretation. Meunier and Velde (2004) have written a book on illite; what follows here is largely drawn from their work. Muscovite has K between the 2:1 layers, held there by electrostatic attraction to charge-unsatisfied oxygens of the silicon-oxygen network: these oxygens are bonded to one silicon and one aluminium (Fig 6.11). Muscovite has one K and one tetrahedral Al for every three Si (i.e.  $\text{KAl}_2[\text{AlSi}_3]\text{O}_{10}(\text{OH})_2$ ).

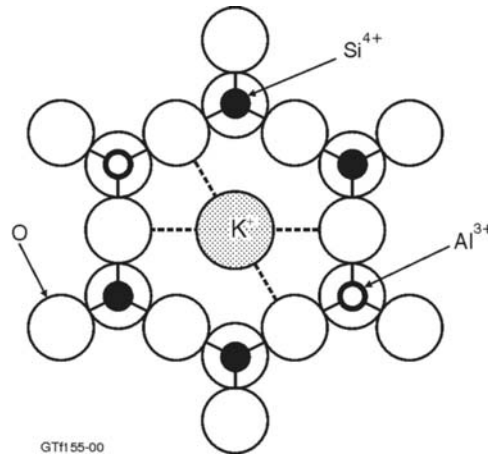


**Figure 1.11:** Part of the tetrahedral sheet of mica showing the bonding of K to basal oxygens which are charge unsatisfied because of  $\text{Al}^{3+} \leftrightarrow \text{Si}^{4+}$  substitution.

Illite has less Al replacing Si in the tetrahedral sheet, and correspondingly less K, with a formula suggested to be  $\text{K}_{0.9}\text{Al}_2[\text{Si}_{3.1}\text{Al}_{0.9}]\text{O}_{10}(\text{OH})_2$ . The illite structure is thought to incorporate in some way 90% muscovite-like domains and 10% pyrophyllite-like domains, and although the octahedral sheet composition need not be pure Al, illites are essentially dioctahedral. The K in illite is still sufficient to hold the 2:1 layers firmly together, so illite is a 10-Å layer silicate. Illite has a CEC of no more than 50 mmoles +/-kg.

What has made the understanding of illite difficult is that random interstratification of smectite with illite can occur with little change in the position of the 10-Å XRD reflection. The smectite component introduces high CEC and many illites have been reported with CECs of the order of 300 mmoles +/-kg. According to Meunier and Velde, these all have interstratified smectite. Deconvolution of the 1.0 nm XRD peak generally shows it to be composed of a well-crystallized illite plus poorly crystallized illite ± smectite.

## Kaolin

Kaolin is a general term that includes kaolinite, dickite, nacrite and halloysite. It is an aluminosilicate, formed during weathering of all the alumino-silicate primary minerals such as feldspars, muscovite, feldspathoids and zeolites as well as illite, smectite, and vermiculite. Kaolinite, dickite and nacrite are platy, commonly forming hexagonal crystals 0.1-2  $\mu\text{m}$  across and about one tenth as thick. Halloysite has the same composition as kaolinite, but with water between the layers. Its layers are not flat, but are curled or rolled, generally occurring either in tubes or spheres, although platy halloysite with curled edges has been described (Fig. 6.12).

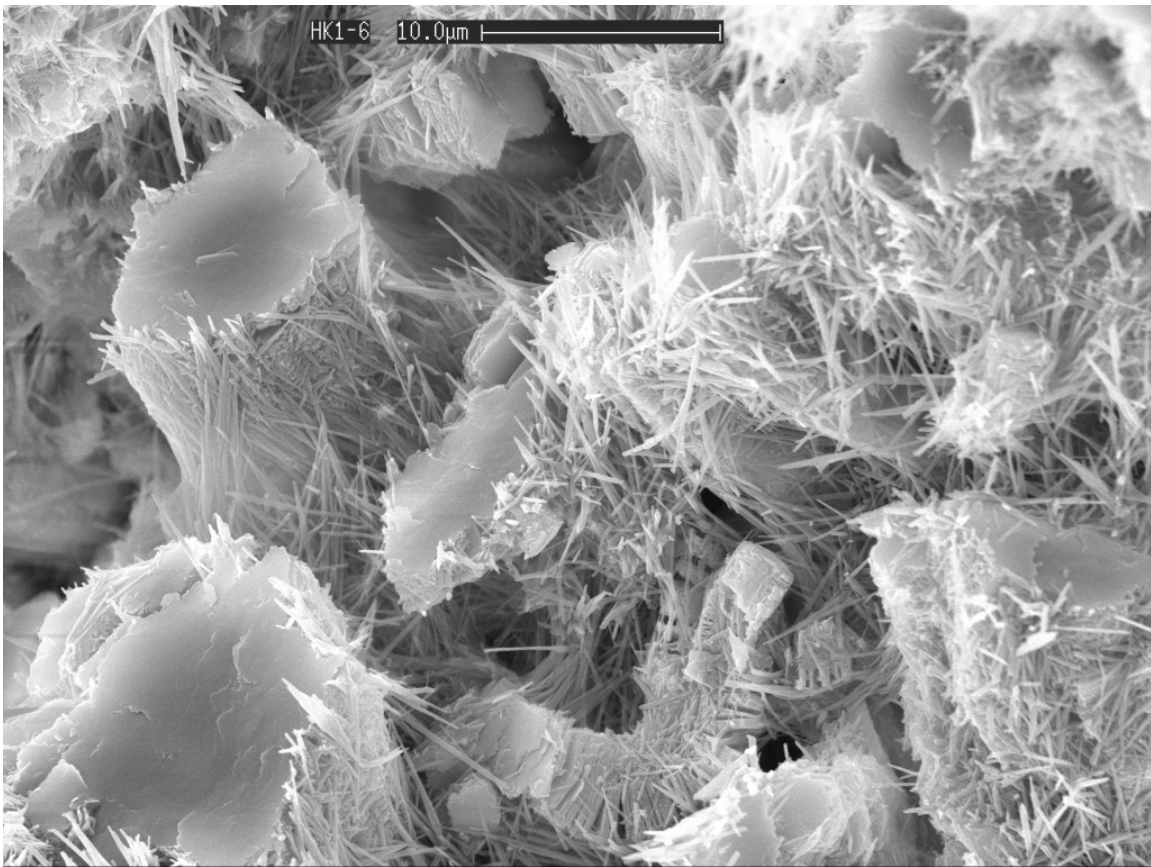


**Figure 1.12:** Scanning electron micrograph of tubular halloysite surrounding kaolinite crystals, the products of granite weathering, Hong Kong. (Photo R.A. Eggleton).

Kaolin has a very low cation exchange capacity, of the order of 20-40 mmole<sup>+ve</sup>/kg. The composition of kaolinite is simple and constant ( $\text{Al}_2\text{Si}_2\text{O}_5(\text{OH})_4$ ). There is no structural exchange site: cation exchange in kaolinite derives from surface and edge exchange sites.

Kaolinite *sensu strictu* is a triclinic mineral having regular stacking of the 1:1 layers yielding a 1-layer structure, 0.72 nm thick (*001* spacing). Dickite is a polytypic variant, in which the layer sequence alternates through alternate positioning of the vacant site in

the octahedral layer (Newnham and Brindley, 1956). This yields a 2-layer unit cell with  $d(001) = 1.42$  nm; the individual layers are still 0.72 nm thick. The first X-ray reflection from dickite has an 0.72-nm spacing as it does kaolinite. However, because of the doubled unit cell, this reflection in dickite is indexed as  $002$ . Because both polytypes are defined on the basis of their regular stacking, the terms are only applicable to regularly stacked crystals, and XRD is needed to establish this. Identifying which kaolin mineral is present requires a well-ordered crystal, yielding a good sequence of  $hkl$  X-ray reflections. While there is some difference in the infra-red patterns of kaolinite and dickite, infra-red results are ambiguous at best if disordered kaolinite or any other clays are present.

Regularly stacked kaolin is best developed in hydrothermal deposits and in *in situ* weathering profiles. Kaolinite is particularly common in weathering profiles on granites and other aluminous igneous rocks, and on shales and arkoses among sedimentary rocks. Transported or sedimentary kaolin is most commonly disordered: the layer sequence is random, yielding an XRD pattern like that shown in Figure 1.8b.

Dickite, which is not common, is known from hydrothermal rocks (see for example Choo and Kim, 2004) and as an authigenic mineral in shales (Veniale *et al.*, 2002) and in sandstones (Bayliss and Loughnan, 1965).

Nacrite is a third variant, even rarer than dickite. It is generally regarded as a hydrothermal mineral. It also has a 2-layer structure, but the interlayer shifts are in the direction perpendicular to those of dickite and kaolinite (Zheng and Bailey, 1994).

### **Interstratified clays**

In plan, all the clay silicates have the same structure: a hexagonal silica-oxygen sheet (or sheets) and a hexagonal octahedral sheet. They therefore have little difficulty stacking different layer types on top of one another. Illite and smectite layers may alternate, building up random sequences (ISISSIISISSIIS) or regular sequences (ISISISIS, or IISIISIIS). Kaolinite and smectite may alternate in soil clays, and both biotite and chlorite weather to vermiculite through an intermediate random (or sometimes ordered) interstratification, as described above. There is a vast literature on interstratified clays (also incorrectly called mixed-layer clays) because they are formed during diagenesis of shales and are common in sedimentary basins.

### **Sepiolite-palygorskite**

Two fibrous Mg-rich chain-silicates that are found in the regolith are sepiolite and palygorskite. They both have a high exchange capacity of around 300 mmoles  $+^{ve}$ /kg and a high surface area ( $\sim 900$  m<sup>2</sup>/g). They adsorb metal cations very effectively, and also absorb more than twice their own weight of water. Sepiolite and palygorskite form in saline evaporitic environments, both marine and terrestrial, such as under arid conditions, in closed basins where high salinity ground-waters accumulate. A reaction between detrital clays, largely smectite, and high-Mg alkaline water derived from mafic rock weathering is generally envisaged (Weaver & Beck, 1977). Callen (1984) summarized the environments of sepiolite-palygorskite deposits and notes a marked relation between latitude (30°-40° N and S) and the occurrence of these minerals, interpreting this as a

control by aridity on their continental formation. Palygorskite deposits are widespread in paleochannels on the Eyre Peninsula, South Australia (Keeling and Self, 1996), associated with dolomite and illite-smectite clays.

---

## OXIDES AND OXYHYDROXIDES

---

### **Silica minerals**

Quartz is far and away the most abundant and ubiquitous mineral in the regolith. Most quartz is residual from bedrock, whether locally derived or transported. There are several reasons for its abundance in the regolith beyond its abundance in crustal rocks; note that feldspar is twice as abundant in rocks, yet is quite rare in regolith. Quartz is the hardest of the common rock-forming minerals, and it has very poor cleavage. Under mechanical stress it does not fracture readily, thus maintaining relatively large grains, and it is resistant to abrasion. Such potential fractures as it does have often appear to be spaced at about 20  $\mu\text{m}$  (Moss *et al*, 1973), so when quartz does fracture, the smallest particles produced are in the silt-size range so that unlike clay minerals, they do not wash away easily. It is also the least soluble of the common rock forming minerals in normal ground water (pH around 6). It is from 10 to 100,000 times less soluble than feldspar for example. Dissolution kinetics are in any case slow. From laboratory measured rates of dissolution (see for example White and Brantley, 1995), a 200  $\mu\text{m}$  quartz grain would take of the order of 2 million years to dissolve.

As outlined at the start of this chapter, the chemical weathering of silicates releases silica into solution. Particularly in arid climates, the dissolved silica is liable to be precipitated, generally as micro-crystalline aggregates. Quartz may precipitate, particularly coating pre-existing quartz, but more common are the silica varieties chalcedony, moganite and opal. Chalcedony and moganite have structures based on multiple twinning of quartz, whereas the opal structure may have cristobalite (Opal C) or tridymite-like units (Opal T), both (Opal CT), or be X-ray amorphous (Opal A). Opal yields very broad XRD maxima, typically having full width at half maximum values of  $\sim 0.5^\circ$

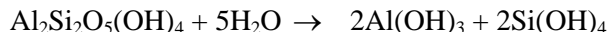
Silica precipitation in the regolith leads to hard-pans, silica veins and crack fillings and to silcretes. Opaline silica is quite abundant in regolith over ultramafic rocks, as the low Al content of the parent rock does not provide for kaolinite as a host for silica. Thiry *et al* (2007) conclude that extensive regions of silica deposition in South Australia in the form of opal, silcrete and red-brown hardpans were formed by a complex interplay of water movement, pH change and climate variation from arid to humid.

### **Al-oxides and hydroxides.**

Continued weathering of aluminosilicates, particularly of kaolin, eventually removes all the silica and leaves alumina minerals.

Gibbsite is the most common alumina mineral ( $\text{Al}(\text{OH})_3$ ), with boehmite ( $\text{AlO}(\text{OH})$ ) quite common, whereas diaspore ( $\text{AlO}(\text{OH})$ ), corundum and other polymorphs of  $\text{Al}_2\text{O}_3$  are rare. Gibbsite and boehmite are the main components of bauxite, and so are important as

ores of aluminium; they are referred to in the mining industry as tri- and mono-hydrate respectively.



Kaolinite + water → gibbsite + silica in solution

On the basis of crystal size, gibbsite and boehmite can be classed as clay minerals, as in most weathered rocks they occur as sub-micron sized crystals, however they generally yield clear, sharp XRD patterns. Heating, either through metamorphism or forest fire, can convert gibbsite and boehmite to corundum ( $\alpha$ -alumina), or the less stable polymorphs  $\gamma$ -,  $\chi$ - or  $\varepsilon$ -alumina (see the section on poorly crystalline minerals below).

### Fe-oxides and hydroxides

As described in the section on clay silicates, an important step in the weathering of primary rock-forming minerals is the oxidation of ferrous iron to ferric. Below the water table, where the conditions are likely to be reducing, dissolution releases ferrous iron to the ground water. As soon as ferrous iron reaches an oxidizing environment, for example above the water table, ferric iron precipitates within the weathering solution as ferric hydroxide, which then evolves to the mineral ferrihydrite (Schwertmann 1985).

Ferrihydrite has an approximate composition  $5\text{Fe}_2\text{O}_3 \cdot 9\text{H}_2\text{O}$ . Ferrihydrite is the brown rusty scum visible at springs, where water seeps from cracks in rocks, or as an 'oil slick' on some swamp water. Ferrihydrite crystals range from about 2 nm in diameter to 7.5 nm. The degree of organization of these particles is low, and the X-ray pattern is very simple and weak, with broad lines. Much ferrihydrite in regolith is missed because it does not yield a marked diffraction pattern. The difficulty of characterising this nanophase material is well illustrated by Michel et al. (2007).

The surface area of ferrihydrite crystals ranges from 200-800  $\text{m}^2/\text{g}$ . Ferrihydrite is a strong adsorber of phosphate, silica, organic molecules, and heavy metals. In the laboratory, ferrihydrite transforms to a more stable oxide-hydroxide (goethite, usually) over a period of a few years. In the soil it probably passes in and out of solution with the seasons. Ferrihydrite is of the order of 100 times more soluble in normal ground water than the other Fe oxides or oxyhydroxides.

Most ferrihydrite is associated with bacteria (*Gallionella* & *Lepthotrix*) which gain their energy from the oxidation reaction  $\text{Fe}^{2+} \rightarrow \text{Fe}^{3+} + \text{e}^-$ . Ferrihydrite also precipitates from ferric iron solution as pH increases. Ferric iron is soluble at pH 2 (very acid), becoming less so with increasing pH. At pH 4 the solubility is negligible (about 1 in 10 million). Very acid waters (mine waters, some lakes such as Lake Tyrell in western Victoria) can hold appreciable ferric iron in solution, which precipitates as ferrihydrite on dilution (because the pH increases) or on input of alkaline water. Soils derived from pyritic ( $\text{FeS}_2$ ) rocks or coastal muds are commonly acid enough to mobilize iron, from whence it may rise to the surface and precipitate through rain dilution or oxidation.

Cyclic dissolution and precipitation of Fe by reduction/oxidation alternation or pH change moves iron away from reducing areas toward oxidizing areas and is responsible for most of the brown/yellow colour banding of soils and weathered rocks. Precipitation at the top of the water table may yield an iron hard-pan.

Goethite FeO(OH) is the most common of the soil iron minerals; goethite is the first conversion product from ferrihydrite. It is a yellow-brown mineral, forming as needle-shaped crystals about 1  $\mu\text{m}$  long in synthetic preparations, but typically more equant in soils. Together with ferrihydrite, goethite imparts most of the brown colour to soils.

The surface area of soil goethite ranges from 6-200  $\text{m}^2/\text{g}$ , which gives goethite considerable adsorptive ability. Heavy metals such as Cu, Pb, and Zn are adsorbed to the extent of about 1  $\mu\text{mol}/\text{m}^2$  (20  $\mu\text{mol}/\text{g}$ ). Goethite is also an effective anion adsorber, notably of phosphate. At normal regolith pH, phosphate values of about 2-3  $\mu\text{mol}/\text{m}^2$  have been measured both in laboratory and the field. Much of the superphosphate ( $\text{Ca}(\text{H}_2\text{PO}_4)$ ) ploughed into fields becomes unavailable to plants in quite a short time because it is sequestered by goethite.

Al occurs in goethite substituting for Fe, up to 32 mole% (Fitzpatrick & Schwertmann, 1982). In the regolith, goethite formed in hydromorphic environments, such as mottles, concretions and ferricretes tends to have lower Al substitution (0-15 mole%), whereas freely drained regolith such as saprolites and bauxites have Al substitution ranging from 15-32 mole% (Fitzpatrick, 1988). Fitzpatrick & Schwertmann (1982) explain the difference as resulting from lower pH and therefore higher Al activity in the more freely drained regolith. Al substitution is readily estimated from the X-ray diffraction pattern of goethite; substitution of Al reduces the unit cell dimensions (Schulze, 1984) as well as reducing the mean crystalline dimension.

Because many regolith goethites are extremely fine-grained, they give rather broad XRD peaks, and this can lead to misleading estimates of the cell dimension, and in turn of the Al substitution. Schulze (1984) explains this problem and suggests ways to overcome it. Using full-profile XRD analysis, the cell dimensions of goethite can be reasonably well determined.

Lepidocrocite is the FeO(OH) polymorph with the oxygens in approximate cubic close packing. Recognizable by its orange colour, lepidocrocite is a relatively uncommon mineral, forming in preference to goethite as a direct oxidation product of ferrous iron and in preference to ferrihydrite if oxidation is slow. It therefore indicates reductomorphic soils. Lepidocrocite, or the very rare polymorph akaganéite, also seem to be precipitate rather than goethite in the presence of  $\text{Cl}^-$ .

Hematite ( $\text{Fe}_2\text{O}_3$ ) is very common in warm or arid regolith, and is red when fine-grained. Its intense colour may mask the presence of goethite. The surface area for soil hematite is about 100 $\text{m}^2/\text{g}$ , much the same as goethite. The hematite-goethite ratio in soils increases with soil temperature (decreasing latitude) and decreases with soil moisture content. Locally, hill tops are richer in hematite, valleys in goethite; globally, the arid regions have hematite rather than goethite. Hematite has similar adsorption properties to

goethite and can also be responsible for the fixation of phosphate. Hematite can accept up to about 15 mole % Al in the structure (Fitzpatrick & Schwertmann, 1982); such high levels indicate hematite crystallization from solutions saturated with Al (Schwertmann & Kämpf 1985, Fitzpatrick 1988). Determination of the extent of Al substitution is very difficult. As with goethite, high Al tends to reduce the crystal size of the hematite making EMP analysis impossible, and Stanjek and Schwertmann (1992) have shown that cell dimensions are at best equivocal as estimators of Al substitution in hematite.

Magnetite ( $\text{Fe}_3\text{O}_4$ ) is a member of the spinel group of minerals. It is not fully oxidized, having one  $\text{Fe}^{2+}$  and two  $\text{Fe}^{3+}$ . It is not as common in regolith as other  $\text{Fe}^{3+}$  minerals. Although some may be produced directly by bacteria, most is residual from magnetite in parent rocks.

Maghemite  $\text{Fe}_2\text{O}_3$  is also a spinel, although its formula is the same as that of hematite. Written as a spinel, maghemite is  $\text{Fe}_8\text{O}_{12}$ , compared with magnetite,  $\text{Fe}_9\text{O}_{12}$ . Maghemite can form by the oxidation of magnetite, and some soil maghemite may result from the oxidation of  $0.1 \mu\text{m}$  crystals of magnetite formed by bacteria. Most maghemite probably forms in soils by the dehydration of goethite or lepidocrocite during fires. Lepidocrocite can transform easily to maghemite, as both have cubic close-packed oxygen substructures. Goethite has a structure based on hexagonal close packing, and normally dehydrates to (hexagonal) hematite. In the presence of organic matter it is thought that maghemite is the common dehydration product. Early in a bushfire, plant fragments in the soil burn providing hot, reducing conditions capable of converting ferrihydrite or goethite to  $\text{Fe}_3\text{O}_4$  or possibly  $\text{FeO}$ . As the fire passes and the carbon is consumed, the reduced oxides change to maghemite. Maghemite is strongly magnetic, and a hand magnet is the quickest means of identification (assuming no magnetite is present).

Maghemite is dense ( $5 \text{ g/cm}^3$ ) and stable in the weathering environment. Maghemite-rich ferruginous nodules and grains accumulate in stream channels where they are particularly obvious in magnetic surveys. Paleochannels can be readily detected by their magnetic signature.

### **Anatase**

The polymorph of  $\text{TiO}_2$  most abundant in the regolith is anatase. It commonly is found as very small ( $0.1 \mu\text{m}$ ) crystals, and is a major constituent of the fine-grained alteration assemblage known as leucoxene. Anatase has a cream-coloured appearance when it is concentrated, but mostly it is dispersed uniformly through silicate weathering products.

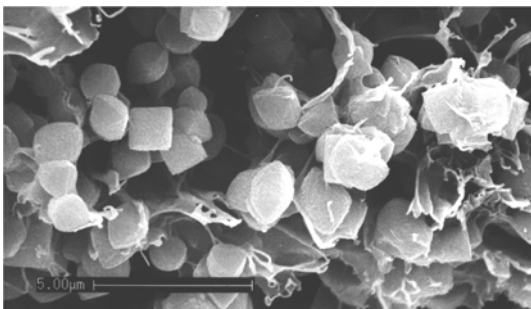


**Figure 1.13:** Crystals of anatase about  $0.1 \mu\text{m}$  across with smectite in altered titanite (Tilley and Eggleton, 2005).

In the lateritic and bauxitic parts of regolith profiles and in silcretes, anatase content commonly reaches 2 to 3% and in some silcretes reaches as high as 40% (Thiry and Simon-Coincon 1996)

Anatase has one very prominent XRD peak at 0.35 nm, generally sharp and well resolved from the nearby 0.36 nm kaolin 002 peak. As little as 0.5% anatase can be detected from this peak, although as it is commonly the only anatase peak distinguishable in the XRD pattern, it is wise to cross check a conclusion about anatase with chemical evidence for TiO<sub>2</sub>.

### **Mn oxides and hydroxides**

In the weathering environment, Mn becomes oxidised to the tetravalent state. The mineralogy of manganese oxides and hydroxides is complex: the more common regolith species are the layer structures having cations other than Mn between MnO<sub>6</sub> octahedral sheets: vernadite ( $\delta$ -MnO<sub>2</sub>), incorporating Ba or K, lithiophorite ((Al,Li)MnO<sub>2</sub>(OH)<sub>2</sub>), birnessite ((Na,K)<sub>4</sub>Mn<sub>14</sub>O<sub>27</sub>·9H<sub>2</sub>O), and the cryptomelane-coronadite-hollandite group (K,Pb,Ba)<sub>2-1</sub>Mn<sub>8</sub>O<sub>16</sub>), which have large cations in tunnels which are bounded by columns of MnO<sub>6</sub> octahedra.

Other Mn-oxides and oxyhydroxides include pyrolusite and nsutite (MnO<sub>2</sub>), romancheite (containing Ba) todorokite (containing Ca, Na, and K), chalcophanite (ZnMn<sub>3</sub>O<sub>7</sub>·3H<sub>2</sub>O) and asbolane. (Ostwald, 1992, Parc *et al.*, 1989).

K-bearing Mn oxides have been used to date regolith by K-Ar and Ar-Ar methods (see Chapter 2).

---

## OTHER MINERALS

---

### **Sulfates**

Gypsum is a common evaporite mineral in arid environments, occurring both in lake deposits and in the regolith over sulfides. The composition of gypsum varies little from CaSO<sub>4</sub>·2H<sub>2</sub>O.

Jarosite-natrojarosite (K,Na)Fe<sub>3</sub>(SO<sub>4</sub>)<sub>2</sub>(OH)<sub>6</sub> precipitate from a reaction between sulfuric acid formed by pyrite oxidation and surrounding silicates. These minerals are common in regolith where pyrite is weathering, and are particularly so in acid-sulfate soils and mine dumps. Brown (1971) showed that jarosite is only stable in the presence of goethite at pH below 3. Such extreme pH levels are reached during sulfide weathering and also in saline lakes such as Lake Tyrrell, western Victoria, Australia, where sulfidic muds oxidize. The persistence of jarosite into environments of higher pH is attributed by Brown to the slowness of its conversion to goethite. Jarosite, which is isostructural with the crandallite group described below, can take a wide range of metals into its structure, substituting either for the large alkali cation or for the octahedrally coordinated Fe<sup>3+</sup>. Metals released by acid sulfate weathering of sulfide ores such as Ag, Pb, Tl, Cu or Hg

may reside in jarosite (Becker and Gashrova 2001), to be released to the environment when the acidity is neutralized causing jarosite to dissolve.

Alunite ( $\text{KAl}_3(\text{OH})_6(\text{SO}_4)_2$ ) is found in hydrothermal advanced argillic alteration, and associated with acid lake and groundwaters, where it crystallizes by reaction between clays and sulfuric acid from pyrite weathering. Alunite is also widespread in arid southern Australia associated with gypsum, kaolin and opal, where it has been suggested that it forms from sulfate-rich groundwaters (Bird *et al* 1989) under low pH conditions associated with the oxidation of ferrous iron (ferrolysis) rather than from sulfide weathering (Thiry *et al* 2007).

## **Carbonates**

The major carbonate mineral of the regolith is calcite ( $\text{CaCO}_3$ ). Of the other rhombohedral carbonates dolomite ( $\text{CaMg}(\text{CO}_3)_2$ ) and magnesite ( $\text{MgCO}_3$ ) are found quite commonly, and siderite ( $\text{FeCO}_3$ ) and ankerite ( $\text{CaFe}(\text{CO}_3)_2$ ) rather rarely. Calcite develops in the regolith in many environments, and where Ca is abundant in the bedrock, particularly in semi-arid climates, large regions of regolith cemented by calcite are found, generally termed calcrete. Uncemented aggregates of carbonate mineral are termed Regolith Carbonate Accumulations (RCAs); these may be dolomitic or magnesitic rather than calcic. Magnesite may be abundant in high Mg terrains, for example as regolith carbonate accumulations following the weathering of ultramafics such as at Kunwarrara in central east Queensland (Wilcock, 1998) or on the Yilgarn of Western Australia (Wells 2005; Gaudin *et al.* 2005). Dolomite and high Mg-calcite occur in some Australian inland regolith, notably in South Australia (Milnes & Hutton, 1983) and western New South Wales (Hill *et al* 1999, McQueen *et al* 1999). These authors also report an increase in the Mg content of Ca-Mg carbonates with depth.

Metal carbonates such as those of Cu (malachite and azurite), Pb (cerussite), Zn (smithsonite) and Ni (gaspéite) are well known from the supergene region of weathered ore bodies, and the list can be expanded to include carbonates of almost all mono- and divalent metals.

## **Phosphates**

The significance of the crandallite group of phosphates in the regolith was established by Norrish (1975), Norrish & Rosser, (1983)). The group includes crandallite ( $\text{CaAl}_3(\text{PO}_4)_2(\text{OH})_5 \cdot \text{H}_2\text{O}$ ), gorceixite ( $\text{BaAl}_3(\text{PO}_4)_2(\text{OH})_5 \cdot \text{H}_2\text{O}$ ), and florencite ( $\text{CeAl}_3(\text{PO}_4)_2(\text{OH})_6$ ) and this isomorphous series can host large divalent cations such as Ca, Ba, Sr, Pb, trivalent ions such as Al, Fe, Sc, Y and the REE, and tetrahedrally coordinated groups such as  $\text{PO}_4$ ,  $\text{AsO}_4$ ,  $\text{SO}_4$ . Of these, the phosphates form a highly insoluble family of minerals that are quite stable in the weathering environment. Banfield and Eggleton (1989) and Taunton *et al* (1999, 2000) have shown the importance of rare-earth phosphates in controlling the phosphorous availability in a weathered granite profile.

## Poorly crystalline minerals

Amorphous minerals were originally so-called because they lacked a crystal shape. The term has become extended to minerals that are not detectable by methods based on crystallinity such as X-ray diffraction. Techniques such as scanning and transmission electron microscopy have shown that many 'amorphous' minerals do have well-defined morphology. They may be composed of very small, or rather imperfect crystals, such as ferrihydrite has, or they may have curved morphology, such as allophane. Both kinds of minerals yield X-ray diffraction patterns with broad, indistinct maxima and are better termed 'poorly diffracting'. Their presence has been long known to soil scientists (Gieseking, 1975), and routinely estimated by chemical extractions. Examination of regolith minerals by transmission electron microscopy and differential X-ray diffraction has allowed mineralogical characterisation of these materials, and their importance in regolith mineralogy and geochemistry is gradually being recognised (Tilley & Eggleton, 1995, 1996), Singh & Gilkes (1995).

Allophane is a hydrated aluminosilicate, formed as spheres about 5 nm across. It does not have a single composition, but ranges from  $\text{Al}_2\text{O}_3 \cdot \text{SiO}_2$  to  $\text{Al}_2\text{O}_3 \cdot 2\text{SiO}_2$ . It is difficult to recognize because it gives very poor X-ray reflections (broad bands centred at about 1.5 nm, 0.34 nm, and 0.25 nm). It is most common in soils derived from volcanic ash, and so is particularly abundant in Japan and New Zealand.

Imogolite is a thread-like mineral of composition about  $\text{Al}_2\text{O}_3 \cdot \text{SiO}_2 \cdot 2.5\text{H}_2\text{O}$ , abundant in volcanic derived soils. The threads are bundles of 2 nm diameter tubes. At pH 7, both allophane and imogolite have CECs of the order of 200-300 meq/kg.

### Hisingerite

Generally thought to be a rare amorphous alteration product of iron sulfides, carbonates and silicates, hisingerite has been shown to be a ferric form of spherical halloysite (Eggleton & Tilley 1998). Many specimens of hisingerite have come from mines at depths below the level normally regarded as within the regolith, though the mineral itself is the product of oxidation and hydration. Hisingerite has a formula close to  $\text{Fe}_2\text{Si}_2\text{O}_5(\text{OH})_4$ , and other than the substitution of Mn, Mg and a small amount of Al for Fe, nothing is known about its chemistry. Its fabric of concentric 1:1 layers forming spheres about 1.4 nm in diameter gives it a high surface area and a high adsorption potential.

### Aluminium-iron oxyhydroxides

Pisolitic bauxites and laterites commonly yield very weak X-ray diffraction patterns. Tilley & Eggleton (1996) and Singh & Gilkes (1995) have shown that these near surface regolith materials may contain a high percentage of ultra-fine-grained minerals occurring as crystals with diameter less than 10 nm, including  $\chi$ - and  $\epsilon$ -alumina, maghemite, akdaleite ( $5\text{Al}_2\text{O}_3 \cdot \text{H}_2\text{O}$ ) and very fine goethite. These minerals have extremely high surface areas ( $\sim 500 \text{ m}^2/\text{g}$ ). Thus, they may provide important sinks for adsorbed trace metals. No work has been done on their geochemistry.

## Resistate minerals

Important components of the residual weathering products are the mineral group commonly called ‘resistates’ or ‘resistant minerals’. These are minerals not significantly affected by the weathering process. Above, quartz has been considered in some detail, and this is probably the most common resistate under most weathering conditions, but it will not be discussed again here.

Other common resistates include the minerals that occur as trace components in parent rock, but which are concentrated by depletion during the process of weathering. The most common are zircon, rutile, ilmenite, magnetite (and other spinels), garnet, tourmaline, and monazite. Much rarer resistates include cassiterite, corundum, gold and diamond. Resistates have been used as indicators of the degree or extent of weathering, particularly zircon and Ti-resistates (see Taylor and Eggleton 2001 for a discussion).

Additionally most of these resistate minerals are denser than quartz and the majority of regolith minerals, and are collectively known as “heavy minerals”. Because they are denser, they tend to concentrate as lenses and beds as they are eroded, transported, winnowed and deposited. They form a significant ore in many unconsolidated sedimentary sequences.

---

## MINERAL WEATHERING

---

How a primary mineral responds to the weathering environment depends significantly on its ferrous iron content and its solubility at pH around 6: the pH of most soil and regolith waters. The iron in ferrous minerals is quickly oxidized as soon as they reach the oxidizing weathering front. In almost every instance, oxidation of the iron strongly affects the mineral structure, creating nanometric channels and cavities into which water penetrates, accelerating dissolution.

Iron-free minerals dissolve in water very approximately in order of their content of the more soluble elements Ca and Mg. Thus olivines and pyroxenes weather faster than feldspars, and anorthite weathers more readily than albite. Table 6.2 lists the common minerals in order of their solubility on a logarithmic scale with quartz set at 10 and glass at 1. The order is based on experimental results and on field observations, and is only presented as a guide. In different situations, and depending on the mineral’s actual composition and internal integrity (determined by the density of twin planes, dislocations, inclusions, fractures) the susceptibility to weathering may be different. The list includes the Fe-bearing minerals biotite, augite, hornblende and olivine, and their position at the more soluble end of the list is at least partly because of the oxidation of ferrous iron.

**Table 6.2:** Relative mineral solubilities (base-10 logarithmic scale, large numbers = least soluble). Order established from experimental results in the literature (White & Brantley 1995), modified by field observations.

gibbsite	11
beidellite	10
quartz	10
kaolinite	10
microcline	9
muscovite	9
sanidine	7
albite	7
biotite	7
augite	7
oligoclase	6
andesine	5
hornblende	4
diopside	4
bytownite	4
anorthite	3
forsterite	2
glass	1

Wilson (2004) and Taylor and Eggleton (2001) give extensive descriptions of mineral weathering.

## 2. THE “ENVIRONMENT” IN MINERALOGY

---

The type of mineral and its physical and chemical properties are used as time keepers (absolute ages), as markers of specific geological events (impacts), as biomarkers (magnetite, calcite), and as indicators of particular physiochemical conditions (acidic, icehouse, greenhouse) – past and present. The question often asked in identifying and studying near surface mineralogy (minerals that dominate the regolith), is what is their significance to the environment? Can we interpret the environment conditions prevailing during their formation (pH, Eh, temperature etc) and therefore use them as indicators of current environmental conditions or to predict or monitor future environmental problems? Furthermore, if we know particular physico-chemical property of a mineral, can we use it to minimize or eliminate specific environmental problems (mimic their natural behaviour)?

The mineralogical diversity in the near surface is being used to infer paleo and recent undisturbed or pure environments and to study, monitor and remediate important contaminated environmental issues. Central to any study of mineral based investigation and monitoring of environmental problem is the accurate identification (often including identifying an aspect of the mineral such as disorder, compositional variation and quantification) of the mineral or minerals associated or linked with the problem and knowledge of their likely formative conditions.

Particular areas where minerals are playing important roles either as markers of specific environment or as indicators of spatial and temporal extents of environmental change produced by human activity are: metalliferous and minewastes, acid sulfate soils and dusts arising from natural, mining and urban activities. Besides these human induced problems, near surface mineralogy has been used to infer particular aspects of the natural environment. Although ‘environment’ in geosciences is mostly associated with geochemistry, it is worth noting a quote by a geochemist: “when attempting to interpret most forms of geochemical data, three rules should always be applied: mineralogy, mineralogy, mineralogy”. As a link to geochemical information, mineralogy is critical to the source of the ions, the mechanism by which the ions are produced and ultimately their resting place.

### 1 Minerals as indicators of specific environment conditions (chemical and physical)

The environment parameters that can be inferred from the presence of a specific mineral are

- pH
- Redox conditions
- Presence of specific anions
- Drainage with landscape position and
- Temperature & climo-sequences
- Transported versus *in situ* regolith

Minerals can be used as indicators of specific environmental parameters on a variety of scales ranging from the micro (thin section) to macro (hand specimen) to profile (vertical differences) to landscape (hydrology, topography) to even continental scale. Much of this summary of minerals and their environmental processes and significance, borrows from Fitzpatrick (1988), Eggleton & Taylor (2001) and Bingham et al (2002).

### 1.1. pH – Acid or Alkaline with dominant anion

The pH is the master variable and pH of surface and groundwaters (shallow and deep) have a direct effect on the precipitation and stability or persistence of secondary minerals in the regolith. Often, the corollary is also true: presence of specific mineral or mineral assemblage is an indicator of pH and dominant anion present in the present or past environment. The main limitation in this inference is that the minerals indicative of the pH may dissolve or transform to another mineral on change of the pH conditions and thereby not be distinctive markers of previous pH's. It is possible to also add an extra variable in the form of dominant anion in the surrounding environment (vadose and groundwaters) to pH and infer both these variables from the minerals present.

Figure 2.1 provides a guide to ranges of pH (acid, neutral or alkaline) and dominant anion (Cl, SO<sub>4</sub>, CO<sub>3</sub>, Si-OH) from the minerals found in the regolith environment or sedimentary rocks. For example, in acid conditions such as those found in acid sulfate soils (AAS) or acid mine drainages (AMD) where the weathering of sulphides and oxidation of iron and sulphur species generates acid conditions, results in the dominance of iron-sulfate minerals such as jarosite and alunite. In addition, common minerals in the regolith - quartz and kaolinite - dissolve due to the low pH releasing Si and Al, which combine in the acid environment to form Al-Si precipitates.

Anion	Chloride	Halite		
	Sulfate	Jarosite	Gypsum	
		Alunite	Bloedite	
	Carbonate		Calcite	Magnesite
Silicate	Silica	Kaolin	Feldspar	
		Smectite		
		Acid	Neutral	Alkaline
		<b>pH</b>		

**Figure 2.1:** Typical minerals indicative of pH ranges with Presence of dominant anion.

At the wide range of neutral pH, presence of sulfate species will result in the formation of a range of sulfate minerals such as gypsum (CaSO<sub>4</sub>.H<sub>2</sub>O), bloedite (Na<sub>2</sub>Mg(SO<sub>4</sub>)<sub>2</sub>.4H<sub>2</sub>O), thenardite (Na<sub>2</sub>SO<sub>4</sub>) and barite (BaSO<sub>4</sub>). Most of these sulfates are indicative of evaporitic environments with a vertical or lateral close by source of sulfate, such as weathering of pyrite. The sulfate released from weathering of pyrite migrates and combines with Ca, Na and Ba to form the above minerals at varying stages of drying or evaporation. If chloride is the major anion, then halite precipitates which is ubiquitous in saline environments, with pH varying from mildly acidic to neutral.

The other end of the pH scale, magnesite (MgCO<sub>3</sub>) and calcite (CaCO<sub>3</sub>) are likely indicators of alkaline solutions having high carbonate ion content such as groundwaters found surrounding weathered ultramafic rocks.

## 1.2 Redox Conditions

Specific minerals in the regolith are indicators of redox state of the environment under which they formed. They form and persist in a restricted Eh-pH range of oxidation potential. Figure 2.2 illustrates the minerals with their approximate Eh-pH ranges. Pyrite (black) and mono-sulphides (“black ooze”) are indicators of reducing environments, where sulphur reducing bacteria catalyze oxidation of organic matter and link it to reduction of  $\text{Fe}^{3+}$ . However, if high  $\text{CO}_3^{2-}$  ion is present in pore waters as is the case in alkaline reducing environments, siderite ( $\text{FeCO}_3$ ) will be the dominant mineral present. Oxidizing acid conditions favour the formation and persistence of iron-sulfate minerals -jarosite and schwertmannite. Jarosite is stable over a longer period while schwertmannite is metastable and transforms to goethite with time (months to a year). Therefore, the presence of jarosite and schwertmannite is used as an indicator of acid conditions ( $\text{pH} < 4$ ) and this pH – mineral stability linkage has been used to spatially and temporally map surface acid conditions via hyperspectral remote sensing. Goethite and kaolinite are indicative of wide oxidizing pH range from mildly acidic to neutral to alkaline conditions.

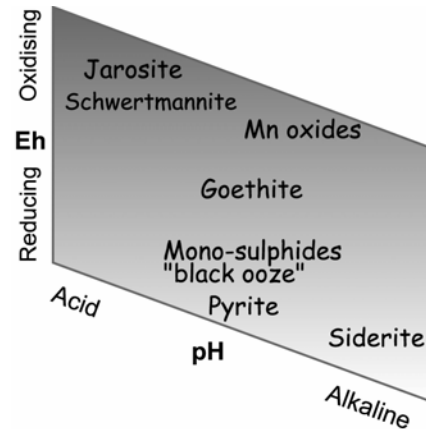


**Figure 2.2:** Common minerals in the regolith indicative of range of redox conditions (modified after Taylor & Eggleton 2001).

The chemistry of individual minerals can also provide information on pH conditions during time of formation. The presence of Al-substituted goethite (15-30% Al) suggests acid conditions because Al goes into solution phase only at low pH's. Al-poor goethite will imply neutral pH.

## 1.3 Drainage or water activity

The rate of flow of groundwater vertically and laterally (landscape) through a profile, sediments or sedimentary rock can affect the nature of the minerals that form, and the presence of resulting minerals can be used as indicators of the rate of flow of water or in thermodynamic terms – the water activity. The inference of drainage and organic matter activity can be extended from a landscape and profile scale to micro scales.

Slow rate of water movement through a regolith profile allows the water to become saturated with the ionic components being released due to the weathering of minerals, and therefore potentially achieve equilibrium with specific secondary minerals. In a vertical profile, the weathering of a mafic rock results in the release of Ca, Mg, Si, Fe, Al to varying degrees due to the weathering of primary minerals and slow water flow or impeded drainage can result in high ionic concentrations of all or some of the released components in the groundwater, leading to the formation of **calcite-smectite-goethite** assemblage. A similar profile under rapid flow or free drainage conditions is likely to attain saturation in Al, Si and Fe resulting in the **kaolinite-goethite and/or hematite** association. However, these assemblages cannot unambiguously be used to infer profile drainage, because local or regional climatic conditions can play as important a role. Arid or semi-arid conditions can result in little water passing through the profile giving the same mineralogical assemblage as “impeded” drainage.

Iron oxides and hydroxides provide a good indicator of water activity and organic matter. The red hematite is favoured over brown goethite in low water activity and low organic matter environments and therefore free flowing profiles and macro and micro sites with lower water

saturation will show dominance of red hematite due to low water activity. In contrast, slow draining profiles or macro or micro regions having longer saturation will show brown or yellow (kaolinite + goethite) areas.

In many deep weathering profiles, red-grey mottles dominated by hematite + kaolinite assemblage overly yellow-brown with grey mottles dominated by goethite + kaolinite ( $\pm$  smectite and illite). The vertical mineralogical sequence points to the varying water saturation regime. Coarse mottled zones are considered to represent the limits of fluctuating water tables in highly weathered regolith profiles. After the wet season, the water table recedes quicker near the top of the mottled zone, therefore the rapid drying and longer period of dryness favours rapid oxidation of  $\text{Fe}^{2+}$  resulting in the formation of reddish hematite and ferrihydrite. Conversely, the longer duration of saturation lower down in the profile favours yellow-brown goethite with possible illite and smectite. There are many profiles removed from current water table that show these mottled features, and paleo water table conditions can be interpreted from these features.

On a macro scale, periodic saturation of parts of the profile can result in dissolution of minerals at specific sites and precipitation of released ions as minerals at another site, according to reduction-oxidation conditions within the unit or micro site. The saturation and associated redox conditions mainly affect minerals dominated by redox sensitive major elements, namely iron and manganese oxides and hydroxides, and the distribution of these minerals can be used as sign of saturation conditions.

Many regolith units (and micro sites), especially the subsoil units and ferricretes, show red

or brown or yellow mottles in grey matrix, or grey zones in a red-brown matrix. These mottled features are referred to as redoximorphic features and are essentially formed in response to redox conditions within the particular unit. Many of these features are formed along pores which could be biological in origin (fauna and flora) and some form in matrix. A common redoximorphic feature is the formation of a grey narrow zone along pore which grades into a yellow zone and then into a matrix with red masses (Figure 2.3, top). The grey coloured zone is referred to as redoximorphic depletions and any red-brown mottled masses or zones are referred to as redoximorphic accumulations. Their formative processes are considered to be the partial saturation of the specific regolith unit, where saturation occurs along the macro and micro voids. If organic matter is present (roots), oxidation of organic matter results in the formation of reducing conditions leading to the reductive dissolution of Fe-oxides/hydroxides along the pore. The  $\text{Fe(II)}$  released, migrates away from the pores into the oxidized matrix and depending on the saturation conditions oxidizes and forms either hematite (drier parts) or

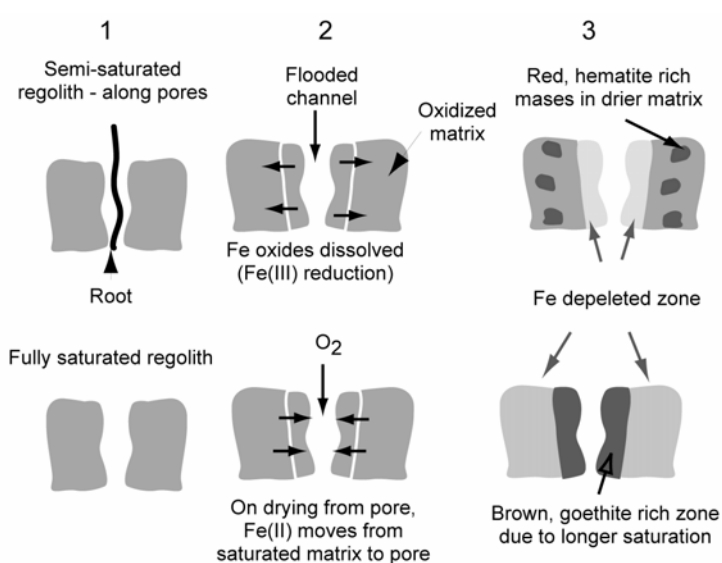


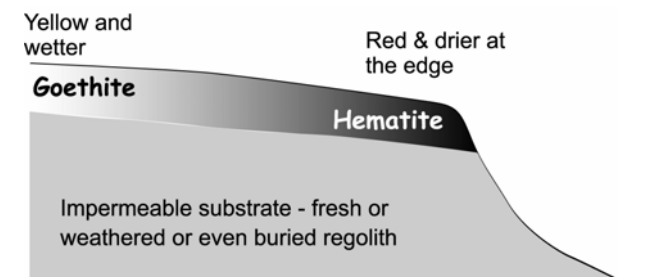
**Figure 2.3** Development sequence of redoximorphic features in periodically saturated regolith unit (above) and full saturated unit (below). The two saturation conditions result in different iron oxide/hydroxide accumulations within matrix (above) and along pores (below). Concepts are from Vepraskas (1992).

goethite (yellow). Generally, a narrow zone of goethite (yellow) is adjacent to the grey depleted zone and grades into red matrix or masses. In regolith units fully saturated for a significant period (waterlogged surface and subsoil units) and bearing organic matter, reducing conditions can occur through the matrix thereby reducing part of the Fe oxides in the matrix with significant amounts of Fe(II) in saturated unit (figure 3, bottom). Subsequent drying of the unit results in rapid influx of oxygen along the larger voids and slower influx through the matrix. The oxygen gradient developed from matrix to pore, leads to migration of Fe(II) from the matrix to the pores where the saturation conditions along matrix and slow Fe(II) oxidation favours brown-yellow goethite.

Brown-yellow pore linings with pale yellow to grey matrix are therefore indicative of regolith units saturated for a longer period of time. In contrast, grey redox depletion zones along pores and voids with red matrix accumulations, are indicative of regolith units periodically saturated.

#### 1.4 Landscape or Catenary Position

Regolith minerals can be used as indicators of past landscape position, but interpretation is a combination of drainage and paleo-landscape evolution or substrate type. The iron oxides, especially hematite and goethite, having their genetic pathways controlled significantly by water activity or saturation, provide the best indicators of drainage linked to catenary position.



In general, on concave slopes with incised edges, red, hematite edges grade inwards to brown-yellow goethite dominant soils (figure 2.4A).

**Figure 2.4A:** Hematite dominates the incised edges because of free drainage and existence of drier conditions, while goethite dominates inwards due to presence of wetter conditions.

This sequence is interpreted as drier or freely draining edges favour hematite while inwards, slower drainage favours goethite.

On convex slopes without incision, hill crests have better drainage while valley bottoms are poorly drained and accordingly the drier hill crests will be richer in hematite and therefore have redder soils, while the valley bottom soils are dominated by goethite and therefore are coloured brown-yellow (figure 2.4B).

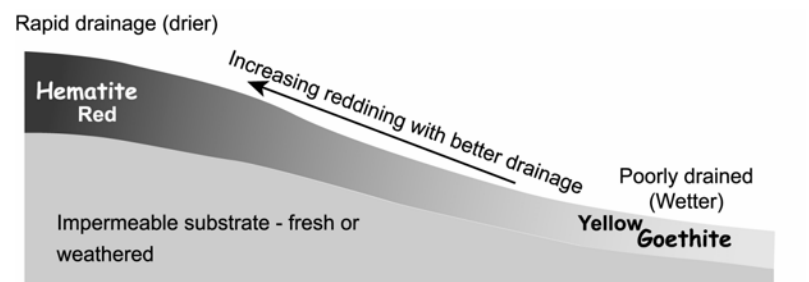


**Figure 2.4B:** Hematite dominates on better drained hill tops as compared to poorly drained, yellow valleys.

However, drainage can be impeded due to the nature of the underlying substrate and are not a function of elevated recharge areas (hill tops) versus lower discharge areas (valleys floors) or incised edges, but of drier versus wetter. If impermeable substrates are closer to the surface, infiltration is slow and upper regolith is wetter for a longer duration leading to yellow-brown goethite e at higher areas as compared to the lower areas (figure 2.4C).

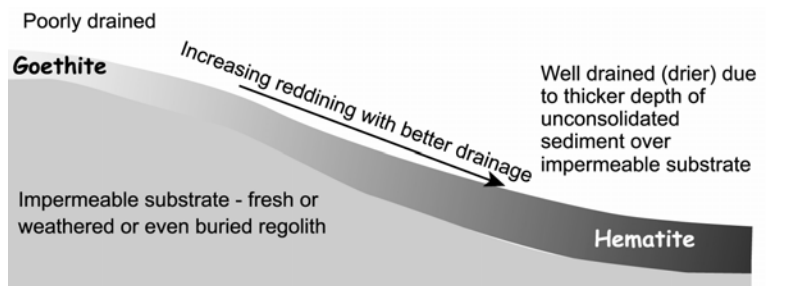


**Figure 2.4C:** Variation in thickness of unconsolidated sediment can result in yellow soils (goethite) forming in higher parts of landscape due to poor drainage while lower parts due to thicker sediment form red (hematite) soils.

In arid and semi-arid regions, lateral, landscape changes in soil and duricrust mineralogy are potential indicators of pH changes along the landscape. Groundwater in contact with weathered silicate rocks when it seeps to the surface is generally acidic (especially in arid settings). Along the groundwater water flow path from higher areas to valley floors, the waters start acidic and gradually become alkaline and increase their total dissolved solids (TDS) or salinity. This pH-TDS evolution of shallow groundwaters along weathered landforms is reflected in the precipitation of different minerals and their main duricrust types (figure 2.4D): closer to the tops is silcrete or microcrystalline quartz and opal A; further down is calcrete cemented by calcite and finally dolomite in the valley floors signifying alkaline pH. Therefore, other factors remaining same, a catenary change in silica-carbonate mineralogy of the regolith is a good indicator of paleo or present pH change.

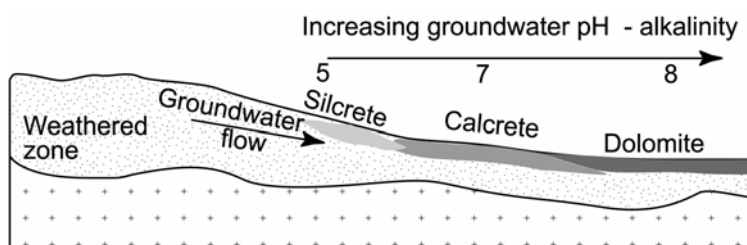


**Figure 2.4D:** Variation in regolith mineralogy (precipitates) with landscape position and pH change. Modified from Carlisle (1983)

### 1.5 Temperature & Climate

Generally, there are few reliable mineral indicators of current and past temperatures. The main indicators are the iron oxides and hydroxides. Maghemite, commonly found in glaucofanites (nodules, pisolites, mottles) within soil and on the surface as ferruginous lag, is a likely indicator of forest-fires. Iron oxides (goethite, hematite) present in soil matrix and in glaucofanites when heated to temperatures above 300°C in the presence of organic matter (top soil organics), transform to maghemite. Therefore, the presence of maghemite is used as an indicator of forest fires. However, maghemite also forms via the oxidation of primary magnetite and the gradual transformation of lepidocrocite in slowly oxidizing conditions.

On a continental scale, hematite shows dominance over goethite in the warmer, humid northern parts of southern hemisphere continents as compared to the temperate, but cooler south, where goethite predominates. Although other factors affect hematite versus goethite formation (water activity, organic matter), general observations suggest that warmer climates are favourable for hematite formation and preservation. Other studies indicate an altitude-climate relationship between hematite and goethite. The yellow soils dominant in goethite occur under cooler wet climates at higher altitudes, while the redder hematite dominates in lower altitudes where warmer temperatures and drier conditions prevail.

## **1.6 Transported vs *in situ* regolith**

Regolith is broadly classified into that produced as a result of weathering of the basement rocks (*in situ*) and that produced due to the transportation processes, which is essence is surficial sediments. Commonly, the weathering overprint on surficial sediments precludes definite identification of *in situ* from transported regolith, a boundary which is critical in mineral exploration programs.

One method proposed to identify the *in situ* – transported boundary is to measure the “crystallinity” of kaolinite throughout the regolith profile. Kaolinite is the most common layer silicate in the regolith and occurs in most parts of the regolith profiles and therefore lends itself as a good marker to estimate specific environment parameters. Well “crystalline” kaolinite as estimated via  $hk0$  d-values from XRD or via the depth of separation in the 2160 and 2177 nm doublet absorption features in reflectance spectra is suggested to be an indicator of *in situ* regolith because the slow formation allows it to crystallize without many defects. In contrast, poorly “crystalline” kaolinite commonly occurs in regolith materials that have a transport history with suggestions that sedimentary transport creates defects in the kaolinite. Using the reflectance spectra of kaolinite from different parts of a profile, it is easy to work out the boundary between transported and *in situ* regolith. However, kaolinite “crystallinity” is not always shown to be related to sedimentary processes.

## 2 Minerals in Mine Environments

The mine environment has several artificially created landform elements, all of which play a role in affecting the surrounding environments. Figure 2.5 shows a typical open cut mine and its associated artificial landscape elements mainly waste heaps, waste rock piles, tailings dams and access roads for heavy vehicles. Associated with waste piles/heaps, tailings dams and abandoned open cut mines are the major short and long term environmental issues that have mineralogy as the source and tracer.



**Figure 2.5:** An open cut mine with its surrounding artificial landform elements. The waste rock piles have a streak of brown-greenish-grey material (jarosite, schwertmannite) coming off them and sometimes ending in blue materials (Cu-sulfates).

The mining process, by its very nature of extracting and processing minerals, results in creating mineralogical wastes and associated environmental issues. The main environmental impacts of mining include the mineralogical and geochemical evolution of rocks exposed in open cut mines, in waste rock and mill tailings that result in the oxidation of sulphide minerals consequently producing acid conditions in surface soils and surface and groundwaters and heavy metal pollution. Another, less studied environmental impact from mining is the effect of mineral dusts created during excavating, crushing and metal processing on human health and ecology.

### 2.1 Sulphide oxidation and acid generation

Waste piles from most metal bearing mines contain a suite of primary minerals with sulphides being common. The weathering of sulphides in the waste piles is the primary issue of environmental concern, but natural weathering and geochemical evolution of a mine waste pile either attenuates the environmental impacts or increases it. A schematic view of geochemical-mineralogical evolution of a waste pile is shown in figure 2.6 where the weathering of sulphides, subsequent generation of acid conditions, the potential buffering from other minerals and the formation of secondary minerals is shown. From an environmental perspective, it is important to evaluate the types of sulphides and other primary minerals, their content,

buffering reactions and the spread of acid conditions away from the point source (waste piles). Mineralogy is central to achieving all these and the processes are summarized below.

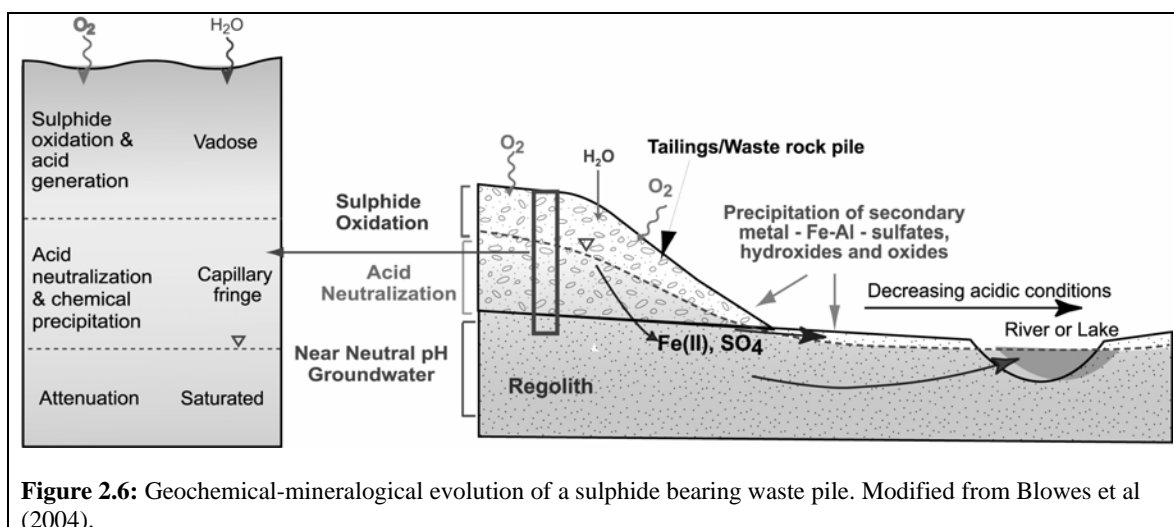
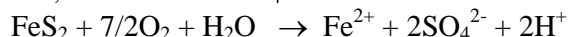


**Figure 2.6:** Geochemical-mineralogical evolution of a sulphide bearing waste pile. Modified from Blowes et al (2004).

The main sulphide minerals that are oxidized in mine wastes and open pits are pyrite and pyrrhotite, but other sulphides are also be oxidized and release ions to the environment. The entire pyrite (and other sulphide) oxidation process is complex involving chemical, electrochemical and biological reactions and is dependant on several factors such as oxygen supply, mineral grain size, pH, presence or absence of microorganisms.

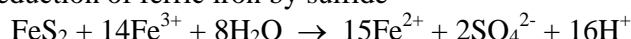
The overall pyrite oxidation reaction by atmospheric oxygen results in one mole of pyrite producing one mole of  $\text{Fe}^{2+}$ , two moles of  $\text{SO}_4^{2-}$  and two moles of  $\text{H}^+$  according to the reaction



However, the rate of oxidation and dissolution of sulphides is dependant on the availability of oxidants at the weathering front or the sulphide mineral surface. The common oxidants available around sulphide ore bodies are  $\text{Fe}^{3+}$  and  $\text{O}_2$ , but oxygen is considered to be a less effective oxidant than ferric iron. The main pathway for sulphide dissolution incorporates ferrous iron oxidation via oxygen according to the reaction



This is followed by reduction of ferric iron by sulfide



For the above reactions, the rate limiting step is considered to be the ferrous iron oxidation by oxygen, which is slow at low pH (Nordstrom & Southam 1997). However, specific microorganisms that enzymatically oxidize iron and thereby increase the amount of  $\text{Fe}^{3+}$  to attack the sulphide surface will increase sulphide mineral dissolution kinetics (Nordstrom & Southam 1997). The mechanism of sulphide dissolution via enzymatic oxidation on the sulphide surface with direct microbial contact is still debated, but results do indicate preferential colonization of sulphides by specific microbes rather than other minerals (Baker & Banfield 2003). Studies in natural environments indicate microbial induced rate for Fe (II) released from sulphide weathering accounting for 75% of the total Fe(II) release.

## 2.2 Mineralogical indicators of acid conditions – secondary minerals

The  $\text{Fe}^{2+}$  and  $\text{SO}_4^{2-}$  released due to sulphide oxidation and subsequently oxidized in mine wastes and open pits results in the formation of single or an assemblage of *secondary* minerals, mainly iron oxihydroxides and iron-sulfates, such as **ferrihydrite** ( $\text{Fe}_5\text{HO}_8.4\text{H}_2\text{O}$ ), **schwertmannite** ( $\text{Fe}_8\text{O}_8(\text{OH})_6\text{SO}_4$ ), **jarosite** ( $\text{KFe}_3(\text{SO}_4)_2(\text{OH})_6$ ) and **gypsum** ( $\text{CaSO}_4.2\text{H}_2\text{O}$ ).

The presence of these minerals can be used as indicators to near surface acidic conditions. Studies indicate that schwertmannite and jarosite appear to be the primary iron-sulfate minerals that form due to  $\text{Fe}^{2+}$  oxidation and hydrolysis in acid waters containing sulfate ions in a pH range of 2 – 4.5, while ferrihydrite and goethite appear to be products of  $\text{Fe}^{2+}$  oxidation at slightly higher pH's of 4.5-6 (Swayze 2004). Schwertmannite is unstable and transforms to goethite at low pH over a period of months to a year. Therefore, presence of schwertmannite and jarosite is used as indicator of ongoing acid or acute acid conditions and identification of these minerals provide an indirect method to firstly recognize acid conditions, and secondly, spatially map acid conditions ( $\text{pH} < 4$ ) around mine environments. The link between specific minerals and acidic conditions, and the easy identification of these minerals via reflectance spectroscopy, is being used to spatially and temporally map acid conditions via hyperspectral remote sensing (Swayze 2004).

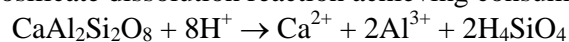
### 2.3 Acid Neutralizing Reactions and Minerals

Although sulphide minerals (mainly pyrite) cause the acidification of surface and shallow groundwaters and regolith, the weathering of other minerals helps to minimize the acidity, and therefore it is important to establish and quantify the mineralogy of not only sulphide ore but of gangue. Waters moving through mine-waste piles and open cut mines react with sulphides and create acid waters with the likely formation of particular suite of soluble and less soluble secondary minerals (jarosite, schwertmannite, gypsum, ferrihydrite). The acid waters are discharged into adjacent near-surface waters or into the shallow groundwater, but chemical reactions with gangue minerals result in the gradual increase in the pore water pH. Gangue mineralogy plays a critical role in providing a natural buffer to the acid producing reactions of sulphide oxidation. The main pH buffering reactions in mine environments are the dissolution of carbonate minerals, hydroxide minerals and aluminosilicate minerals. Carbonate mineral dissolution at low pH is a sink for  $\text{H}^+$  according to



Dissolution of carbonate minerals results in raising the pH of surface and pore waters and releasing Ca, Mg, Fe and Mn to the solution. Carbonates are also the most soluble primary minerals and therefore dissolve first when pH drops due to sulphide oxidation.

In a vertical sequence of mine waste rocks composed of sulphides and gangue (carbonate, aluminosilicates, oxides and hydroxides), sulphide oxidation commences at the top due to the influx of oxygen and oxygenated waters resulting in acid conditions (figure 6). Dissolution of carbonate minerals near the top in response to the onset of acid conditions buffers the pH. Cations released from the dissolution of sulphides and carbonates result in the formation of soluble iron-sulfates (copiapite, schwertmannite) and less soluble iron-sulfates (jarosite, gypsum) and secondary hydroxides such as gibbsite, goethite and ferrihydrite in the wastes and along the water flow directions. In the sequence of solubility products of primary and secondary minerals and kinetic factors in the mine wastes, these secondary hydroxides and soluble sulfates tend to dissolve next thereby buffering the pH. In combination with hydroxide dissolution, aluminosilicates minerals such as layer silicates (chlorite, biotite, muscovite), feldspars, biotite, pyroxenes and amphiboles also dissolve resulting in acid-neutralization reactions, but their dissolution is not rapid (slow kinetics) as in the case of carbonates and hydroxides. The aluminosilicate dissolution reaction achieving consumption of  $\text{H}^+$  is



The reaction sequence of sulphide oxidation, acid production and subsequent acid-neutralization via primary and secondary mineral dissolution in mine wastes and tailings are used to predict (via laboratory tests) the acid producing and acid-neutralization capacity of the

materials. Both **static** and **kinetic** tests are used on materials from mine sites to predict whether the sample, based on its mineralogy, will be acid producing on weathering, and if so, what will be its acid-neutralizing capacity.

These tests are known as **acid-base account (ABA)**, which involves determining acid-producing potential (AP) of a sample (mainly oxidation of sulphides), and determination of base (weathering of carbonates, hydroxides and aluminosilicates) that is likely to be released or neutralization potential (NP). The result is expressed as Net Neutralization Potential (NNP) = NP – AP. If NP > AP, indicates sample is likely to be acid-neutralizing while NP < AP indicates sample likely to be acid generating. Underpinning these tests is the mineral type and quantity in the mine wastes, and therefore it is important to quantify the mineralogy and its reactivity.

The static and kinetic tests have a mineralogical basis because they are measuring mineralogical weathering reactions. A summary of static and kinetic tests is:

- Static Tests (Sobek Test, NAG test, Lawrence test). In this test, the sample is ground and total S measured to provide an estimate of acid producing potential (AP). The sample is then ground and reacted with 25% HCl to estimate the “fizz” rating which provides neutralizing potential (NP).
- Kinetic Tests. These tests simulate field flow conditions in the lab (humidity cells, columns) to estimate rates of weathering in addition to S content. The samples are exposed to repeated weathering cycles by reacting the samples with oxygenated water followed by the measurement of amount of metals leached. The amount of metal released with time is used to estimate the rate at which “waste rock” minerals react (chemically weather) and are therefore able to buffer the AP with time.

## 2.4 Metal Sorption

The secondary minerals formed as a result of oxidation of iron and sulphur in mine environments, as well as those found in the regolith, especially iron and manganese oxides and hydroxides and clay layer silicates (smectite, kaolinite), are mainly fine grained with large surface areas and hydrolysable surfaces. Both these mineral factors make most regolith minerals good sorbers of metals from solution, especially the Fe and Mn oxides and hydroxides.

The secondary mineral crystals bear surface functional groups (unsatisfied bonds) and are amphoteric and therefore act as both an acid and a base. In presence of water, hydrogen ( $H^+$ ) and hydroxyl ( $OH^-$ ) ions are attracted to the surface atoms and form surface complexes with the solid. The type of total charge present on the surface, either negative or positive, will depend on the pH (supply of  $H^+$  or  $OH^-$ ). The pH where the total positive charges equal the total negative charges on a mineral surface is known as point of zero charge (PZC). For most oxides and hydroxides of Fe and Mn found in the regolith, PZC is in pH range of 7-9. The sorption of metals onto oxides and hydroxides is strongly dependant on solution pH, with cation (Zn, Pb, Cu, Ni) adsorption increasing with an increase in pH. The opposite is true for oxyanions ( $AsO_3^{3-}$ ,  $CrO_4^{2-}$ ,  $MoO_4^{2-}$ ) where oxyanion sorption decreases with increasing pH. The reason for this the surface competition based on solution pH and PZC of the mineral. At lower solution pH values (more  $H^+$ ) than the PZC of the mineral, increasing number of surface sites become positively charged (extra  $H^+$ ), thereby causing the solid to adsorb oxyanions. At higher solution pH values, the solid surface sites become negatively charged, and adsorb cations preferentially.

On a molecular level, adsorption can be further divided into:

- **Outer-sphere complex** - where a water molecule is present between the ion or molecule that it binds to the surface oxygens of the mineral. In general, outer sphere complexes involve electrostatic binding and are thus less stable than inner-sphere complexes.  
 $\underline{\text{S}}\text{OH} + \text{M}^{2+} = \underline{\text{S}}\text{OHM}^{2+}$  ( $\underline{\text{S}}$  - is metal atom at surface of solid,  $\text{M}^{2+}$  is metal atom in solution)
- **Inner-sphere complex** – where no water molecule is present between the ion that binds to the solid surface i.e. the ion binds (generally through covalent bonds) directly to the solid surface without an intervening molecule.  
 $\underline{\text{S}}\text{-OH} + \text{M}^{2+} = \underline{\text{S}}\text{-OM}^+ + \text{H}^+$
- **Diffuse swarms** – are weakly associated with the mineral surface possibly through numerous layers of water molecules. A newer variety that is close to diffuse swarms and is being researched is known as clusters.

Studies of iron hydroxides from acid mine drainages show a high concentration of metals (Zn, As, Pb) associated with ferrihydrite and goethite. Therefore, these minerals act as natural retardants or hosts of metal species released due to the weathering of sulphides in the waste and tailings.

### 3 Health Effects of Mineral Dusts

Although people are exposed to a myriad of mineral dusts, only a select number of natural and anthropogenic minerals are recognized to impact adversely on human health. Most of these dust materials are either individual or multiple mineral assemblages and the common ones known to affect health are:

- Mineral dusts composed of asbestos or fibrous minerals, silica, coal, clay and iron minerals, cement etc., released into air due to mining, construction, demolition or natural degradation of household products.
- Volcanic ash and gases
- Soil and dusts containing heavy metals, organic contaminants or pathogens released due to mining activities (mineral processing and smelting) or naturally blown dust

**Table 1:** Minerals and materials with known cases to affect health.

<b>Mineral</b>	<b>Definition or types</b>
Asbestos	Highly fibrous silicate minerals that separate into long, thin, strong fibers and useful for their insulating, heat and chemical resistance. Technically restricted to chrysotile (serpentine) and actinolite, tremolite, anthophyllite, amosite and crocidolite (amphiboles). Fibers having length:width ratio of 10:1
Asbestiform	Other minerals resembling asbestos in habit
Crystalline Silica	Microcrystalline quartz and polymorphs – cristobalite and tridymite
Coal	Organic rich matter with variable amounts of accessory minerals such as sulfides, carbonates, clay minerals, crystalline silica and other silicates.
Other Silicates	Talc, pyrophyllite, kaolinite, vermiculite and zeolite (erionite)
Nanoparticles	Carbon nanotubes

#### 3.1 Diseases arising from minerals

Several diseases have been linked to inhalation (and sometimes ingestion) of mineral dusts. The diseases or health problems arising from acute or chronic exposure to mineral dusts are:

- Asbestosis: progressive lung fibrosis that results in shortness of breath and eventual death by lung or heart failure
- Lung Cancer: Caused mainly by exposure to high levels of chrysotile, crocidolite and amosite, with a long latency period (10-20 years). Similar to cancer caused from excessive smoking.
- Mesothelioma: Cancer caused due to lining of the lung cavity. Caused mainly by exposure to crocidolite.
- Pleural effusion: Accumulation of fluid between the layers of the membrane that line the lungs.
- Silicosis: Lung disease caused by inhalation of silica dust over long resulting in the inflammation and scarring of lung tissue. Three types can be identified; *chronic silicosis*, results with the development of inflammation and scarring due to exposure to low amounts of silica over long periods (> 20 years); *accelerated silicosis*, occurs from exposure to larger amounts of silica over shorter durations (5-15 years), and *acute silicosis* results from short term exposure to high amounts of silica which leads to lung inflammation resulting in acute shortness of breath and low blood oxygen levels.
- Other lung or breathing diseases such as asthma (inflammatory disorder of airways) and emphysema (damage to air sacs in the alveoli), shortness of breath.

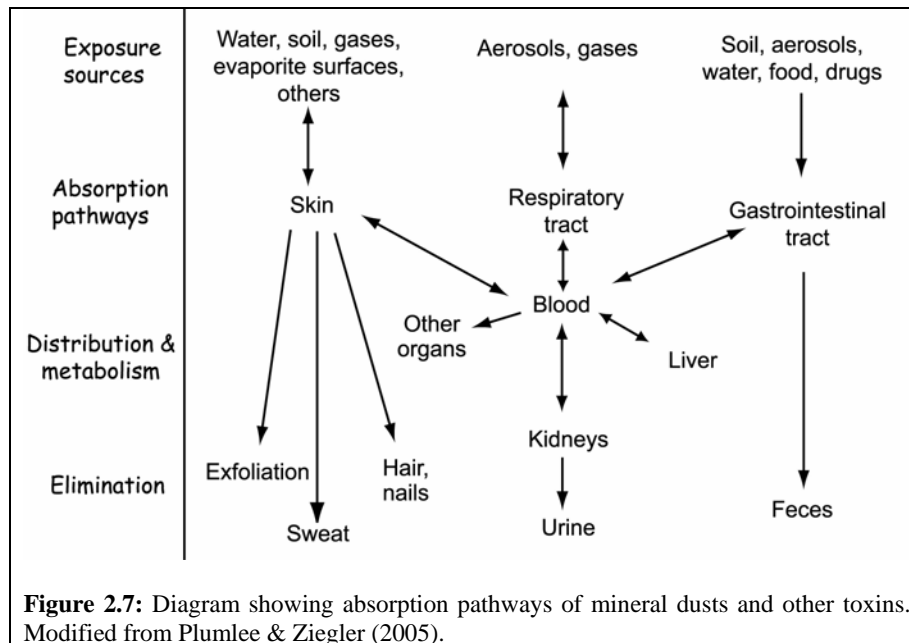
- Pathogen initiated diseases where the pathogen is adsorbed or associated with the mineral or mineral dusts – valley fever, naturally occurring anthrax.

**Table 2:** Examples of minerals, their sources and known health effects (modified from Plumlee & Ziegler 2005).

<b>Mineral</b>	<b>Potential sources</b>	<b>Primary exposure pathways, health effects</b>
Asbestos	Dusts from: industrial, commercial products (insulation, brake linings, building products), natural sources (weathering & erosion of asbestos bearing rocks)	<i>Inhalation:</i> lung cancer; pleural effusion, plaques, mesothelioma cancer. <i>Ingestion:</i> Has been proposed as a trigger of GI cancers.
Crystalline Silica	Dusts from mining, erosion of friable silica-rich rocks and industrial activities	<i>Inhalation:</i> Silicosis, industrial bronchitis with airflow limitation. Associated illness include silica nephropathy, lung cancer.
Coal dust	Dusts produced from coal mining, processing and combustion activities	<i>Inhalation:</i> “Black lung”- includes progressive massive fibrosis, chronic airway obstruction or bronchitis, emphysema
Other mineral dusts	Dusts of talc, kaolinite, erionite, sulphides, sulfates, Fe oxides & hydroxides	<i>Inhalation:</i> Mineral specific fibrosis such as talcosis <i>Ingestion:</i> Release of associated metals into the system can cause numerous diseases

### 3.2 Exposure Pathways, biodegradability and toxicology of minerals

The health effects of minerals depend on **dose response** (higher the amount of specific mineral(s) in the air, the greater the toxicological response) and **routes of exposure** and associated clearance mechanisms (figure 2.7). The best studied exposure pathway for mineral dusts is via the respiratory tract (inhalation), but increasingly the intake via skin (absorption) and mouth (gastrointestinal tract) are being recognized as critical for some minerals. Besides the dose response, the health effects of inhaled minerals depend on type of mineral inhaled, the concentration of the specific mineral (fibre) in the air, the solubility and reactivity of the mineral in the respiratory tract and the size and shape of the mineral.



To deal with the toxicological effects of mineral dusts, the solubility of the mineral at a particular body site (respiratory tract) is critical, because longer the mineral persists without dissolution, the greater its abundance in the particular organ and more acute the resulting effects. Alternatively, heavy metal and toxic metal hosting minerals, if easily dissolved, can release those metals into the body fluids and tissues and caused toxicity depending on dose rate. Accordingly, **biodurability** is the measure of a substances resistance to clearance by dissolution of body fluids, and **biopersistence** is the measure of a substances resistance to all chemical, physical and biological clearance mechanisms. Linked to biopersistence is **biosolubility**, which is the degree to which a substance is soluble in the various body fluids and **bioreactivity** is the extent to which the substance can modify key body fluid parameters such as pH, concentration of major electrolytes. **Bioaccessible** minerals are those that are readily biosoluble (less biodurable) and are therefore easily dissolved in body fluids and pose less of a health risk in terms of respiratory diseases. Figure 10 in Plumlee and Ziegler (2005) shows a plot of bioreactivity and biosolubility of several earth materials, from which asbestos and crystalline silica are the least biosoluble and most biodurable.

The extent of health risk of an inhaled mineral is dependant on the **morphology** (size, shape) of the minerals and their biodurability (and bioaccessibility), the latter being controlled by the minerals solubility in particular body fluids. The **size** and **shape** of the minerals inhaled dictates the limit to where they can be carried in the respiratory tract and the degree to which they can be cleared from particular sites by various bodily mechanisms. Particles < 10  $\mu\text{m}$  (“PM<sub>10</sub>”) are mainly inhaled with only smaller sized particles (< 5  $\mu\text{m}$ ) commonly penetrating deeper into the respiratory system (Figure). The defense mechanism for larger particles is the mucous lining the airways, with the mineral bearing lining being cleared through the trachea and bronchi via coughing. Particles < 2  $\mu\text{m}$  is size reach the alveoli from where they are either exhaled, trapped or cleared via the biological defense mechanisms. The mineral clearance mechanisms in the alveoli proceed either through dissolution of the mineral and subsequent absorption of released ions into the tissue or through engulfing of the mineral by alveolar macrophage cells (phagocytosis).

Even finer mineral particles such as those described as “nano-particle” (< 100 nm in size), are suggested to have greater inflammatory response because of their larger surface area which

may inhibit efficient functioning of phagocytosis. However, studies are being conducted to evaluate the dose-response effects of nano-particles on health. For biodurable minerals such as asbestos and crystalline silica, the bodily mechanisms of clearance, such as phagocytosis, are not efficient to discard them from the alveoli. Toxicological studies suggest that the morphology (fibrous habit and length:width ratio) appears to be an important factor precluding easy clearance from the respiratory tract, with longer fibres being less easily cleared and penetrating deeper into lung tissue.

The other factor controlling the biodurability and biopersistence of the minerals is their particle **solubility** and their **dissolution rates** in body fluids or their bioreactivity. The dissolution rates of minerals are a complex function of mineral structure, chemistry, particle size and shape, and studies have suggested differential dissolution based on these mineral parameters. For example, amphibole asbestos is less readily dissolved in lung fluids than chrysotile asbestos, which enables amphibole asbestos to endure longer in lung tissue and subsequently trigger fibrosis and cancer. Furthermore, the same mineral with different morphology (length, width, “curlyness”) and trace chemistry can show different biodurabilities and in turn affect disease rate. For example, a study demonstrated that similar amphibole minerals from different localities but with different mineral fiber lengths showed different biological activity.

Controlled toxicological studies suggest that biodurability and toxicological effects of minerals (especially asbestos and asbestiform) appear to be strongly linked to the morphology (size, shape) and chemistry of the mineral (especially surface chemistry) rather than just a mineral species, and it is therefore important to identify mineral characteristics via different instrumental techniques such as optical, SEM and TEM, rather than merely identify the presence of asbestos. Furthermore, the dose rate or particles per milliliter or cubic meter (m<sup>3</sup>) of air is critical, with higher dose rates for toxic minerals overriding the lung clearance mechanisms and contributing to accumulation of fine mineral particles in the lung and subsequent diseases.

Although public perception of mineral dusts and health risks is dominated by asbestos and silica in the workplace, there are other mineral groups that occur in working environments such as mine environments, where the effects of the mineral dusts on health are not well established. As mentioned in the mine environments section, weathered mine wastes contain a combination of a variety of minerals. In terms of reactivity, the minerals in the mine waste include

- Bioreactive minerals: sulphides, iron-sulfates and iron hydroxides. These groups contain potentially bioaccessible metals such as As, Zn, Cu, Pb, Hg, either within their structure (sulphides) or adsorbed onto their surfaces. Furthermore, many of the sulfates and iron hydroxides are in the nano-particle range and therefore easily bioaccessible.
- Biodurable minerals: Quartz.
- 

The range of factors will govern the bioaccessibility of metals incorporated and absorbed to the mine waste minerals, the main factors being the type of the mineral, its grain size and the amount of encapsulation by other less or more biodurable minerals. In terms of mineral types, carbonates are easily dissolved (most soluble) in acid fluids of stomach and intestines, but sulphides, sulfates and hydroxides may survive the time they take to pass through gastrointestinal system. However, the finer grain size of the hydroxides and sulfates can make them reactive and increase their solubility. Further, metals adsorbed onto the mineral surfaces can be exchanged with ions in the stomach fluids and be easily bioavailable, with As and Pb being the most harmful. The inhalation effects of mine site related bioreactive minerals remain unclear.

### 3. X - R A Y S

#### HISTORY

Röntgen 1895: Wurzburg, discovered unknown penetrating rays coming from the anode of a cathode ray tube. Later moved to Munich.

Ewald 1912, in Munich was studying the structure of crystals.

von Laue 1912 was interested in the diffraction of light by 2-D lattices. After discussions with Ewald, he suggested passing X-rays through a crystal, reasoning that if crystals were built on a 3-D lattice, and X-rays were waves, they should interact to produce diffracted beams. Used X-ray tube in Sommerfeld's lab with two of Sommerfeld's assistants; Friedrich and Knipping.

Moseley: relation between atomic number and X-ray wavelength:  $1/\lambda = K(Z - \sigma)^2$   
 where Z is the atomic number of the element emitting the X-rays, K is a constant  
 ( $= 8.23 \times 10^4$  for the K-series,  $\sigma \sim 1$ )

**To analyse**

elements  
 molecules  
 bonds between atoms  
 crystals/phases  
 morphology

**use**

XRF, INAA, AA, wet chem  
 Chromatography.....  
 Infra-red.....  
 XRD, TEM  
 Optics, SEM

Some methods depend on the energy of the actual thing analysed:

- Flame photometry: sees outer electron transitions ( $E = 2 \text{ eV}$ )
- Infra-red: bond stretching and bending ( $E = 0.2 \text{ eV}$ )
- XRF: inner electrons ( $E = 20 \text{ keV}$ )

Electromagnetic radiation: waves, with an associated energy (E) and wavelength ( $\lambda$ ).

Radio	micro-waves	infra-red	light	ultra-violet	X-rays	$\gamma$ -rays
m	mm	$\mu\text{m}$	nm	nm	nm	pm
$\lambda \ 10^6\text{-}1$	100-1	100-1	700-450	100-10	5 - 0.01	10-0.1
am-fm			red-blue			
FM104.7						
2.86m						

$E = hc/\lambda$  , whence  $E = 1.24/\lambda$  if  $\lambda$  is measured in microns ( $\mu\text{m}$ ,  $10^{-6} \text{ m}$ )  
 $E = 1,240/\lambda$  if  $\lambda$  is measured in nanometres (nm,  $10^{-9} \text{ m}$ )

Hot atoms also emit electromagnetic energy, the peak wavelength is given by the equation:

$$\lambda_{\max}T = K \quad \text{where} \quad K = hc/4.965k$$

It would require 10 million degrees to generate  $3\text{\AA}$  X-Rays.

## X-RAY GENERATION

1. When high energy (speed) electrons strike atoms, they may lose their energy in steps, emitting quanta at each step, of any energy up to the maximum they have left. If the energy loss in a single event is high, the quantum may be in the X-ray range, if small, in the heat range. This process produces a continuous spectrum of X-rays.
2. Some electrons may strike an electron of the target material and eject it from its stable position. The consequent electron is called a photo-electron; its energy tells things about the material it came from but is not considered here.

The photo-electron leaves an electron hole in the atom it left; the atom is thus ionized. This is an unstable arrangement, the hole is filled by the nearest electron in a higher energy position - like pulling a book suddenly from the bottom of a stack; the one above drops down, which causes all the ones above it to drop. The analogy is not perfect; sometimes an electron further out beats one closer to the hole. This doesn't happen with book stacks.

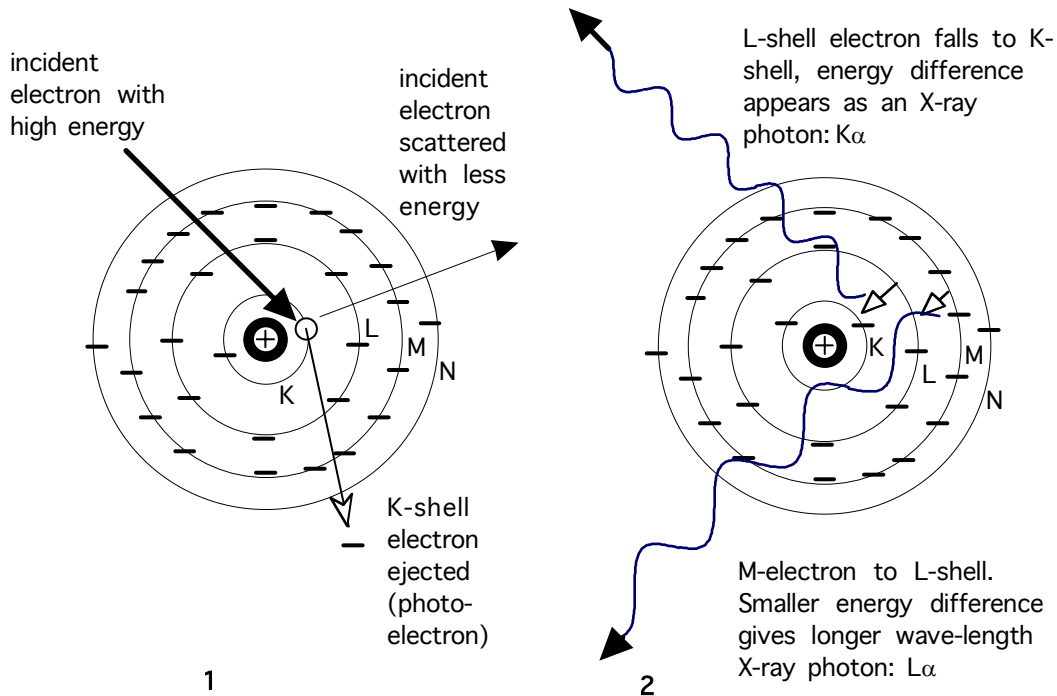


**Figure 3.1:** Diagram representing the generation of characteristic X-rays.

The higher electron "falls" to a level of lower potential energy, giving up the difference in energy between its initial and final positions, as you do if you fall off a wall. This energy quantum is in the X-ray range if the hole was created in the inner shells of an atom. Because the electron energy levels of atoms are discrete, and depend on the atom species, i.e. element dependent, each quantum is:

- a) always of the same energy for a given transition from a given element.
- b) different for every element.

Hence the X-rays emitted by this process, in contrast to the white radiation, are characteristic of the element.

3. X-rays behave also like particles. They have the ability to eject electrons from atoms in the same way as electrons do. Hence the process described in 2. holds also for atoms subjected to X-rays; photo-electrons are ejected, and characteristic X-rays produced. The original X-ray that produced the photo-electron is lost (its energy is used in ejecting the photo-electron; it is absorbed).

X-ray diffraction targets are designed to produce K-shell radiation. Commonly Cu or Co are selected as target metals, with Fe, Cr and Mo used for special purposes. All produce both  $K\alpha$  and  $K\beta$  radiation.  $K\beta$  is the more energetic, originating in an  $M \rightarrow K$  transition, and so has the shorter wavelength. As we will see, X-ray diffraction requires monochromatic radiation, therefore the continuous radiation from the target, and the K radiation need to be removed in order to leave just one wavelength.

There are two ways to remove  $K\beta$  radiation. One is to make use of the fluorescence phenomenon and absorb it before it reaches the sample for diffraction studies. Photo-electrons are created very efficiently when the energy of the X-ray causing photo-emission is just sufficient to do it. An example is the emission of Ni K electrons. They require an energy equivalent to  $1.49\text{\AA}$  for their generation, and the wavelength of  $\text{Cu}_{K\beta}$   $1.39\text{\AA}$ . The  $K\alpha$  wavelength for Cu is  $1.54\text{\AA}$ , so  $\text{Cu}_{K\beta}$  is able to excite Ni K electrons,  $\text{Cu}_{K\alpha}$  is not. By putting a thin Ni foil in the X-ray beam, over 90% of the  $K\beta$  radiation from Cu is absorbed, and only a few percent of the  $K\alpha$  is absorbed. Thus almost monochromatic  $K\alpha$  is produced. The same can be done for Co radiation using an Fe filter and so on.

The second way, and the better way, it to use diffraction itself to select the desired radiation. Without any explanation here, a crystal monochromator for X-rays is typically a graphite or Si-metal single crystal positioned after the sample, so that all X-rays coming from it are eliminated except the desired  $K\alpha$  radiation.

$K\alpha$  radiation is actually made up of two slightly different energies,  $K\alpha_1$  and  $K\alpha_2$ . For Cu,  $K\alpha_1 = 1.5405$ ,  $K\alpha_2 = 1.5443$ . The difference is quite detectable in X-ray diffraction scans, but is usually not a problem, or can be allowed for by calculation.

### Scattering of X-rays by materials.

When an X-ray beam strikes a crystalline substance, most of the energy is transmitted. Some is scattered coherently, that is, diffracted by the crystals. Some is scattered randomly, or incoherently, some is absorbed and leads to fluorescent radiation. The incoherent and fluorescent radiation contribute to the background on which the diffracted X-rays are superimposed.

---

---

## DIFFRACTION

---

---

There are two parts to the theory of diffraction by a crystal: Laue, or Bragg diffraction from the lattice, and the intensity of the diffracted X-rays. We will first look at diffraction by atoms, then by crystals.

### 1) Diffraction by an atom

When X-rays interact with atoms, the electrons scatter them. The scattering does not change their wavelength. The amplitude of the scattered wave from an atom is proportional to the number of electrons around it, thus Pb scatters 207 times more intensely than does H.

Imagine an X-ray passing an atom, and consider the X-ray scattering by 2 of its electrons.

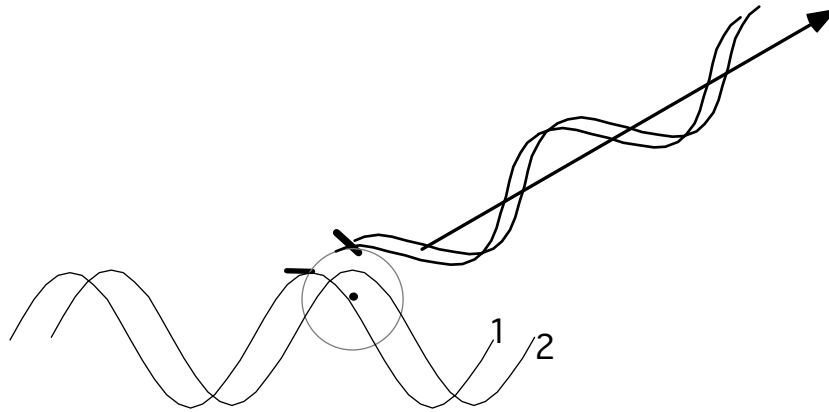


**Figure 3.2:** Scattering of X-rays by 2 electrons of an atom.

The wave first strikes the left electron (in position 1, Figure 3.2). This sends a weak scattered wave in all directions, like the ripples in a pond when a fish jumps, but we will look at one direction only, at about  $30^\circ$  to the direction of the incident wave. A little later the wave is in position 2, and X-rays scatter from the second atom. In the straight forward direction ( $0^\circ$  from the incident beam), the scattered X-ray wave is in step with the scattered wave from the first atom, because these two are going at the same speed in the same direction as the incident wave. But in the direction at  $30^\circ$ , the path from

electron 1 to electron 2 is longer than the path in the  $0^\circ$  direction, so these two waves are a little out of step. The sum of the amplitudes of two equal waves in step is twice the amplitude of either. However if they are out of step the sum is less than this, by an amount depending on the separation of their wave fronts (say their crests). This difference is called their *phase* difference.

Phase is measured in fractions of a wavelength, using a sine or cosine function. Waves repeat every wavelength ( $\lambda$ ) and cosines repeat every  $2\pi$  (measuring in radians). The amplitude of a wave at position  $x$  is calculated as  $\cos(2\pi x/\lambda)$ . When  $x=0$ ,  $A=1$  ( $\cos(0)=1$ ). When  $x=1$ ,  $A=\cos(2\pi)=1$ . When  $x=0.5$ ,  $A=\cos(2\pi/2\lambda) = -1$ .

The sum of two waves is mathematically expressed as the sum of their cosines, so in these examples, the  $0^\circ$  wave amplitude is  $E\cos(0) + E\cos(0) = 2E$  where  $E$  is the scattering power of one electron,  $0$  is their phase position. The wave amplitude in any other direction (say at  $30^\circ$ ) is  $E\cos(0) + E\cos(2\pi x/\lambda)$  where  $x/\lambda$  is the phase difference. Note that  $x/\lambda$  is independent of wavelength. In the drawing of Fig 21, the second wave is about  $0.07$  of a wavelength behind the first, so the net amplitude would be  $E\cos(0)+E\cos(2\pi*0.07) = 1.9E$ . The exact value of  $x/\lambda$  will depend on the distance between the two electron as well as the direction of scattering. At higher angles,  $x/\lambda$  will be greater, so the total intensity from the electrons will be less. When all the electrons in an atom are considered, the total scattering varies with angle in the manner shown in Fig 3.3.

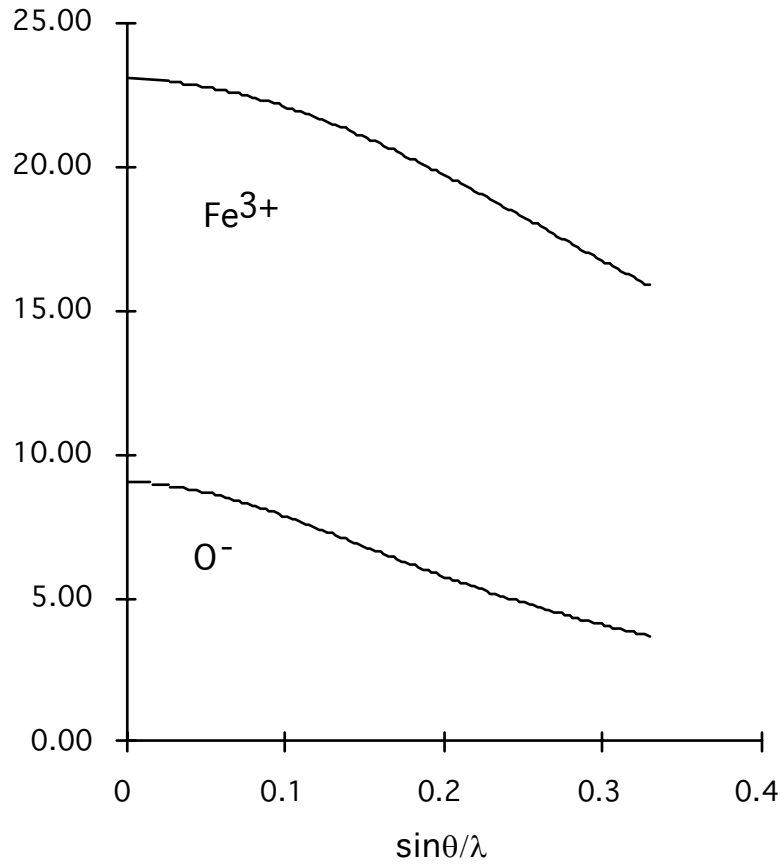


**Figure 3.3:** Scattering factor curves for Fe<sup>3+</sup> and O<sup>-</sup>.

## 2) X-ray scattering by a crystal

Scattering by a crystal is no different in principle from scattering by electrons. We will start with a crystal made up of one atom kind on a primitive lattice. The symmetry is not important at this stage, because all the atomic positions are related to the unit cell itself. An atom at (0.1, 0.2, 0.3) is one unit cell away from an atom at (1.1, 0.2, 0.3) regardless of crystal system.

*One-dimension - a row of atoms*

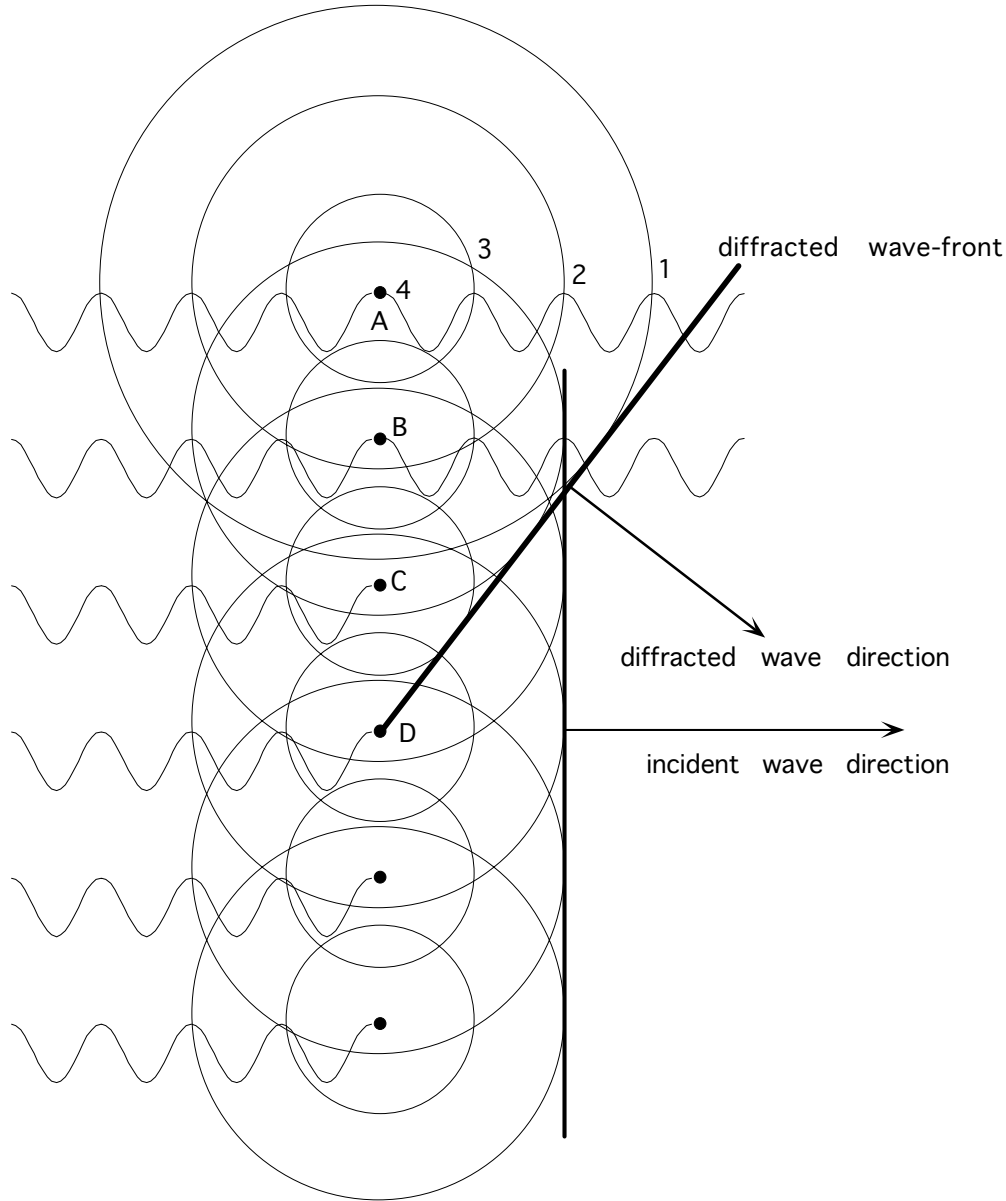


**Figure 3.4:** One dimensional row of atoms scattering X-rays.

Figure 3.4 depicts an X-ray wave train striking a row of equally spaced atoms. Each atom becomes a point scatterer, sending out a circular wave. The first wave (1) hits all atoms at the same time, in the forward direction ( $0^\circ$ ) the ripples from each atom line up. Then the second wave arrives, and it too sends out ripples. The forward wave front from wave 2 is marked. This wave front is a tangent to all the second ripples from all the atoms. Its amplitude would be, from atoms of atomic number  $Z$ :

$$Z\cos(2\pi*0) + Z\cos(2\pi*0) + \dots = nZ \text{ for } n \text{ atoms.}$$

Another tangent, or another wave front, can be seen as a tangent to ripple 1 from atom A, ripple 2 from atom B, ripple 3 from atom C and the about to start ripple 4 from atom D. This wave front is made up of waves that are each one wavelength behind the adjacent wave. Mathematically, the amplitude of this wave would be:

$$Z\cos(2\pi*3) + Z\cos(2\pi*2) + Z\cos(2\pi*1) + Z\cos(2\pi*0) + \dots = nZ,$$

where the digits 0, 1, 2 ,3 are the path differences (in wavelengths) between adjacent waves.

So in the forward direction, and in this new direction, there would be a pile up of waves, leading to a strong X-ray signal.

If we pick a different direction to consider, such as in Fig 3.5, the waves do not line up crest on crest, so the resulting amplitude must be less than  $nZ$ .

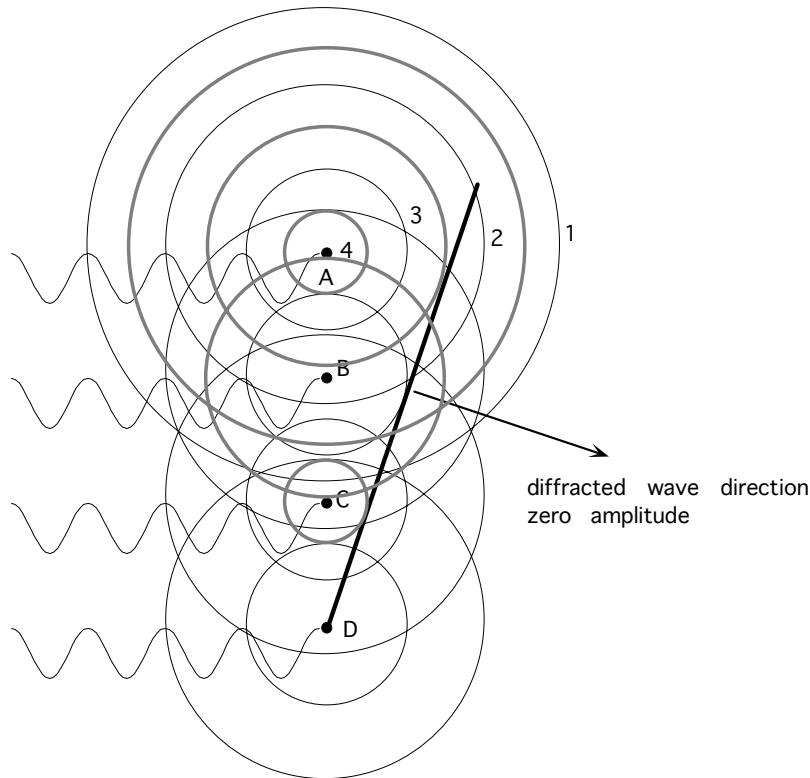


**Figure 3.5:** Destructive interference in X-ray scattering from a row of atoms.

In Fig 3.5, the troughs of the ripples half way between the crests (phase =  $\lambda/2$ ) are shown as grey circles. The direction shown has a line-up of a trough from atom A with a crest from atom B with a trough from atom C with a crest from atom D. The resulting amplitude will be (using \* to denote multiplication):

$$Z\cos(2\pi*3/2) + Z\cos(2\pi*1) + Z\cos(2\pi*1/2) + Z\cos(2\pi*0) + \dots \\ = -Z + Z - Z + Z \dots = 0$$

In any random direction, the phase difference will be some fraction of a wavelength, let's say 1/50th. Then the amplitude will be (starting at the 49th atom and working back to the first instead of the other order we have been using))

$$Z\cos(2\pi*0) + Z\cos(2\pi*(1/50)) + Z\cos(2\pi*2/50) + \dots + Z\cos(2\pi*25/50) + \dots + Z\cos(2\pi*49/50)$$

$$= Z + 0.99Z + 0.97Z + \dots - Z - 0.99Z - 0.97Z \dots + 0.99Z + \dots = 0$$

This result shows the fundamental nature of diffraction by a regular lattice. Either the direction is exactly right for the scattered waves all to line up crest on crest, and a strong signal be received, or the wave from one atom is cancelled exactly by the wave from another somewhere along the lattice row. The longer the row of regular atoms (the bigger the crystal) the more exactly all the waves are cancelled except in the very precise direction where the crests all align. Figure 25 shows the mathematical result for various numbers of rows of atoms. The calculation is of amplitude squared (Intensity). When there are only a few atoms, there is not complete cancellation between the intensity maxima and minima, and wavelets are created. These can be detected occasionally from groups of very tiny crystals if all are the same size. Mostly, however, there are random numbers of atoms from crystallite to crystallite in a real mineral, and the wavelets are undetectable. Once the crystallite reaches as few as 50 atoms in a row, the peaks are so sharp they are almost spikes. The breadth of the peaks can be used to estimate crystal size.

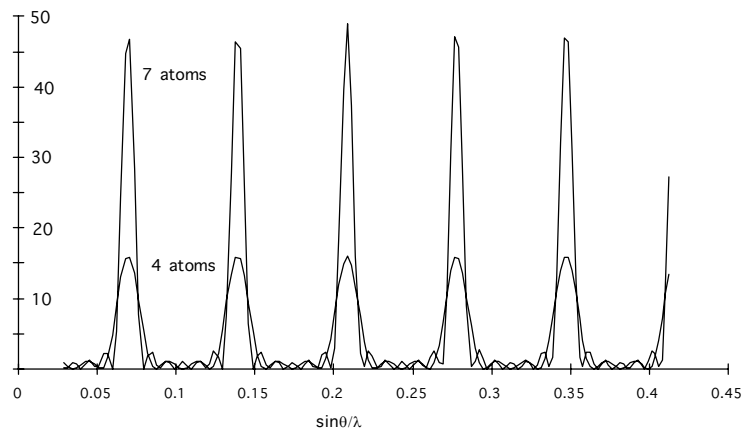


**Figure 3.6:** Diffracted intensity from rows of equally spaced atoms: broader, lower curve from 4 atoms, higher sharper curve from 7 atoms.

### ***2-dimensions***

There is no real difference between 1- and 2-D theory. The principles work the same way, the diffracted waves interfere constructively in a selected direction, in all other directions interference is destructive. The result is a 2-dimensional pattern of maxima. Figure 3.7 shows a 2-dimensional section from a 3-dimensional diffraction pattern of the mineral calciotantite. Each black spot comes from Ka radiation diffracted from a set of

atomic planes (see below). The “tail” radiating out from each spot comes from the white radiation.

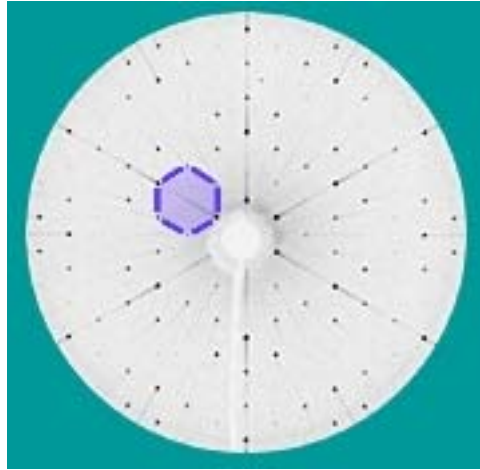


**Figure 3.7:** Hexagonal single crystal diffraction pattern (calcioantite)  
Image courtesy Canadian Museum of Nature, T.Scott Ercit

### *3-dimensions*

The addition of the third dimension leads to the requirement that the wave crests from atoms in each of the 3 lattice directions X, Y, Z, must all add up in the same direction. This is not inevitable, unlike 1- and 2-D diffraction where it doesn't matter how the incident X-rays strike the lattice, diffraction will always occur in some direction. In a real crystal, three sets of orientation relations have to be satisfied at once, known as the Laue equations. We are not going to examine the Laue equations, but rather we will consider Bragg's relation for X-ray diffraction by a lattice.

Bragg noticed that for the rare orientations that a crystal did diffract X-rays, the incident and diffracted beams made equal angles with a crystallographic plane. It looked as though the crystal plane reflected the X-rays. Unlike the reflection of light from a mirror, there were only very specific angles at which any plane acted like a mirror to X-rays. Bragg appreciated that the process was actually constructive interference from all the atoms in the crystal, and the crystal could have been ground into the shape of a sphere and have no actual planar surfaces; the X-rays still came and went as though reflected from lattice planes.

We'll begin again with a row of atoms.

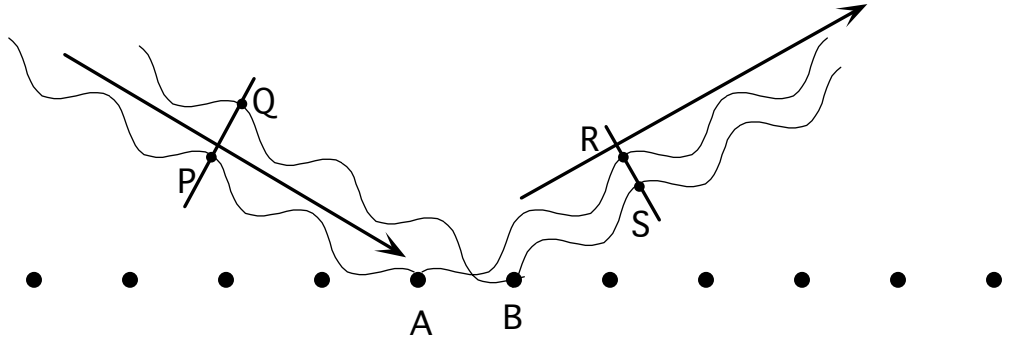


**Figure 3.8:** X-rays "reflecting" from a row of atoms.

If a wave train strikes a row of atoms at any angle, for the waves to be scattered with ZERO path difference (not just in phase, but with the same crests all lined up), the incident and scattered directions must be at equal angles to the line of atoms (ie., "reflection"). In Fig 3.8, the wave is striking atom A at its crest, having struck atom B a bit earlier just up from a trough. The crest of the ripple from A will only align with the crest of a ripple from B if the path  $PAR = QBS$ , that is, if the angles from P to A and A to R are the same.

Extending to a plane of atoms doesn't affect the story.

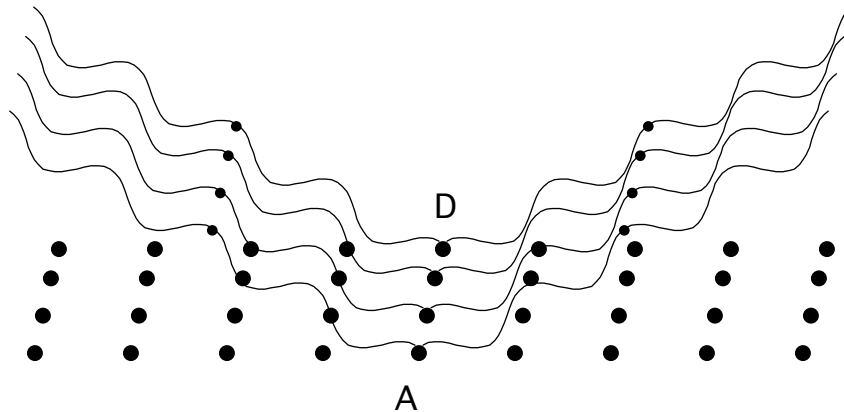


**Figure 3.9:** X-rays "reflecting" from a row of atoms.

If atom A (Fig 3.9) is scattering a crest, so are all the atoms in the row AD, therefore all the atoms in the plane are scattering in phase provided the angle of incidence equals the angle of diffraction.

Adding the third dimension limits crystal diffraction to very few directions. We now require that all the atoms from the first plane diffract in phase (reflection condition), and that all the atoms from a parallel plane below the first are scattering in phase. All we need to find is the condition that ONE atom of the plane below is in phase with ONE atom of the first plane, because if it is, it must be in phase with all the other atoms of this plane (since they are all scattering in phase).

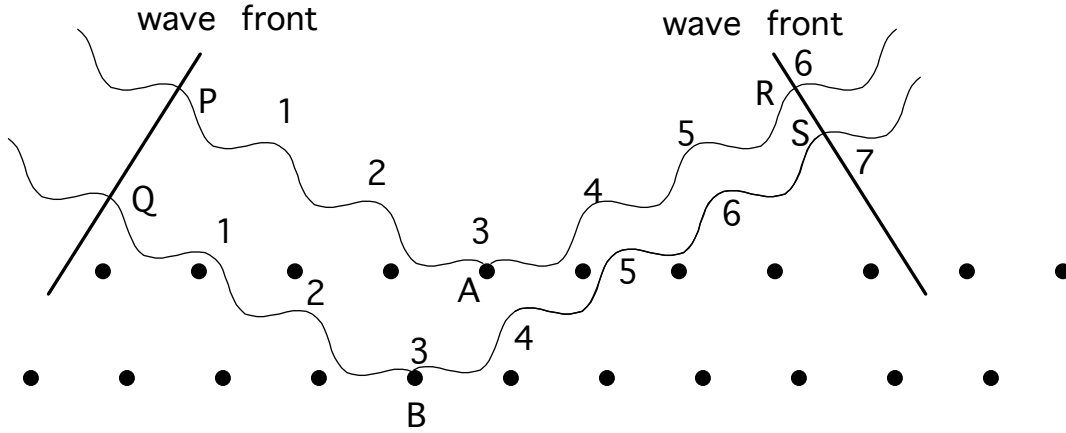


Figure 3.10: In-phase scattering from two atoms in successive planes in a crystal.

Figure 3.10 shows two rows of atoms, one above the other, being part of two parallel planes of atoms. The wave front approaching from the left strikes an atom of the top row, and wavelets spread out, with zero path difference in the reflection direction as in the 2-D case. The same wave front also strikes an atom of the second row, and if the scattered wave from this atom is to be in phase with the wavelets from the upper atom, the path QBS must be exactly one (or 2, or 3) wavelengths longer than the path PAR. In Figure 29, the waves are counted, there are 6 along the path PAR, 7 along QBS. Figure 30 simplifies the geometry of this diagram.

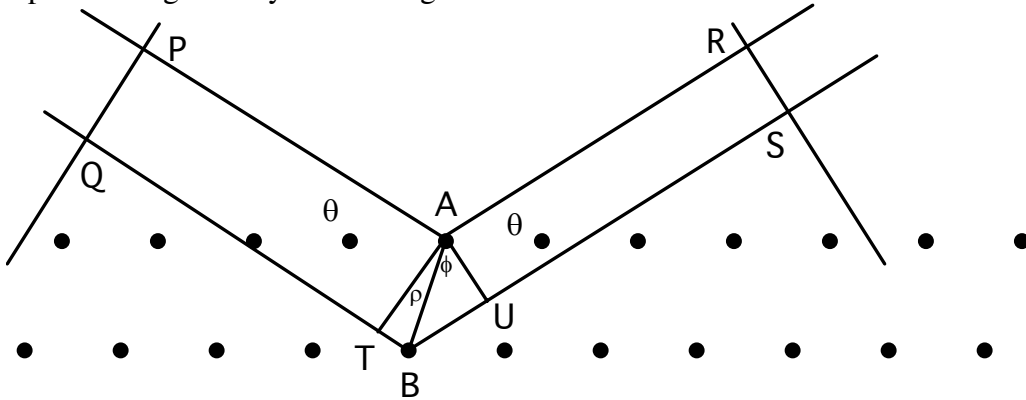


Figure 3.11. Ray path diagram for Bragg diffraction.

In Fig 3.11, for PQ and RS to be wave fronts, QBS-PAR must be  $\lambda, 2\lambda, 3\lambda, \dots, n\lambda$ . Since A is scattering a wave, AT and AU must be wave fronts, therefore  $TBU=n\lambda$ .

$$\begin{aligned}
 TB &= AB\sin(\rho) \\
 AU &= AB\sin(\phi) \\
 \therefore TB+AU &= AB(\sin(\rho)+\sin(\phi)) \\
 n\lambda &= AB.2\sin((\rho+\phi)/2)\cos((\phi-\rho)/2)
 \end{aligned}$$

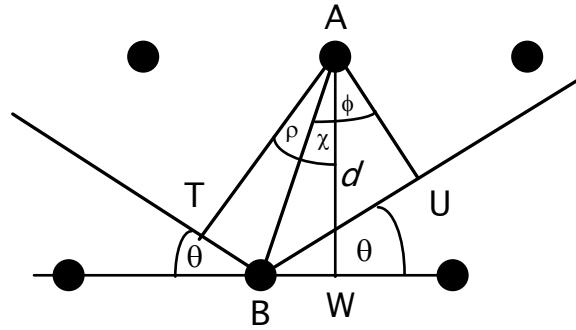


Figure 3.11a: -enlargement of part of fig 30.

From Fig 3.11a,

$$\begin{aligned}
 (\rho + \phi) &= 2\theta \\
 \text{(quadrilateral ATBU has angles } A = \rho + \phi, T = 90, B = 180 - 2\theta, U = 90, \\
 \therefore \rho + \phi + 180 - 2\theta &= 180, \text{ hence } \rho + \phi = 2\theta) \\
 (\rho + \chi) &= \theta \\
 \text{(quadrilateral ATBW has angles } T, W = 90, \text{ hence } (\rho + \chi) = \theta) \\
 (\phi - \chi) &= \theta \\
 \therefore (\phi - \rho)/2 &= \chi \\
 \therefore n\lambda &= 2AB\sin(\theta)\cos(\chi) \\
 \text{but } AB\cos(\chi) &= d \text{ (distance between lattice planes)} \\
 \therefore \underline{n\lambda} &= \underline{2d\sin(\theta)} \\
 &\text{Which is the Bragg relation}
 \end{aligned}$$

### Indices of Bragg reflections

Whenever X-rays diffract from a crystal there is a lattice plane positioned symmetrically to the incident and diffracted beams, and the Miller indices of this lattice plane are given to the X-ray reflection. Thus we speak of the 001 reflection, or the 122 reflection (no brackets), or we refer to  $d_{001}$ , meaning the distance between successive (001) lattice planes. (Note that in this context, (001) refers to the whole family of lattice planes parallel to the basal face of the crystal (001). A mica crystal 1 mm thick would have  $10^6$  (001) lattice planes but only one (001) face (and an  $00\bar{1}$ ) face).

Imagine the mica crystal oriented with its XY plane parallel to the X-ray beam, and that it is slowly rotated about an axis parallel (001) (Fig 15). The distance  $d_{001}$  for mica is  $10\text{\AA}$ , so using Bragg's equation, diffraction will first occur when:

$$\begin{aligned}
 \lambda &= 2d_{001}\sin\theta \\
 \lambda &= 2.10.\sin\theta
 \end{aligned}$$

A common radiation for X-ray machines is  $\text{CuK}\alpha$ , with a wavelength of  $1.5418\text{\AA}$ .

$$\begin{aligned}
 \therefore \sin\theta &= 1.5418/20 \\
 \sin\theta &= 0.07709
 \end{aligned}$$

$$\theta = 4.42^\circ$$

A second diffracted beam will occur when  $n=2$ . This is known as the second *order* diffraction from (001).

$$\begin{aligned} 2\lambda &= 2d_{001}\sin\theta \\ 2\lambda &= 2 \cdot 10 \cdot \sin\theta \\ \lambda &= d_{001}\sin\theta \\ \lambda &= 10 \cdot \sin\theta \\ \therefore \sin\theta &= 1.5418/10 \\ &= 0.15418 \\ \theta &= 8.87^\circ \end{aligned}$$

And a third will occur when  $n=3$  (the 3rd order diffraction from (001))

$$\begin{aligned} 3\lambda &= 2d_{001}\sin\theta \\ \therefore \sin\theta &= 3 \cdot 1.5418 / 2 \cdot 10 \\ \sin\theta &= 0.23127 \\ \theta &= 13.37^\circ \end{aligned}$$

and so on.

The crystal will produce a diffracted beam only at these particular angles, and will continue to yield diffracted beams out to the geometric limit when  $\sin\theta = 1$  ( $\theta=90^\circ$ ), or as close as possible. At this limit,  $n\lambda=2d_{001}$ . If  $\lambda = 1.5418$ , the maximum detectable value for  $n$  will be  $2 \cdot 10 / 1.5418 = 12.97$ . Thus only up to  $n=12$  will be actually detectable with this set-up.

We shall repeat these calculations for the two minerals chlorite ( $d_{001} = 14.4$ ) and kaolinite ( $d_{001} = 7.2$ )

	chlorite	kaolinite
n	$\theta$	$\theta$
1	3.07	6.15
2	6.15	12.37
3	9.24	18.74
4	12.37	25.36
5	15.53	32.37
6	18.74	39.97
7	22.01	48.55
8	25.36	58.93

When the path difference from successive layers of the chlorite lattice is  $2\lambda$  (second order), the scattering angle is  $6.15^\circ$ . Exactly the same angle occurs from kaolinite when  $\lambda=1$ . This equivalence is easily recognised when we know what the minerals are, but in most real examples the *identity* of the mineral is being sought. There is no obvious way to know that a reflection at  $6.15^\circ$  results from  $2\lambda$  path difference from chlorite or  $1\lambda$  from kaolinite. or indeed  $3\lambda$  from some other mineral with a lattice spacing of  $21.6\text{\AA}$ .

We get around this unknown by pretending it doesn't exist. When the identity of the mineral is unknown, we assume for the time being that  $n=1$ , and solve the simpler version of Bragg's equation:  $\lambda = 2d\sin\theta$ . The experiment yields an angle, which we convert using the known value of  $\lambda$  to obtain the unknown d-spacing. So if diffraction occurs at  $\theta=6.15^\circ$ , we deduce it came from lattice planes at  $7.2\text{\AA}$ . In fact, if the mineral was chlorite, it came from lattice planes at twice this spacing, but as there is no way of knowing this until the mineral has been identified as chlorite, we don't let it bother us. We simply say that chlorite has a d-spacing of  $7.2\text{\AA}$ , among others. When we do discover that chlorite is the mineral, we know to call this reflection the second order from the (001) lattice planes. The shorthand then is to call this reflection the 002 reflection from chlorite, or  $d_{002}$ . The table of angles calculated for chlorite and kaolinite, once the indices are included, looks like:

		chlorite	kaolinite
n	indices	$\theta$	$\theta$
1	001	3.07	6.15
2	002	6.15	12.37
3	003	9.24	18.74
4	004	12.37	25.36
5	005	15.53	32.37
6	006	18.74	39.97
7	007	22.01	48.55
8	008	25.36	58.93

If the chlorite pattern was obtained from an initially unknown mineral, the information we would have would be:

unknown		
hkl	$\theta$	d
?	3.07	14.400
?	6.15	7.200
?	9.24	4.800
?	12.37	3.600
?	15.53	2.880
?	18.74	2.400
?	22.01	2.057
?	25.36	1.800

From these data we would have to deduce that the pattern was a sequence of reflections from a crystal with a 14.4-Å lattice spacing. This would be fairly easy if these were the only reflections present, but in a real case, 14.4 Å is only one of the lattice spacings of a chlorite. There are also the (100), (010), (110), (011), (101), (111), (210),..... planes that can diffract, and each of these can diffract with  $1\lambda$ ,  $2\lambda$ ,  $3\lambda$ .... path difference. The possibilities are many, and next will look at the general case of the angle of diffraction from the  $hkl$  plane of any lattice.

The orthorhombic crystal system provides a medium complicated example, in that all the angle are  $90^\circ$ , which makes the geometry simple, but  $a \neq b \neq c$ .

In Fig 3.12, a rectangular lattice has a (11) lattice plane. (Or think of it as (110) in a 3-D lattice)

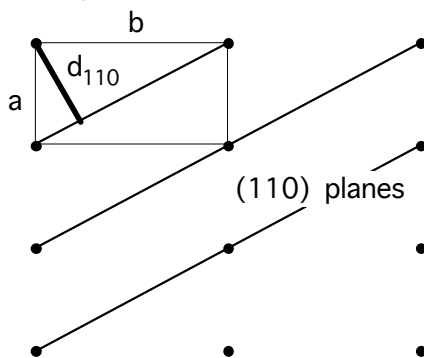


Figure 3.12: Rectangular lattice showing  $d_{110}$ .

$$d_{110} = b \sin \phi = a \cos \phi$$

$$d^2 = b^2 \sin^2 \phi$$

$$d^2 = a^2 \cos^2 \phi$$

$$d^2/b^2 = \sin^2 \phi$$

$$d^2/a^2 = \cos^2 \phi$$

$$d^2/b^2 + d^2/a^2 = \sin^2\phi + \cos^2\phi$$

$$\text{but } \sin^2\phi + \cos^2\phi = 1$$

$$\therefore 1/d^2 = 1/a^2 + 1/b^2$$

For  $hk0$ , the lattice plane cuts the x-axis at  $a/h$ , and the y-axis at  $b/k$ , so the algebra begins:

$$d_{110} = b\sin\phi/k = a\cos\phi/h$$

and concludes as:

$$1/d^2 = h^2/a^2 + k^2/b^2$$

The same algebra works in 3-D, yielding:

$$1/d^2 = h^2/a^2 + k^2/b^2 + l^2/c^2$$

Notice that the relation between  $d$  and  $a, b, c$  is reciprocal, and this is true of diffraction generally:  $\sin\theta$  and  $d$  are reciprocally related.

As the symmetry gets higher, the equation becomes simpler: for the **tetragonal**,  $a=b$ , so

$$1/d^2 = (h^2+k^2)/a^2 + l^2/c^2$$

and for the **cubic**,  $a=b=c$ , so:

$$1/d^2 = (h^2+k^2+l^2)/a^2$$

in the **hexagonal**, the X-axes are at  $120^\circ$ , which introduces some extra geometry, but the result is:

$$1/d^2 = 4(h^2+hk+k^2)/3a^2 + l^2/c^2$$

in the **monoclinic**, the angle  $\beta$  must be allowed for:

$$1/d^2 = h^2/a^2 \sin^2\beta + k^2/b^2 + l^2/c^2 \sin^2\beta + 2hl \cos\beta/acs\sin\beta$$

and in the **triclinic** the geometry gets out of hand!

$$1/d^2 = (h^2 \sin^2\alpha/a^2 + k^2 \sin^2\beta/b^2 + l^2 \sin^2\gamma/c^2 + 2hk(\cos\alpha \cos\beta - \cos\gamma)/ab + 2kl(\cos\beta \cos\gamma - \cos\alpha)/bc + 2hl(\cos\alpha \cos\gamma - \cos\beta)/ac)/(1 - \cos^2\alpha - \cos^2\beta - \cos^2\gamma + 2\cos\alpha \cos\beta \cos\gamma)$$

The next table shows the d-spacings for crystals with similar cell dimensions in 3 different crystal systems:

h	k	l	d-cubic	d-ortho	monoclinic
0	1	0	5.430	6.600	6.600
1	0	0	5.430	5.430	5.103
1	1	0	3.840	4.193	4.037
0	0	1	5.430	3.700	3.477
0	2	0	2.715	3.300	3.300
1	0	1	3.840	3.058	2.729
1	0	-1	3.840	3.058	3.044
0	1	1	3.840	3.227	3.076

Notice here that there are many d-spacings the same in the cubic example (because  $a=b=c$ ); in the orthorhombic negative indices don't change d whereas they do in the monoclinic (cf 101 with  $10\bar{1}$ ), and that in the monoclinic the  $\beta$  angle affects any d-spacing involving h or l (cf 100 orthorhombic with 100 monoclinic).

In this small example, the cubic pattern only has 3 different d-spacings, the orthorhombic has 7 and the monoclinic 8. As more hkl values are included the difference for the monoclinic increases, eventually reaching a bit less than double the orthorhombic.

The next table shows a slightly more extended set of d-spacings, but reordered, with overlapping d-spacings together. Overlap is indicated by the column M, the multiplicity of the d-spacing. All d-spacings that overlap by symmetry are included in the multiplicity. (eg. 110 and 101 in the cubic). Multiplicity has the same value as the number of faces in the form with the same symbol. In the cubic, there are 6 faces in the form  $\{100\}$ , the cube, 8 in the form  $\{111\}$ , the octahedron. Note that although the cubic pattern is listed out to  $d=1.451\text{\AA}$ , it still has fewer d-spacings than does the monoclinic pattern, listed only out as far as  $1.740\text{\AA}$ .

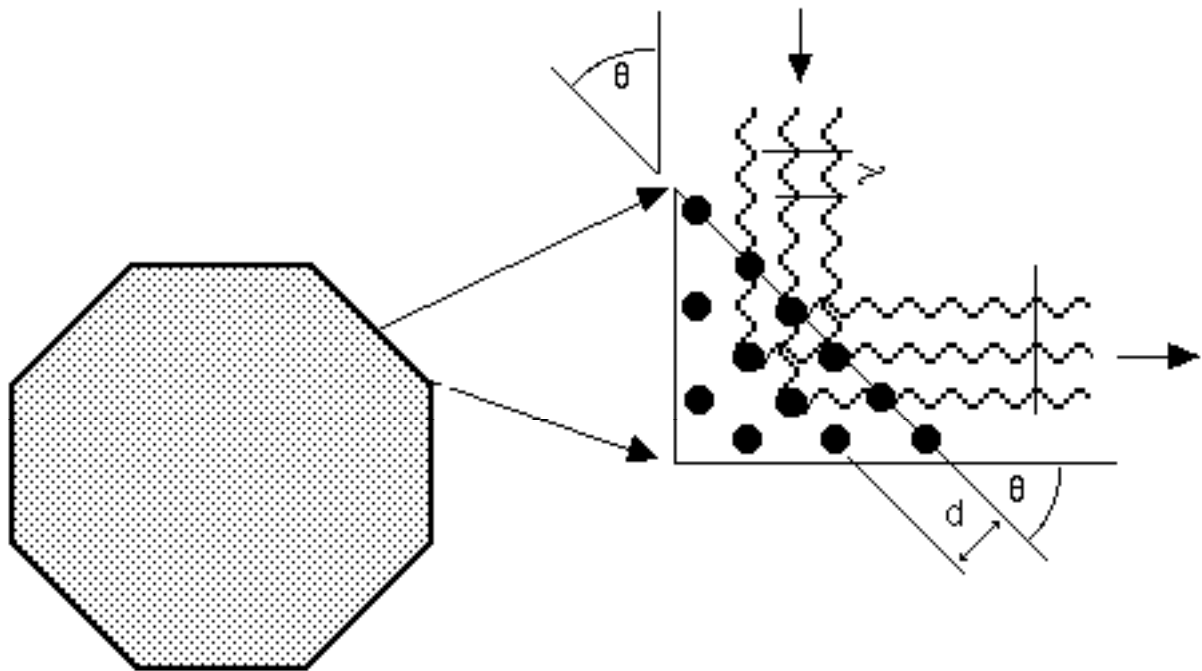
h	k	l	M	d-cubic	h	k	l	M	d-ortho	h	k	l	M	d-mono
1	0	0	6	5.430	0	1	0	2	6.600	0	1	0	2	6.600
1	1	0	12	3.840	1	0	0	2	5.430	1	0	0	2	5.103
1	1	1	8	3.135	1	1	0	4	4.193	1	1	0	4	4.037
2	0	0	6	2.715	0	0	1	2	3.700	1	0	-1	2	3.480
2	1	0	24	2.428	0	2	0	2	3.300	0	0	1	2	3.477
2	1	1	24	2.217	0	1	1	4	3.227	0	2	0	2	3.300
2	2	0	12	1.920	1	0	1	4	3.058	1	1	-1	4	3.078
2	2	1	24	1.810	1	1	1	8	2.774	0	1	1	4	3.076
3	1	0	24	1.717	2	0	0	2	2.715	2	0	0	2	2.551
2	2	2	8	1.568	2	1	0	4	2.511	2	0	-1	2	2.506
3	2	1	48	1.451	0	2	1	4	2.463	1	0	1	2	2.502
					2	0	1	4	2.189	0	2	1	4	2.394
					2	0	2	4	1.529	2	1	0	4	2.380
										1	1	1	4	2.340
										2	0	1	2	1.786
										2	0	-2	2	1.740

In summary, each beam of X-rays diffracted from a lattice can be indexed according to the Miller indices of the lattice plane which makes a symmetric angular relation to the incoming and diffracted beam. The Miller indices of the plane are multiplied by the order of diffraction - the path difference in numbers of wavelengths scattered from successive hkl planes.

## Summary of XRD

X-rays striking crystals undergo similar diffraction. Crystals are composed of atoms arranged in a repetitive array. The interval between identical atom groups is of the order of 1 nanometer, comparable to the wavelength of X-rays (about 0.15 nm in normal experiments).

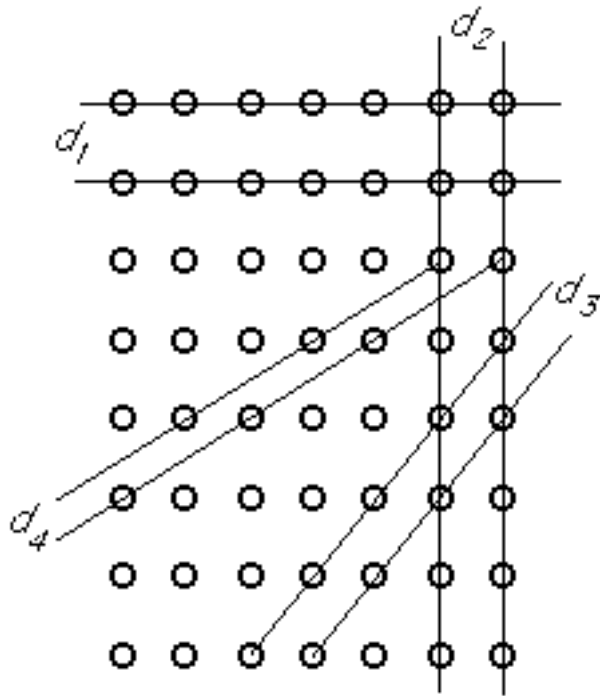
X-rays are scattered from crystals in directions determined by the wavelength, the atomic spacings, and the orientation of the crystal to the X-rays.



If wavelength, spacing between atoms, and orientation are suitable, cooperative scattering (diffraction) of X-rays occurs, according to the Bragg relation:

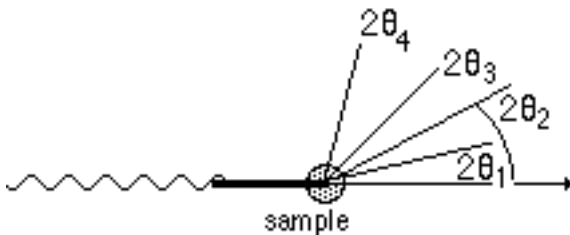
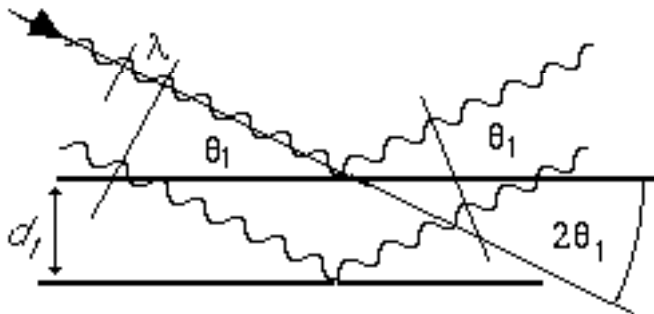
$$\lambda = 2d \sin \theta$$

A crystal has many possible planes of atoms, and therefore many different values for the distances between them,  $d$ . A given crystal can therefore diffract a fixed wavelength X-ray beam in a number of different directions  $\theta$ , each corresponding to a different value of  $d$ .



In practice, the crystal is rotated in the X-ray beam, allowing different planes to be presented at their appropriate angle to the beam at a different time, so that a succession of diffracted X-ray beams occurs. These may be recorded on a film or detected by a radiation counting instrument (such as a Geiger or scintillation counter)

On the rectangular lattice left, four planar directions are marked, with successively smaller  $d$ -spacings between them.



If X-rays strike the crystal and the crystal happens to be positioned so that the planes  $d_1$  are angled at the angle  $\theta_1$  to the beam, Bragg diffraction will occur, sending a diffracted beam away at an angle  $2\theta_1$  to the incoming X-ray beam.

If the sample is rotated in the X-ray beam, other planes will at some time also be positioned at angles  $\theta_2$ ,  $\theta_3$ ,  $\theta_4$  etc to the beam, allowing the Bragg relation to be satisfied for  $d_2$ ,  $d_3$ ,  $d_4$ , etc. successively as the crystal is turned.

## 4. SAMPLE PREPARATION

---

---

### RANDOMLY-ORIENTED SAMPLE

---

---

Samples submitted for quantitative XRD analysis should ideally be randomly-oriented to overcome preferred orientation of the crystallites. Preferred orientation may have several causes. Preferred orientation can arise due to crystal shape, good cleavages or insufficient grinding.

#### **Crystal shape**

When different minerals crystallise they commonly do so in various shapes. Crystals having a needle-like morphology (e.g. amphiboles) tend to settle with their long axes perpendicular to the gravity field. As an example, tip out a box of matches onto your desk and note their orientations. The chances of finding a match standing on its end is very slim indeed. If the matches were crystals, it can be seen that diffraction of X-rays occurs predominantly from those planes parallel to the z-axis, hence  $hk0$  reflections in an XRD trace would have an enhanced intensity. Similarly, crystals having a platey morphology (most clays) tend to lie with their z-axis parallel to the gravity field. A simple analogy is to empty a deck of playing cards onto a table; most if not all of the cards will lie flat. The chance of finding a card standing on its end is extremely small. Substituting the cards with say kaolin crystals, one can clearly see why the  $00l$  reflections are the main reflections seen in oriented samples due to their preferred orientation.

#### **Cleavage**

Many minerals possess planes of weakness in their crystal structures. When such minerals are crushed and ground they will have a tendency to break or "cleave" along these planes of weakness. When the mineral powder is applied to a sample holder the crystallites will tend to orient themselves so that their cleavages are perpendicular to the gravity field. This effect is greatly enhanced if the crystallites are initially suspended in a fluid (e.g. water, ethanol or acetone) before they settle. The fluid provides a medium through which crystals can rotate into their most stable position. An example of preferred orientation due to cleavage is that of the mineral mica. The covalent bonding within mica sheets is extremely strong compared to the weak van der Waals forces between the sheets. Consequently, when mica is crushed and ground, it will tend to break parallel to these sheets. Since the plane parallel to these surfaces is the (001) plane, and this plane is preferentially exposed to X-rays during XRD, enhancement of the  $00l$  reflections occurs.

#### **Grinding**

To optimise diffraction and improve diffraction statistics, samples should ideally be ground to between 1 and 10  $\mu\text{m}$ . This can be achieved by using an agate mortar and pestle until the sample "feels" smooth and not gritty. Grinding is also effective in

breaking up well-formed crystals so that they do not preferentially lie on crystal faces. Electrostatic forces between crystallites begin to dominate over gravitational forces as the crystallites become finer. As a result, smaller crystallites do not suffer as much preferred orientation as larger crystallites because electrostatic attraction between adjacent crystallites is generally sufficient to prop up ones that would normally lie flat.

### Side-packing holder

A sample submitted for XRD analysis must be randomly oriented to overcome preferred orientation of crystallites. Preferred orientation may be the result of several reasons. Preferred orientation can arise due to crystal shape, good cleavages or insufficient grinding. To optimise diffraction and improve diffraction statistics, samples should ideally be ground to between 1 and 10  $\mu\text{m}$ . This can be achieved by using an agate mortar and pestle until the sample "feels" smooth and not gritty. Grinding is also effective in breaking up well-formed crystals so that they do not preferentially lie on crystal faces. Sedimentation of a sample using a fluid such as water, alcohol or acetone often enhances preferred orientation, as the fluid provides a medium through which crystals can rotate into their most stable position; usually on cleavage planes, if the mineral has good or perfect cleavages. Preferred orientation due to cleavage can be quite a problem. To overcome preferred orientation in such a sample, directional pressure and/or shearing of the sample during packing must be kept to a minimum. One of the best methods available to overcome preferred orientation of crystals while retaining the maximum number of crystals exposed to X-rays, is by gently packing a sample side-ways into a holder. A side-packing holder may be constructed as follows.

### Side-packing holder for the Siemens D500 series X-ray diffractometer

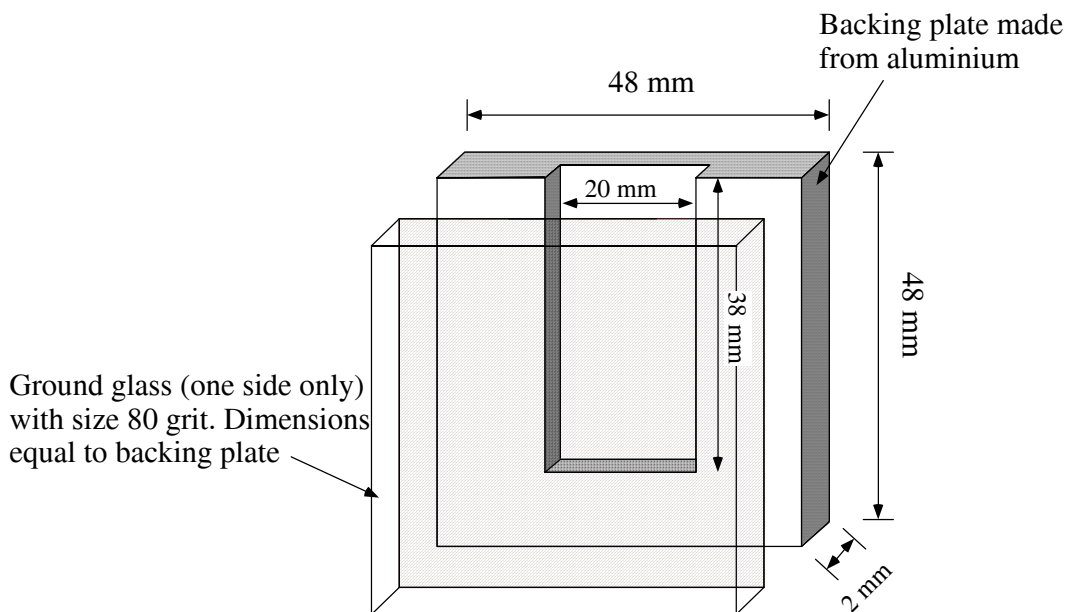


Figure 4.1

To load the holder with a sample, simply spoon the sample in with a spatula or via a funnel made from a rolled piece of waxed paper. As loading proceeds, gently tap the side of the holder on the bench. When the holder is loaded, carefully remove the frosted glass ensuring that there is no side-ways movement of the glass during its removal. The sample is now ready for analysis.

---

---

## ORIENTED SAMPLE

---

---

Preferred orientation can be used to your advantage for the qualitative analysis of clay minerals. The distance between successive layers in the clay structure is generally different for different clays. However, the inter-atomic spacings within the layers are usually quite similar. By orienting a clay sample prior to XRD analysis, enhancement of the  $00l$  peaks, which commonly show the greatest differences in d-spacing, enables easier identification of clay minerals. Further tests such as ethylene glycol saturation and heat treatment (commonly @  $350^{\circ}\text{C}$ ) can be employed for discriminating between smectite, vermiculite and chlorite.

An oriented sample is prepared by passing a clay slurry through a Millipore<sup>®</sup> filter by suction (see figure 4.2).

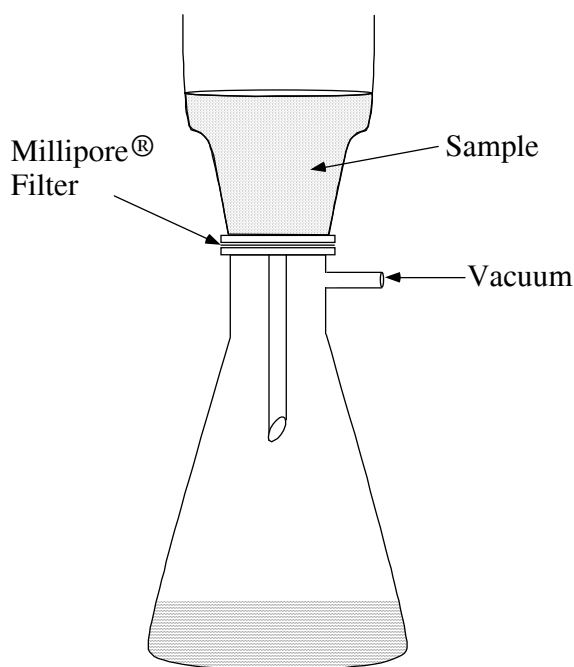


**Figure 4.2**

Once the water has been drawn out of the sample, 0.1 M solution of  $\text{MgCl}_2$  is pipetted onto the clay cake which forms on the Millipore<sup>®</sup> filter. The sample is then washed with a few millilitres of distilled water. The procedure effectively replaces any exchangeable cations with  $\text{Mg}^{2+}$ , standardising the interlayer spacing of smectite and leaves the sample sufficiently salt-free for XRD analysis. Now for the tricky part! The clay cake is transferred from the Millipore<sup>®</sup> filter onto a glass tile. This requires patience and much experience. We suggest that you practice on another sample until you get the knack. The filter is inverted so that the clay cake comes in contact with the glass tile. A drop of water

is added to the back of the filter. Carefully, the filter paper is removed, leaving behind (hopefully!) the clay cake on the glass tile (see figure 4.3).

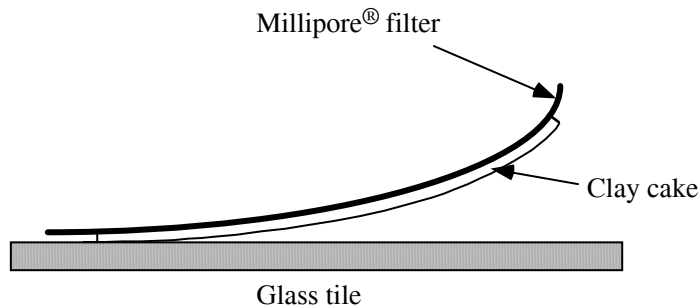


**Figure 4.3**

This method for obtaining an oriented clay sample is preferred over more simpler sedimentation methods because there is no differential settling of clay particles due to density variations. In other words, clay and other fine minerals such as iron oxides are homogeneously distributed throughout the sample.

---

---

### **LOW BACKGROUND HOLDER**

---

---

Sometimes it is not possible to have sufficient sample to side-pack. The method of pipetting a suspension of the sample onto a glass tile is reasonably successful if there is sufficient material to cover the glass. If the sample is too thin, a scattering band from the glass will be evident in the XRD pattern. Preferred orientation may be a problem with this method as well. To overcome preferred orientation with this method the sample can be dusted onto a glass tile that has an extremely thin smear of vaseline. Once again, if there isn't sufficient material to cover the vaseline and glass, a scattering band will be evident in the XRD pattern.

The best method currently available is the use of a low-background holder made from a pure crystal, either a natural or synthetic quartz crystal or silicon metal. To make a low background holder, you must first obtain a crystal that has no obvious flaws or cracks otherwise diffraction can occur at the site of these defects. Next you must ensure that the cut you are going to make is not parallel to any planes that would Bragg diffract X-rays. This is not as difficult as it sounds as there is an infinite number of possible cuts but only a finite number of planes diffraction can occur from. With quartz, we recommend that a cut  $\sim 5^\circ$  to the 001 plane (or  $5^\circ$  from the plane perpendicular to the length of the crystal) should work in most cases. Once a cut has been made, a similar cut parallel to this surface must be made to produce a tile. The tile has to be of sufficient thickness to avoid breakage but thin enough to fit in the diffractometer holder. The surface of the quartz tile must be ground perfectly flat and then polished.

---

---

A sample may be applied to a low background holder either by dusting onto a thin vaseline smear or by depositing a suspension via a pipette. Dusting of the sample onto a vaseline smear virtually eliminates preferred orientation, however may introduce scattering bands (associated with the vaseline). Deposition of the sample in suspension via a pipette eliminates the scattering band problem but enhances preferred orientation.

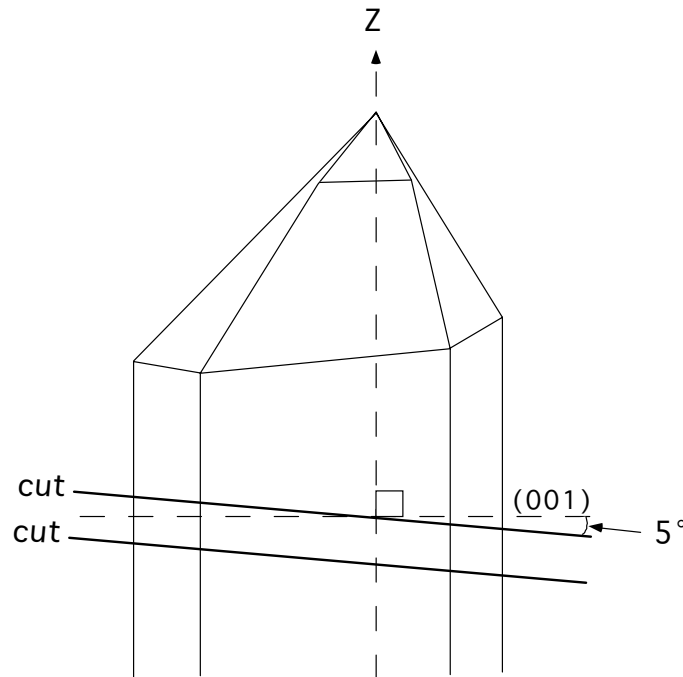


Figure 4.4

A sample may be applied to a low background holder either by dusting onto a thin vaseline smear or by depositing a suspension via a pipette. Dusting of the sample onto a vaseline smear virtually eliminates preferred orientation, however may introduce scattering bands (associated with the vaseline). Deposition of the sample in suspension via a pipette eliminates the scattering band problem but enhances preferred orientation.

---

---

### INTERNAL STANDARDS FOR ANALYSIS OF POORLY-DIFFRACTING MATERIAL (PDM)

---

---

Selection of an internal standard depends on many variables:

1. Ideally the internal standard should have a similar mass absorption coefficient to minerals you want to analyse, to minimise the absorption contrast caused by particle size variations. If you can't avoid this, use a radiation that gives similar mass absorption coefficients.

2. The standard should have no cleavage to minimise preferred orientation and the use of orientation corrections in SIROQUANT.
3. The standard should have a similar density to the minerals you are analysing, particularly if you are using a slurry mount as differential settling causes the heavier minerals to settle first thereby a greater amount of the lighter minerals are exposed to the X-rays.
4. The crystals should be close to 1  $\mu\text{m}$  in size to minimise the use of Brindley particle size corrections.
5. The standard should be wholly crystalline. You can test this by running standards with standards of known crystallinity. For example, I would test with a ground up quartz crystal or similar crystal (however only grind for the minimum amount of time required or you may end up amorphising some of your quartz). Synthetic standards are fine if they are formed under conditions that result in total crystallisation. Some so-called corundums for example, are formed by a heating process, where insufficient heating may result in an alumina product composed of corundum, and transitional aluminas such as gamma-alumina (i.e. poorly-diffracting). Some ZnO samples have appreciable (20%) amorphous ZnO, which renders them useless.

It is extremely important that sample preparation be carried out in the correct manner as well. The sample itself should be between 1 and 5  $\mu\text{m}$  in size with preferred orientation eliminated or kept to a minimum (i.e. side-packing of the powdered specimen is recommended). Certainly Siroquant has a correction for preferred orientation, however it cannot cope with a high degree of preferred orientation.

## 5. CRYSTAL SYMMETRY

---

### THE 14 BRAVAIS LATTICES

---

Crystallographic lattices can have 3 kinds of symmetry: translation, reflection, and rotation. While geometric objects such as an octagon or a 5-pointed star can have other rotational symmetry, and pictures and magnetic materials have colour symmetry, there are only 14 different ways that a repeating lattice can have symmetry, and these are known as the Bravais lattices.

Translation symmetry consistent with a lattice are the unit cell translations and half cell translations.

Planar symmetry elements are reflection (mirror) planes or reflection coupled with half-cell translation (glide planes).

Rotational symmetry elements are simple rotation through  $2\pi/n$  where  $n=1, 2, 3, 4$  or  $6$ , or rotation coupled with cell translation (screw axes).

Unit cells may be *primitive* (P), that is, having one lattice point per cell. In Figure 1a, an oblique cell is drawn with one lattice point per cell. It may look like 4 lattice points per cell, but if the cell edges are shifted slightly (Fig 1b, note that where you conceptualise the unit cell is immaterial, it doesn't HAVE to be fixed on a lattice point, though it usually more convenient to do so), it is clear that there is only one lattice point inside the unit cell.

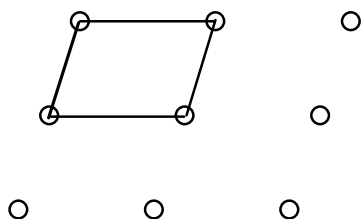


Figure 1a

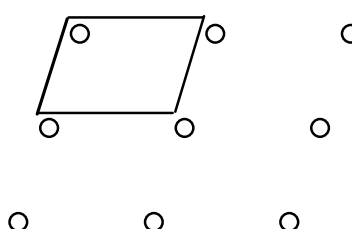


Figure 1b

Lattices may be *centred* (C), having a lattice point at the corners and at the centre of the unit cell. Fig. 2a shows a rectangular P-cell (a 2-D lattice), with mirror symmetry, and Fig 2b shows a centred rectangular lattice with mirror symmetry. The centred lattice has two lattice points per cell.

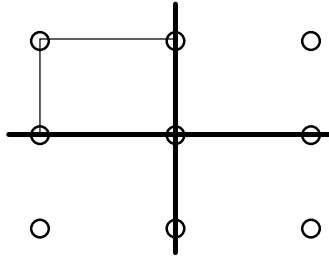


Figure 2a

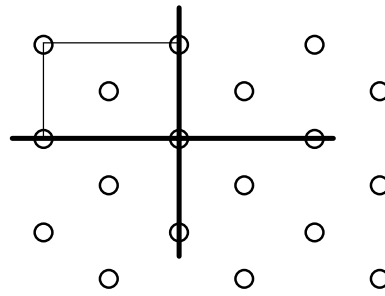


Figure 2b

The lattice of Fig 2b could be described using two equal translation vectors (Fig 3), but these would not be parallel to the symmetry planes, and so this cell is not used.

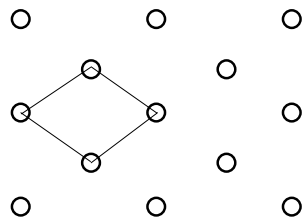


Figure 3

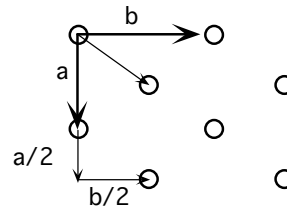


Figure 4

The centred lattice of Fig 2b has 2 types of translation vectors: the unit cell translations  $(a, b)$ , and half-cell translations  $(a/2, b/2)$  (Fig 4). Alternatively, the two half cell translations can be regarded as one half diagonal translation  $(a+b)/2$ .

In addition to its mirror symmetry, the C-lattice has glide-plane symmetry. the mirrors pass through the lattice rows, the glides pass half way between them (Fig 5)

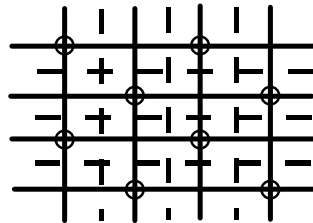


Figure 5: C-lattice with mirror and glide planes

In 3-D, centred lattices may exist on any of the 3 faces of a unit cell. Centring the top (001) face of a cell (C-cell) is no different from centring the front (100, A-cell) or side (010, B-cell) face in terms of the fundamental symmetry; one can be changed to the other by turning the cell about. Centring all 3 faces is different (known as an F-cell), and a lattice can be centred at its centre of gravity (right in the middle: body-centred, or I-cell).

The 14 Bravais lattices that result from combining symmetry with centring are:

	<b>P</b>	<b>A,B,C</b>	<b>I</b>	<b>F</b>	
triclinic	P	=P	=P	=P	
monoclinic	P	C	=C	=C	
orthorhombic	P	C	I	F	
tetragonal	P		I	=I	
hexagonal;	P				R
cubic	P		I	F	

(Trigonal lattices can be referred to hexagonal lattices)

In the monoclinic system, A, and C are interchangeable, while a B-lattice can be redefined as a P-lattice. In the tetragonal, hexagonal, and cubic systems, A and B cells do not conform to the definition of a lattice, and C-cells can be redefined to other lattices.

## UNIT CELL COORDINATES

A crystal is conceived as a repeating array of unit cells. The unit cell has a size and shape ( $a, b, c, \alpha, \beta, \gamma$ ) unique to the crystal species. The cell edges are the translation vectors by which the full crystal is considered to be created by repetitions of the unit cell.

One corner of the cell is given the coordinate  $(0,0,0)$ ; this is the cell origin, and is usually placed at the back, lower, left corner of the cell. The other 7 cell corners then have coordinates such as  $(1,0,0)$ ,  $(0,1,1)$ , etc.

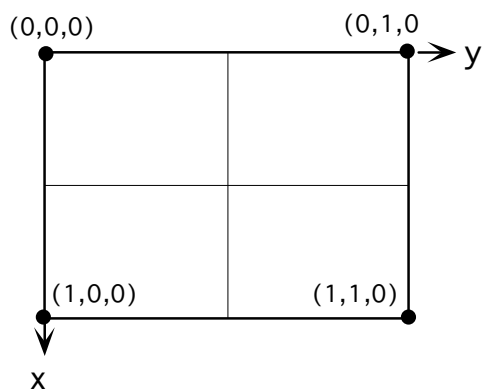


Figure 6: The coordinates of the four corners at the base of a unit cell

A crystal is also described by its symmetry (space group) and by the positions and type of each atom in the unit cell. Both the position of the symmetry element and of each atom are given in  $(xyz)$  coordinates, where the coordinate is a fraction of the particular cell edge.

Atoms within the unit cell have  $(xyz)$  coordinates such that  $0 \leq x < 1$ . Any coordinate  $> 1$  or  $< 0$  is logically in another cell, and since all unit cells are identical, they are crystallographically

equivalent, thus the coordinate  $x=1.34$  is the same as the coordinate  $x=0.34$ . (It is this repetition from cell to cell that lies at the heart of the theory of X-ray diffraction. Both the crystal, and the X-ray wave form are repeating phenomena; one unit cell is the same as the next, one wave form is the same as the next. A mathematical expression that holds for one unit cell holds for all.)

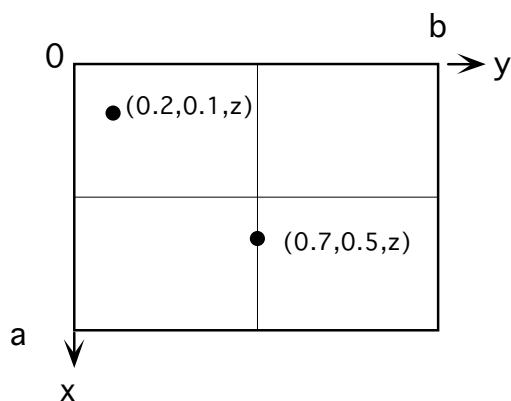


Figure 7

Figure 7 shows a unit cell with dimensions  $a, b, c$ , containing two atoms. One, whose coordinates are  $(0.2, 0.1, z)$  has an actual distance from the origin of  $0.2 \times a$  Å in the X-direction,  $0.1 \times b$  Å in the Y-direction, and with its  $z$ -coordinate unspecified. The other has coordinates  $(0.7, 0.5, z)$ . The coordinates of the atoms are expressed as fractions of the cell edges, not in units such as Ångstroms or nanometres, thus the coordinates have no units. The atomic coordinates for crystalline copper, gold, and caesium, for example, are all the same, even though the nature of these elements differs, as do their unit cell dimensions. Because they happen to be iso-structural, they have identical atomic coordinates. The same is true of, e.g., halite and periclase; they both have cubic symmetry ( $Fm\bar{3}m$ ), and the same atomic coordinates:

Na1	0,0,0	Mg1
Na2	1/2, 1/2, 0	Mg2
Na3	1/2, 0, 1/2	Mg3
Na4	0, 1/2, 1/2	Mg4
Cl1	0, 1/2, 0	Ox1
Cl2	1/2, 0, 0	Ox2
Cl3	0, 0, 1/2	Ox3
Cl4	1/2, 1/2, 1/2	Ox4

only the cell edges (and the atoms themselves) differ.

Symmetry elements themselves have a restricted set of possible positions  $(0, 1/4, 1/2, 3/4)$  as described above. Suppose a mirror exists parallel to  $(010)$ , positioned at  $y=0$ :

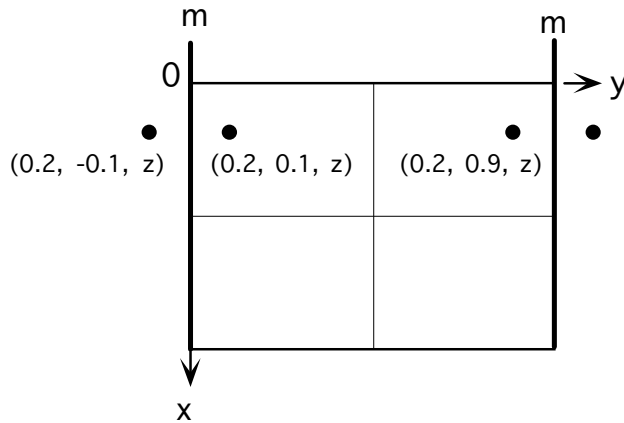


Figure 8

an atom at (say)  $(0.2, 0.1, z)$  has a symmetry related atom of the same species at  $(0.2, -0.1, z)$ , which is its mirror equivalent. Because a crystal is built of repeating unit cells, any atom at  $(xyz)$  has an identical atom at  $(x, y+1, z)$  for example. Thus the mirror equivalent of the first atom has a translation equivalent at  $(0.2, -0.1+1, z)$ , that is, at  $(0.2, 0.9, z)$ . This third atom is necessarily the same distance from the line at  $y=0.5$  parallel to  $(010)$  as the first atom is, only on the other side. That is, atom 3 is the mirror image of atom 1 just as atom 2 is, and there must be a mirror at  $y=0.5$

The mathematics of mirrors would imply that an  $(010)$  mirror at  $y=0$  operates on an atom at  $(xyz)$  to create another at  $(x,-y,z)$ . Naturally no such activity really takes place. The electrostatic attractions and repulsions that stabilise crystals cause the atoms to be positioned in certain symmetrical ways, such that, for example, atom pairs show positional relationships. But to succinctly describe a crystal, it is generally simplest to describe the symmetry and a minimum group of atoms (the so-called asymmetric unit). From these, the whole unit cell can be built up.

---



---

## SPACE GROUPS

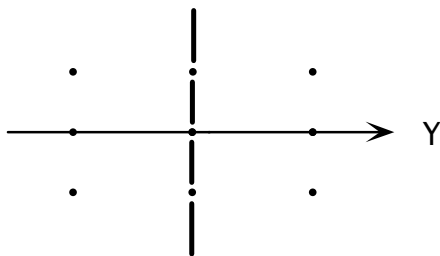
---



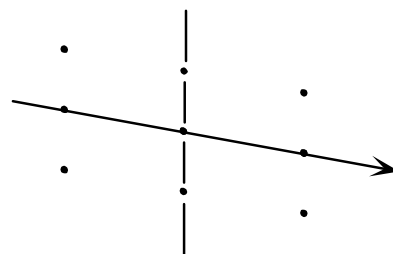
---

Crystallographic space groups are the 230 different ways in which symmetry elements (translation, reflection, rotation) can be arranged in space within the constraints of a lattice.

For example, a reflection plane (mirror) can only exist in a lattice having two axes at right angles.



mirror perpendicular to lattice axis



mirror not possible if lattice oblique

Figure 9

Lattice axes in the plane of the mirror may be inclined, since the mirror does not force orthogonality of axes in its own plane:

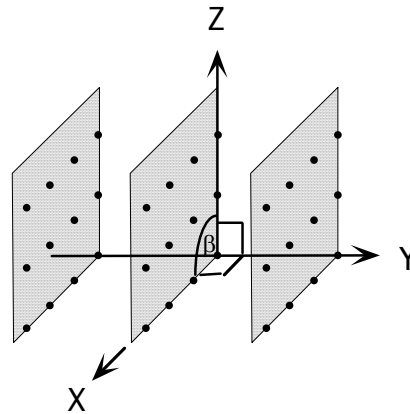


Figure 10: Mirror planes (shaded) in a monoclinic lattice.

Similarly a diad axis imposes the same perpendicular condition on the lattice; the lattice vector parallel to the diad must be at  $90^\circ$  to the other two lattice vectors, but they may be mutually inclined.

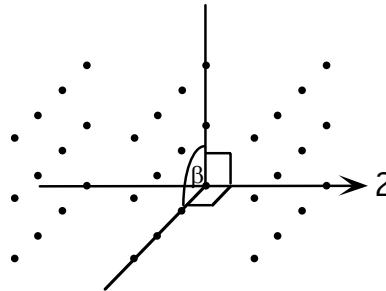


Figure 11: Diad (2) in a monoclinic lattice.

A consequence of the lattice translations is that symmetry elements along lattice rows also repeat half-way between lattice rows:

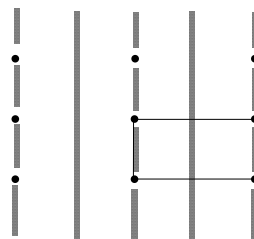


Figure 12: Mirrors at 0, 0.5 (i.e., on the lattice rows and half-way between them)

This is a general result; any symmetry element at coordinate zero repeats at coordinate 0.5, or if at, say coordinate 0.25, there is another at 0.75. Except in the high symmetry systems (trigonal, hexagonal, cubic) symmetry is only found at 0, 0.25, 0.5 and 0.75 of the cell edge.

Space group symbols use a code with up to a 4-positions:

In all systems, the 1st position is the lattice type

P Primitive: P  
A centred on (100)  
B centred on (010)  
C centred on (001)  
I Body centred  
F All face-centred

### **Orthorhombic**

1st position: Lattice type (P,C,I,F)  
2nd position: axes// to X, planes perpendicular to X (= parallel to (100))  
3rd position: axes// to Y, planes perpendicular to Y (= parallel to (010))  
4th position: axes// to Z, planes perpendicular to Z (= parallel to (001))

e.g. C 2/m 2/c 2<sub>1</sub>/a  
short form: Cmca

### **Monoclinic**

1st position: Lattice type (P, C)  
2nd position: 1 (no symmetry parallel to X or (100))  
3rd position: axes// to Y, planes perpendicular to Y (= parallel to (010))  
4th position: 1 (no symmetry parallel to Z or (001))

e.g. P 1 2/c 1  
short form: P2/c

### **Triclinic**

1st position: Lattice type (P)  
2nd position: 1 (no symmetry)

e.g. P1

### **Tetragonal**

1st position: Lattice type (P, I)  
2nd position: axes// to Z, planes perpendicular to Z (= parallel to (001)) (because Z is the high symmetry axis)  
3rd position: axes// to X (=Y), planes perpendicular to X (=Y) (= parallel to (100)=(010))  
4th position: axes// to [110], planes perpendicular to [110]

e.g. P 4/n 2/b 2/m  
short form: P4/nbm

### **Hexagonal, trigonal**

1st position: lattice type (p, r)  
2nd, 3rd, 4th positions as for Tetragonal

e.g. P 6/m 2/c 2/c  
short form: P6/mmc

### **Cubic**

1st position: Lattice type (P,I,F)  
2nd position: axes// to X (=Y=Z), planes perpendicular to X (=Y=Z) (= parallel to (100)=(010)=(001))  
3rd position: triads (//[111])  
4th position: axes// to [110], planes perpendicular to [110]

e.g. F 4/m  $\bar{3}$  2/m  
short form: Fm3m

## DESCRIBING CRYSTAL STRUCTURES

It would be possible to describe the structure of a crystal by giving its cell size and shape and the location and species of every atom in the unit cell. This approach would ignore the computational advantages of recognising symmetry. A unit cell of a simple compound like olivine ( $\text{Mg}_2\text{SiO}_4$ ) has 28 atoms, but of these only the positions of 7 need to be known if the symmetry is known.

To draw the structure, or to have a computer draw it, or to calculate many crystal properties, the algebraic expressions for the positional relation between two symmetry equivalent atoms needs to be determined. We saw earlier how a mirror parallel to (010) passing through (0,0,0) relates two atoms at (x,y,z) and (x,-y,z). This kind of relation can be written for all symmetry elements.

Suppose in the example above the atom has a y-coordinate of zero. The mirror would then relate the atom to itself. This is a special kind of place for the atom to be, actually lying on a symmetry element, and such a coordinate is known as a *special position*.

Atom positions have a *multiplicity* associated with them, depending on their relation to the symmetry. In the cases above, the atom at (x,y,z) is in a *general position* with a multiplicity of 2, the atom at (x,0,z) is in a special position with a multiplicity of 1.

In Fig 6, the black atom at the intersection of the mirror planes has a multiplicity of 1, the grey atom lying on a mirror plane has a multiplicity of 2, the white atom on neither plane has a multiplicity of 4.

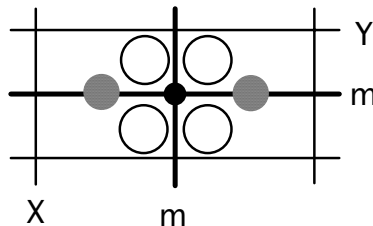


**Figure 6:** Special and general positions.

Position	mult	sym m	code	coordinates	example
General	4	(i)	1	$x,y,z; x,-y,z; -x,y,z; -x,-y,z$	(white atom)
Special	2	(h)	m	$1/2,y,z; 1/2,-y,z$	(grey atom)
Special	2	(g)	m	$0,y,z; 0,-y,z$	(not occupied)
Special	2	(f)	m	$x, 1/2, z; -x, 1/2, z$	(not occupied)
Special	2	(e)	m	$x, 0, z; -x, 0, z$	(not occupied)
Special	1	(d)	mm	$1/2, 1/2, z$	(black atom)
Special	1	(c)	mm	$1/2, 0, z$	(not occupied)
Special	1	(b)	mm	$0, 1/2, z$	(not occupied)
Special	1	(a)	mm	$0,0,z$	(not occupied)

The minimum multiplicity for C-cells and I-cells is 2, because the lattice translation of  $(a+b)/2$  duplicates any and every atom, and for F-cells is 4.

The formulae have been worked out for all of the 230 space groups, and are presented in the International Tables for X-ray Crystallography, Vol 1. A typical page is shown below.

Either graphical or algebraic expressions are sufficient for a human to construct a model of the crystal. For a computer, some algorithm must be programmed. A common approach is to use a matrix that provides an equation relating atoms. In the example above, to convert  $x,y,z$  to  $x,-y,z$ , the x-coordinate must be multiplied by 1, y by -1, z by 1. In high symmetry space groups, coordinates  $(x,y,z)$ , may have a symmetry equivalent  $(z,x,y)$ , or more complex combinations. Thus each coordinate needs room for information about any of x, y, or z, plus any translation symmetry.

In SIROQUANT, the identity symmetry code is 1 0 0 0 for the x position, which is interpreted as: for the x-coordinate take 1 times the read in x value plus zero times y plus zero times z plus zero. Similarly, the y-coordinate would be handled as 0 1 0 0, and z as 0 0 1 0. For a symmetry related atom at  $(x,-y,z)$ , the code is: {1 0 0 0 0 -1 0 0 0 0 1 0}  
For an atom at  $x+1/2, 1/2-y, z$ , the code is {1 0 0 0.5 0 -1 0 0.5 0 0 1 0}

Some programmers are kind, and build all 230 space groups into their programs, so all that the computer needs is the coordinates of the asymmetric unit and the space group number.

---



---

## SPACE GROUP DIAGRAMS

---



---

A space group diagram shows a unit cell shape consistent with the crystal system, the symmetry elements of the space group in standardised diagrammatic form, and all symmetry related motifs of one general position.

For an orthorhombic space group, the diagram uses a rectangular cell, generally viewed down Z, although the direction can be changed to be most convenient

Mirror symmetry perpendicular to the page is shown as a bold line.



Mirror symmetry parallel to the page is shown as two joined bold lines at right angles.



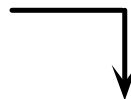
a-, b-, or c-glide symmetry having the translation direction in the plane of the page is shown as a broken bold line



a-, b-, or c-glide symmetry having the translation direction perpendicular to the plane of the page is shown as a dotted bold line:



a-, b-, or c-glide symmetry parallel to the page is shown as a mirror with an arrow on one of the bold lines to indicate the glide direction:



A diagonal glide having the translation direction perpendicular to the plane of the page is shown as a bold dot-dash line:



A diagonal glide having the translation direction parallel to the plane of the page is shown as a mirror plus a diagonal arrow:



Examples using the motif of the number "7" are shown in Figures 13a and 13b

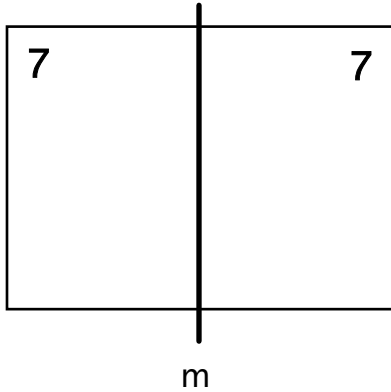


**Figure 13a:** Mirror  $\perp y$ .

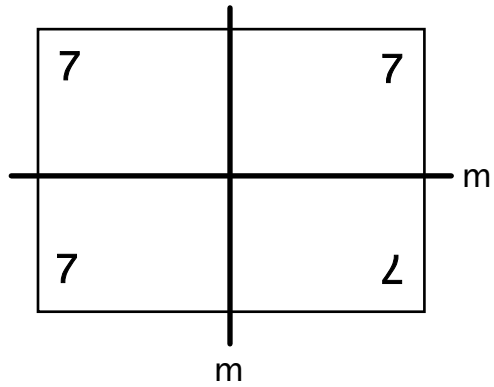
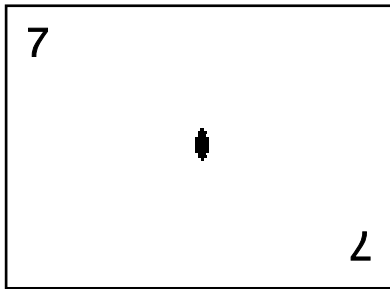


**Figure 13b:** Mirrors  $\perp x$  and  $\perp y$ .

Axes of symmetry are shown as geometric shapes appropriate to the rotational type (eg, a triangle for a 3-fold rotation axis or triad) if the axis is perpendicular to the paper. Only diads parallel to the paper are ever shown (Cubic space groups are too complex for 2-D representation), and diads are represented as an arrow.



$\updownarrow$ , 2: diad

**Figure 14a:** Diad perpendicular to the page.

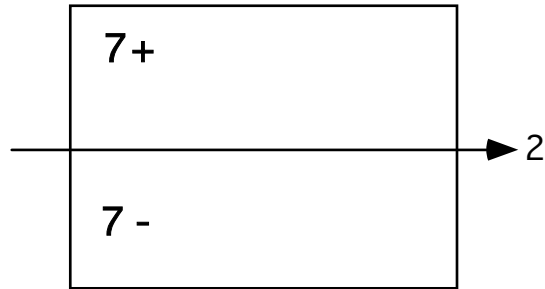


**Figure 14b:** Diad parallel to the page.

Note that in Figure 14b, a new symbolism (+, -) has been introduced to show that the initial motif had a positive z-coordinate, and its rotational symmetry equivalent, where the diad is positioned at  $z=0$ , has a negative z-coordinate.

Combining symmetry may generate more symmetry. Figure 15 shows an (010) mirror with a diad //Y. A centre of symmetry results from this combination. When an axis (R) is positioned perpendicular to a mirror (m), the symmetry is coded as "R/m"

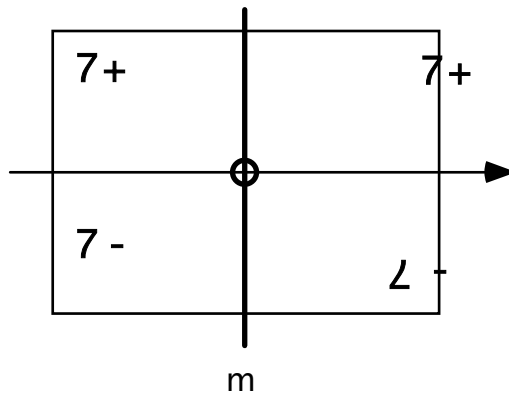


**Figure 15:** Mirror with a perpendicular diad, and a symmetry centre at their intersection.

Once the diagrams become complex, using an asymmetric motif like a “7” becomes rather complicated. In practice, a stylised motif of a small circle is used. If the circle is above the plane of the paper it has a “+” associated, a “-” if below. If symmetry relates a second motif as far below  $z=0.5$  as the original was above  $z=0$ , the motif has “1/2-” associated. If mirror symmetry relates a second motif to the first, this relation is shown by using a “Q” rather than an “O”

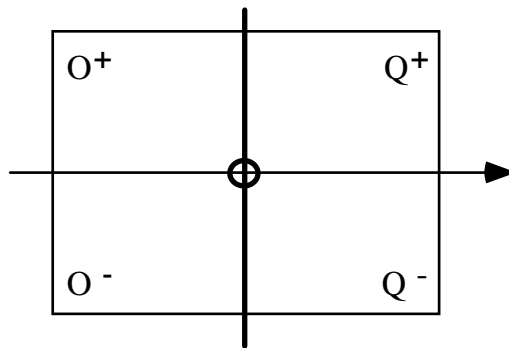


**Figure 16:** Symbolism for the general position in space group P2/m

Glide symmetry combines reflection across the symmetry plane with half-cell translation. Figure 17 shows an a-glide (translation component =  $a/2$ ) oriented parallel to (010).

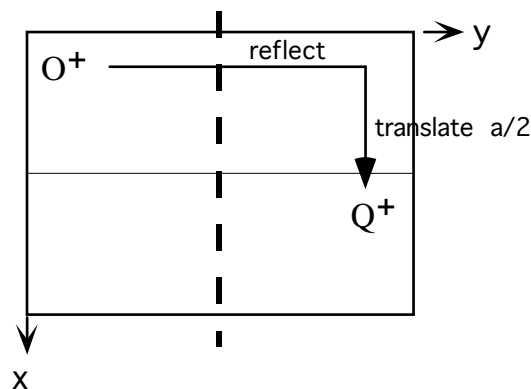


**Figure 17:** a-glide//(010)

The path from the original motif ( $O^+$ ) to the symmetry equivalent  $Q^+$  is shown by the lines labelled “reflect” and “translate  $a/2$ ”.

Combining a glide plane with a rotation axis (diad) at right angles again introduces a centre of symmetry (Fig 18):

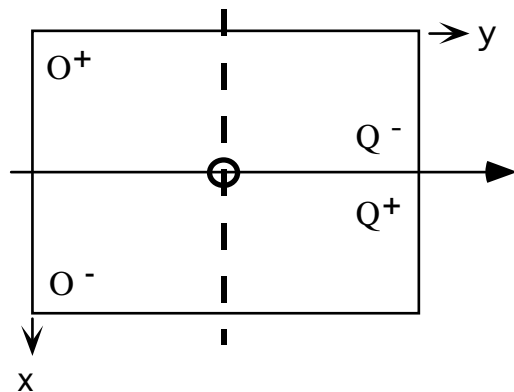


**Figure 18:** Space group  $P2/a$ .

Translation rotation axes (screw axes) operate by rotating the motif through  $360/n^\circ$ , and translating by  $t/n$ , where  $t$  is the cell translation. In the orthorhombic system, only 2-fold rotation occurs, so the operation of a screw diad parallel to  $Z$  would be  $180^\circ$  rotation coupled with  $c/2$  translation (Fig 19). The symbol for a screw axis is  $R_n$ .

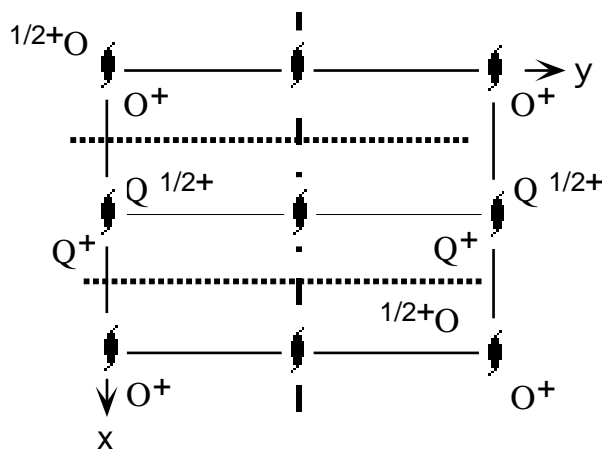


**Figure 19:** Space group  $Pca2_1$ .

---

---

## 6. Intensity of X-ray diffraction

---

---

### Structure factor

We have now seen that a lattice diffracts X-rays in certain directions only, and that these directions have indices  $hkl$ . We saw earlier that the scattering of X-rays from crystals could be seen as the sum of wavelets scattered from successive atoms, and that these atoms lay on a lattice. We also have seen how a crystal is made up of many atoms of different species, occupying different parts of the unit cell. When all these parts come together, we have the total X-ray scattering from the crystal.

To begin, let us consider a simple P-lattice and a simple I-lattice. The P-lattice has atoms at the cell corners. If Bragg diffraction occurs, all these atoms must be scattering in phase, and the total intensity is  $Nf$  where  $N$  is the number of atoms in the crystal, and  $f$  the atomic scattering factor of the atom.

Figure 6.1a shows this situation for the 001 reflection, and Fig 6.1b the same arrangement for an I cell, viewed along the X-axis. Evidently if the waves from successive lattice planes are in phase (but  $1\lambda$  behind each other), the waves from the centred atom in the I-cell example must be  $\lambda/2$  behind the waves from the lattice corners.

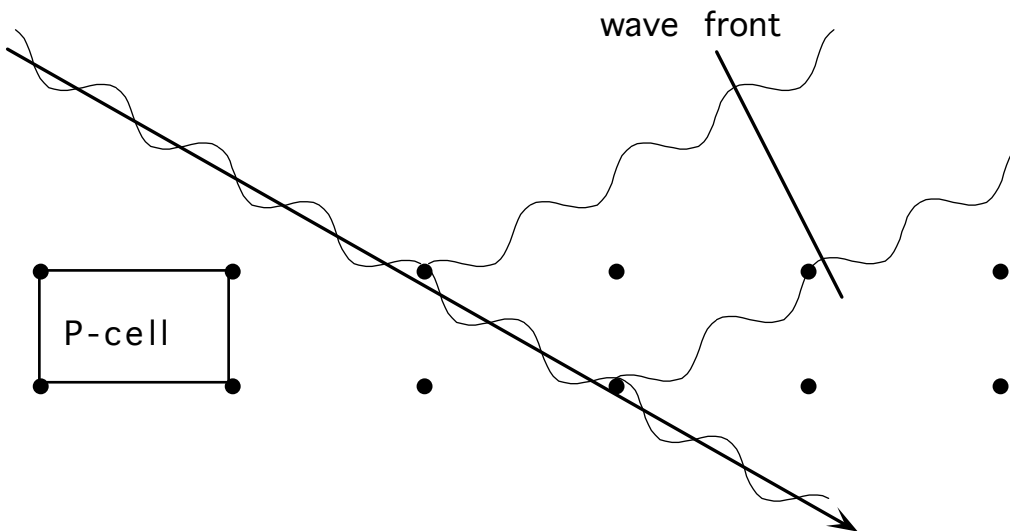


**Figure 6.1a:** 001 reflection from a P-cell.

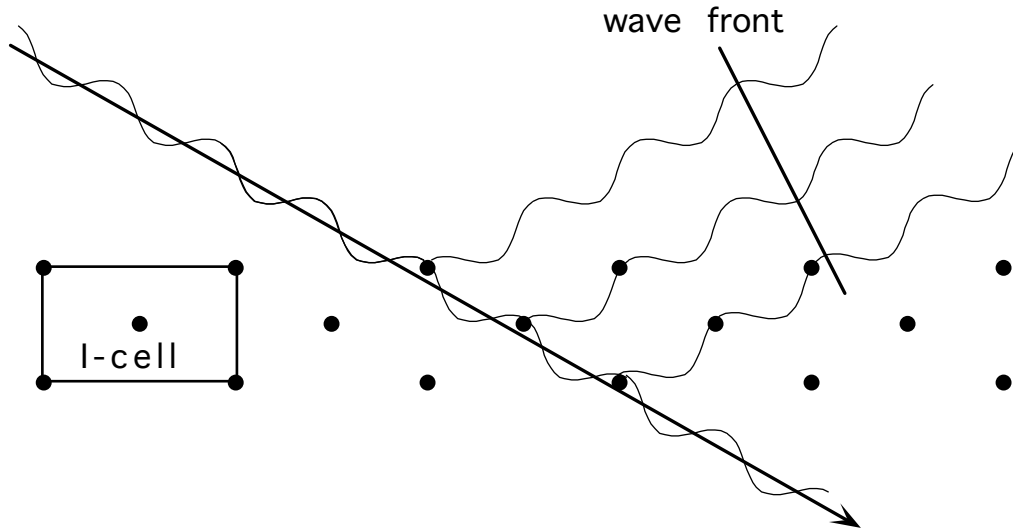


**Figure 6.1b:** 001 reflection from an I cell.

Note that in Fig 6.1a, all waves from all lattice points will add (crests all aligned) whereas in 6.1b, the wave from the centred atom is half a wave out of phase with that from the corner atom, so the net amplitude will be zero.

Fig 6.2 shows the I-cell for the 002 reflection. The path difference for the corner atoms of the lattice is  $2\lambda$ , and for the centred atom it is  $\lambda$ , thus all waves add and the result is non-zero.

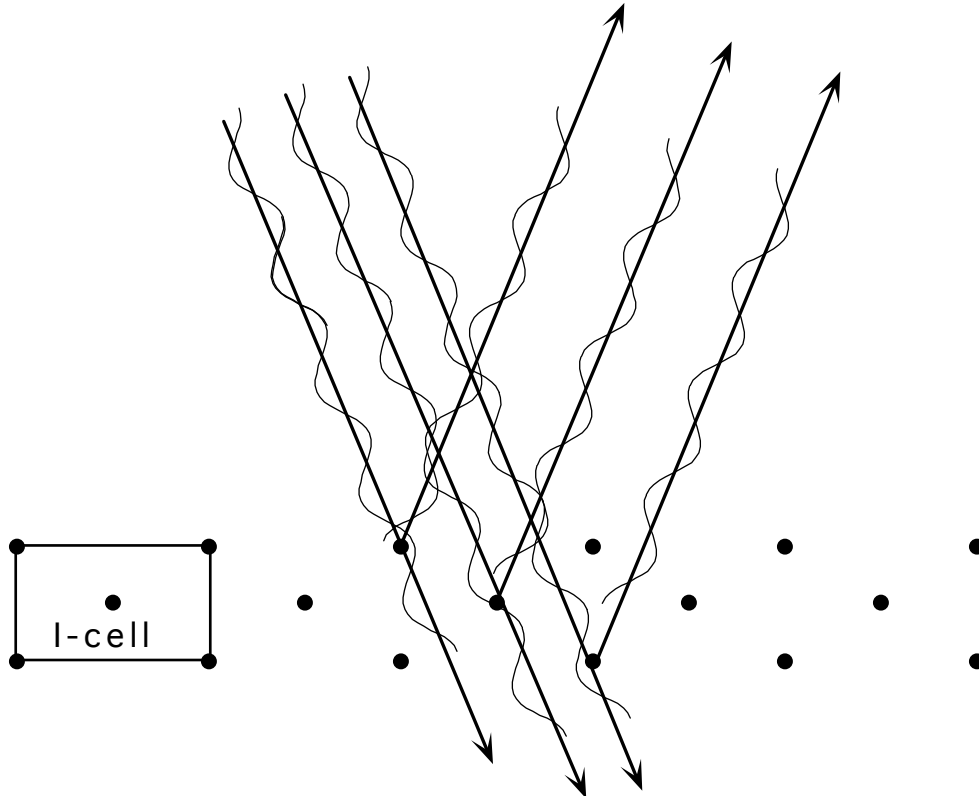


**Figure 6.2:** 002 reflection from an I-lattice.

This result, shown graphically for one type of lattice with more than one lattice point per cell, can be generalised for all reflections and all atoms in a cell, using Fourier series. Remember that the sum of several scattered waves can be expressed by the sum of cosine terms of the phase difference between the waves.

For a first order Bragg reflection, successive lattice planes are one wave behind each other. The phase difference is therefore  $2\pi$ . In the case of the 001 reflection, waves from lattice points at  $z=0$  and  $z=1$  are  $2\pi$  apart. For 002, waves from  $z=0$  and  $z=1$  are 2 waves ( $=4\pi$ ) apart. In general, the phase difference for an atom at  $z$ , relative to an atom at zero is  $2\pi hz$ . If  $h=1$  (first order) and  $z=0.5$  (middle of the cell), then the phase difference is  $2\pi/2 = \pi$ . Since these are lattice points in the case of the I-cell,  $f$  is the same for both, so the resulting wave amplitude is:

$$A = f\cos(0) + f\cos(\pi) = 0$$

For the 002 reflection

$$A = f\cos(0) + f\cos(2\pi \cdot 2/2) = 2f$$

For the 003 reflection

$$A = f\cos(0) + f\cos(2\pi \cdot 3/2) = 0$$

and so on.

We can now expand this equation to all  $hkl$  and all  $xyz$ . If the atom previously considered at  $z=1/2$  is not the same type as the atom at  $z=0$  (ie, the cell is not centred but primitive, with 2 different types of atom in the cell, say an iron at  $z=0$  and an oxygen at  $z=0.5$ , then, taking  $f_{Fe}=26$  and  $f_{Ox}=8$ ,

For 001:

$$A = 26 \cos(0) + 8 \cos(2\pi/2)$$

$$A = 26 - 8 = 18$$

For 002

$$A = 26 \cos(0) + 8 \cos(2\pi)$$

$$A = 26 + 8 = 34.$$

The expression for any  $hkl$  is:

$F_{hkl} = \sum f_i \cos 2\pi(hx_i + ky_i + lz_i)$  where the summation is taken over all atoms (i) in the cell, and  $F_{hkl}$  is called the structure factor, or sometimes the geometric structure factor.

This is a summation that becomes very tedious if there are more than 4 atoms or so in the unit cell. The calculations are easy to perform on a spread-sheet, though you quickly run out of memory if the crystal is very large, and then the job is done by programming a larger machine.

The equation above is valid for centrosymmetric crystals only. If the crystal is non-centrosymmetric, a sine term is also needed, and the maths gets complex. In case you are reading a book, the term above ( $F_{hkl}$ ) equals the amplitude (A) for centrosymmetric crystals, but  $F_{hkl} = \sqrt{\{\sum f_i \cos 2\pi(hx_i + ky_i + lz_i)\}^2 + \{\sum f_i \sin 2\pi(hx_i + ky_i + lz_i)\}^2}$  for non-centrosymmetric crystals.

The table shows an example of a few structure factor calculations for NaCl :

h	k	l	Na			hx+ky+lz(G)	cos 2πG	fcos 2πG	Cl			hx+ky+lz(G)	cos 2πG	fcos2 πG
							fNa =	11					fCl =	17
			x	y	z				x	y	z			
1	0	0	0	0	0	0	1	11	0	0.5	0	0	1	17
1	0	0	0.5	0.5	0	0.5	-1	-11	0.5	0	0	0.5	-1	-17
1	0	0	0.5	0	0.5	0.5	-1	-11	0	0	0.5	0	1	17
1	0	0	0	0.5	0.5	0	1	11	0.5	0.5	0.5	0.5	-1	-17
<b>F=</b>	<b>0</b>						sum Na=	0					sum Cl=	0
1	1	0	0	0	0	0	1	11	0	0.5	0	0.5	-1	-17
1	1	0	0.5	0.5	0	1	1	11	0.5	0	0	0.5	-1	-17
1	1	0	0.5	0	0.5	0.5	-1	-11	0	0	0.5	0	1	17
1	1	0	0	0.5	0.5	0.5	-1	-11	0.5	0.5	0.5	1	1	17
<b>F=</b>	<b>0</b>						sum Na=	0					sum Cl=	0
							fNa =	11					fCl =	17
			x	y	z				x	y	z			
1	1	1	0	0	0	0	1	11	0	0.5	0	0.5	-1	-17
1	1	1	0.5	0.5	0	1	1	11	0.5	0	0	0.5	-1	-17
1	1	1	0.5	0	0.5	1	1	11	0	0	0.5	0.5	-1	-17
1	1	1	0	0.5	0.5	1	1	11	0.5	0.5	0.5	1.5	-1	-17
<b>F=</b>	<b>-24</b>						sum Na=	44					sum Cl=	-68
2	0	0	0	0	0	0	1	11	0	0.5	0	0	1	17
2	0	0	0.5	0.5	0	1	1	11	0.5	0	0	1	1	17
2	0	0	0.5	0	0.5	1	1	11	0	0	0.5	0	1	17
2	0	0	0	0.5	0.5	0	1	11	0.5	0.5	0.5	1	1	17
<b>F=</b>	<b>112</b>						sum Na=	44					sum Cl=	68
2	1	0	0	0	0	0	1	11	0	0.5	0	0.5	-1	-17
2	1	0	0.5	0.5	0	1.5	-1	-11	0.5	0	0	1	1	17
2	1	0	0.5	0	0.5	1	1	11	0	0	0.5	0	1	17
2	1	0	0	0.5	0.5	0.5	-1	-11	0.5	0.5	0.5	1.5	-1	-17
<b>F=</b>	<b>0</b>						sum Na=	0					sum Cl=	0
2	2	0	0	0	0	0	1	11	0	0.5	0	1	1	17
2	2	0	0.5	0.5	0	2	1	11	0.5	0	0	1	1	17
2	2	0	0.5	0	0.5	1	1	11	0	0	0.5	0	1	17
2	2	0	0	0.5	0.5	1	1	11	0.5	0.5	0.5	2	1	17
<b>F=</b>	<b>112</b>						sum Na=	44					sum Cl=	68
2	2	1	0	0	0	0	1	11	0	0.5	0	1	1	17
2	2	1	0.5	0.5	0	2	1	11	0.5	0	0	1	1	17
2	2	1	0.5	0	0.5	1.5	-1	-11	0	0	0.5	0.5	-1	-17
2	2	1	0	0.5	0.5	1.5	-1	-11	0.5	0.5	0.5	2.5	-1	-17
<b>F=</b>	<b>0</b>						sum Na=	0					sum Cl=	0

### **Temperature factor (B)**

The equation for the structure factor assumes that the atoms are exactly at  $(x,y,z)$ . In fact, thermal vibration smears the atom over a volume whose mean centre is  $(x,y,z)$ . This leads to a diminution in the atomic scattering factor which is exponential in  $\sin\theta/\lambda$ . The extent of thermal vibration depends on the temperature, and on structural properties of the crystal. A correction factor ( $=e^{-B(\sin^2\theta/\lambda)}$ ) is applied to all the structure factors. B is determined in the process of full crystal structure determination. Values range from 0.1 to 2, and values of 0.5 for cations and 1 for anions are usually adequate for powder diffraction calculations. B assumes the thermal vibrations are isotropic. For accurate work, anisotropic temperature factors, with up to 6 parameters are used. With B incorporated, the structure factor is

$$F_{hkl} = \Sigma(f_i \cos(2\pi(hx_i + ky_i + lz_i))) \cdot e^{-B(\sin^2\theta/\lambda)}$$

### **Diffraction by a powder**

Single crystal diffraction is used primarily to elucidate the atomic structure of a new crystalline species. It is very rarely used in geology, where the primary aim is to identify a mineral that cannot be identified by other methods (such as petrography). Very commonly, XRD is used to identify fine-grained mixtures of minerals. We therefore need to understand the results of many crystals diffracting all at once. In developing the Bragg relation, it was pointed out that diffraction only occurred at very specific orientations of the lattice to the X-ray beam, and that the crystal had to be turned until it exactly met the Bragg condition before diffraction would occur. An alternate strategy is to use millions of crystallites ( $5\mu\text{m}$  size), oriented at random, and trust to statistics to ensure that all Bragg orientations will occur in a stationary sample (as well as many non-Bragg orientations). In terms of maximising the diffracted intensity, this approach is very inefficient, since maybe only 1% of the crystallites ever get to diffract, but it is very efficient in terms of preparation time and data collection time.

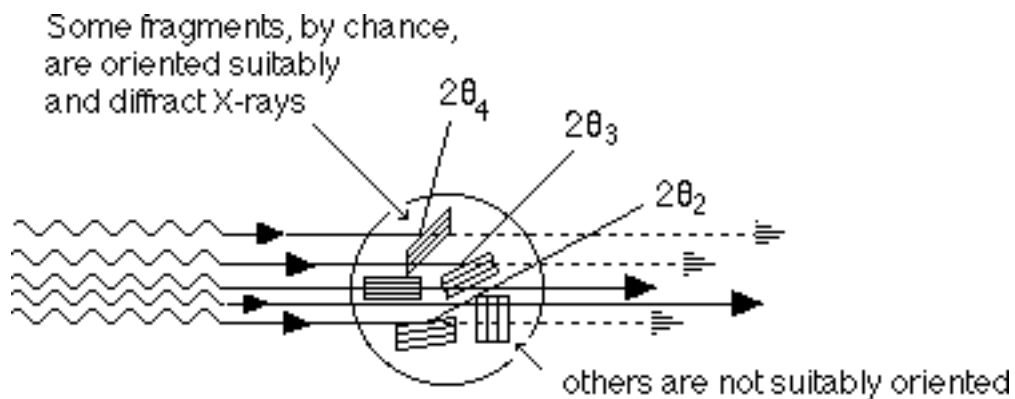


Figure 6.3

In the summary above, you will see that the angle between the incident beam and the diffracted beam is  $2\theta$ . If a crystal has a d-spacing such that its Bragg angle is  $\theta$  to the

incident beam, and there are 10,000 crystallites in a powder all oriented so that this plane is at  $q$  to the beam, but all are differently oriented, the diffracted beams from them all must lie along the surface of a cone of semi-angle  $2\theta$ .

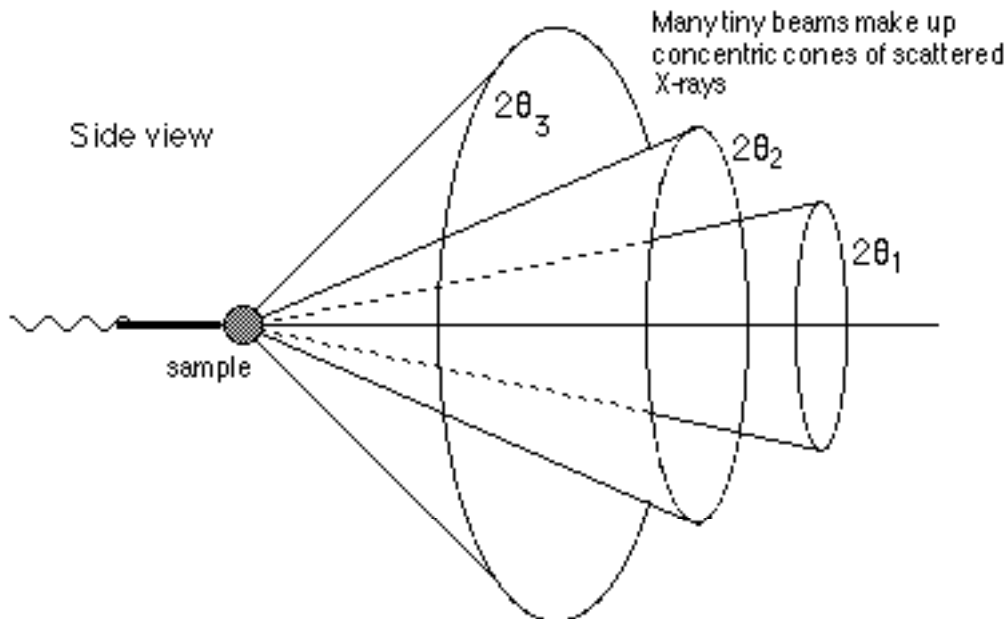


Figure 6.4

The diffraction angles  $2\theta_1$ ,  $2\theta_2$ ,  $2\theta_3$ , ..etc can be easily measured by putting a film around the sample, or by scanning an X-ray detector from  $0^\circ$  to  $180^\circ$  of  $2\theta$ . Provided the crystallites are random, and the sample is sufficiently small, accurate measurements of both d-spacing and intensity can be obtained.

This technique - X-ray powder diffraction - has two instrumental variations. The older, and now less commonly used technique uses a rod of sample, about 1 mm long and 0.2 mm diameter, cohered with an X-ray transparent amorphous glue like nail polish, irradiated by a 1mm diameter X-ray beam in a camera with a cylindrical film surrounding the sample. Camera diameters are either 57.3 or 114.6 mm, constructed to these sizes so that 1mm of film represents  $0.5^\circ 2\theta$  or  $1^\circ 2\theta$ . Angles can be measured from a film to an accuracy of  $0.05^\circ$ . The technique can produce a very usable film from a powder crushed from a crystal fragment as small as 0.2 mm in diameter.

The most commonly used technique, and the major technique for clays, is X-ray powder diffractometry. In a powder diffractometer, the X-rays are detected by scanning an electronic detector from  $0^\circ$  to a maximum of about  $120^\circ 2\theta$ . The sample is prepared as a flat surface, generally about 1 cm square or so, and preferably 0.5 to 1mm thick. Thus the technique is not really suited to very small quantities of powder.

The detector, like the film, can only record Bragg reflection from lattice planes that are in the right position to diffract. The construction of the diffractometer takes advantage of

so-called “focussing” geometry, which requires that the surface of the sample be on a tangent to a circle passing through the source of X-rays, the sample, and the detector.

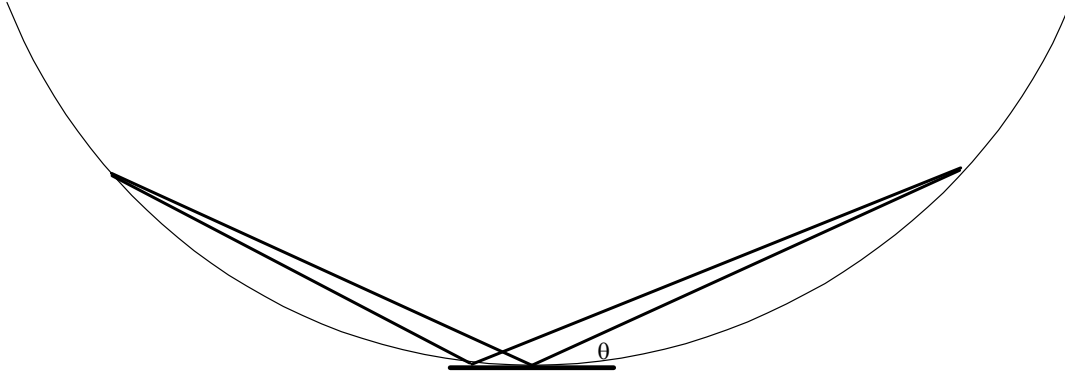


**Figure 6.5**

Any lattice plane oriented tangential to the “focussing circle” is in the Bragg position, and provided the detector is positioned suitably, a diffracted beam will be recorded. Even though in reality the sample is flat, it is close enough to the circle to be regarded as tangential over its 1 or 2 cm length (Fig 6.5).

This geometry ( $\theta$  in,  $\theta$  out) can only be maintained if the sample is rotated at half the speed the detector is rotated, so the instrument is designed in so-called  $\theta/2\theta$  geometry; the sample surface turns to present a changing angle  $\theta$  to the beam, and the detector turns twice as fast to maintain an angle of  $2\theta$  to the direct beam.

The surface of a holder (maybe a glass plate or a cavity holder) is covered by powder (Figure 6.6). All orientations may be present, in which case only those lattice planes parallel to the surface of the sample will be detected (because for all other orientations the detector is in the wrong place at the right time).

Some fragments, by chance, are oriented suitably and diffract X-rays to the detector

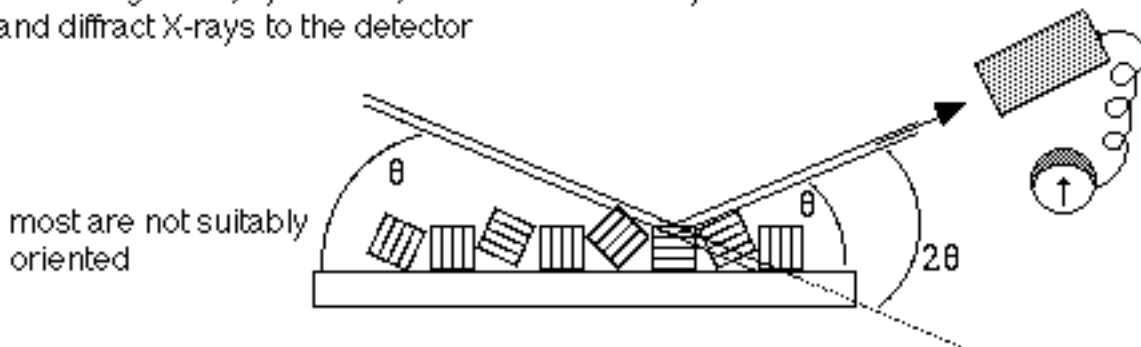


**Figure 6.6**

Provided the sample is quite random in orientation of the crystallites, every Bragg plane will find itself parallel to the sample surface in one crystallite or another, and every possible Bragg reflection will be detected as the detector scans over the range of  $2\theta$ .

### **Multiplicity (M)**

As we saw earlier, symmetry causes overlap of scattering at various Bragg angles. Because there are 6 cube {100} faces, these planes (100), (010), (001) and their negatives all diffract at the same angle. Thus the peak caused by the appropriate orientation of (100) is added to by diffraction from (010) and (001). For the {111} form, there are 8 faces, and therefore 8 overlapping XRD peaks. The number of faces in the form is called the multiplicity of the reflection.

### **Lorentz-polarisation factor (Lp)**

The detector scans at a constant rate, collecting X-rays as it passes across each of the Bragg angles for the particular crystal. Provided the orientation of the crystallites is random, the intensities will be accurately related to the Structure Factors  $F_{hkl}$ . The relation, however, is not direct, because of an effect known as the Lorentz effect. If, as is to be hoped, each Bragg angle  $\theta$  is satisfied by the same number of crystallites, one can imagine that the cones of scattered X-rays shown in Figure 6.4 to be made up of equal numbers of tiny rays directed out from the sample. A small angle cone of rays must have a higher density of rays than a high angle cone, which would pose no problem if the intensity of the whole cone were collected. But an X-ray detector has a limited width window (about 1 cm wide), and the cone of rays is spread over a distance  $2\pi L \sin\theta$  by the time it reaches the detector, ( $L$  is the distance from sample to detector window, typically 120 mm)(Fig 6.7). Thus for a  $30^\circ$   $\theta$ , only about 1/36th of the rays are collected, whereas for a  $10^\circ$   $\theta$  about 1/13th of the rays are detected. Other geometric factors also affect the detection of the X-rays, including a polarisation factor, leading to an overall correction known as the Lorentz-polarization factor, or  $L_p$  factor. For a powder:

$$L_p = (1 + \cos^2 2\theta) / (\sin^2 \theta \cos \theta)$$

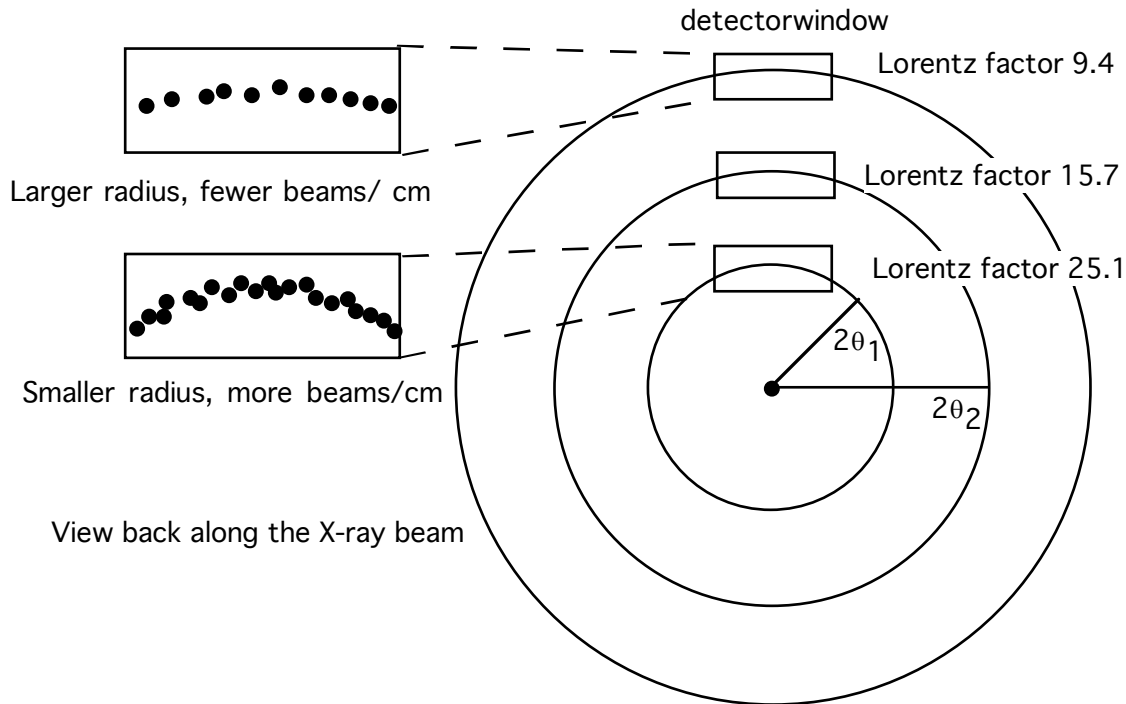


**Figure 6.7:** Diagram showing the origin of the Lorentz factor correction for powder diffraction.

### Absorption

The last of the factors affecting the intensity of X-rays diffracted from a crystal that is intrinsic to the sample is absorption. When x-rays strike matter several processes occur which decrease their intensity. Diffraction scatters a small amount of the energy away from the direct beam, reducing its ability to contribute to the diffracted intensity derived from further in to the sample. Diffraction is elastic scattering (no overall loss of energy). Inelastic scattering also occurs (Compton scattering) which further reduces the intensity, but not by much. The major reduction results from interaction with the electrons of the crystal and the displacement of the electrons from their stable energy levels. Outer shell electrons are easily displaced, absorbing some of the X-ray energy, and causing heating in the sample. Inner shell electron require more energy to shift, and in the extreme case, all the energy of an X-ray quantum may be absorbed and the electron ejected from that atom. In these processes there is no overall energy loss. The energy absorbed by the sample is re-emitted as radiation of a longer wavelength, but the net result is a loss to both the incident and diffracted X-ray beams, and consequently a reduction in the intensity observed at the detector.

The relation is exponential. For a sample length  $x$ :

$$I = I_0 e^{-\mu x} \quad \text{where } \mu \text{ is the linear absorption coefficient.}$$

The linear absorption coefficient ( $\mu$ ) depends on the density of the crystal, the composition of the crystal, and the wavelength of the incident X-rays. Tables of the mass

absorption coefficient ( $\mu/\rho$ ) for all elements and for all the commonly used X-ray targets have been tabulated, and from these  $\mu$  can be calculated according to:

$$\mu = \rho \sum g_i (\mu/\rho)_i$$

where  $g_i$  is the mass fraction of the  $i$ th element (obtained from the known chemical composition of the crystal) and  $(\mu/\rho)_i$  its mass absorption coefficient. Clearly  $\mu$  cannot be calculated for an unknown sample, and this correction can only be applied once the identity of the material is known. Absorption is usually only considered for quantitative phase analysis.

Absorption becomes severe when the sample being X-rayed contains an element with a K-shell energy slightly less than the energy of the X-ray. In this situation, a great deal of the incident energy is used up in creating photo-electrons and causing X-ray fluorescence. Absorption is not therefore simply related to wavelength and atomic number. It decreases approximately in proportion to the third power of wavelength, but rises sharply when an energy is reached that allows photo-emission. Particularly inconvenient in this regard are the pair of Cu  $K\alpha$  radiation and Fe-rich samples, because Cu radiation excites characteristic radiation in Fe. Fe-rich samples are best studied with Co-radiation.

### Preferred orientation

A major factor affecting the intensities of diffractometer experiments is the degree to which the powder sample is truly random. Because only lattice planes parallel to the sample surface are in the Bragg position when the detector is placed to receive their diffraction, any preferential orientation of planes parallel to this surface will enhance this lattice plane at the expense of all others. So, for example, flakes of mica deposited on a glass slide will all lie with (001) parallel to the slide surface, and only 001, 002, 003,...etc diffracted beams will ever be detected by a diffractometer (Fig 6.8). Similarly, calcite will tend to orient with its cleavage {104} parallel to the surface, and amphiboles will lie with their z-axis (prism zone) parallel to the surface, enhancing {hk0} reflections at the expense of {hkl} and {001}.

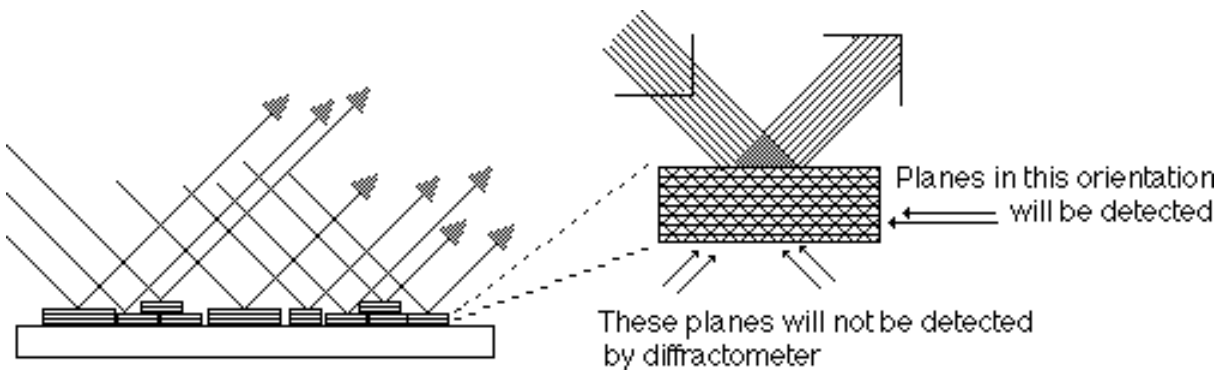


**Figure 6.8:** Preferred orientation in diffractometry.

It is almost impossible to eliminate this effect from minerals with excellent cleavage. Random orientation can be approached by using a grease as the substrate, though this increases the background scattering. Packing the sample so that its surface is never pressed or flattened also helps. For quantitative analyses, a preferred orientation factor can be included in the calculation of theoretical intensity, but a correction to bad data is never as good as good data in the first place.

When all factors are taken into account, the intensity (I) is calculated from:  $I = MALpF^2$

### **The pattern**

The resulting pattern consists of sharp diffraction maxima (peaks) positioned at various angles ( $\theta$ ) (Fig 6.9). Most machines record  $2\theta$  as the angle because  $2\theta$  is the angle between the incident X-ray beam and the diffracted beam. The positions of the peaks mark the angles at which the Bragg condition is satisfied, each peak has associated hkl indices. The intensities of the peaks vary because F, their structure factors varies. The maximum intensity of any peak decreases with increasing angle because of the decrease in f (atomic scattering factor), B (temperature factor) and Lp factor.

This pattern is a "finger-print" of the crystalline substance, because the peak positions depend on the cell dimensions and lattice shape, and the peak intensities depend on the atomic structure. Unless a pattern of the particular phase is on file, the substance cannot be identified by this technique, although much could be discovered about a completely unknown or new crystalline substance by X-ray diffraction. To identify an "unknown", a data file (the International Centre for Diffraction Data, or ICDD file) is used (Formerly known as the JCPDS PDF (Powder Diffraction File). This file is arranged in order of the position (d-spacing) of the most intense diffraction maxima (peaks). For the pattern below (Fig 6.9), the d-spacing of the peak at  $36.2^\circ$  would define the group in which to search, the peak at  $26.4^\circ$  would then be used to search within that group, then the other stronger peaks used to find a good overall match. Confirmation would follow by reference to every peak in the pattern.

### Typical X-ray diffraction pattern

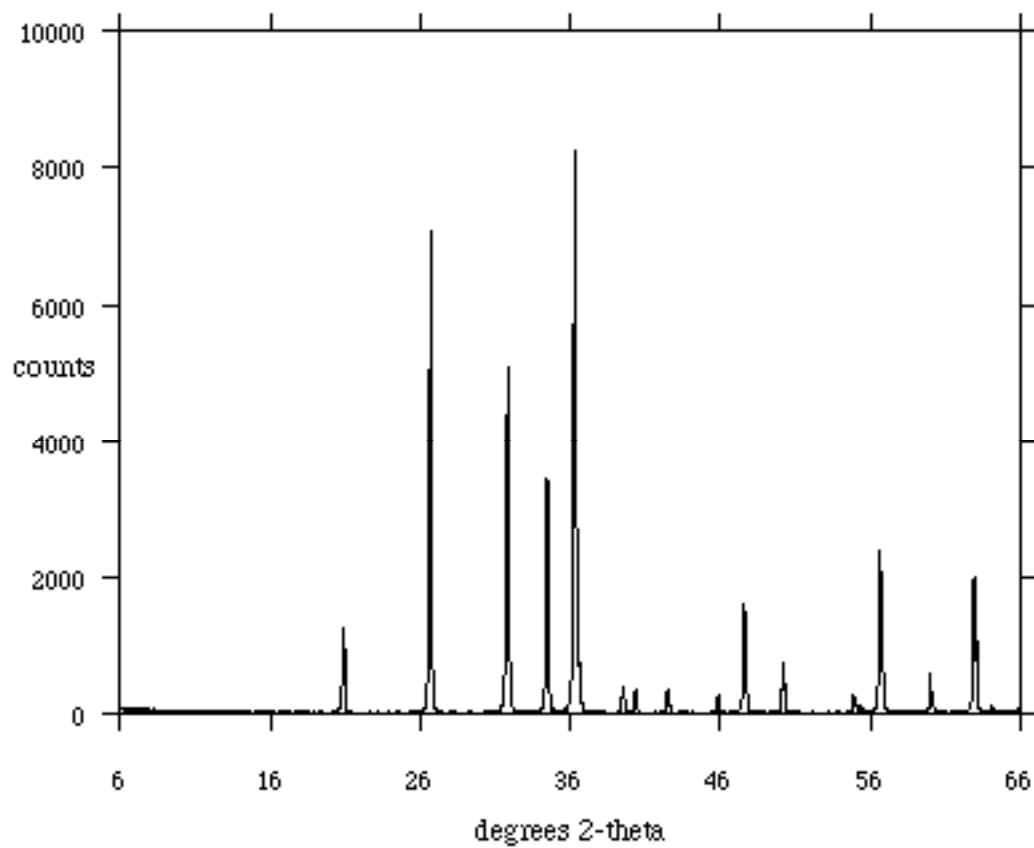


Figure 6.9

## 7. X-RAY IDENTIFICATION OF CLAY SILICATES

All the clay silicates have similar structures, their major differences to X-rays come from different thicknesses of the layer, and therefore show as different basal spacings,  $d_{001}$ . To enhance this difference, clay samples are settled from water onto a glass slide so that the basal planes all lie flat. For better preferred orientation, the sample can be centrifuged onto a porous tile or suction filtered onto a millipore filter.

Distinction between clays can then be made from the first reflection: 7.2 Å from kaolin, 10 Å from illite, 14.2 Å from chlorite or vermiculite, 15 Å from smectite. But inevitably it is not quite so simple. Smectite, chlorite and vermiculite peaks may occur in the one sample and overlap, and chlorite has a strong 7.2 Å line exactly on top of kaolinite, and so kaolinite may be hidden from detection. A full protocol of tests is needed to make a certain identification.

1. Fully disperse the clay in water, extract a subsample and make an XRD oriented clay mount.
2. Run a diffractometer scan from  $4^\circ 2\theta$  to  $40^\circ 2\theta$  Cu  $K\alpha$ .
3. If any scattering exists in the region of  $5-10^\circ$ , Mg-saturate and rerun, to ensure vermiculite is fully expanded to 14.5 Å
4. Saturate the sample with ethylene glycol (24 hours over ethylene glycol at  $50^\circ$ ) and run  $3^\circ$  to  $20^\circ$  to look for smectite, which expands to 17 Å with glycol.
5. Heat to  $300^\circ$ . Smectite and vermiculite collapse to 10 Å, chlorite (14.2 Å does not).
6. Heat to  $550^\circ$ . Kaolinite (7 Å) vanishes, chlorite (14, 7 Å) does not.

### Summary of the results of simple clay silicate XRD tests.

Note that most clays give prominent second and higher order reflections at  $d_{001}/2$ ,  $d_{001}/3$ ,  $d_{001}/4$  etc. e.g., oriented kaolinite has peaks at 7.2 Å, 3.5, 2.4 Å, illite at 10 Å, 5 Å, 3.33 Å, 2.5 Å etc. The second order from smectite (7.5 Å) is often weak, while a reflection at about 3.1 Å may be present

All clays, if not absolutely perfectly oriented, give an 020 reflection at about 4.5Å. Halloysite cannot be stopped from showing its 020 by sample preparation as it is not a platy mineral and is always random.

Mineral	basal		spacing ( $d_{001}$ ) glycolated	300°	550°
	as collected	Mg-saturated			
kaolinite	7.2	7.2	7.2	7.2	gone
halloysite	10	10	10	7	gone
illite	10	10	10	10	10
smectite-Na	12.5	15	17	10	10
smectite-Ca	15	15	17	10	10
vermiculite-Na	12.5	14	14	10	10
vermiculite-Mg	14	14	14	10	10
chlorite	~14.2	~14.2	~14.2	~14.2	~14.2

Interstratified clays give an XRD pattern which varies with the degree of regularity of the sequence. A perfectly regular illite-smectite gives sharp reflections at  $(10+15)\text{\AA} = 25\text{\AA}$ ,  $12.5\text{\AA}$ ,  $8.33\text{\AA}$ ,  $6.25\text{\AA}$  etc. Random illite smectite gives a broad peak between 15 and  $10\text{\AA}$ , with its maximum closer to the d-spacing of the more abundant component. Various treatments move the peak according to the effect on each component; e.g. glycolating a random IS mineral yields a poor peak around  $(17+10)/2 = 13.5\text{\AA}$ , and a better one at  $(10+17/2)/2 \sim 9\text{\AA}$ . With some figuring, a randomly interstratified clay can be fairly well interpreted, but it is often sufficient just to note its presence.

---

### OCTAHEDRAL SHEET DIMENSION: THE b-AXIS

---

The cell dimensions of the clay silicates and the oxy-hydroxides of iron and aluminium are determined by the size of the metal-oxygen octahedron. Trioctahedral minerals have a larger octahedral sheet than dioctahedral minerals, both because the structure collapses somewhat about the vacant site in a dioctahedral structure, and because the ionic radius of  $\text{Al} < \text{Mg}$ , and of  $\text{Fe}^{3+} < \text{Fe}^{2+}$ . Since the octahedral sheet is trigonal in symmetry, it has 3 equivalent X-axes, but it is more convenient to describe the lattice using the same axes as most clays have. These are the so-called ortho-hexagonal axes, in which  $a = \sqrt{3}b$ . Along the Y-axis of this arrangement are 3 metal octahedra (Fig 7.4), all of which are occupied in the trioctahedral species, only two in the dioctahedral clays. The b-axis is therefore 3 times the O-O distance in a metal-oxygen octahedron. Some examples are:

Mineral	composition	b-axis	cation radius
Greenalite*	$\text{Fe}_3\text{Si}_{2.4}\text{O}_{6.6}(\text{OH})_{2.4}$	$9.7\text{\AA}$	0.77
Brucite	$\text{Mg}_3(\text{OH})_6$	$9.3\text{\AA}$	0.72
Nontronite	$\text{Fe}_2\text{Si}_4\text{O}_{10}(\text{OH})_2$	$9.06\text{\AA}$	0.65
Gibbsite	$\text{Al}_2(\text{OH})_6$	$8.68\text{\AA}$	0.53

\* Greenalite is a modulated layer silicate, but the octahedra determine the cell edge, not the unusual tetrahedral sheet.

Note that the dioctahedral species have much smaller b-axes than the trioctahedral. This leads to an easy distinction between the two classes of minerals using the very strong 060 reflection. Dioctahedral species have  $d_{060} \leq 1.51\text{\AA}$ , whereas the trioctahedral group have  $d_{060} > 1.51\text{\AA}$ .

To measure the 060 reflection the sample must be random; any preferred orientation so diminishes the 060 intensity that its measurement becomes questionable.

---

## EFFECT OF DEFECTS ON THE XRD PATTERN

---

### Point defects

No natural crystals are perfect. The lattice continuity is interrupted by the presence of random extra atoms, or missing atoms. These occur spontaneously and their extent can be predicted from thermodynamics. They cause random scattering of incident X-rays, and contribute to the general background radiation of an XRD pattern.

### Line defects

Line defects are of two types: edge dislocations and screw dislocations. Both occur where a plane of atoms terminates inside a crystal, causing the planes on either side to be distorted around the edge of the terminated plane. If the edge is straight and parallel to a lattice plane, the defect is an edge dislocation (Fig 7.1), if the defect spirals through the crystal, it is called a screw dislocation. Identifying dislocation types requires electron microscopy.

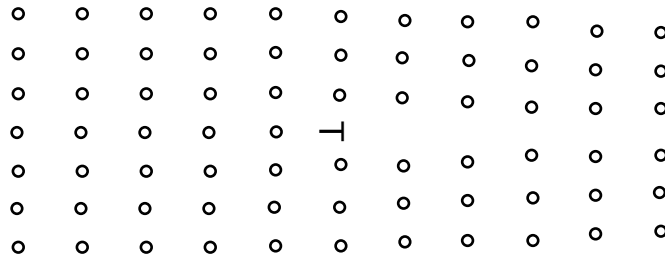


Figure 7.1: Edge dislocation The position of the dislocation is marked "T".

The lattice orientation of a crystal changes very slightly across a dislocation, causing the exact Bragg condition for the crystal to extend over a small angular range. This introduces broadening of the diffraction peak, as the Bragg condition is met for different parts of the crystal at different angles. The dislocation also interrupts the regularity of the lattice repeat ( $a$ ,  $b$  or  $c$ ); for example if the terminating plane is parallel to (001) as in Fig 7.1, the  $c$ -repeat will be  $=c$  before the plane terminates, then in the next unit cell it will be  $<2c$ , and gradually decrease to  $c$  again over successive unit cells. For this region of the crystal  $c$  is variable, hence (001) won't "know" exactly what  $d$ -spacing it should be, and cooperative diffraction will occur over a wider angular range than expected. Again, the diffraction peak will be broadened, and some scattering will occur well away from the Bragg peaks, introducing more background.

### Grain boundaries.

At grain boundaries both point and line defects accumulate, so these areas become rather glass-like. The X-ray scattering from glasses is almost random; glasses yield broad humps centred on the mean interatomic distances in the glass. Silica glass, for example,

gives a hump at about  $4\text{\AA}$ , corresponding to Si-Si distances in cristobalite and tridymite. Such "glassy" regions between crystallites adds further to the background scattering.

### Crystal size

As we saw in the development of diffraction theory, the very existence of Bragg maxima (XRD "lines") depends on lattice regularity and repetition. Only relatively regular lattices with many repeating unit cells yield sharp XRD peaks. If the unit cells only repeat for a short distance, waves scattered from one unit cell at a small angle to the ideal Bragg direction will not be eliminated by destructive interference from a more distant cell. This leads to broadening and lowering of the Bragg peak (Fig 7.2). Such peaks are poorly resolved from each other and from the background, and in the extreme case (crystals of 5-10 nm diameter) may become undetectable by routine analysis.

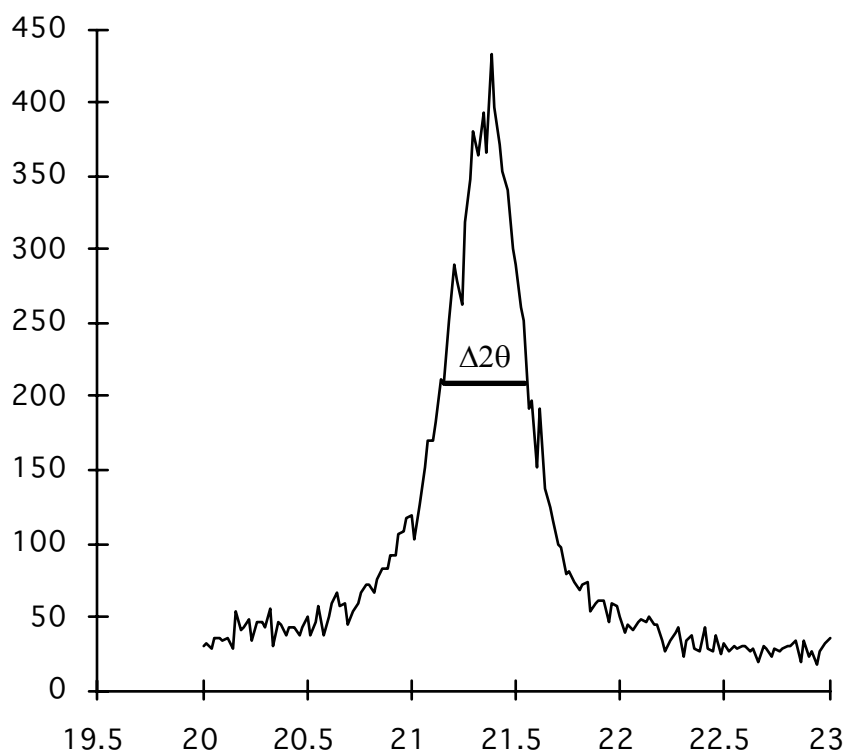


**Figure 7.2:** Peak broadened by small crystal size (ca  $250\text{\AA}$ )

### Crystal size estimation

The broadening of the diffraction peak can be used to estimate the size of the diffracting domains in the crystal. (Peak broadening is commonly referred to as being related to "crystallinity". It is actually related to the size of the coherently diffracting domain. The domains may be themselves be perfect (have high crystallinity) but be very small and produce broad peaks. Crystallinity is not a well-defined term.)

Because the width of the XRD peak depends on the number of cooperatively diffracting unit cells, a relation can be found between the peak width and the domain size. Peak width is defined as the width of the peak at a point half-way up, and is known as the width at half maximum or the half-width for short; its symbol is  $\Delta\theta$  and it is measured in radians. The true half-width must be corrected for instrumental broadening of about  $0.2^\circ$  ( $\Delta\theta_I$ ), broadening which arises because all diffractometers have diverging beams and the sample is not truly positioned on the "focussing" circle.

If the half-width observed is  $\Delta\theta_o$ , the crystal half-width  $\Delta\theta = \sqrt{(\Delta\theta_o^2 - \Delta\theta_I^2)}$ . From  $\Delta\theta$ , the crystal size (L) can be estimated from the Scherrer equation:

$$L = 0.9\lambda/\Delta\theta.\cos\theta$$

The accuracy of this estimate is quite low, because only in the rarest case are the crystallites all the same size. In the example of Fig 7.2,  $\Delta\theta_o = 0.4^\circ$ , from which  $L = 233\text{\AA}$ . Normally one would only quote L to a precision of about 5 nm (eg, a crystal size estimate calculated as  $233\text{\AA}$  would be quoted as  $\sim 250\text{\AA}$  (25 nm)

A second effect of small crystal size is a shift in the position of the Bragg maximum. The intensity of X-ray diffraction peaks depends on the structure factor (F) and the  $L_p$  factor, both of which can change significantly over a small angle. F depends on  $hkl$ , values which are necessarily integers from the derivation of the Laue equations or the Bragg equation. But if diffraction is occurring from a non-ideal crystal, the strict integer values of  $hkl$  are lost, and one can imagine that at a small angle to the true Bragg position, an index can be regarded as, say  $0.9h$ . Or considering the 00l sequence from a layer silicate, the region between 001 and 002 can be regarded as a region of continuous scattering, with indices 001, 001.1, 001.2, 001.3.....001.9, 002, 002.1, or any finer divisions of l you wish. Taken to the extreme, the structure factor F can be calculated for scattering from one unit cell alone as  $F = \sum f_i \cos(2\pi l z)$  where  $l$  is now a continuous variable, not an integer.

Now suppose that  $F^2$  is rapidly declining as the index increases, and we are looking at a low angle peak (say 110 from goethite). The intensity at  $h,k < 1$  is greater than the intensity at the exact Bragg position ( $h,k = 1$ ), and the  $L_p$  factor is greater also. These combine to make the peak shape asymmetric, higher to the low angle side. The located peak position, whether found by eye or computer algorithm, will be to the low angle side of the true Bragg position, and the observed d-spacing will be wrong (Fig 7.3).

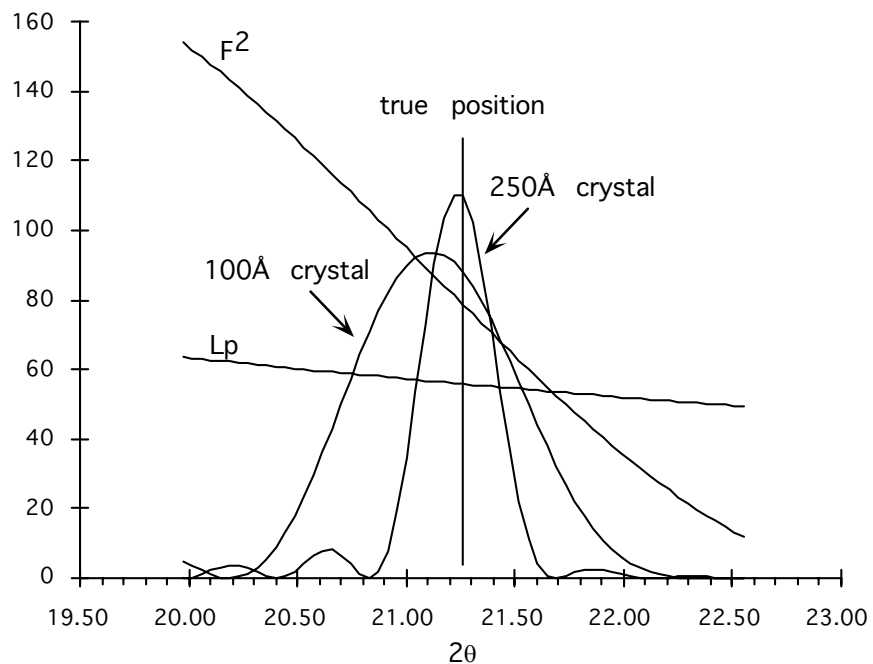


**Figure 7.3:** Peak displacement for goethite 110 reflection caused by small crystal size.

### Stacking faults

Clays and other layer-structured crystals commonly have stacking faults. These are changes in the successive position of the layers. A perfect clay crystal has each layer repeating in regular crystallographic continuity. Two factors lead to a breakdown of this regularity. Clay layers are hexagonal (Fig. 7.4), but the full symmetry of most clay minerals is lower, monoclinic or triclinic.

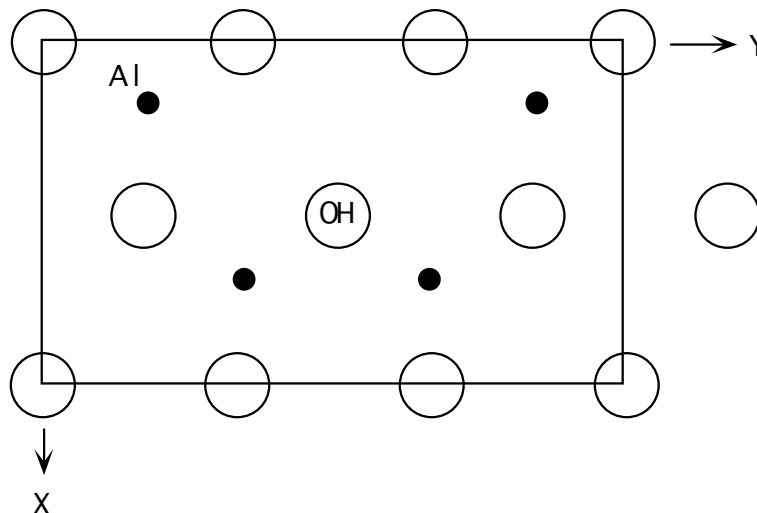


**Figure 7.4:** Hexagonal arrangement of the octahedral sheet.

This low symmetry results from the distribution of Al and Si not being hexagonal, and also from the positioning of one layer above the next. The Al/Si distribution reduces the

layer symmetry to orthorhombic, (Fig. 7.5) and the H-bonds between layers cause offsets that introduce  $\beta$ -angles, causing monoclinic or triclinic stacking.

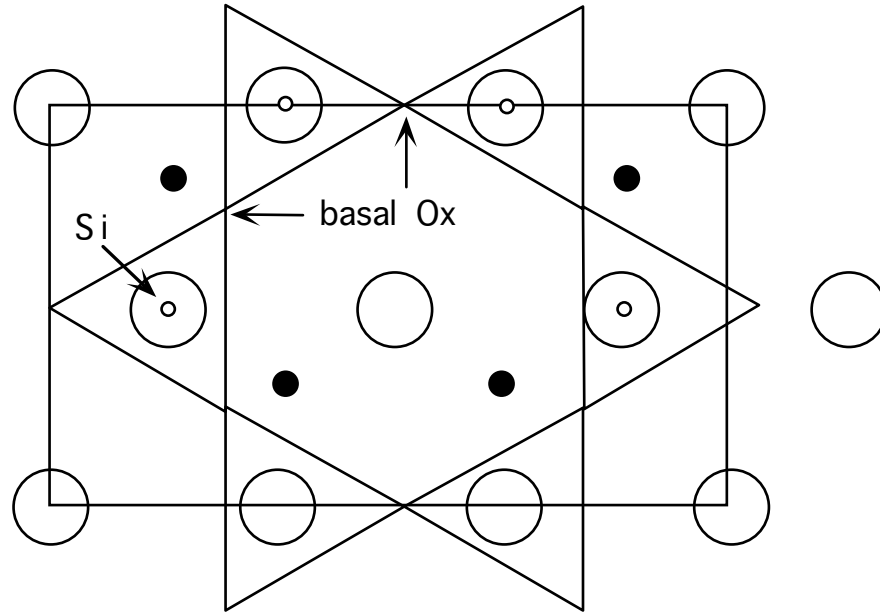


Figure 7.5: Hexagonal arrangement of the tetrahedral sheet.

But because of the hexagonal layer shape, there is very little energy difference between positioning one layer on the next in the same orientation, or in an orientation rotated by  $60^\circ$ ,  $120^\circ$ , or  $180^\circ$  (Fig 7.6a). Alternatively, because the oxygen positions repeat at intervals of  $b/3$ , layers may be displaced by  $b/3$  in any of the directions  $[010]$ ,  $[110]$ , or  $[\bar{1}10]$  and still maintain good H-bonding (Fig 7.6b). Such deviations from perfect lattice regularity are called stacking faults.

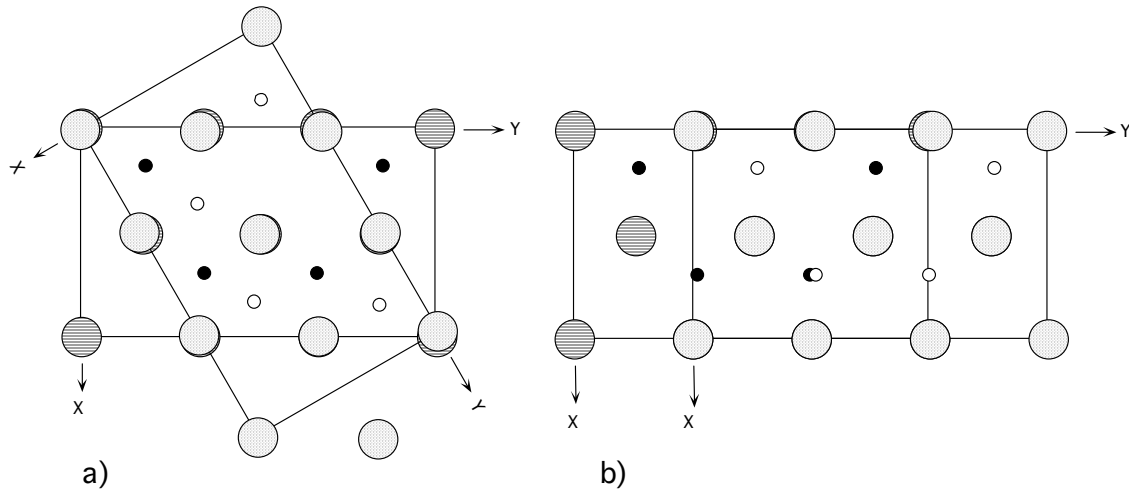
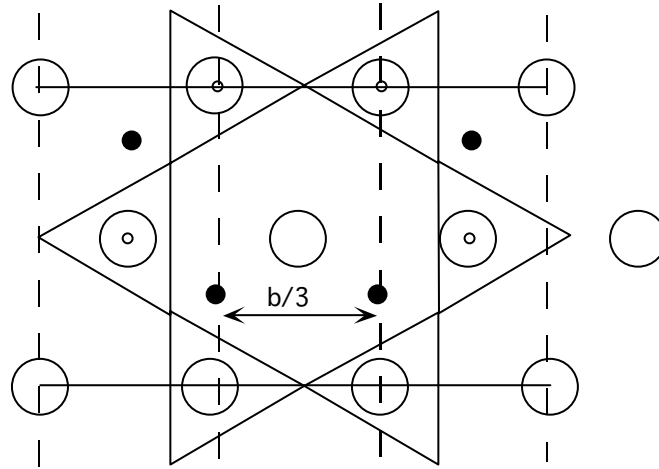


Figure 7.6: a) Clay unit cells superimposed after  $60^\circ$  rotation and b) after  $b/3$  translation. In both cases, the atoms lie on the  $b/6$  planes.

Stacking faults in clays affect some XRD reflections and not others. Firstly, they have no effect on the 00l reflections. Thus the normal peaks used for clay identification will not yield any information about this type of disorder. The word “crystallinity” is usually used to refer to lattice perfection, so a clay of low “crystallinity” would have many stacking faults interrupting the c-axis regularity, but yield very sharp 00l reflections. By contrast, a clay with no stacking faults but with very thin crystals would yield broad low 00l peaks.

Secondly, they have no effect on reflections for which  $k=3n$ , where  $n$  is an integer (not the  $n$  of the Bragg equation; just to be confusing, the reflection 060 has its Bragg  $n=6$  ( $=k$ ), but the  $n$  in the usage  $k=3n$  would be 2. Sorry, but that’s how the language evolved.) The reason that stacking faults do not affect  $k=3n$  reflections lies in the hexagonal nature of the layers. The oxygens and the cations of the octahedral layer and the silicons repeat at intervals of  $b/3$ . (Fig 7.7)



**Figure 7.7:** Clay unit cells showing  $b/3$  repetition.

Brucite ( $Mg(OH)_3$ ), a simple octahedral sheet, has cell edge  $3.15\text{\AA}$ , the equivalent layer silicate, say biotite, has  $b=9.3\text{\AA}$ . Clay layers have to stack in such a way as to maintain H-bonding from oxygen to oxygen, and since the oxygens repeat every  $b/3$ , the H-bonds can form provided the oxygens are correctly aligned, and they don’t care about the rest of the structure (Fig 7.8). Provided this regularity is maintained, for the  $k=3n$  reflections all atoms except the basal oxygens of the tetrahedral sheet line up, and sharp, strong reflections occur. All clays give strong reflections for 00l, 20l, 13l, 06l and 33l reflections. However for other reflections, the Bragg condition becomes lost, because for these, there is no c-repeat. The reflection 021, for example, becomes meaningless because there is no regular repeat of the lattice (Fig 7.9b).

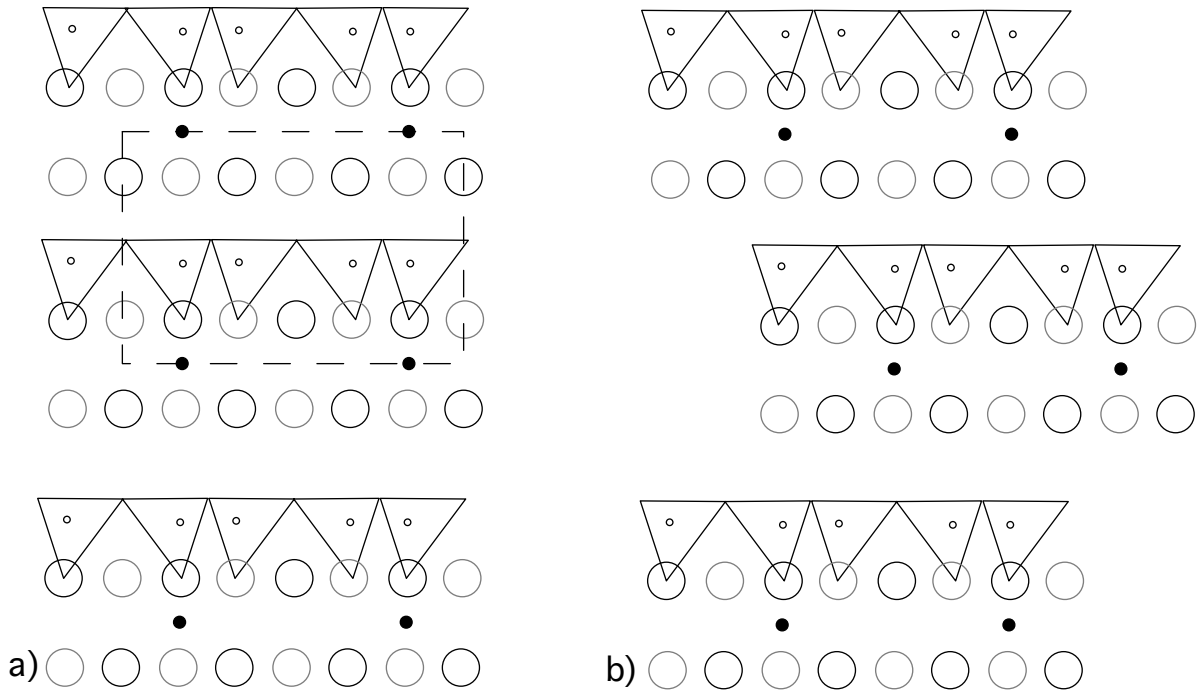


**Figure 7.8:** a) Regular stacking of kaolin layers. b) irregular layer stacking. Both stackings maintain the same oxygen registry across the interlayer.

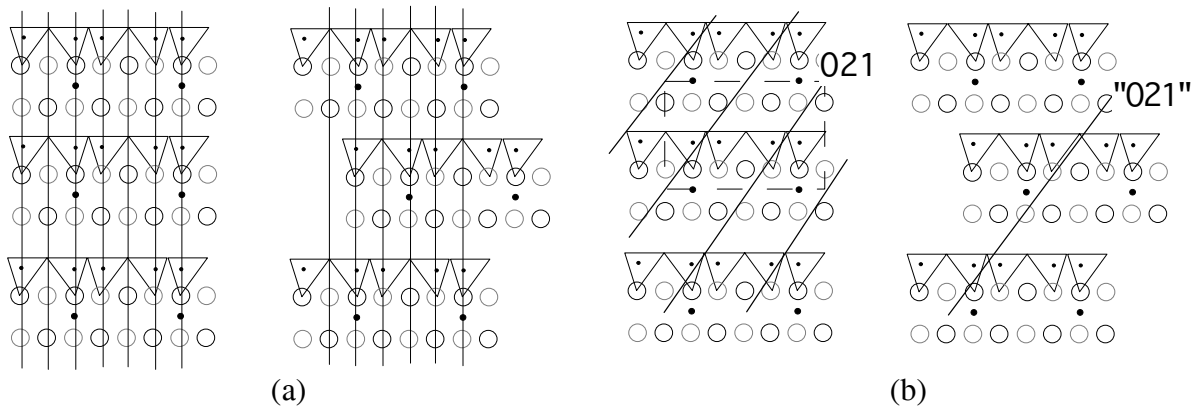


**Figure 7.9:** a) 060 planes maintained through either regular or irregular stacking. b) 021 planes exist in a regularly stacked clay, but not in the irregular stacking. (The expected "021" does not pass through identical parts of the structure in successive layers).

For a regularly stacked clay, for example kaolinite, the reflection 020 is sharp and fairly strong (at about 4.45Å). 110 and  $\bar{1}10$  superimpose because, although it is triclinic, their d-spacings are very close, and these are followed by , 111,  $\bar{1}11$ ,  $\bar{1} \bar{1}1$  021, and 0  $\bar{2}1$  at higher angles as discrete sharp peaks (Fig 7.10).

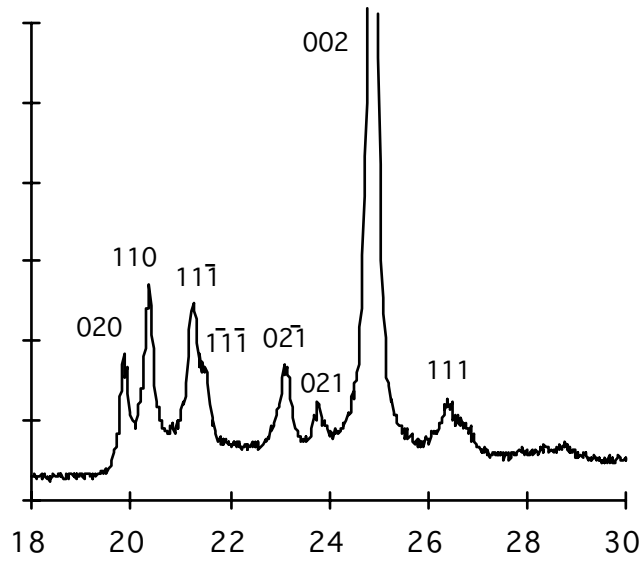


**Figure 7.10:** XRD pattern of the 02l, 11l region of a well-ordered kaolinite

For an irregularly stacked clay, the diffraction pattern shows a sharp intensity climb at the low angle side of the 020 Bragg position, followed by a gradual decline in intensity toward higher angle. One way to understand this is to recognize that the *c*-repeat is very large (in effect, the whole crystal dimension in the *Z*-direction), thus if  $1/d^2 = k^2/b^2 + l^2/c^2$  and *c* is (say) 250Å, then 020 will be at 4.450Å, 021 at 4.449Å and so on (see Table)

l	d
0	4.450
1	4.449
2	4.447
3	4.444
4	4.439
5	4.433
6	4.425
7	4.416
8	4.406
9	4.394

The "peaks" simply merge into a continuous asymmetric peak (Figs 7.11, 7.12).

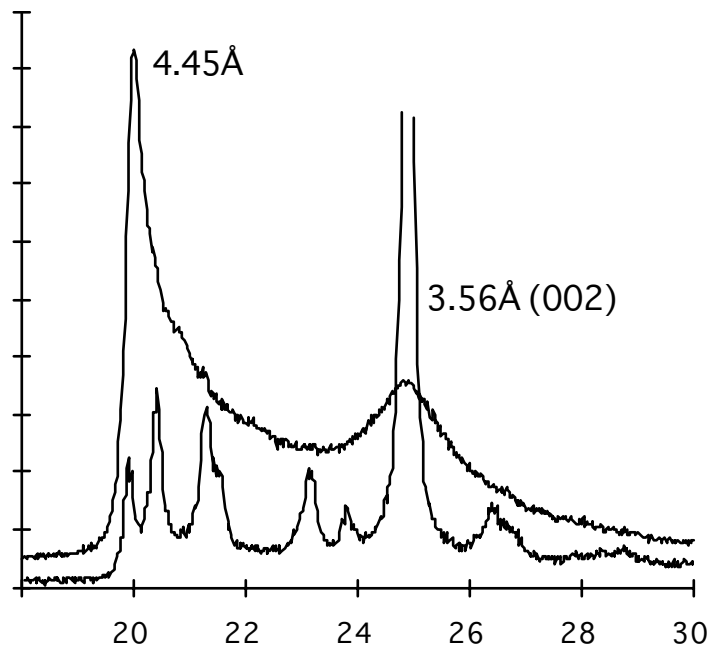


**Figure 7.11:** XRD pattern from an irregularly stacked and very thin clay tubular halloysite). The 02, 11 band is asymmetric and the 002 peak is very broad. The pattern from Fig 7.10 is shown for contrast.

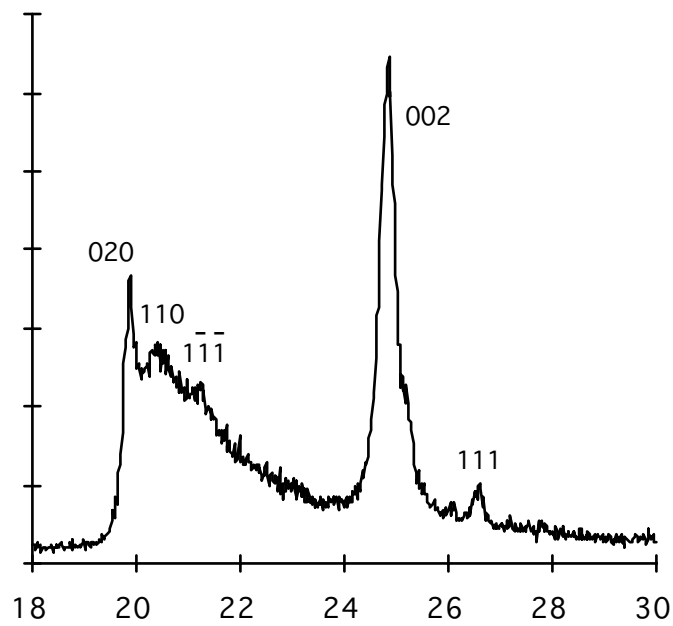


Figure7.12: XRD scan of the 02, 11 region of a poorly ordered kaolinite. Patterns like this are typical of many soil kaolinites.

---



---

**ATOMIC RADII** (Ångstrom units)

---

Shannon and Prewitt (1969)

element	ionic coordination #				covalent	van der Waal's
	iv	vi	viii	xii		
Li <sup>+</sup>	0.59	0.74				1.52
Be <sup>2+</sup>	0.27				0.96	
	1.11					
B <sup>3+</sup>	0.12				0.85	
C <sup>4+</sup>	-0.08				0.77	1.7
N <sup>5+</sup>					0.72	1.55
O <sup>2-</sup>		1.35			0.68	1.52
F <sup>-</sup>		1.28			0.67	1.47
Ne						1.54
Na <sup>+</sup>		1.02	1.16			
	1.86					
Mg <sup>2+</sup>	0.49	0.72			1.30	
	1.60					
Al <sup>3+</sup>	0.39	0.53			1.23	
Si <sup>4+</sup>	0.26	0.40			1.17	2.1
P <sup>5+</sup>	0.17				1.13	1.8
S <sup>6+</sup>	0.12					
S <sup>2-</sup>		1.80			1.13	1.8
Cl <sup>-</sup>				1.80	1.13	1.75
K <sup>+</sup>				1.65		
Ca <sup>2+</sup>			1.12	1.35	1.6	
Ti <sup>4+</sup>		0.60				
Mn <sup>2+</sup>		0.82				
Fe <sup>2+</sup>		0.77				
Fe <sup>3+</sup>	0.49	0.645				

## 8. Other methods

---

---

### X-ray Fluorescent Analysis (XRF or XFA) and electron microscopy

---

---

The physics of X-ray fluorescence was introduced earlier, where it was shown that a high energy electron striking an atom could eject one of that atom's own electrons. Because electrons do not penetrate very far into solids, most of this happens very near the surface (within 100 nm), so many of the ejected electrons (secondary electrons) are emitted into the vacuum above the impacted solid. These electrons are collected for Scanning Electron Microscopy (SEM) to be discussed below. Some of the incident electrons are also scattered back from the sample,

In addition to the secondary electrons, some of any subsequent X-radiation may be directed out of the specimen. Although the electron beam may be only one micrometre in diameter, the total excited region of the sample is about 5  $\mu\text{m}$  across, as incident and secondary electrons ricochet through the sample. The fluorescent X-rays may be derived from any energy level change between electron shells:

L  $\rightarrow$  K transition produces K-radiation;  $K_{\alpha 1}$  and  $K_{\alpha 2}$

M  $\rightarrow$  K transition produces K-radiation;  $K_{\beta}$

M  $\rightarrow$  L transition produces L-radiation;  $L_{\alpha 1, 2, 3}$

N  $\rightarrow$  M transition produces M-radiation;  $M_{\alpha}$

etc.

Because the energy of an electron is a unique characteristic of its atom type and shell position, each emitted X-ray has an energy that is characteristic of that electron transition; therefore measuring the X-ray quantum's energy identifies the atom type from which it emerged. Measuring the number of quanta allows a determination of the number of atoms of that type - i.e., allows a chemical analysis. Elements of lower atomic number than carbon do not generate X-rays of sufficient energy to be detected by routine laboratory instruments, so analysis is limited to elements of atomic number 6 or greater. The technique works particularly well for silicate minerals.

Arriving at a relationship between the intensity and energy (equivalent to wavelength) of emitted X-rays and the weight percent of the elements that produced them requires considerable prior knowledge of electron and X-ray physics, knowledge that is fortunately now well established. In practice, a Scanning Electron Microscope is used to form a focussed beam of electrons, about 1  $\mu\text{m}$  in diameter. The sample to be analysed is put under this beam, in a vacuum, having previously been coated with a thin (10 nm) coat of carbon to conduct the incident electrons away. An X-ray detector, capable of discriminating the energy of the X-ray, and of counting the number of quanta of each discriminated energy, is positioned above and to one side of the specimen. Just how finely the detector can discriminate energy depends on its type.

Energy dispersive detectors are solid-state devices, able to discriminate to within about 150 electron volts (eV) (out of a range from 1-15 keV). They are common adjuncts to SEMs, and are invaluable for analysis of major element content. They are not sufficiently sensitive to analyse elements present in trace amount (<0.1 wt %). The technique is called Energy Dispersive X-ray Analysis - EDXA. Wavelength dispersive detectors are carefully cut single crystals which provide a diffraction grating, essentially using Bragg's Law with a known *d*-spacing but unknown wavelength (the opposite of a normal diffraction experiment where wavelength is known and fixed and *d*-spacing is analysed). Remembering that the energy and wavelength of radiation are linked by the equation  $E=hc/\lambda$ , Bragg's Law can be used by measuring the diffraction angle  $\theta$ , solving for  $\lambda$  and so obtaining E. Wavelength dispersive detectors discriminate very closely - to within 5 electron volts - and can analyse to ppm (mg/kg) levels. The Technique is called Wavelength Dispersive X-ray Analysis - WDXA.

For a qualitative analysis (what elements are present, roughly in what proportion), any kind of sample small enough to fit in the SEM can be examined. For quantitative analysis a smooth, flat surface is needed, and most analysts prefer to use a polished specimen. This is difficult to obtain with clay-rich samples, but it is nonetheless quite easy to distinguish one clay mineral from another, provided the particles are larger than 5  $\mu\text{m}$  - i.e., larger than a clay particle! Masses of a single clay species can generally be well analysed, and it is advisable to have studied a sample by optical microscopy and XRD before attempting analysis so that you know its fabric well enough to understand the analytical results.

The example analysis below is of a garnet. The instrument must be calibrated using standards of known composition; for this analysis the following standards and electron beam energies (kilovolts) were used:

Standards :

Na K	Albite 15kv
Mg K	MgO 15kv
Al K	Albite 15kv
Si K	Sanidine $\text{KAlSi}_3\text{O}_8$
K K	Sanidine $\text{KAlSi}_3\text{O}_8$
Ca K	Diopside
Ti K	$\text{TiO}_2$ 15kv
Mn K	Pure Mn 15kv 1
Fe K	$\text{Fe}_2\text{O}_3$

The technique analyses elements. The analysis for oxygen is generally less accurate than that of elements of higher atomic number, so most geologists recast silicate analyses in terms of the constituent oxides. For anhydrous minerals such as this garnet, the analytical totals (whether element wt % or oxide wt %) should be close to 100. For clays, the water in the structure is not analysed by electron probe methods (hydrogen does not generate X-rays), so the totals are always <100%, and you will need to have a good idea of what you are analysing if you are to assess the analytical quality as you go. The software puts a \*

beside results that are close to or below the detection limit of the method, so you know not to take any notice of the figure.

### Analysis

Elmt	Spect. Type	Element %	Atomic %	Oxide	Wt %	Nos. of ions
Na K	ED	-0.05*	-0.05*	Na <sub>2</sub> O	-0.07*	-0.01*
Mg K	ED	8.23	7.48	MgO	13.64	1.50
Al K	ED	12.05	9.87	Al <sub>2</sub> O <sub>3</sub>	22.76	1.97
Si K	ED	19.07	15.01	SiO <sub>2</sub>	40.80	3.00
K K	ED	0.07*	0.04*	K <sub>2</sub> O	0.08*	0.01*
Ca K	ED	5.27	2.91	CaO	7.38	0.58
Ti K	ED	0.15*	0.07*	TiO <sub>2</sub>	0.25*	0.01*
Mn K	ED	0.35*	0.14*	MnO	0.45*	0.03*
Fe K	ED	11.40	4.51	FeO	14.66	0.90
O		43.42	60.01	12.00		
Total		99.95	100.00		99.95	
Cation sum						8.00

Comparing the analysis with the spectrum (Figure 8.1), it is clear that there is a simple relationship between the position across the spectrum (the energy of the characteristic X-rays) and atomic number. For this K-series spectrum, the lowest atomic number element detected is carbon on the left, followed by oxygen, then Mg, Al, Si, Ca and Fe. The carbon X-rays arise from the carbon coat put over the sample to conduct the incident electrons away.

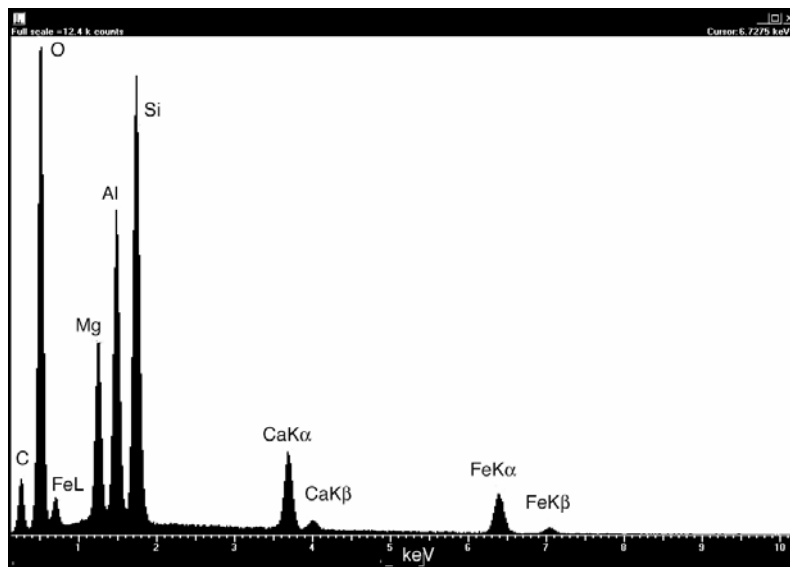
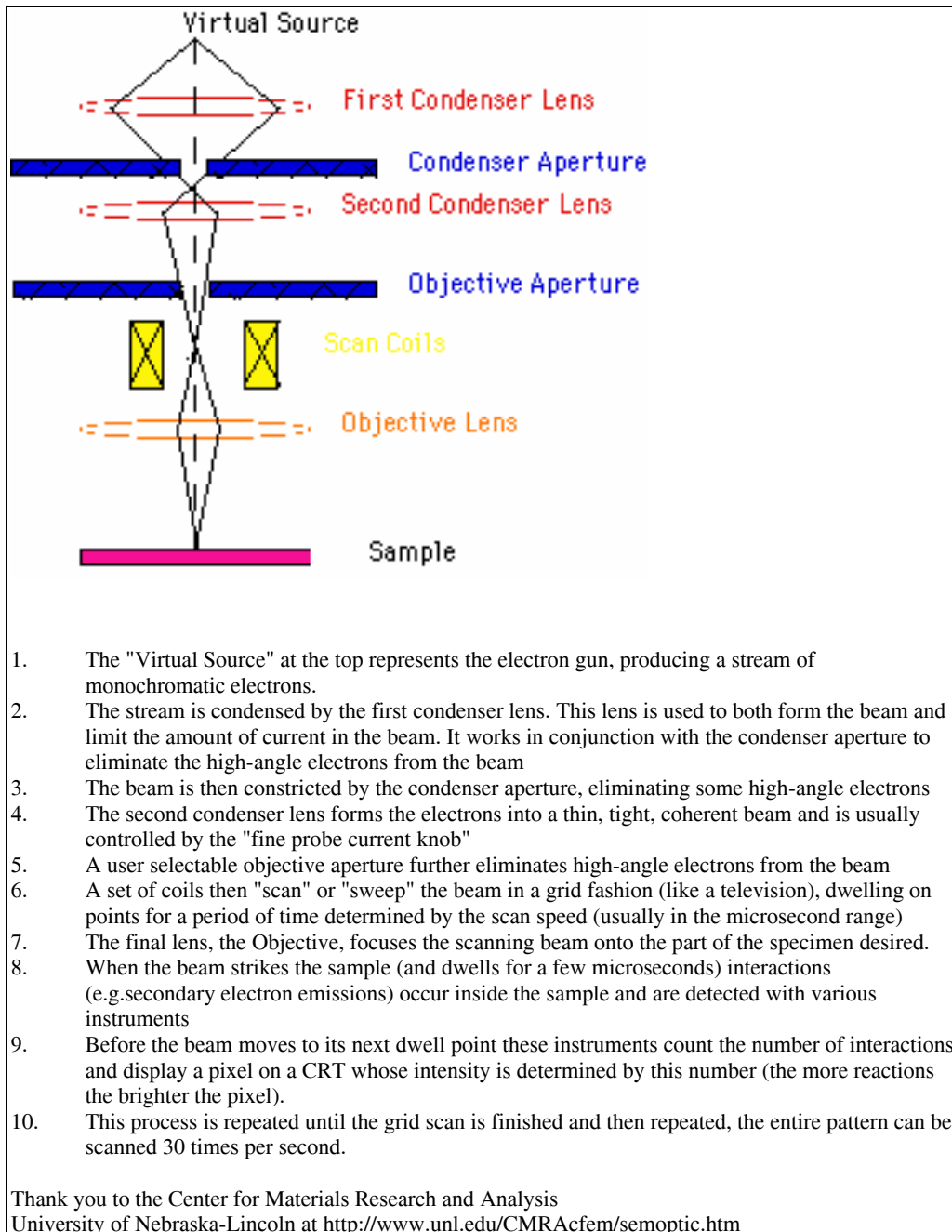


Figure 8.1.

## Scanning Electron Microscopy (SEM)

A scanning electron microscope forms an image from electrons scattered off or emitted by the specimen. The procedure requires a finely focussed electron beam to be scanned over the sample in a raster pattern.



The two main modes of operation in a scanning electron microscope use either secondary electrons or back-scattered electrons. The secondary electron mode is generally

considered to be the normal mode of operation. Images produced by this method display variations in topography, so the images look 3-dimensional. In the back-scattered electron mode, the images produced have bright areas corresponding to relatively high atomic number elements while the darker areas contain elements with lower atomic numbers. In both modes, the detectors collect electrons and an image is displayed on a monitor. The image can be recorded on photographic film or down-loaded to a computer.

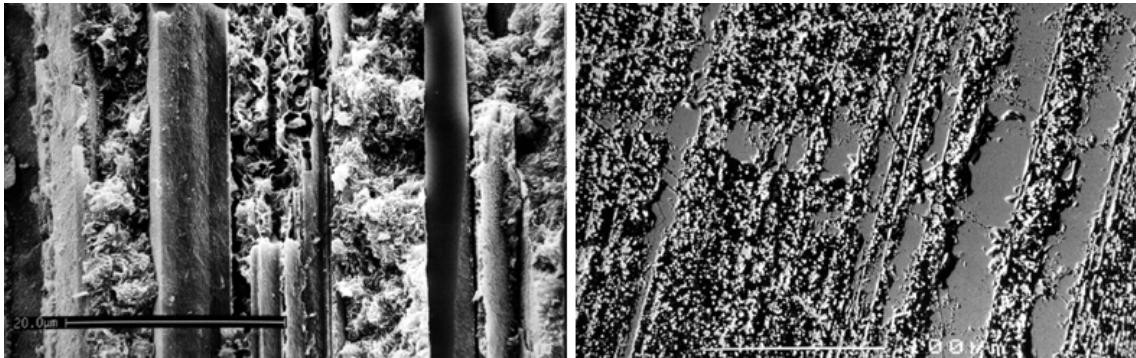


**Figure 8.2a**

**Figure 8.2b**

Examples of scanning electron microscopy of the same sample; secondary electron mode (Fig 8.2a) and back-scattered electron mode (Fig 8.2b)

---

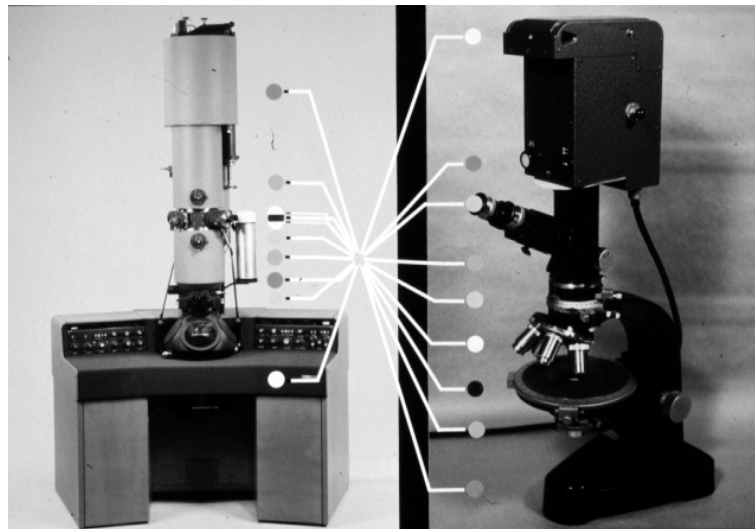


**Figure 8.3**

## Transmission Electron Microscopy (TEM)

Figure 8.3 shows the relationship between a transmission electron microscope (left) and a light microscope (right). An electron microscope is analogous to an upside-down light microscope. The main differences are the utilisation of electrons instead of visible light for "illumination" and the use of electromagnetic coils for focussing the radiation rather than glass lenses. A light microscope uses electromagnetic radiation of visible wavelengths ranging from violet (430 nm) to red (690 nm) to obtain a magnified image of small, nearby objects whereas a transmission electron microscope uses electrons of a specific energy. For example, the electron beam in a 100 kV electron microscope has an effective wavelength of  $3.7 \times 10^{-3}$  nm which is of the order of  $10^5$  times shorter than visible light. A relationship exists between the resolving power of a microscope and the wavelength of radiation used; the shorter the wavelength the higher the resolving ability. The relationship reveals that the optimum resolving power of a 100 kV electron microscope is 2.3 Å whereas a light microscope has a limiting resolution of approximately 1 μm. This is why electron microscopes are so useful for imaging very small particles such as viruses and clay crystals whereas if a light microscope was used for the job, their structures would be hopelessly concealed by diffraction. Selected area electron diffraction (SAED) is a technique that makes use of diffraction from crystal layers. The regularly repeating layers of atoms in a crystal make an ideal diffraction grating. The distance an electron beam is diffracted from the central non-diffracted beam is governed by the spacing of the atomic layers. The wider the spacing, the closer the diffracted beam is to the central non-diffracted spot. Two types of diffraction pattern are commonly observed during SAED; a ring diffraction pattern (Fig 8.4a) and a spot diffraction pattern (Fig 8.4b).

**Ring diffraction pattern**

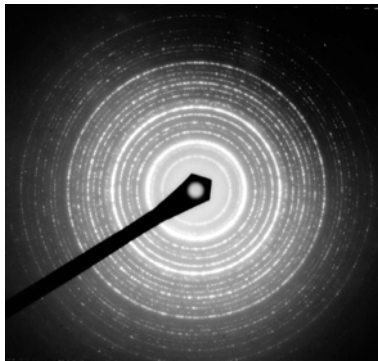


**Figure 8.4a**

**Spot diffraction pattern**



**Figure 8.4b**

A ring diffraction pattern tells the microscopist that the material is composed of a multitude of randomly-oriented crystals - a powder pattern. A spot diffraction pattern on the other hand (particularly if it looks symmetrical) is from a single crystal. By making careful measurements of the ring diameters and/or distances of spots from the central non-diffracted beam, it is possible to calculate the d-spacings within the crystal lattice. The formula used in these calculations is derived from the Bragg equation:  $n\lambda = 2d\sin\theta$ .

If  $R$  is the distance from the central spot to the diffracted spot (or ring) and  $L$  is the camera length, then  $Rd = \lambda L$  where  $\lambda L$  is the camera constant.

### **Sample preparation for TEM**

There are two main methods of sample preparation for TEM; ion-beam thinned specimens supported on a copper grid and powdered ones supported on a holey carbon-coated grid.

#### *Ion-beam thinned specimens*

Firstly, to make an ion-beam thinned specimen, a 30  $\mu\text{m}$  thin-section of the material has to be made. Crystalbond™ adheres the thin-section to a supporting glass slide (usually a microscope slide). A copper grid is glued to the area of interest with Araldite™. Using a pin, the material surrounding the grid is broken away. The slide is then heated on a hot plate and the copper grid together with the specimen is removed with forceps. An ion-beam mill is then used to gradually erode the specimen until small holes are made in it. A thin layer of carbon is then precipitated onto the specimen. At the edges of these holes, the specimen is generally thin enough for electrons to pass through and thus an image can be obtained.

#### *Powder mounted specimens*

All that is required for this method is to ultrasonically disperse in ethanol a powdered specimen and then pipette this onto a holey carbon-coated grid which rests on filter paper. The sample does not require any additional carbon coating as the membrane upon which the particles lie is sufficient for dissipating any build-up of charge.

### **Sample preparation for SEM**

Before you can prepare a sample for SEM you need to know what mode you are going to operate in. If you require information on the chemical composition of the sample by using energy dispersive X-ray analysis (EDXA) and back-scattered electron microscopy, then the best sample to use is a very flat, polished section that has been carbon-coated. Alternatively, if you require good quality 3-dimensional-looking images then a broken fragment mounted on an aluminium stub and coated with a very thin (200 Å) layer of gold is all that is needed.

---

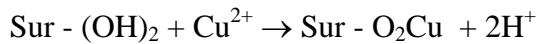
## **ADSORPTION AND ION EXCHANGE**

---

Adsorption refers to the attachment of ions to a mineral surface, or in sites within the mineral accessible to weathering solutions. Adsorbed ions are accidental to the structure of the host mineral, and in many instances adsorbed ions are exchangeable. Extensive coverage of the mechanisms and processes of surface adsorption on soil materials are provided by Sposito (1984, 1989), Davis & Kent (1990) and Schindler (1990).

The outer surface ions of the common regolith minerals are oxygen. In acid solutions, the mineral surface is protonated (the surface layer becomes hydroxyls) and positively charged. As the surrounding solution becomes more alkaline, the surface oxygens tend to lose their protons, leaving a negatively charged surface. The change from a positive to a negative surface depends on the mineral, occurring at different pH for different minerals. The pH at which the net surface charge is zero is called the point of zero charge (PZC). At pH below the PZC, the surface is positively charged and is an anion adsorber, at pH above the PZC the surface is a cation adsorber. Surface chemists define several points of zero charge depending on the method of determination, including a point of zero net charge (PZNC) and a pristine point of zero charge (PPZC) (see Sposito (1989), Davis & Kent (1990) for an extended coverage of this topic). Some values of PZC for the major regolith minerals are listed in Table 7.3.

Cations in solution are invariably surrounded by a coordination shell of water molecules. Adsorption sites for ion complexes on silicates and oxides can be grouped into three. If the surface of the mineral has a stronger attraction for the cation than have the water molecules, the cation adsorbs directly to the mineral surface, and is termed "inner sphere" adsorption (Fig. 8.5.a). Adsorbed cations in inner sphere sites are strongly held and difficult to displace. Examples are the interlayer site in vermiculite (10-Å), where K<sup>+</sup> is bonded directly to the basal oxygens of two adjacent tetrahedral sheets, divalent metals adsorbed on oxide surfaces and anions such as [HPO<sub>4</sub>]<sup>2-</sup> adsorbed to the surface of goethite. If Sur represents the mineral surface, the adsorption of a cupric ion can be written as:



Inner sphere adsorbed ions may not be readily exchangeable, and for this reason they are of major importance in geochemical prospecting, because they can remain adsorbed through extremes of other ion concentrations.

Where the mineral surface anions attract the hydrated cation less strongly, the water shell is retained, and the adsorption is termed "outer sphere" (Fig. 8.5b). Such adsorbed cations remain bound to the mineral surface as long as there is no competing ion of higher concentration; Outer sphere sites are typical ion exchange sites such as the hydrated Na<sup>+</sup>, K<sup>+</sup>, Ca<sup>2+</sup> and Mg<sup>2+</sup> ions in the smectite interlayer (Davis & Kent, 1990)

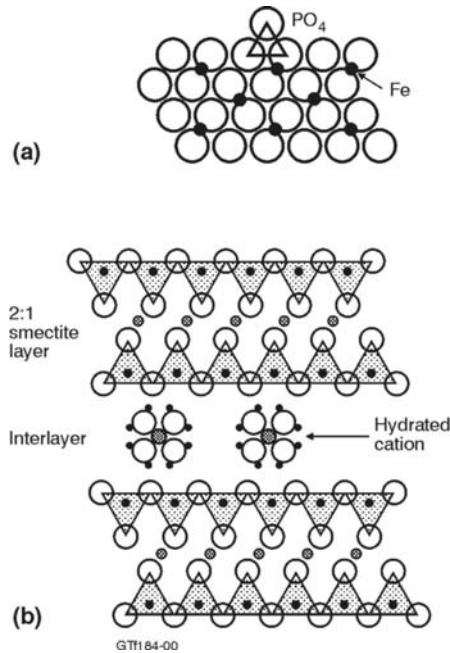


**Figure 8.5:** Adsorption sites on mineral surfaces. (a) inner sphere adsorption of  $[PO_4]$  on goethite (after Parfitt, 1978). (b) outer sphere adsorption of hydrated cations in the smectite interlayer.

Outer sphere complexes bond to similar parts of the mineral surface as do inner sphere complexes, but the cations, with a surrounding hydration shell of water molecules, are relatively weakly bonded through the electrostatic attraction of the hydration complex for the negative charge excess on the mineral.

Any charged mineral surface attracts a cloud of weakly associated hydrated ions. Where these are not specifically bound to the mineral surface, they are termed diffuse-ion swarms. The more readily exchangeable outer-sphere ions and diffuse-ion swarms are important in soil science and for bioavailability. Diffuse ions are not directly associated with any site in the mineral, but are retained at the surface by weak electrostatic attraction of the charged ion aqueous complex for the surface of the mineral.

### Cation exchange capacity

The clay silicates, particularly smectites and vermiculite, are important as temporary repositories for cations in the regolith. They exhibit the property of cation exchange, which arises in minerals whose structure or surface have weakly bound cations. A cation with a stronger binding force may displace a more weakly bound cation, such as a  $Ca^{2+}$  compared with a resident  $K^+$ , or the influx of a high concentration of a soluble cation, such as Na, may swamp and so displace the resident cation. All mineral surfaces exhibit this property, and clays, because of their small particle size and therefore larger surface area, exhibit high exchange capacity. Surface cation exchange is pH dependent; kaolinite, for example shows cation exchange at pH 7, but at pH 4 the surface is neutral and the cation exchange capacity is zero.

Some minerals have sites within their structure where a weakly bound cation is essential, though non-specific. Such exchangeable cations can be displaced by other cations. The zeolites have such sites within silica cages, and among the clay silicates, smectites have exchange sites in their interlayer region. The difference between the two aluminous smectites - montmorillonite and beidellite, lies in the origin of their exchange capacity. For montmorillonite, interlayer cations balance a positive charge deficiency that arises in the octahedral sheet ( $Al_{1.8}$  compared to  $Al_2$  required for a neutral 2:1 layer). For beidellite and nontronite, the interlayer cations balance a charge deficiency arising in the tetrahedral sheet as a result of  $Al \leftrightarrow Si$  substitution,  $Ca_{0.2}$  compensating for  $[Si_{3.6}Al_{0.4}]$  when  $[Si_4]$  would yield a neutral 2:1 layer).

Cation exchange capacity (CEC) is reported in terms of millimoles of positive charge per kg ( $mM^+/kg$ ), though the older literature refers to milliequivalent weight/100 g of clay. Millimoles are used because only a small weight of cations are exchangeable. The equivalent weight of an ion (the exchange ion in this case) is the weight that could exchange with one gram of hydrogen. For a divalent ion such as  $Ca^{2+}$ , this is half a mole or 20 g (Atomic weight of  $Ca = 40$ ). So an exchange capacity of  $400 mM^+/kg$  ( $=40 meq/100$ ) means that if  $Ca$  were the only exchange ion present, 1 kg of clay can hold  $400 \times 20 / 1000 = 8$  g of  $Ca$  on its exchange sites.

#### Values of Cation exchange Capacity (CEC)

It is clear from the discussion above that ion exchange capacity depends on three main factors:

- the amount of surface on which ions can adsorb,
- the pH
- the presence of structural charge

CEC therefore needs to be measured at a standard pH in order to compare truly between samples. This commonly means that the determination needs careful chemical treatment to maintain a constant and known pH.

Values of CEC at a standard pH will then depend on the surface area, which essentially means on the grain size. A kaolinite sample may be composed of fairly large particles (for example 2  $\mu m$  diameter books) or of much smaller and thinner crystals (0.5  $\mu m$ ). The smaller the crystals, the higher is the CEC. Illite CEC depends also on particle size. Illite's CEC partly derives from its having a charge unsatisfied outer surface. The Al-Si substitution in the mica tetrahedral sheet requires an interlayer cation ( $K^+$  in the case of illite). The outer two surfaces of an illite crystal would have their  $K^+$  ions held in inner sphere adsorption sites, held much less strongly than are the  $K^+$  ions sandwiched between two 2:1 layers in the interior of the crystal (these interior ions are not exchangeable). The CEC of illite therefore depends on the ratio of surface layers to interior layers. When this value is low (large, thick crystals), the CEC is low ( $100 mM^+/kg$ ), but values as high as  $400 mM^+/kg$  are found in very fine illite.

Smectites and vermiculites have a high CEC because they have a very high surface area and have structural exchange sites between every 2:1 layer. Values range from 600-1500 mM<sup>+</sup>/kg, with an average value of about 1000 mM<sup>+</sup>/kg

**Cation exchange capacities of clays (mM<sup>+</sup>/kg)**

<b>Mineral</b>	<b>range</b>	<b>typical</b>
Kaolinite	30-150	40
Halloysite	50-500	250
Muscovite		20
Illite	100-400	250
Smectite	600-1500	1000
Vermiculite	1000-1500	1200

Measurement of CEC

CEC is measured by displacing the exchange ions using a high concentration solution of a standard ion not likely to be present on the original clay (e.g one molar ammonium acetate, 0.1 molar barium or silver chloride) buffered to pH 7. Either the ion retained on the clay is measured (e.g. Ag or Ba can be determined by X-ray fluorescence spectrography on a pressed pellet of the dried, Ba-exchanged sample) , or the displaced exchange ions measured on the displacing solution by atomic absorption spectroscopy or other ion-specific techniques. See Wilson (1994) for procedures. Measuring the displaced ions gives much more information because all the exchange ions can be determined.(e.g. Na, K, Ca, Mg). But some samples may have exchangeable Al or H, thus the measured total CEC will be low unless these are also determined. Determined the retained ion provides a measure of total CEC but not of the individual ions. Measuring both provides a cross-check.

---

## THERMAL METHODS

---

Thermal methods of mineral analysis depend on some change in the mineral during heating, normally between 100°C and 1200°C. Changes may be loss of a component (e.g. H<sub>2</sub>O, CO<sub>2</sub>), a phase change without loss of a component (e.g. α-quartz to β-quartz transition at 573°C), or a phase change with loss of component (e.g. kaolinite dehydroxylation and conversion to metakaolin at about 500°C).

Many such changes occur over a fairly narrow temperature interval, and so determination of the temperature of a change is a qualitative determination of the presence of a particular mineral. Measurement of weight change, or of the amount of an evolved gas, or of the heat gained or lost during the transition allows a quantitative estimate of the clay.

### Thermogravimetric analysis (TGA)

This is the simplest of the main thermal methods. Typically, a small (0.2g) sample is heated on a sensitive balance, and the weight change recorded. Quantitative analysis of the evolved material is possible, and from this an estimate of the amount of that mineral can be made. For example kaolinite has 14% H<sub>2</sub>O by analysis, which is lost at about 500°C. Measurement of the total water lost over an interval from 450°C to 600°C can be used to estimate total kaolinite, provided no other minerals in the sample lose weight over this interval. Some TGA machines measure only weight loss, other apparatus (e.g. LECO moisture analyser) measures H<sub>2</sub>O and CO<sub>2</sub> evolved separately.

The thermodynamic phase rule tells us that during a reaction from phase A to phase B, while both phases are present, there will be no change in temperature (for example ice in water stays at 0°C even on a hot day until all the ice is melted). Thus heat added to the sample is absorbed with no rise in temperature of that sample.

### Differential Thermal Analysis (DTA)

If heat is applied equally to an inert substance and a reactive one, their temperatures will rise until the reactive one undergoes a phase change. At this temperature, if the reacting sample is using energy it will stay at a constant temperature despite being heated, while the inert sample will rise in temperature. If the reaction releases energy, the reactive sample's temperature will rise faster than that of the inert sample. In either case, there will be a difference in temperature between the inert standard and the reacting substance, and this temperature can be measured to reveal the presence of a thermal event. Reactions that give off heat are termed *exothermic* while those that absorb heat are *endothermic*, and this difference is readily seen by such an experiment.

### Differential Scanning Calorimetry (DSC)

This technique is very similar to DTA, but more informative. In DSC the heat applied to the sample and inert standard is controlled automatically to maintain both at the same temperature. The instrument measures the difference in energy being applied to the

sample and standard, allowing measurement of heat capacity, of heat change during a reaction, and of the rate of a reaction.

---

## INFRARED SPECTROSCOPY

---

### INTRODUCTION

Spectroscopy is the study of the interaction of electromagnetic radiation with matter. In a mineralogical or geological context, spectroscopy is applied to study energy transitions in atoms and molecular configurations that make up minerals. Spectroscopic methods are used to probe the minerals *local* structure such as site symmetry and local chemical and crystallographic environment (bonding), and it does not depend on long range periodicity of structure. There are several spectroscopic techniques, but all work on the same principle on energy interaction with matter.

As energy is central to the spectroscopic techniques, it is important to understand the electromagnetic spectrum and the different energy phenomena associated with it (figure 8.6).

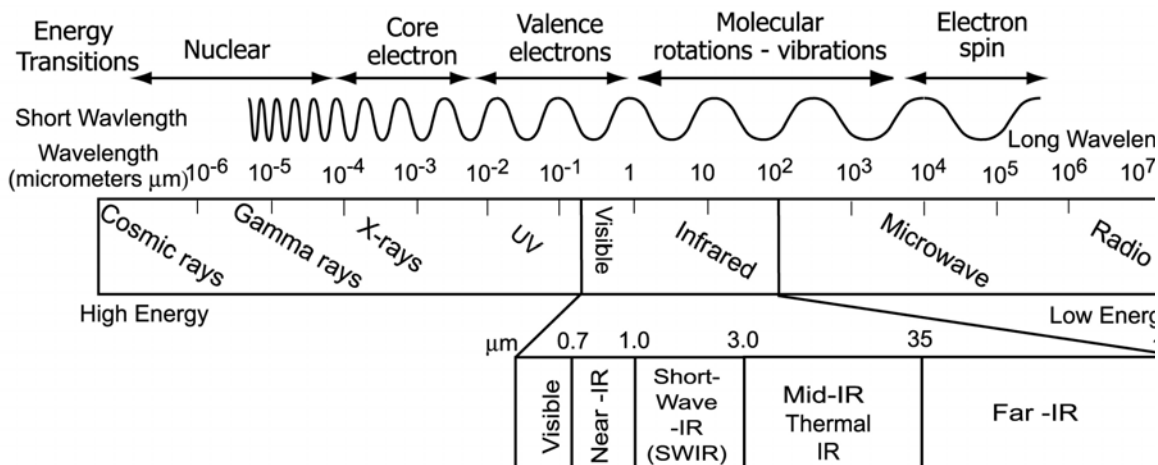


**Figure 8.6:** The electromagnetic spectrum with the associated phenomena creating the energy transitions. Infrared part of the spectrum is commonly divided into visible, NIR, SWIR, mid and far infrared.

### ENERGY TRANSITIONS IN MINERALS

When a molecule interacts with EM radiation, the energy is absorbed and the molecule is promoted, or is said to experience a transition to a higher energy state (called excited state). In order for absorption to occur, the energy of the radiation must match the energy difference between **quantized energy levels** of the molecule. Quantized means that the energy can only contain certain discrete levels.

When radiation of energy  $\Delta E = E_2 - E_1$  strikes a molecule, the energy is promoted from lower energy state ( $E_1$ ) to a higher energy state ( $E_2$ ). Radiation of energy other than  $\Delta E$

will not be absorbed. As reflectance is an inverse measure of absorbance, the amount of reflectance from a sample can be measured to acquire information about the molecules in the sample. This energy states as seen in EM principles

$$\Delta E = h\nu = hc/\lambda = hc\nu$$

Where  $h$  is the Planck's constant ( $6.626 \times 10^{-34}$  J s) and  $c$  is the speed of light ( $3 \times 10^8$  m.s<sup>-1</sup>).

From the above equation it is apparent that radiation can be represented by its frequency ( $\nu$ ), its wavelength ( $\lambda$ ), or its wavenumber.

The energy transitions between the two states occur over the entire electromagnetic spectrum, with energy differences representing specific phenomena. In the lowest energy range, energy transitions associated with the spin of nuclei can occur, which are small (figure 8.6). For the infrared part of the EM spectrum, electronic transitions involving valence electrons and molecular vibrations involving stretching and bending of atomic bonds between atoms are the transition phenomena. These different transitions within minerals can be studied using incident radiation of particular wavelength, and in this section, the effect of infrared radiation on energy transition in minerals is considered and evaluated in order to identify the specific atom(s) and molecule(s) in minerals, which in turn are used to identify the mineral.

## TYPES OF INFRARED TECHNIQUES

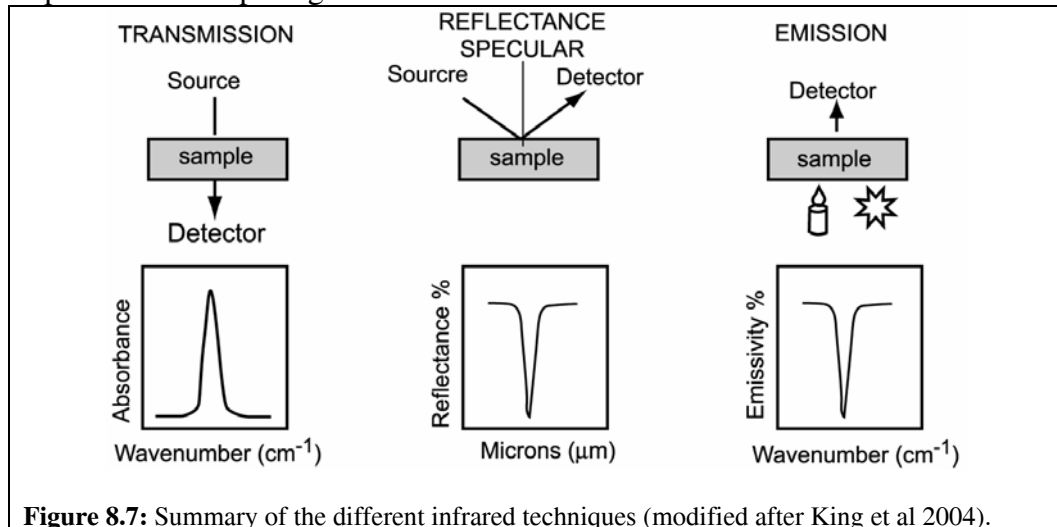
Any infrared technique will have a

- **Source** of radiation. The sources used are either unpolarized (quartz halogen source), bright, pulsed polarized (lasers), or thermal sources.
- **Sample.** This is the sample of interest. Some techniques require the sample to be specially prepared while reflectance can measure the IR spectra from the sample in its natural state.
- **Detector.** The detector converts the energy received from the sample into an electrical current or potential and finally into a signal. The choice of detectors depends on the wavelength or frequency range in which the spectra are collected, with the NIR detectors made of semi-conductor materials such as In(Ga)As or HgCdTe, while thermal or mid infrared region detectors are thermocouples and pyroelectric ones.

The infrared techniques involve collecting spectra from a sample. The spectra can be collected and displayed in different formats depending on the task at hand. Each of the types has different geometry and sample preparation methods. The types are (figure 8.7)

- **Reflectance.** Here the spectra collected are from the same side as the source with the energy being reflected or scattered from the sample. The samples require minimal preparation and therefore this method is suitable for field and lab collection of spectra as well as from a large number of samples.
- **Transmission.** The spectra collected are from the opposite side of the sample to that of the source, and this technique is mainly used in the laboratory and requires proper sample preparation such as powdered sample pressed into a disc.

- **Emission.** The sample itself is the source of energy. The sample needs to be at a different temperature to that of the detector and/or have different emissivity in the spectral region of interest. To record the spectra in detail, it is best to heat the samples so the sample signal is different from that of the instrument.



Of the above three methods, **reflectance** spectroscopy will be described in detail because it is a technique being increasingly used for mineral identification in exploration and environment, it is easy and fast to collect spectra in this mode, and sample preparation required is minimal.

## REFLECTANCE SPECTROSCOPY

When infrared radiation strikes an object (earth material), the energy received back or reflected to the detector is a function of two main fundamental processes: scattering and absorption. Scattering is process by which radiation (photons) are reflected or refracted from the grain surfaces and depends on the “roughness” of surfaces. Several absorption processes occur in a sample depending on the wavelength of radiation such as electronic transitions and sub-molecular vibrations that provide information about the composition of the materials. The complex interaction between scattering and absorption on and within a sample governs the amount of radiation received by the detector (or reflectance).

The *spectra* or *spectral signature* from a sample is measured by recording the amount of radiation reflected from the sample as a function of *frequency* ( $\nu$ ) or *wavelength* ( $\mu\text{m}$  or  $\text{nm}$ ) of the incident radiation, with the reflected radiation being ratio against a suitable background (calibrated). Spectra from a sample (reflectance vs wavelength) will have peaks and valleys, with the valleys representing absorption processes within the sample at the particular wavelength. For example, take a molecule with two quantized energy states that is subjected to radiation. The resulting reflectance against wavelength (or constantly increasing energy) from the molecule is recorded as a spectrum. A point is reached where the energy between the two quantized energy levels of the molecule matches the incident radiation and the molecule is promoted from the lower energy state to a higher energy state. The energy of the incident radiation is absorbed by the molecules and the spectrum

registers this wavelength as lower reflectance. Therefore, it is critical to understand the causes of the absorption features and the wavelengths at which they occur, so compositional, and thereby mineralogical information regarding the sample can be obtained.

### **Absorption Processes**

There are two general absorption processes: electronic and vibrational, and each provides information on different energy transitions within the mineral.

#### **Electronic Processes**

Electronic processes in atoms and molecules occur dominantly in the visible to near infra-red regions. Several types of electronic transitions are observed in the UV to infrared spectral range and the ones important to minerals are:

##### *.Crystal Field Effects*

These are energy transitions where electrons from one orbital are promoted to a higher energy orbital in the same atom. Generally, such electronic transitions occur in the ions that have their d-orbital unfilled, such as the transition state elements –  $\text{Fe}^{2+}$ ,  $\text{Fe}^{3+}$ ,  $\text{Mn}^{2+}$ ,  $\text{Mn}^{3+}$ ,  $\text{Cr}^{3+}$ . These transitions involve absorption in the visible to near infrared and are the prime cause of colour in minerals. The absorption features produced on the reflectance spectra of minerals by crystal field effects are typically broad.

##### *Charge Transfer Effects*

These transitions occur when an electron from an orbital on one atom absorbs enough energy to jump to a higher energy orbital of an adjacent atom. Such energy transitions can occur when electron jumps from an anion to cation ( $\text{O}^{2-}$  to  $\text{Fe}^{3+}$ ) or from a cation to anion. In minerals, the Fe-O transitions exhibit this type of energy transition. Charge transfer effects are confined to the ultraviolet to visible portion of EM spectrum. The Fe-O transition absorbs energy in blue-green region of the visible spectrum, and therefore the iron oxides ( $\text{Fe}^{3+}$  oxides such as goethite and hematite) appear in shades of red to the eyes. The main absorption features of Fe-O are in the UV with broad wings extending almost to 0.7  $\mu\text{m}$  in the visible part of the spectrum. The extreme width of the absorption feature is due to the *wide range of energy levels available to electrons within molecular structures*. The width of an absorption feature in a mineral is controlled by the *nature and co-ordination of the anions* present, which determines the extent of charge transfer between oxide and hydroxide ions to  $\text{Fe}^{3+}$  ions.

##### *Conduction Band Effects*

Electronic transitions where an electron escapes from the localized orbital on an atom to the conduction band and moves freely in the entire solid are called conduction band effects. Such type of energy transition is typical of semi-conductors and is shown by the sulphide minerals. Conduction band effects occur in the visible to ultra-violet range.

### *Spectral Features in the Visible Near Infrared Region*

The spectral features in the 0.4 to 1  $\mu\text{m}$  region are dominated by the transition elements (Fe, Mn, Cr, Ni, Cu) which give rise to the crystal field and charge transfer effects described previously. In minerals, the iron is dominant transition element giving rise to electronic absorption features in this region. Ferric ion ( $\text{Fe}^{2+}$ ) in the Fe-O bond, shows intense absorption of the shorter wavelengths (UV) due to the charge transfer effects. Iron also produces absorption features due to the crystal field effects especially in the common Fe(III) oxides goethite and hematite (figure 8.8).

Charge-transfer associated features are broad and therefore non-discriminatory for iron oxides at least, but features due to crystal field effects are narrower and therefore suitable to an extent to discriminate mineral species. For example, crystal field transitions in hematite due to  $\text{O}^-$  are at 0.84  $\mu\text{m}$  while crystal field transitions in goethite due to  $\text{OH}^-$  take place at 0.90-.092  $\mu\text{m}$  (figure 8.8).

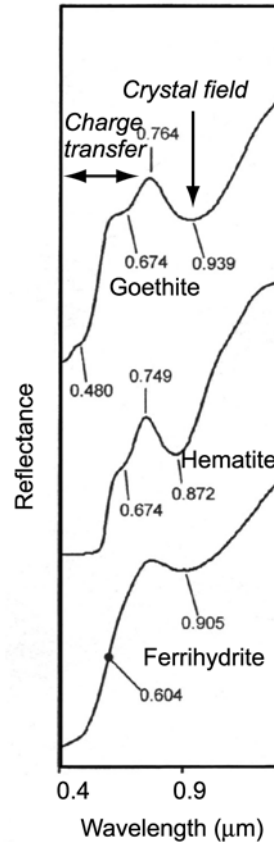


**Figure 8.8:** Absorption features in iron oxides due to electronic transitions

Atoms bonded together give rise to molecules. All rocks are made up of minerals, which are made up of atoms bonded together in a specific geometry (crystal structures). Therefore there are molecular configurations in minerals and the interest is in identifying minerals by scrutinizing their entire spectra or parts of their spectra.

The vibrational processes involve the *bending* and *stretching* of the bonds between the atoms i.e. molecular vibrations. The interatomic forces between atoms control the precise frequency of the vibrations similar to springs connecting two vibrating masses. The frequency of vibration depends on the

- Strength of the bond in a molecule and
- The masses of each atom in the molecule.

In general, a molecule containing  $N$  atoms will have  $3N-6$  vibrational modes called *fundamentals*. Each vibration can also occur at roughly multiples of the original fundamentals. When the additional vibrations involve multiples of a single fundamental mode they are called *overtone*s. When the additional vibrations involve different modes of vibrations, they are called *combinations*.

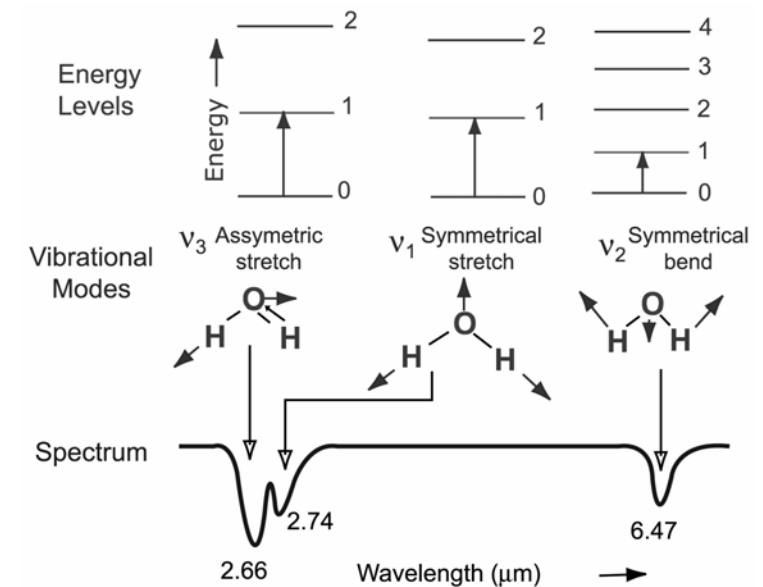


**Figure 8.9:** A vibrational-energy level sketch for the water molecule.

The greek letter nu ( $\nu$ ) and a subscript are used to denote frequencies of fundamental vibrations. A molecule having fundamental vibrations  $\nu_1$ ,  $\nu_2$ ,  $\nu_3$ , will have overtones at approximately  $2\nu_1$ ,  $3\nu_2$ ,  $2\nu_3$  and combinations at approximately  $\nu_1 + \nu_2$ ,  $\nu_2 + \nu_3$ , and so on. Any of the higher overtones are considerably weaker than the last. These weak absorptions can be measured and information acquired from 2<sup>nd</sup> and 3<sup>rd</sup> overtones. A vibrational-energy-level diagram for the water molecule (which is common in reflectance spectra) is shown in figure 8.9. Three fundamental vibrations ( $\nu_1$ ,  $\nu_2$ ,  $\nu_3$ ) are horizontally separated. A representation of the infrared absorption spectrum with corresponding energy transitions from ground state to first excited state is shown.

### Absorption Features Relevant to Short Wave Infrared Region

The 1-3  $\mu\text{m}$  (1000-3000 nm) region (referred to as SWIR), is dominated by the energy-level transitions of vibrational *combinations* and *overtone*s of the fundamentals that occur in the mid-infrared region. The critical features due to vibrational energy-level transitions in the SWIR region are from the stretching and bending of the

- Hydroxyl (OH) bond
- Water (H<sub>2</sub>O)
- Carbonate (CO<sub>3</sub>)
- Ammonia (NH<sub>4</sub>)

The hydroxyl anion is crucial, because its bonding with specific ions in the minerals provides a diagnostic absorption features at specific wavelengths. The cation-OH's producing the diagnostic features are

- Al-OH
- Fe-OH
- Mg-OH

Minerals with the above bonds will show absorption features in the reflectance spectra and therefore can potentially be identified (figure 8.10). Minerals that do not have the typical H<sub>2</sub>O, OH, Mg-OH, Al-OH, Fe-OH and CO<sub>3</sub> arrangements, will not show absorption peaks in this region and in turn show high reflectance.

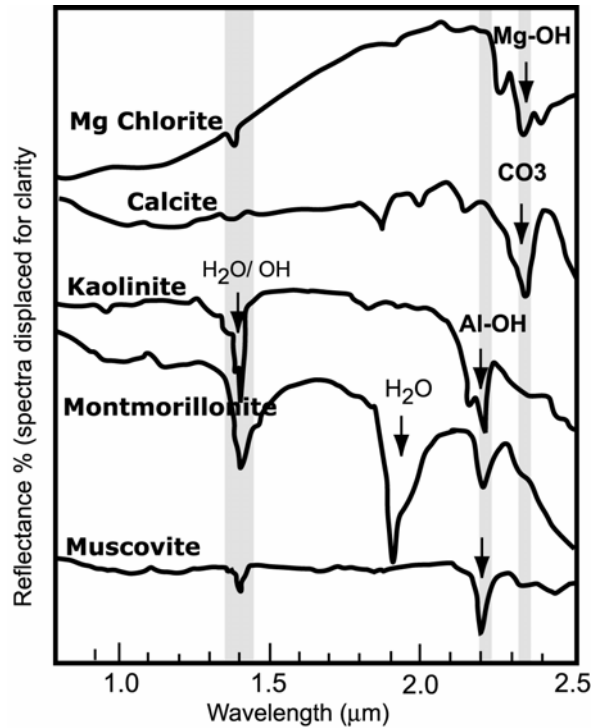


**Figure 8.10:** Some spectra of minerals showing vibrational absorption features, with the common ones being OH, H<sub>2</sub>O, Al-OH, Mg-OH and CO<sub>3</sub>.

**Table 8.1:** Major absorption features for minerals in the 1-2.5 μm region. The absorption peaks are the related overtones and combinations of the fundamentals that occur in the mid to far infrared.

Molecule	Absorption peak	Minerals showing feature
H <sub>2</sub> O	1.9 μm	Smectites, vermiculite, sulfates
OH	1.400 μm, 1.75-1.85 μm in some minerals	Amphiboles, smectites, vermiculites, kaolinite, jarosite, gypsum
Al-OH	2.16 -2.22 μm	Kaolinite, smectites, vermiculites, micas
Mg-OH	2.30 - 2.36 μm	Mg-chlorites, amphiboles, Mg-smectite
Fe-OH	2.23 – 2.295 μm	Fe-chlorite, biotite, Fe-smectite (nontronite)
CO <sub>3</sub>	2.30 – 2.35 μm	Calcite, dolomite, siderite, magnesite,

### Factors Affecting Reflectance Spectra of Minerals

Reflectance spectra are sensitive to several local structure of minerals including compositional and disorder changes in combination with grain sizes including mixture of

minerals. Unlike XRD which is largely sensitive to crystal structure of the sample, the sensitivity of reflectance spectroscopy to several parameters of the sample, makes interpreting the spectra difficult. But it also provides a valuable diagnostic tool to derive information of several parameters of the mineral for many samples. Reflectance spectroscopy is affected by

- Composition of minerals
- Crystallinity (or order)
- Particle Size
- Mixtures of minerals

#### ***4.3.1 Composition***

Compositional differences of individual mineral groups can be expressed in subtle shifts in the reflectance spectra of micas, chlorites and carbonates (provided no overlap occurs with other mineral absorption peaks). The composition differences are highlighted in the shifts in the wavelength of the absorption peaks but does not change the overall spectral signature of the mineral. Examples of compositional variations are found in

- Carbonates, where the Ca to Mg increase in the carbonate shifts spectral absorption peak to lower wavelength from calcite to dolomite to magnesite.
- Sericites, where the Al to Fe increase in micas shifts the spectral absorption peak to higher wavelength from muscovite (2.19  $\mu\text{m}$ ) to phengite (2.22  $\mu\text{m}$ ).
- Chlorites, where the substitution of Fe for Mg shifts the most intense absorption peak from 2.36  $\mu\text{m}$  (Mg rich) to 2.26  $\mu\text{m}$  (Fe-rich).

#### ***4.3.2 Crystallinity***

Minerals can have short range disorder in their structure, which with other factors such as grain size and dislocations is referred to as crystallinity. With reflectance spectra it is possible to differentiate between “crystalline” and “poorly crystalline” kaolinite. For the asymmetric absorption doublet at 2.16-2.18, well crystalline kaolins have a increased sharpness of the 2.16 feature while the poorly crystalline kaolins have a broad doublet.

#### ***4.3.3 Particle Size***

The particle size of the sample and individual minerals can affect the spectra. Generally, smaller particles show brighter spectra. Different sizes of individual mineral can cause a broadening and subtle shifting of primary absorption peaks. For example, hematite 0.9  $\mu\text{m}$  peaks shows broadening and shifting of the maximum absorption to longer wavelengths with an increase in grain sizes. Therefore, in a mixture of minerals with close or overlapping absorption peaks, it is difficult to differentiate between particle size or composition differences.

#### ***4.3.4 Mineral Mixtures***

Most natural samples are made up of mineral mixtures, and how these mixtures affect the spectral signatures is important for proper identification of minerals. Mineral mixtures can be expressed in the spectra as either linear or non-linear.

In linear mixtures, the mixed spectrum= X% mineral1 + Y% mineral2 +.... The absorption intensities likely to reflect the proportions of each mineral in the mixture. Unfortunately, this is rare in natural sample mixtures because of the varying mineral mixtures are influenced by several non-linear factors such as different absorption

coefficients between different minerals, the type of mixture whether it is intimate or a coating, and multiple scattering with the volume of the mixed minerals.

For non-linear mixtures which is mostly applicable to natural samples, intensity of absorption features do not correspond to proportion of particular mineral in mixture. Therefore, some minerals will affect the spectra stronger than others irrespective of their percentage of the total. For example, clay minerals (phyllosilicates) will dominate spectrum in mixtures of carbonates and clays, while talc will dominate a mixture of clay minerals. Furthermore, feldspars and quartz do not show absorption in the SWIR range therefore a sample with significant feldspars will be biased to the clay minerals. The greatest effects on non-linear contribution to the spectra is found with opaque minerals such as sulphides, which in minor quantities are known to significantly lower the overall reflectance of the spectra.

### **Spectral Interpretation**

The simplest method to conduct spectral interpretation is to match known patterns of minerals to the unknown patterns. However, this is difficult and awkward if you don't know approximately what is in the sample, and especially if mixtures are present. Dividing the spectra into different parts makes the interpretation easier. An approach to interpret spectra with several mineral spectra and causes for absorptions shown in figure 8.11.

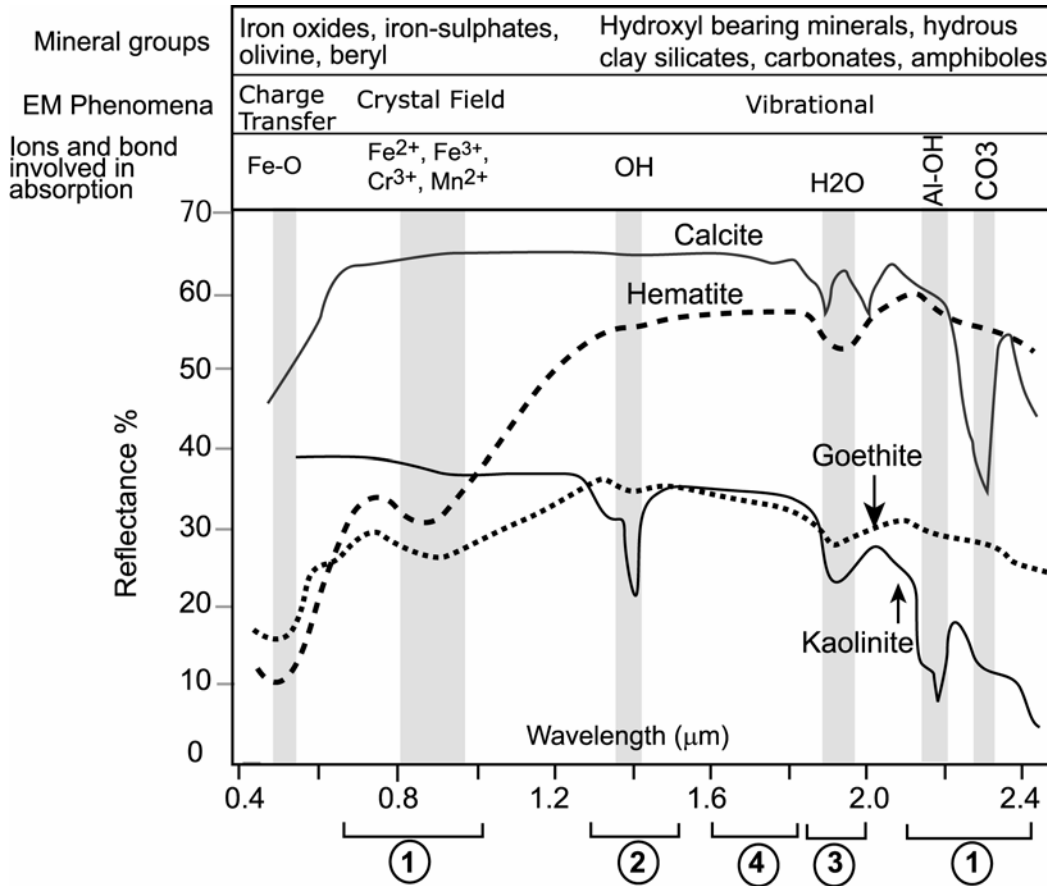


**Figure 8.11:** Spectra of hematite, goethite, kaolinite and carbonate with the main absorption causes of absorption features. Circled numbers are the sequence of steps recommended to follow to interpret unknown spectra.

The first step is to view the spectra in the 2-2.4  $\mu\text{m}$  range and note the wavelengths and shapes of deepest absorption features. Using this compare with library to narrow down the minerals. Also look at the .5-1.0  $\mu\text{m}$  region to identify any iron bearing minerals. Absorption peaks in this region indicate pure iron minerals (hematite, goethite) or iron bearing silicates (Fe- chlorite) and sulfates (jarosite). A comparison with library spectra will identify major mineral.

The next step (2) is view the features in the 1.3-1.5  $\mu\text{m}$  region to aid in confirmation of the features found in step 1.

Step 3 is to look at the water absorption feature at 1.9  $\mu\text{m}$  to determine whether water bearing minerals exist. The depth and shape provide a clue, with deeper features indicative of water bearing minerals (smectite).

For the last step, look at 1.55 – 1.85  $\mu\text{m}$  region to see if any absorption features are present. Absorption in this range is diagnostic of sulfates (gypsum, jarosite).

The advantage of reflectance spectra are its rapid collection from untreated samples. Thus spectra are being increasingly collected from core and drill cuttings to provide downhole mineralogical information. The viewing of spectra from downhole samples provides a quick and efficient method to view mineralogical changes occurring downhole. Further, it is possible to extract compositional information on micas and highlight in situ against transported regolith. The acquisition of downhole changes in iron and phyllosilicate mineralogy, mineral composition and possible regolith unit demarcation, have made reflectance spectra an important tool in the mining environment.

## 9. RIETVELD METHOD OF QUANTITATIVE XRD USING SIROQUANT

---

---

### BACKGROUND

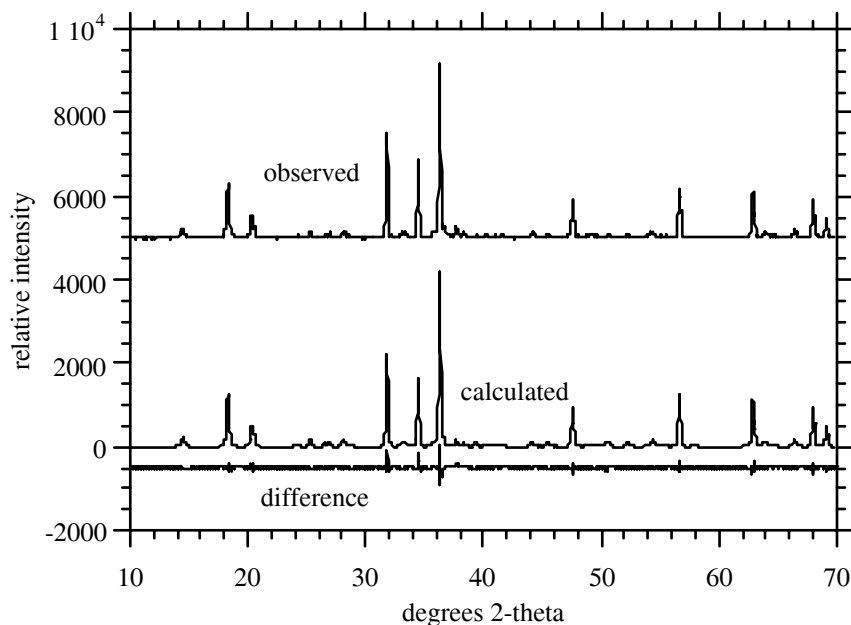
---

---

Quantitative X-ray diffraction techniques traditionally involved the measurement of the intensity of chosen peaks and subsequent comparison with those in standard calibration mixtures. However, these methods were tedious, as standards needed to be made up for a variety of situations and intensity anomalies caused by angular dependent aberrations such as preferred orientation often made the method unreliable.

The foundations for multiphase profile analysis of the complete powder diffraction pattern were first laid down by Rietveld (1969). He showed that it was possible to replicate a measured diffraction profile with a calculated pattern. The advantage of full profiling is that residual errors caused by intensity aberrations inherited from sample preparation or from using imperfect structural models tend to be positive and negative over the full diffraction profile leaving the Rietveld phase scaling factors largely unaltered (Taylor, 1991). Other workers including; Hewat (1973), Wiles & Young (1981), Will, Huang & Parrish (1983), Hill & Howard (1986) and (Taylor, 1991) have since refined the technique, culminating in the writing of *Siroquant* .

Siroquant is a Rietveld-type multiphase analysis program which replicates a measured diffraction pattern by employing a least-squares fitting routine which adjusts the scaling factors until the calculated profile best approximates the measured one. In the process, a differential pattern is produced which indicates the degree to which the calculated pattern replicates the measured one. As an additional means of determining the degree of fit, the statistical parameter,  $\chi^2$  (chi-squared), is displayed after each least-squares fitting routine. Ideally, a perfect match is attained when  $\chi^2 = 1$ , however this seldom occurs. Generally, a good fit is indicated when the  $\chi^2$ -value is less than 3. The quantity of individual minerals present within a sample is calculated from their respective scaling factors and absorption coefficients. Figure 8.1 displays a typical Siroquant analysis of a bauxite that had 33.3% ZnO added to the sample as an internal standard. Generally, an internal standard is not required, however it is essential when quantifying the amount of amorphous and/or poorly-diffracting material in a sample.



SIROQUANT RESULTS

Scan File : A:\a10259.cps 01-04-1980  
 Jacaranda 1.5m 9.51-4mm (Background Removed)  
 Task File : C:\SQBETA\demo.tsk  
 Global Chi<sup>2</sup> : 2.63

PHASE	WEIGHT%	ERROR
Gibbsite	41.5	0.34
Boehmite	8.4	0.27
Hematite	12.9	0.21
Quartz	0.1	0.13
Anatase	2.7	0.13
Zinc oxide	34.5	0.23

**Figure 9.1:** A typical Siroquant analysis of bauxite containing an internal standard of 33.3% ZnO.

As mentioned, Siroquant has the provision for quantifying the amorphicity of a sample. The presence of poorly-diffracting material (PDM) in a sample causes a reduction in the diffracted intensity of the crystalline phases. The amorphicity of a sample may be due to a number of reasons. Minerals that are composed of particles smaller than several hundred Å, have broad diffraction patterns. The diffraction lines may be so broadened that they are lost in the background. Glassy materials have no three-dimensional periodicity and therefore give no diffraction lines. Disordered structures may have streaking in the reciprocal lattice, thereby contributing as well, to the poorly-diffracting material content of a sample (*pers. com.* John C. Taylor, 1993).

Rietveld analysis alone cannot quantify amorphicity. However, the addition of an internal standard (corundum or quartz are recommended) of known concentration, facilitates the quantification of the poorly-diffracting weight fraction. Siroquant uses the following equations in the quantification of poorly-diffracting material (Taylor, J. C. *pers. com.*, 1993):

Equation 1  $X_D = 1 - Y_S / X_S$

Equation 2  $X_I = X_D / (1 - Y_S)$

$X_D$  = weight fraction of PDM in the sample containing an internal standard,

$Y_S$  = weighed weight fraction of the internal standard,

$X_S$  = Siroquant weight fraction of the internal standard.

$X_I$  = weight fraction of PDM in the original sample containing no internal standard.

As the addition of an internal standard causes dilution of the sample with a subsequent loss in the intensity of diffraction peaks, it is preferable to run a sample without an internal standard, as well. The sample without the internal standard is used specifically for the purpose of quantifying well-crystallised phases while the sample containing the internal standard is used only for the amorphicity determination. To obtain the final quantification, the results from both samples are combined and normalised within the Siroquant program.

---

---

## METHODOLOGY

---

---

### **Create a task file**

This is a file of the minerals you know are present in the sample. SIROQUANT will not find any minerals itself. If a mineral is present but not listed in the Task File, it will not be quantified. If “amorphous” content is estimated, any crystalline minerals not in the task file will be included as part of any “amorphous” content.

**Load a .RAW file** – that is, the diffraction pattern.

### **Calibration**

At low angle the X-ray beam extends beyond the sample. This means all that part of the beam that does not hit the sample does not diffract to the detector, so the measured intensity results from only a percentage of the incident intensity. Beyond a particular angle all the beam strikes the sample so diffracted intensities are thereafter correctly in proportion to each other.

The calibration correction enhances the lower angle reflections proportion to the area of the beam not striking the sample. Also, it corrects for changes in the sample volume that is diffracting X-rays.

### **Background subtraction**

X-ray scattering from a sample includes non-Bragg scattering. This must be subtracted from the observed pattern. The shape of the background scattering is a smooth curve, higher in intensity at low angle. SIROQUANT provides a “Manual Background Subtraction” which works well for well-crystallized samples but which needs your help for most regolith materials. The presence of amorphous or poorly-diffracting material has the effect of introducing scattering bands into the XRD pattern in the 20 to 30° region. A scattering band is also present when using a glass sample holder. When quantification of amorphous or poorly-diffracting material is required, it is advisable to subtract the scattering bands during the background removal procedure, otherwise the quantity of well-crystallised material may be over-calculated. An apparent increase in the background level may be caused by peak overlap. In such cases, care must be exercised to ensure that not too much background is removed, otherwise phases associated with the peak overlap may be under-calculated. Apply the Manual Background Subtraction, then correct it to follow a uniformly decreasing smooth curve as in Figure 62.

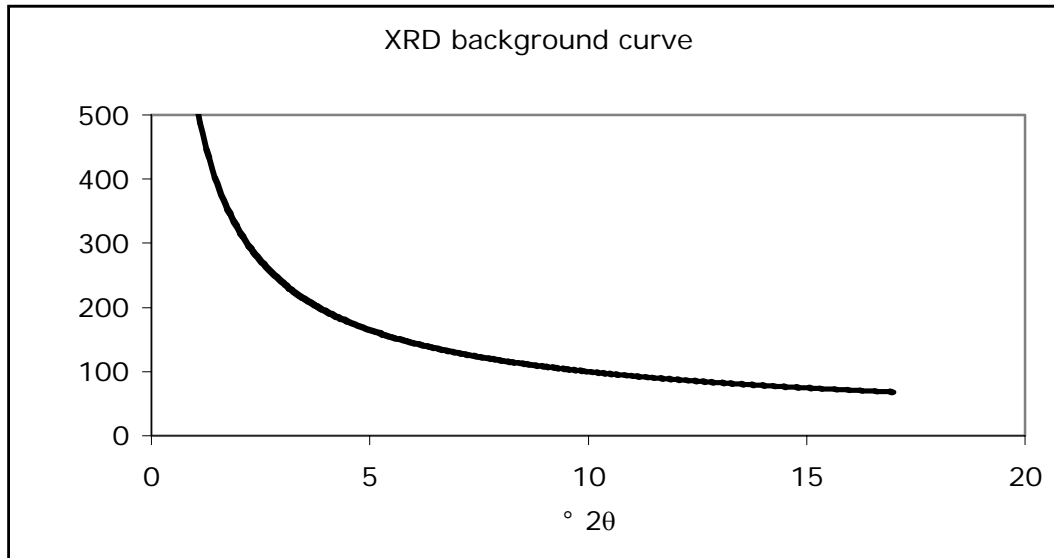


**Figure 9.2:** Shape of the background in an XRD pattern.

### **Initial quantification**

The pattern is now ready to be quantified.

First run the program set to Auto Prescale.

Second, look at the results to see which minerals are abundant.

If there is quartz, or an internal standard, then change the settings to "Refine Instrument Zero" and the peak width W for those minerals only.

Next turn off those variables and select whatever seems to need fixing from the most abundant mineral – peak width, orientation or cell parameters.

Next turn those variables off and vary parameters for the next phase needing help.

And so on.

---

## SIROQUANT for minerals

---

### 1. General issues concerning minerals

Laboratory and industrial chemicals have a formula. They obey Dalton's Laws of constant composition and multiple proportions: NaCl, KCN, NaNO<sub>3</sub>, K<sub>2</sub>CO<sub>3</sub>. These chemicals have fixed compositions, and their component atoms are in integer ratios.

Many minerals also obey these laws in the same simple way: quartz - SiO<sub>2</sub>, rutile -TiO<sub>2</sub>, galena – PbS, gibbsite – Al(OH)<sub>3</sub>. All minerals obey these laws, but some do so in a less obvious way. To show conformity with the Law of Multiple Proportions, many mineral formulae need to be written as 'site' formulae. Olivine - A<sub>2</sub>SiO<sub>4</sub>, for example, has a structural site, here denoted by 'A', which may contain Mg, Fe, or Mn in any proportion as long as the total is 2 atoms. And small amounts of many other divalent elements may reside in the A-site of olivine.

This has an immediate effect on Siroquant. Since Siroquant matches an observed pattern to a calculated pattern, the data must be available to make that calculation. But the composition of olivine is infinitely variable, from pure Mg<sub>2</sub>SiO<sub>4</sub> to pure Fe<sub>2</sub>SiO<sub>4</sub> or to Mn<sub>2</sub>SiO<sub>4</sub>. Obviously Siroquant cannot provide an exact match to any particular olivine XRD pattern, since both the positions of the lines and their intensity change as the Mg:Fe:Mn ratio changes.

Olivine is really a fairly easy mineral to quantify, because refinement of cell parameters allows a match with the d-spacings of the unknown, and geological experience, coupled with a relation between cell edge and chemistry, allows a formula to be selected close to the unknown sample's composition.

The commonest of all minerals, feldspar, is much more difficult to handle. Like olivine it has variable composition, from KaAlSi<sub>3</sub>O<sub>8</sub> to NaAl Si<sub>3</sub>O<sub>8</sub> to CaAl<sub>2</sub>Si<sub>2</sub>O<sub>8</sub>. Worse, unlike olivine which in any particular rock will have a constant composition, feldspars generally have a range of composition in one crystal. Na-Ca feldspar – plagioclase - is commonly compositionally 'zoned', generally with a Ca-rich core and an Na-rich rim. On top of that, K-feldspar can be monoclinic or triclinic, and the triclinic angles range from about 90° to 94° depending on the mineral's geological history. Just identifying a mineral as K-feldspar is only the first step; next the cell parameters need to be determined, and from them the K-Na ratio and/or the particular structural type established. Guides to doing this are in the section on specific minerals.

Feldspars are probably the worst of the common minerals for Siroquant. But amphiboles are not far behind. Their site formula is: AD<sub>2</sub>M<sub>5</sub>T<sub>8</sub>O<sub>22</sub>Q<sub>2</sub>, where A may be a vacancy or Na, D may be Na, Ca or K, M may be Al, Mg, Fe, Ti or almost any transition element, T is Si mostly plus Al, and Q is (OH), F or Cl. To estimate amphibole percentages accurately with Siroquant, the mineral's formulae needs to be determined by some

method, generally electron microprobe analysis. Then a specific file can be established for that amphibole.

A second problem with minerals, but one not at all confined to minerals, is that of preferred orientation. Many crystals exhibit a property known as cleavage. This is a planar direction, or symmetry related group of planar directions, along which the crystal splits more readily than in any other direction. When such a crystal is crushed for XRD and deposited on a flat substrate, more fragments lie with their cleavage parallel to the substrate than in any other orientation, thus rendering the overall orientation of the powder non-random – the crystals lie on a preferred plane, their cleavage plane. Micas are the worst minerals for this, calcite, with 3 cleavage planes at 74° to each other is difficult to randomise, as are feldspars, which have excellent (001) cleavage and good (010) cleavage. Siroquant can allow for preferred orientation up to a point, but it is much better to be aware of the problem and fix it during sample preparation.

Fibrous minerals have the same problem, causing the prism planes parallel to the fibre direction to be grossly preferred over all other planes.

So the first rule for mineralogical Siroquant is to know your own sample. Know its geological setting, know its mineralogy, and wherever possible, know each mineral's chemistry and make up an appropriate Siroquant file for it. A careful orientation study is invaluable, particularly if you have many samples from the same provenance.

## **2. SIROQUANT variables - which to vary and when not to.**

### Cell parameters

As may be evident from the foregoing general discussion, minerals which exhibit solid-solution (diadochy) will have cell parameters that are determined by their composition. Contrary to that, minerals that do not have a compositional range generally do not show any variation from ideal cell parameters. Therefore do not vary cell parameters of a phase unless you have evidence that it is different from the Siroquant standard phase.

Of the common minerals, quartz shows least variation in cell parameters (effectively none). Those which should generally NOT be varied are:

- Quartz
- Zircon
- Sillimanite
- Kyanite
- Topaz
- Beryl
- Talc
- Pyrophyllite
- Corundum
- Rutile
- Brucite
- Gibbsite

Pyrite  
Galena  
Gypsum  
Fluorite  
Halite

Those which should always be varied (provided there is enough to yield enough well-resolved peaks – see below) are

Olivine  
Garnet  
Epidote  
Pyroxenes  
Amphiboles  
Micas  
Feldspars  
Feldspathoids  
Hematite  
Ilmenite  
Spinel  
Goethite  
Sphalerite  
Carbonates

Before allowing the cell parameters to vary, think about what is happening in the program. Cell parameters are estimated by a least-squares routine, which establishes the best fit between the observational data and the variables – in this case the cell parameters. With one cell parameter (cubic crystal,  $a$ -parameter), one reflection will allow Siroquant to estimate  $a$ . It will be a poor estimate. Generally you need at least 3 times as many observations as you have variables, and more than 4 times is much better. So for a triclinic plagioclase you need to be able to identify at least 18 clear and distinct plagioclase peaks. In most rocks having plagioclase as a major phase, even 30% plagioclase may not be enough to provide this minimum number of observations. In such a case, you should extract some plagioclase crystals as part of your orientation study and run plagioclase alone (or at least as a 60% or better concentrate). From such a scan reliable cell parameters will be obtained, and an even better set if an internal standard such as quartz or ZnO is included. These parameters can then be keyed into the Siroquant file when doing the bulk sample quantification.

#### Peak width

All “good” minerals yield sharp Bragg reflections, and generally the default peak half-width is suitable for these. All minerals present to a reasonable extent (say >15%) may have their peak-width varied at some stage in the Siroquant refinement process, but generally not at first.

“Bad” minerals in this context are those that yield broad Bragg reflections. There are three main reasons:

The crystallites of the mineral are very small (<1  $\mu\text{m}$ );  
The crystals are strained; or,  
The crystals are chemically inhomogeneous.

In each case, allowing the peak-width parameter to vary is essential to achieving a good agreement between the observed and calculated patterns.

Peak broadening caused by small crystal size has a second effect – peak positions are shifted from their ideal Bragg position, generally only low-angle (<20° 2 $\theta$ ) peaks show appreciable displacement. It may be necessary to exclude such peaks once they are recognized, as the formal calculation of peak position assumes ideal crystals, even when the peak-width parameter reveals ultra-small crystals.

A third effect occurs with thin (platey) or fibrous minerals: certain Bragg reflections are broadened, others may not be. The number of coherently diffracting unit cells determines the peak width. Very thin flat crystals may be only a few unit cells thick (001 plane) but many cells wide (010, 100 planes). As a consequence  $00l$  reflections may be broad while  $hko$  reflections are sharp and  $hkl$  reflections in between. Siroquant cannot fully allow for this.

If a fine-grained mineral is present to a small extent, Siroquant does not generally handle the peak-width variable very well. A better strategy is to use a parameter from a previous refinement where that mineral was more abundant, or manually set the peak width until the peak appears to be well-fitted.

#### Preferred orientation

Even though Siroquant has a preferred orientation parameter, it is limited in its ability to fully compensate for poor sample preparation. The correct strategy is to ensure as random a sample as possible. This means careful grinding to reduce the particle size to about 5  $\mu\text{m}$ , followed by loose packing (though not so loose as to introduce sample thickness problems by having the X-rays penetrate unduly deeply into the sample). Spinning the sample allows the X-ray beam to “see” more crystal, but will have no effect on preferred orientation, since the sample is spinning in the plane of that orientation.

### **3. Approach should be guided by geological information**

The nature of the geological sample containing the minerals can help you to plan an appropriate strategy for Siroquant, so again, an orientation study is really essential

#### Coarse-grained (plutonic) igneous rocks

Amorphous material is very unlikely, so it should not be necessary to add an internal standard. However small amounts of alteration minerals may be present either from hydrothermal alteration or weathering. Optical examination by a petrographer is a very good idea before doing a lot of XRD on igneous rocks, and this should reveal the presence of alteration minerals.

Most minerals (other than quartz) in plutonic igneous rocks will not have “ideal” compositions, so the petrographic examination should be directed towards determining the composition of the major minerals, particularly the feldspars. It may well pay dividends to extract concentrates of the major minerals when a suite of samples from the same provenance is being examined. X-ray these concentrates (try to get at least 50% of each of the major minerals in each concentrate) and adjust the Siroquant parameters to yield the best possible fit for cell parameters, composition and peak width. These parameters can then be held constant during quantification of the unknown mixtures. This keeps the number of Siroquant variables to a minimum, and will lead to a more accurate result.

#### Fine-grained (volcanic) igneous

The approach to volcanic rocks is essentially the same as for plutonic, except that glass (amorphous phase) is more likely, and cryptic alteration of fine-grained minerals is also possible. Petrographic examination will help, but may not show much in the fine-grained material. Unless there is clearly no glass or alteration, an internal standard is a wise inclusion.

Solid solution is again a likely problem, but it may be a lot harder to concentrate the major minerals, especially those in the fine-grained matrix of the rock. The structural state of feldspar will also have to be assessed (see section on individual minerals)

#### Metamorphic rocks

Generally approach as coarse-grained igneous.

#### Sedimentary Rocks

Sedimentary rocks tend to be mineralogically simpler than igneous or metamorphic rocks, being dominated either by quartz or carbonates or clays. Sandstones are generally very quartz-rich, but they may contain appreciable feldspar which itself may have altered to clay. Trace minerals such as zircon, anatase, rutile, tourmaline, garnet, ilmenite and magnetite may all be present. If you routinely include these minerals in your refinement of the XRD pattern, check that the main peaks are really present, as Siroquant will almost always find a bit of a designated phase if the background in the region of its main peaks is high enough. Clay-rich sediments are a very different problem. Adding an internal standard is mandatory, because some clays do not always reveal their presence in a bulk XRD scan. (See the section on Regolith and Soils below).

#### Sulfide Ores

Unless alteration minerals are evident, amorphous material is unlikely. If alteration has occurred, sulfate minerals may be present, some of which are soluble in water, and you should consider this possibility during sample preparation.

Solid solution and complex structural variation occurs in some sulfides, so as with the silicates, determine the cell parameters and composition of your material before doing detailed Siroquant analyses.

There are very many sulfide minerals, so you need to be alert for the uncommon, but not before the common minerals have been correctly fitted.

### Regolith and soils

These are the most difficult geological samples to quantify by XRD, and in some cases it is impossible to quantify them using XRD alone. Quantifying the mineralogy of a regolith sample has been a long sought goal of soil and clay scientists. A combination of quantitative phase separation followed by electron microscopy and micro-analysis, X-ray diffraction, sub-sample chemistry, infra-red analysis, and so on and so on..... will use up all your money and most of your time. And yield a good answer!

The main difficulty is that all the known techniques are based around a theoretical (mostly ideal) mineral or a standard sample –often a well-characterized museum specimen. Unfortunately these reference minerals do not always match the real world of regolith clays. Siroquant partly gets around the problem by comparing the unknown X-ray pattern to a suite of reasonably typical clays, but the approach still assumes that the clays diffract as 3-dimensional crystals.

All the alumino-silicate clays, which are most of those in the regolith, have excellent 2-dimensional structures. Mica has a regular 3-D structure, illite almost does, some kaolinites do, others don't, halloysite and smectite do not. The 2-D X-ray patterns from all these clays overlap exactly in the region around 4.5 Å (the *02, 11* band), at about 2.5 Å (the *20, 13* band), and at 1.5 Å (the *06, 33* band), making it impossible to separate the contributions when 2 or more clays are present. The basal (*001, 002* etc) reflections, as is well known, do allow each clay to be recognized – PROVIDED THESE REFLECTIONS ARE PRESENT.

In a normal procedure, a clay fraction (<2 µm size) is extracted, and this is an essential part of a regolith orientation study. This fraction does not represent the silicate clay minerals quantitatively. Much mica and illite and some kaolin remains coarser than 2 µm or stuck to coarser particles, even after determined dispersal. The clay fraction can be used to identify the clays present, but it won't quantify them in the original sample, even if the clay size fraction has been determined quantitatively.

Because of its inherently 2-D character, smectite in a bulk regolith sample occurs as irregular sheets, some only one layer thick, others not much thicker, draped over the coarser particles. When these are X-rayed, the basal 15-Å spacing is almost invisible because too few consecutive sheets are superimposed and Bragg diffraction does not occur, even from a sample whose clay fraction clearly shows smectite (Figure 9.3). When the clay fraction is prepared by sedimentation on to a substrate, several smectite sheets layer one on the other. As few as 6 layers yield a very clear signal.

This means that smectite may be seriously under-estimated by Siroquant. Although smectite's *02,11* band may be show appreciable intensity, Siroquant may attribute this to another clay, such as kaolinite. The greater than expected intensity now attributed to

kaolin's  $02$ ,  $11$  band is allowed for by the orientation parameter, so that what may in fact be a random sample appears to have kaolinite "anti-oriented". That is, the orientation parameter is adjusted by the software as though the kaolinite flakes were sitting on their edges, not their faces or randomly. By this adjustment to the orientation parameter, the relative intensities of the kaolinite  $001$  and  $02$ ,  $11$  bands can be made to fit the pattern, and the smectite content is reduced.

Although the Siroquant estimate of the clays may be seriously in error, the estimate of total clay is usually quite good. This is because all the clay diffraction energy has been accounted for in the  $3hk$  bands, it is just that the proportions are wrong.

Without extra information, it is really impossible to know what has actually happened during the Siroquant analysis. To circumvent the problem adopt the following strategy.

From the orientation study, include the clays you know to be present and of course all the other minerals. This will estimate total clay, and correctly estimate the non-clay minerals. Have the samples measured for their cation exchange capacity (CEC). Smectite has a CEC of about 1000 millimoles of charge/kg (=100 meq/100g). If organic matter is absent, smectite contributes almost all the CEC in a normal well-weathered regolith sample (vermiculite has a similar high CEC and has to be looked out for). So if your sample shows no 15-Å or 14-Å smectite or vermiculite peak, but has a CEC greater than about 100 mmol+/kg, be very suspicious that smectite is present. It may be there as interstratified illite-smectite, or just as smectite, but it will probably be there.

Another approach is to measure weight loss vs temperature on heating (Thermogravimetric analysis). Kaolinite loses structural (OH) over a temperature range of 400-500°C, and the weight loss in this interval can give a fair estimate of kaolinite %. Bulk chemical analysis adds further cross checks to the mineral analysis.

Armed with at least some of this extra information, of which total CEC is probably the most valuable and least expensive, you can return to Siroquant and try to force it to fit more plausibly. One approach is to set the smectite orientation factor to a high value (2 or more) until the ratio of smectite to other clays starts to agree with your other results. Setting a high orientation parameter reduces the calculated intensity for  $001$  and enhances those of the  $hk$  bands. Keep the orientation parameter for the other clays at 1 (this assumes you have made a serious effort to achieve a truly random sample; having quartz and other granular minerals in a bulk sample helps this enormously).

Vermiculite and halloysite add their own complications. Vermiculite has a high CEC like smectite, but it generally gives appreciable  $00l$  reflections and Siroquant is able to handle it fairly well. However it becomes very difficult to quantify both vermiculite and smectite in the sample unless you have several other results (CEC, chemistry, water loss on heating for example). Halloysite has almost the same pattern as poorly ordered kaolinite, though it is possible to quantify both clays using Siroquant's "observed" files for the minerals if they are the only clays in the sample.

“Amorphous”, or poorly diffracting material (PDM)

Some regolith samples, and some volcanic rocks, contain material that yields no diffraction pattern, or only a very diffuse pattern. Among these are volcanic glass, ferrihydrite (the mineralogical equivalent of rust), opal, and some alumina species found in lateritic regolith. An internal standard such as ZnO is essential if PDM is suspected. The first clue to its presence is a high background in the XRD pattern and low maximum peak intensities. A broad background hump between about 4 Å and 2.7 Å is another indicator of PDM. Siroquant includes a routine for estimating PDM content (Amorphous content analysis), based on the inclusion of a known wt% of a standard such as 25 to 30% of ZnO.

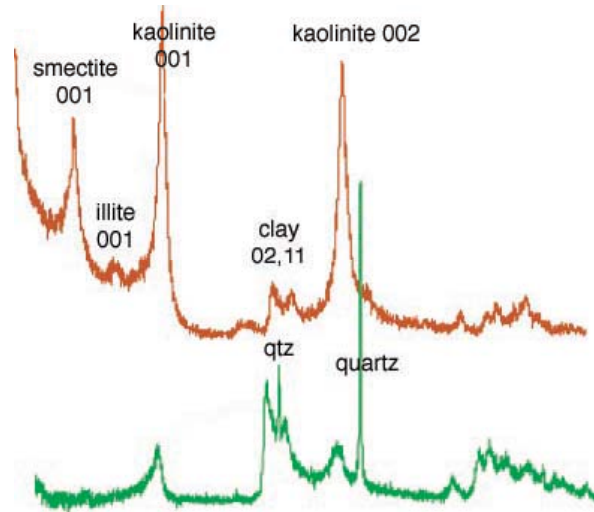


**Figure 9.3:** XRD scans from one sample. The upper pattern is from a <2µm extract, the lower scan is of the bulk sample. Smectite does not appear at all in the bulk sample scan, but the ratio of the 02, 11 band to the kaolinite 001 peak warns of a potential problem. In a random kaolin sample,  $I_{001} > I_{02,11}$ .

#### 4. Choosing the most appropriate mineral from Siroquant’s QUANT.DAT<sup>1</sup> file

It is not possible here to include a treatise on mineralogy, but it is difficult to correctly analyse a rock sample by SIROQUANT if you have no mineralogical knowledge. SIROQUANT will only quantify the phases you give it, so it is important to select the standards that fit your minerals most closely. The following notes assume familiarity with the terms and concepts of mineralogy.

There are many times when it is not practicable to do an orientation study and determine the composition of the minerals in the sample. In such cases a combination of intelligent guessing and trial and error is the quickest way to choose the appropriate SIROQUANT mineral for the sample. Table 1 lists the SIROQUANT entries for the common rock-forming minerals, and the rock types they are most likely to be found in. Lacking

---

<sup>1</sup> The QUANT.DAT file contains the crystallographic data from which SIROQUANT calculates percentages. If you need a mineral not supplied in the standard data base it must be obtained from the supplier.

specific information about mineral composition, use those in boldface print. There are times when a mineral identification routine will select a highly unlikely mineral as its first choice, and it is up to the user to consider if this selection is likely in the particular geological setting of the sample.

### **Alkali feldspar**

There are three structures of alkali-feldspar: sanidine, orthoclase or microcline. If you know the rock type you can make a good guess at the variety: volcanic rocks mostly have sanidine or orthoclase, plutonic rocks orthoclase or microcline. Microcline is triclinic, orthoclase and sanidine monoclinic; examine 2 regions of the XRD pattern to help decide whether the feldspar is monoclinic or triclinic (or to confirm the correctness of the decision made by your mineral identification routine). Look first in the region between 4 Å and 3.3 Å, then in the region between 3 Å and 2.7 Å. Figure 1 shows what to look for.

Figure 9.4 Differences between monoclinic orthoclase and triclinic microcline. A) 3.3- to 4-Å region. B) 2.8-Å region.

Once you have the correct structure, refining the cell parameters will allow a check on the composition. From K to Na--feldspar the cell parameters change, and the composition can be determined from the *a*-parameter alone, or from the cell volume (Fig 9.5). If the composition is close to the K-feldspar end, select either #19 Orthoclase 1 or <#88 Maximum microcline or if intermediate microcline, #87. If the composition is considerably different (say 30%Na-feldspar in the solid solution) it may help to make up your own QUANT.DAT file with 0.7K and 0.3Na in the K-site.

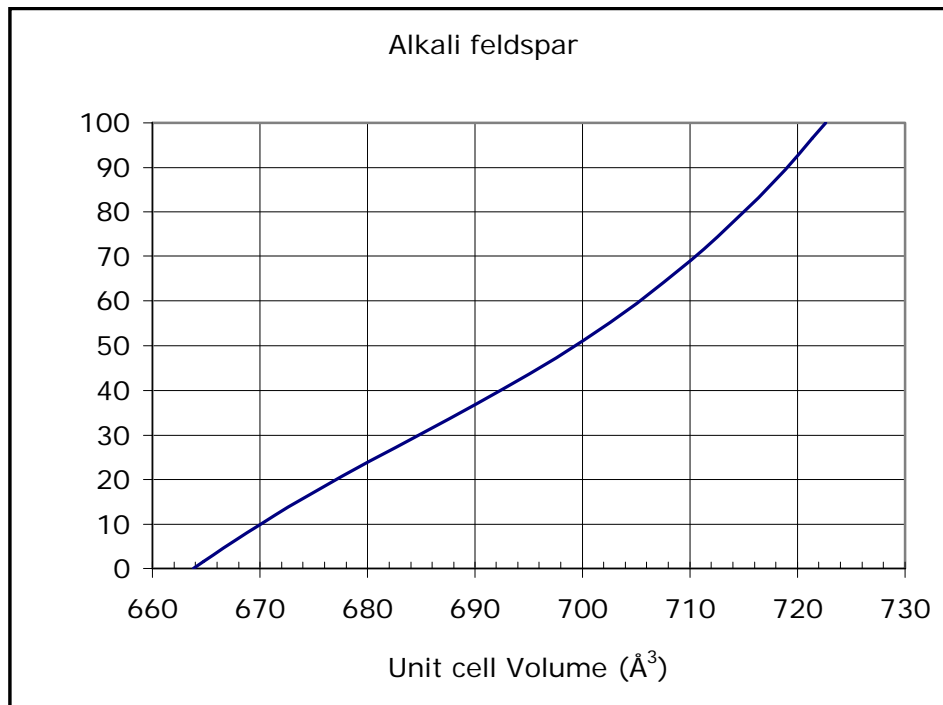


**Figure 9.5:** Relation between unit cell volume and composition of alkali feldspar in terms of % Or (KAlSi<sub>3</sub>O<sub>8</sub>) end member.

## Plagioclase

Plagioclase only has the one structural state – always triclinic. However it has complex microstructures and is generally compositionally zoned within the crystals. As a result the peaks are never very sharp, and an excellent match with a pure standard, such as SIROQUANT uses, is always difficult if not impossible. If the pattern is relatively good, cell-dimension refinement may give a clue to composition by use of the  $\gamma$  cell angle (Figure 9.6). This is unlikely to be reliable if the sample is mixed with K-feldspar, as there are too many peaks overlapping. Purifying the plagioclase as part of the orientation study is the best approach. Electron microprobe analysis, with optical microscope evaluation of the extent of zoning, will yield far more certainty about the plagioclase composition, but still won't ensure a good SIROQUANT match.

In many cases it may be simplest to guess the appropriate standard to use from the geology of the rock. For pegmatites and late stage plutonic rocks or dykes use albite #206 Albite (low) accurate study, NaAlSi<sub>3</sub>O<sub>8</sub>

For granites and similar felsic rocks use andesine #1548 Albite,-Ca,low,An28

For basalts and gabbros use labradorite #1533 Labradorite An52.

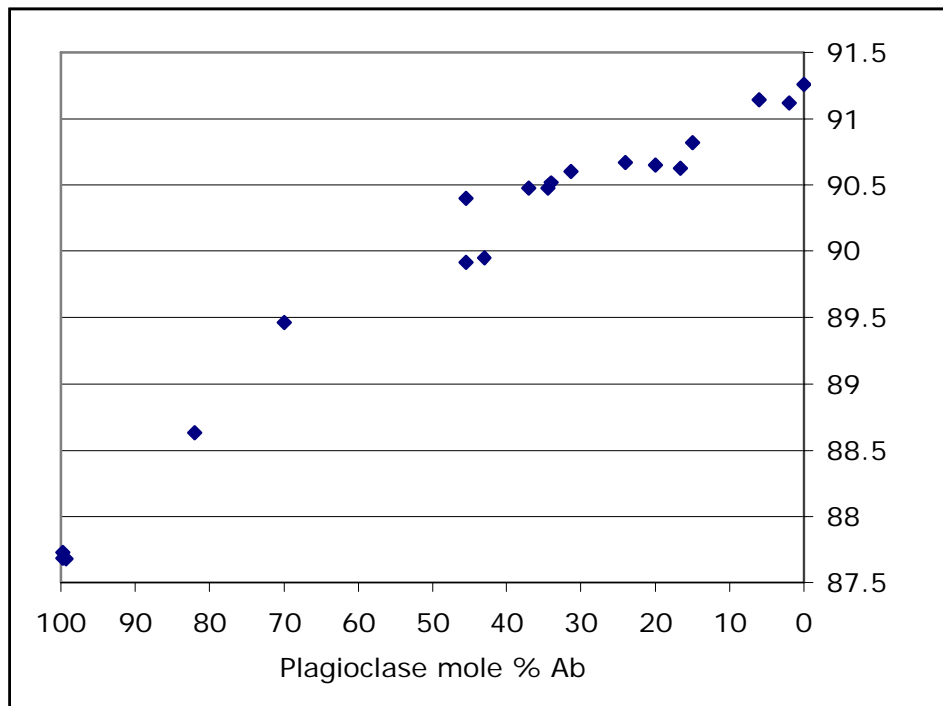


**Figure 9.6:** Plagioclase: relation between  $\gamma$ -cell parameter and composition expressed as mole % Ab (Na-end member).

## Olivine

Olivine should pose no particular problems for SIROQUANT, though you may need to obtain the Mg:Fe ratio and make an appropriate QUANT.DAT file. The composition can be determined accurately from the cell dimensions. Basalts commonly have olivine

compositions at the Mg-end of the solid solution series, and olivine #211 Forsterite,  $\text{Mg}_{0.8}\text{Fe}_{0.2}\text{SiO}_4$  will generally serve.

### Garnet

Garnets have a wide range of solid solution involving at least Ca, Mg, Fe, Al and Mn. The position of the peaks will be well fitted by SIROQUANT by varying the  $a$ -parameter, but the intensities may require knowledge of the garnet variety. Broadly, there are 2 common groups of garnet: dark-coloured “pyralspites”, having Mg-Fe<sup>2+</sup>-Mn variation, and paler-coloured grandites having Al-Fe<sup>3+</sup> variation. The 2 groups are generally distinguishable on colour if the garnets are big enough, though Fe-rich grandites may be dark. The  $a$ -parameter of pyralspites is generally < 11.8 Å, while that of grandites is >12 Å. Regionally metamorphosed rocks such as schists and gneisses tend to have pyralspites, contact metamorphic limestones may have grandites.

### Pyroxene

Most common pyroxenes are augite, found in mafic igneous rocks such as basalts and gabbros. They have a 3-way compositional solid-solution between Ca, Mg and Fe, and three different structure types. The particular structure in a sample (either of the 2 clinopyroxenes augite and pigeonite, or orthopyroxene) should be determinable from the XRD pattern of a concentrate. After this, chemical analysis is the only certain way to get the mineral composition, from which you can select the appropriate SIROQUANT standard to use.

### Amphibole

Like the pyroxenes, amphiboles come in 3 varieties: 2 varieties of clino-amphibole and ortho-amphibole. The compositional variation in amphiboles is large, and picking the appropriate standard demands knowledge of the composition.

### Mica

Unless you are working with unusual rocks, there are only 2 species of mica to consider. Both have the typical strong peaks at 10 Å and 3.33 Å (which generally falls on top of the strong quartz peak at 3.34 Å). Muscovite (K-Al mica) has  $b$ -parameter <9.0 Å and biotite (K-MgFe mica) has  $b$ -parameter >9.0 Å. The strong layer silicate peaks at about 4.5 Å and 1.5 Å easily distinguish these 2 if there is doubt about the identity.

<i>hkl</i>	Muscovite		Biotite	
	<i>d</i> -spacing	intensity	<i>d</i> -spacing	intensity
001	10.0	100	10.0	100
002	5.0	30 to 50	5.0	5 to 20
020	4.49	70	4.59	10
060	1,499	30	1.535	30

In clays and weathered rocks, fine-grained mica, generally termed illite, may occur. True illite has much broader peaks than the other micas, and the  $hkl$  peaks of illite (particularly in the region from 4.5Å to 3.5Å) are weak or absent. Siroquant has an observed file for

illite, which should be used if the mica pattern shows broad peaks and the sample's geology suggests weathering or alteration.

### **Chlorite**

Chlorites have a large compositional variation among their essential octahedral cations Mg, Fe and Al. This variation affects both cell parameters and peak intensities. They also have at least 4 different structure types (known as polytypes), of which the Ila structure is by far the most common, and in most cases should be the only one you consider. The other three types are rare, and restricted to iron formations or some hydrothermal rocks. Look carefully for the polytype defining reflections if you suspect anything other than the Iib polytype (see for example Bailey (1980) for this.

As far as composition goes, typical chlorite from a metamorphic rock such as a phyllite or greenschist is likely to be Mg-rich, and the SIROQUANT entry for #758

Chlorite, Iib 1-layer  $\text{Mg}_{4.54}\text{Al}_{2.12}\text{Fe}_{.46}\text{Si}_{2.85}\text{O}_{18}\text{H}_8$  is probably the most appropriate.

Chlorites from iron-formations are Fe-rich chamosites. SIROQUANT has 3 to choose from, and trial and error may be needed to achieve the best fit.

### **Hematite**

Hematite may contain appreciable Al substituting for Fe, and this changes cell parameters and peak intensities. There is no simple relationship between cell parameters and composition (Stanjek, 1992), but aluminous hematites have a shorter *a*-axis than does pure hematite. If  $a = 5.035 \pm 0.005$ , use hematite. If  $a < 5.03$ , 5 to 10% of the Fe may be replaced by Al. In this case try using #1746 Hematite 12% Al sub. Substitutions of Al beyond 15% are rare.

### **Goethite**

Like hematite, goethite can have Al substituting for Fe. The substitution affects the *b*- (~10 Å) and *c*-cell (~3 Å) parameters in a consistent way (see Schulz, 1984), and refinement of parameters allows an estimation of Al content and therefore the correct selection of which goethite to use. (Note that the orientation of cell parameters for the Siroquant entry differs from that used by Schulze and mineralogical texts). Schulze proposes: Mole% Al =  $1730 - 572c$ . He points out that peak broadening shifts the 110, 111 and 140 peaks appreciably from their ideal Bragg position. If there are sufficient well-resolved goethite peaks for a cell-dimension refinement (more than 9, ideally) but they are broad, it may be a good approach to exclude these 3 peaks.

### **Spinel**

Magnetite is the common spinel of igneous rocks and beach sands, with chromite also very common in these rocks and sediments. Test for magnetism if you suspect magnetite, as these two minerals have very similar *a*-parameters, but chromite is barely magnetic. Other spinels may be determined from the cell-edge, but a microprobe analysis is the best way to be sure you have the right mineral.

## **Carbonates**

The rhombohedral carbonates are quite easy to accurately identify from their XRD pattern. Calcite is generally close to ideal  $\text{CaCO}_3$ , though a little Mg may slightly change the cell parameters. Along the solid solution series dolomite-ankerite  $\text{Ca}(\text{Mg,Fe})(\text{CO}_3)_2$ , any Mg:Fe ratio is possible, but only the end compositions are available in Siroquant. If an accurate quantification is needed it may be necessary to make up a specific QUANT.DAT file at the Mg:Fe ratio of the sample based on #31 dolomite or # 136 ankerite. Similarly for the magnesite-siderite solid solution series, use #129 magnesite or #24 siderite and adjust the Mg:Fe ratio appropriately.

**Table 1:** List of the major rock-forming minerals, their most common rock association, and **recommended selection** when there is no other information.

Mineral	SQ #	Main rock types
<b>FELDSPARS</b>		
Adularia, $\text{KAlSi}_3\text{O}_8$	204	pegmatite
Albite (high), $\text{NaAlSi}_3\text{O}_8$	207	volcanics
Albite (low)	20	granites
<b>Albite (low) accurate study, <math>\text{NaAlSi}_3\text{O}_8</math></b>	206	granites
Albite (high, K-bearing), in cryptoperthite	1542	volcanics
<b>Albite, -Ca, low, An16</b>	1546	granites
<b>Albite, -Ca, low, An28</b>	1548	granodiorites
Albite, high	1543	volcanics
Albite, high, Calif.	1541	volcanics
Albite, high, from cryptoperthite	1525	volcanics
Albite, inter., California	1538	volcanics
Albite, low	1550	granites
Albite, low, Calif.	1545	granites
Anorthite (hexagonal), $\text{CaAl}_2\text{Si}_2\text{O}_8$	254	????
Anorthite (monoclinic), $\text{CaAl}_2\text{Si}_2\text{O}_8$	253	????
<b>Anorthite, An94, Calif.</b>	1528	basalts, mafics
Anorthite, Austria	1530	basalts, mafics
Anorthite, body-centred, $\text{CaAl}_2\text{Si}_2\text{O}_8$	568	basalts, mafics
Anorthite, $\text{CaAl}_2\text{Si}_2\text{O}_8$	153	basalts, mafics
Anorthite, Monte Somma	1536	basalts, mafics
Anorthite, Switzerland, An91	1537	basalts, mafics
Anorthoclase 1, $\text{Ca}_2.03\text{K}_1.34\text{Na}_2.74\text{Si}_{11.98}\text{Al}_3.95\text{O}_{32}$	948	volcanics
Anorthoclase 2, $\text{Ca}_2.28\text{K}_1.90\text{Na}_2.84\text{Si}_{11.81}\text{Al}_4.14\text{O}_{32}$	949	volcanics
Anorthoclase 3, $\text{Ca}_2.10\text{K}_1.56\text{Na}_3.42\text{Si}_{11.71}\text{Al}_4.31\text{O}_{32}$	950	volcanics
Anorthoclase, $\text{Na}_2.67\text{K}_1.27\text{Ca}_2.06(\text{Si}_3\text{Al})\text{O}_8$	867	volcanics
Bytownite	38	basalts, mafics
<b>Bytownite, Ca.85Na.12Al1.84Si2.16O8</b>	938	basalts, mafics
Bytownite, Italy	1527	basalts, mafics
Feldspar, France, -K, Na	1522	???
<b>Labradorite, An52</b>	1533	mafic igneous
Labradorite, $\text{Ca}_{1.1}\text{Na}_{0.9}\text{Al}_3.1\text{Si}_4.9\text{O}_{16}$	332	mafic igneous
<b>Microcline (max), <math>\text{KAlSi}_3\text{O}_8</math></b>	88	granites
Microcline, inter., $\text{KAlSi}_3\text{O}_8$	304	granites
Microcline, inter., Or89Ab11Cn1	1551	granites
Microcline, ordered	1523	granites
<b>Orthoclase 1</b>	19	granites
Orthoclase 2, $\text{KAlSi}_3\text{O}_8$	205	granites
<b>Sanidine</b>	21	felsic volcanics
Sanidine, Germany	1518	felsic volcanics
Sanidine, intergrown, from cryptoperthite	1524	felsic volcanics
<b>OLIVINE</b>		
Fayalite	53	syenite, metamorphosed iron-formation
Forsterite, $\text{Mg}_0.8\text{Fe}_0.2\text{SiO}_4$	211	mafic igneous, contact metamorphics
<b>GARNETS</b>		
Almandine, garnet	1564	regional metamorphism
Almandine, $\text{Fe}_3\text{Al}_2(\text{SiO}_4)_3$	857	regional metamorphism
Andradite, hydrous	1556	contact (skarn) metamorphism
Andradite, Al, Gr68An32, orthorhombic	1555	contact (skarn) metamorphism
Andradite, Al-bearing	1554	contact (skarn) metamorphism
<b>Andradite, <math>\text{Ca}_3\text{Fe}_2\text{Si}_3\text{O}_{12}</math></b>	362	contact (skarn) metamorphism
Garnet (Mn), $\text{Ca}_2.81\text{Mn}_2.55\text{Al}_2.64\text{Si}_3\text{O}_{12}$	1015	contact (skarn) metamorphism
Garnet, magnesian, $(\text{Mg}_2.5\text{Ni}_2)\text{Al}_2(\text{SiO}_4)_3$	766	unusual
Grossular, ferrian, garnet	1562	contact (skarn) metamorphism
Grossular, ferrian, garnet	1563	contact (skarn) metamorphism
<b>Grossular, <math>\text{Ca}_3\text{Al}_2\text{Si}_3\text{O}_{12}</math></b>	59	contact (skarn) metamorphism
Hydrogrossular	1557	contact (skarn) metamorphism
Hydrogrossular	1558	contact (skarn) metamorphism
Hydrogrossular	1559	contact (skarn) metamorphism
Hydrogrossular	1560	contact (skarn) metamorphism
Hydrogrossular	1561	contact (skarn) metamorphism
Pyrope, $\text{Mg}_3\text{Al}_2\text{Si}_3\text{O}_{12}$	60	kimberlite
Spessartine (fluoro), $\text{Mn}_3\text{Al}_2(\text{SiO}_4)_3$	193	regional metamorphism
Spessartine, garnet, synthetic	1566	regional metamorphism
Uvarovite, $\text{Ca}_3\text{Cr}_2(\text{SiO}_4)_3$	858	metamorphic

PYROXENE

Acmite(aegirine),C2/c	1590 syenite
Acmite(aegirine),P21/c	1591 syenite
Aegirine(Acmite)	1046 syenite
Augite	1572 igneous
Augite	1573 igneous
Augite, second entry,Ca.61Fe.49Mg.76(SiO3)2	693 igneous
Augite,Antarctica#1	1577 igneous
Augite,Antarctica#2	1578 igneous
Augite,Antarctica#3	1579 igneous
Augite,China	1574 igneous
Augite,Ethiopia	1576 igneous
Augite,N.Z.	1571 igneous
Augite,Si7Al1.6FeMg3Ca3Na.3O24	607 igneous
Augite,syn.	1575 igneous
Augite,syn.	1580 igneous
Bronzite(o-pyrox.),Si7.4Al.Fe1.6Mg6Ca.24Ti.05O24	608 igneous
Clinohypersthene(pyrox.),Mg.31Fe.67Ca.015SiO3	613 igneous
Clinopyroxene,Ca,Mg,Al	1618 igneous
Clinopyroxene,syn.	1615 igneous
Clinopyroxene,syn.	1617 igneous
Diopside,accurate study	1610 contact metamorphics
Diopside,Ca.8K.073Na.023Mg.95Fe.06Cr.07Al1.02Si2O6	956 contact metamorphics
Diopside,CaMgSi2O6	133 contact metamorphics
Diopside,-Fe,Na	1613 contact metamorphics
	contact
Diopside,ferrous	1612 metamorphics
Diopside,manganooan,Ca.68Mn.44Mg.88(SiO3)2	863 contact metamorphics
Diopside,syn,ferroian	1611 contact metamorphics
Enstatite, ferroan,(Mg,Fe)SiO3	149 igneous
Enstatite, ortho,MgSiO3	631 igneous
Enstatite,clino,syn.	1614 igneous
Enstatite,-Co,syn	1607 igneous
Enstatite,-Fe	1605 igneous
Enstatite,MgSiO3	111 igneous
Enstatite,-Mn	1606 igneous
Fassaite,meteor	1608 meteorite
Ferrosilite,clino	1609 igneous
Ferrosilite,-Mg	1604 igneous
Hedenbergite,CaFeSi2O6	957 contact metamorphics
Hedenbergite,-Fe rich,syn.	1602 contact metamorphics
Hedenbergite,magnesian	1601 contact metamorphics
Hedenbergite,Manganooan	1603 contact metamorphics
Jadeite,NaAlSi2O6	958 high pressure metamorphics
Kanoite,Arabia	1600 ???
Kanoite,pyroxene,Mn1.02Mg.86Ca.12(SiO3)2	864 ???
Kosmochlor	1599 rare
Omphacite,(Ca,Na)(Mg,Fe,Al)Si2O6	199 high pressure metamorphics
Omphacite,Calif.	1598 high pressure metamorphics
Omphacite,S.Africa	1597 high pressure metamorphics
Pigeonite,lunar	1058 moon
Pigeonite,lunar	1059 moon
Pigeonite,terrestrial	1060 igneous
Pyroxene,clino,Ca.8Mg1.2(SiO3)2	903 igneous and metamorphic
Pyroxene,ortho	1596 igneous
AMPHIBOLE	
<b>Actinolite,Ca2(Mg,Fe)5Si8O22(OH)2</b>	215 calc-silicate metamorphic
Anthophyllite,(Mg,Fe)7Si8O22(OH)2	217 metamorphic
Cummingtonite,(Fe,Mg)7Si8O22(OH)2	214 metamorphic
Eckermannite	1654 syenite
Edenite	1653
Gedrite,N.Carolina	1678 metamorphic
Gedrite,N.Hampshire	1679 metamorphic
Glaucophane,ferroan	312 high pressure regional metamorphic
Glaucophane,Na2(Mg,Fe)3(Al,Fe)2Si8O22(OH)2	218 high pressure regional metamorphic
Grunerite,(Fe,Mg)7Si8O22(OH)2	219 metamorphosed iron formation
Hastingsite,-Cl,F	1668 metamorphics
Hastingsite,Ontario	1681 metamorphics
Holmquistite	1661 metamorphics associated with Li-rocks
Holmquistite,clino	1656 metamorphics associated with Li-rocks

Hornblende	150	granitic & metamorphic
Hornblende	1758	granitic & metamorphic
Hornblende(Hastingsite),Si6Al2Fe4Mg.5Ca2NaO24H2	567	granitic & metamorphic
Hornblende(pargasite),Si6Al3FeMg3Ca2Na.4K.6O24H2	566	granitic & metamorphic
Hornblende,No2	1666	granitic & metamorphic
Kaersutite No.1	1061	alkaline volcanics
Kaersutite,oxy	1062	alkaline volcanics
Richterite ,K,F form	325	contact metamorphic & volcanics
Richterite,-K(syn)	1682	contact metamorphic & volcanics
Richterite,-K,	1669	contact metamorphic & volcanics
Richterite,Na-F,Ca2Na4Mg10Si16O48	326	syenite
Riebeckite,(Na,Ca)2(Fe,Mn)3Fe2(Si,Al)8O22(OH,F)2	216	syenite
Tremolite	1583	ultra-mafic & calc-silicate metamorphic
<b>Tremolite,Ca2Mg5Si8O22(OH)2</b>	175	ultra-mafic & calc-silicate metamorphic
Tremolite,fluoro	1667	ultra-mafic & calc-silicate metamorphic
Tremolite,neutron study	1584	ultra-mafic & calc-silicate metamorphic
Tremolite,new refinement	1585	ultra-mafic & calc-silicate metamorphic
Winchite	1658	metamorphics
MICA		
Annite,mica	1624	igneous
Biotite	151	igneous and metamorphic
Biotite, 1M,K(Mg,Fe)3(AlSi3O10)(OH)2	220	igneous and metamorphic
Biotite, 2M1,K(Mg,Fe)3(AlSi3O10)(OH)2	221	igneous and metamorphic
Celadonite,ferrous	1646	basalts
Celadonite,K(Mg,Fe,Al)2(SiAl)4O10(OH)2	85	basalts
Kinoshitalite,mica	1643	rare
Lepidolite,1M,K.8Mg.1Li1.5Al1.8Si3.5O12H2	865	pegmatites
Lepidolite,1M,K.9Na.1Li1.7Al1.95Si3.36O12H2	895	pegmatites
Lepidolite,2M1,	893	pegmatites
Lepidolite,2M2,Si8Al13.2Li6.8K3.5O42F6	322	pegmatites
Lepidolite,3T,K3Al5.3Li4.8Si10.5O31.5F4.5H2	894	pegmatites
Margarite (brittle mica),CaAl2(Al2Si2O10)(OH)2	222	contact metamorphics
Mica, trioctahedral,K1.9Mg4.9(Fe1.7Si6.6)O20F4	996	(a biotite)-igneous & metamorphic
Mica,1M,K.33Fe.05Mg.03Mn.03Al.9(Si1.79Al.21)O6	586	low grade metamorphic, sediments
<b>Mica,2M1,K2.8Ca.5Na.2Al9.0Cr.7Fe.4Mg2.4Si12.4O48H8</b>	995	metamorphic, granite
Muscovite,KAl2(AlSi3O10)(OH)2	82	metamorphic, granite
Paragonite, 2M1, dioct.,Na4.0Al12.0Si12.0O48H8	860	metamorphic
Paragonite,1M,NaAl2(Si3Al)O10(OH)2	861	metamorphic
Paragonite,3T	1630	metamorphic
Phengite	4	metamorphic
Phengite 2M1,Sahara	1645	metamorphic
Phengite,1M,Li-Fe	1648	rare
Phengite,-Mn,2m1	1650	rare
Phlogopite,-Fe	1651	metamorphic, granite
Phlogopite,ferrian,K1.0Mg2.7Fe1.3Si3.1O11.9H3.5	756	some igneous
Phlogopite,fluoro,M1,KMg3AlSi3O10F2	897	some igneous
Phlogopite,KMg3(AlSi3O10)(OH)2	83	some igneous
Phlogopite,N.J.	1649	some igneous
Taeniolite,mica	1640	
Zinnwaldite #1	1620	pegmatites
Zinnwaldite #2	1621	pegmatites
Zinnwaldite #3	1622	pegmatites
Zinnwaldite #4	1623	pegmatites
CHLORITE		
Chamosite (Bish model),(Fe,Al,Mg)6(Si,Al)4O10(OH)8	286	sedimentary Fe-deposits, metamorphics
Chamosite,(Fe,Al,Mg)6(Si,Al)4O18(OH)8	171	sedimentary Fe-deposits, metamorphics
Chamosite-IIb,dis.,Mg3.5Al5.0Fe5.4Si5.7O36H16	757	sedimentary Fe-deposits, metamorphics
Chlorite, chromian,(Cr,Al)2Mg5Si3O10(OH)8	172	rare
Chlorite,Al2Mg5Si3O10(OH)8	84	low-grade metamorphics
Chlorite,dioct.,Al4.2(Si3.2Al.8)O18H8	580	not common; hydrothermal
Chlorite,dioct.,Al4.2Mg.8(Si3.3Al.7)O18H8	585	not common; hydrothermal
Chlorite,di-trioct.,Mg1.9Al3.1(Si2.92Al1.1)O18H8	584	
Chlorite,la(4),Mg5Cr.7Al.3(Si3Al)O18H8	581	sedimentary rocks
Chlorite,lb,(Fe3.4Mg1.3Al1.3)(Si2.7Al1.3)O18H8	579	sedimentary rocks
Chlorite,lb-2,ferroan,Mg2.9Al2.7Fe1.8Si2.6O18H8,	759	sedimentary rocks
Chlorite,IIb(4),chromian,Mg5Cr.7Al.3(Si3Al)O18H8	582	common chlorite of metamorphic rocks
<b>Chlorite,IIb,1-layer,Mg4.54Al2.12Fe.46Si2.85O18H8</b>	758	common chlorite of metamorphic rocks
Clintonite, 1M,(Cr,Al)2Mg5Si3O10(OH)8	173	metamorphic
<b>Hematite</b>	41	any rock type or sediment
Hematite (0%Al sub)	1745	any rock type or sediment

Hematite (12%Al sub)	1746	regolith
Hematite (18%Al sub)	1747	regolith
Hematite (24%Al sub)	1748	regolith
Hydrohematite	1051	
Goethite	42	regolith, hydrothermal
<b>Goethite(0%Al sub)</b>	1749	regolith, hydrothermal
Goethite(12%Al sub)	1750	regolith
Goethite(18%Al sub)	751	regolith
Goethite(24%Al sub)	1752	regolith
SPINEL		
Chromite	1704	igenous, beach sand
Cuprospinel	1705	???
Iron oxide,gamma,maghemite C	1036	regolith
Iron oxide,gamma,maghemite-Q	1037	regolith
Iron oxide-gamma,maghemite_Q, second structure	1039	regolith
Jacobsite	1697	igneous
Maghemite	49	regolith
Maghemite,titanian,Fe1.924Ti.607O4	882	???
Magnesioferrite	1721	???
Magnetite	50	igneous, beach sand
Magnetite,titanian,Fe2.244Ti.608O4	881	igneous
Manganochromite	1731	igneous
Spinel,ferroan,Mg.5Fe.5Al2O4	440	igneous
Spinel,MgAl2O4	110	igneous
Ulvoespinel	1719	igneous
CARBONATE		
Ankerite	136	limestone and altered limestone
<b>Calcite (hex. cell)-use in preference to rhomb.</b>	11	limestone and altered limestone
Calcite (rhomb. cell)	10	limestone and altered limestone
Dolomite	31	limestone and altered limestone
Magnesite,MgCO3	129	altered ultra-basics
Siderite	24	sediments, Fe-formation
<b>Siderite, Hex Cell</b>	117	sediments, Fe-formation
Smithsonite,ZnCO3	426	Zn deposits

---

---

## REFERENCES

---

---

- Azaroff, L. and Buerger, M.J. (1958) *The Powder Method*. McGraw Hill. pp 4-11 (RAE)
- Bailey SW, Brindley GW, Johns WD, Martin RT and Ross M (1971) Summary of national and international recommendations on clay mineral nomenclature. *Clays and Clay Minerals* **19**, 129-132.
- Baker B.J. & Banfield J.F. 2003. Microbial communities in acid mine drainage. *FEMS Microbiology Ecology* **44**, 139-152.
- Banfield JF and Eggleton RA (1989) Apatite replacement and rare earth mobilization and fixation during weathering. *Clays and Clay Minerals*, **37**, 113-127.
- Bayliss P, Loughnan FC and Standard JC (1965) Dickite in the Hawkesbury sandstone of the Sydney Basin, Australia. *American Mineralogist* **50** 418-426.
- Becker U and Gashrova B 2001 AFM observations and simulations of jarosite growth at the molecular scale: probing the basis for the incorporation of foreign ions into jarosite as a storage mineral. *Phys. Chem. Minerals* **28**, 545-556.
- Bingham, J.M., Fitzpatrick, R.W., & Schulze, D.G (2002). Iron Oxides. In *Soil Mineralogy with Environmental Applications*. Soil Science Society of America Book Series no 7. 323-365.
- Bird MI, Chivas AR, Lock DE and Andrew AS (1989) An isotopic study of surficial alunite in Australia: 1. Hydrogen and sulfur isotopes. *Geochimica et Cosmochimica Acta* **53**, 3223-3237.
- Bloss, F.D. *Crystallography and Crystal Chemistry*. Holt, Rinehardt and Winston. New York.
- Blowes, D.W., Ptacek, C.J., Jambor, J.L., & Weisner, C.G (2005). The geochemistry of acid mine drainage. In *Environmental Geochemistry*, **9** (ed. Lollar, S). Treatise of Geochemistry, vol 9, 149-205.
- Brigatti MF, Frigieri P, Ghezzi C, and Poppi L (2000) Crystal chemistry of Al-rich biotites coexisting with muscovites in peraluminous granites, *American Mineralogist* **79**, 1068-1083.
- Brindley GW and Brown G (Eds). 1980 *Crystal Structures of Clay Minerals and their X-ray Identification*. Mineralogical Society, 495 pp.
- Brown JB (1971) Jarosite-Goethite stabilities at 25°C, 1 ATM. *Mineral. Deposita* **6**, 245-252.
- Callen RA (1984) Clays of the palygorskite-sepiolite group: depositional environment, age and distribution. In Singer, A. and Galan, E. *Palygorskite-Sepiolite. Occurrences, Genesis and Uses*. *Developments in Sedimentology* **37**, 1-38, Elsevier.
- Choo, Chang Oh and Kim, Soo Jin (2004) Dickite and other kaolin polymorphs from an Al-rich clay deposit formed in volcanic tuff, Southeastern Korea. *Clays and Clay Minerals*, **52**, 749-759.
- Clark, R.N (2004). Spectroscopy of rocks and minerals, and principles of spectroscopy. In *Infrared Spectroscopy in Geochemistry, Exploration Geochemistry and Remote Sensing*

- (eds. King, P.L et al.). Mineralogical Society of Canada, Short Course Series Vol 33. 17-56.
- Eggleton RA and Tilley DB (1998) Hisingerite: ferric kaolin mineral with curved morphology. *Clays and Clay Minerals*. 46, 400-413.
- Elias M. (2002) Nickel laterite deposits – geological overview, resources and exploitation In: DR Cooke and J Pongratz. eds CODES Special Publication 4, Centre for Ore Deposit Research, University of Tasmania, 205-220.
- Ewald, P,P (Ed) (1962). Fifty years of X-ray diffraction. . IUC. pp 6-73, 265-276 (RAE)
- Fitzpatrick RW (1988) Iron compounds as indicators of pedogenic processes: Examples from the southern hemisphere. pp. 351-396. In J. W. Stucki, B. A. Goodman, and U. Schwertmann. (ed). *Iron in soils and clay minerals*. D. Reidel Publ. Co. Dordrecht.
- Fitzpatrick RW and Schwertmann U (1982 ) Al-substituted goethite - an indicator of pedogenic and other weathering environments in South Africa. *Geoderma* **27**, 335-347.
- Fitzpatrick, R.W (1988). Iron compounds as indicators of pedogenic processes. Examples from southern hemisphere. In *Iron in soils and clay minerals* (eds J.W. Stucki et al). 351-396.
- Gaudin A, Decarreau A, Noack Y and Grauby O (2005) Clay mineralogy of the nickel laterite ore developed from serpentinised peridotites at Murrin Murrin, Western Australia. *Australian Journal of Earth Sciences*, **52**, 231-241.
- Gaudin A., Grauby O., Noack Y., Decarreau A. and Petit S. (2004) Accurate crystal chemistry of ferric smectites from the lateritic nickel ore of Murrin Murrin (Western Australia). I. XRD and multi-scale chemical approaches. *Clay Minerals* **39**, 301-315.
- Gieseking JE (1975) (Ed). *Soil components V2. Inorganic components*. Springer-Verlag, 684pp.
- Hill, R J & Howard, C.J (1986) AAEC Report M112, Lucas Heights Research
- Holland TJB and Powell R (2006) Mineral activity-composition relations and petrological calculations involving cation equipartition in multisite minerals: a logical inconsistency. *Journal of metamorphic Geology* **24**, 851-861.
- International Tables for X-ray Crystallography
- Keeling JL and Self PG (1996) Garford Paleochannel palygorskite. *MESA Journal* **1**, 20-23.
- King, P.L., Ramsey, M.S., McMillan, P., and Swaze, G (2004). Laboratory fourier transform infrared spectroscopy methods for geologic samples. In *Infrared Spectroscopy in Geochemistry, Exploration Geochemistry and Remote Sensing* (eds. King, P.L et al.). Mineralogical Society of Canada, Short Course Series Vol 33. 57-92
- McQueen K.G., Hill S.M. and Foster K.A. (1999) The nature and distribution of regolith carbonate accumulations in southeastern Australia and their potential as a sampling medium in geochemical exploration *Journal of Geochemical Exploration*, **67**, 67-82.
- Michel FM, Ehm L, Liu G, Han WQ, Antao SM, Chupas PJ, Lee PL, Knorr K, Eulert H, Kim J, Grey CP, Celestian AJ, Gillow J, Schoonen MAA, Strongin DR, Parise JB (2007) Similarities in 2- and 6-line ferrihydrite based on apir distribution function analysis of X-ray total scattering. *Chemistry of Materials* **19**, 1489-1496.
- Millot G. (1970) *Geology of clays*. Springer Verlag, New York.

- Moore DM and Reynolds RC Jr. (1989) *X-ray Diffraction and the Identification and Analysis of Clay Minerals*. Oxford University Press Inc., 332 pp.
- Moore, D.M. & Reynolds, R C.Jr. (1989) X-ray diffraction and the identification and analysis of clay minerals. OUP. pp3-55
- Moss AJ, Walker PH and Hutka, J. (1973) Fragmentation of granitic quartz in water *Sedimentology* **20**, 489–511.
- Newnham RE and Brindley GW (1956) The crystal structure of dickite. *Acta Crystallographica* **9**, 759-764.
- Nickel, E.H. (1995) The definition of a mineral. *Canadian Mineralogist* **33**, 689-690.
- Nordstrom D.K. & Southam G. (1997). Geomicrobiology of sulfide mineral oxidation. In *Geomicrobiology: Interactions between Microbes and Minerals* (Banfield J.F. & Nealson K.H), MSA vol 35. 361-390.
- Norrish K and Pickering JG (1983) Clay Minerals. In *Soils: An Australian Viewpoint*. Division of Soils CSIRO, 928 pp CSIRO: Melbourne.
- Norrish K. (1954) The swelling of montmorillonite. *Transactions of the Faraday Society*, **18**, 120-134.
- Ostwald J (1992) Genesis and Paragenesis of the Tetravalent Manganese Oxides of the Australian Continent. *Economic Geology* **87**, 1237-1252.
- Parc S, Nahon D, Tardy Y, and Viellard P (1989) Estimated solubility products and fields of stability for cryptomelane, nsutite, birnessite and lithiophorite based on natural lateritic weathering sequences. *American Mineralogist* **74**, 466-475.
- Plumlee, G.S & Ziegler, T.L (2005). The medical geochemistry of dusts, soils and other earth materials. In *Environmental Geochemistry*, 9 (ed. Lollar, S). Treatise of Geochemistry, vol 9, 263-310.
- Rengasamy P and Olsson KA (1991) Sodicity and soil structure. *Australian Journal of Soil Research* **29**, 935-952
- Ribbe, P,H (Ed) (1992) Minerals and reactions at the atomic scale: Transmission electron microscopy. Min. Soc. America, Reviews in Mineralogy v27.
- Rietveld, H M (1969) A profile refinement method for nuclear and magnetic structures: *Journal of Applied Crystallography* **2**, 65-71.
- Schulze DG (1984) The influence of aluminium on iron oxides: VIII. Unit cell dimensions of Al-substituted goethites and estimation of Al from them. *Clay Minerals* **32**, 36-44.
- Schwertmann U. occurrence and formation of iron oxides in various pedoenvironments. In JW Stucki, BA. Goodman, and U Schwertmann. (eds). *Iron in soils and clay minerals*. 267-308. D. Reidel Publ. Co. Dordrecht.
- Singh B and Gilkes RJ (1995) The natural occurrence of  $\chi$ -alumina in lateritic pisoliths. *Clay Minerals* **30**, 39-44.
- Stanjek H and Schwertmann U (1992) The influence of aluminum on iron oxides. Part XVI: Hydroxyl and aluminum substitution in synthetic hematites. *Clays and Clay Minerals* **40**, 347-354.
- Swayze, G (2004). Using reflectance spectroscopy to evaluate minerals of environmental concern. In *Infrared Spectroscopy in Geochemistry, Exploration Geochemistry & Remote*

- Sensing*. (eds. P.L King et al.). Mineralogical Association of Canada, Short Course Volume 33.181-196.
- Taunton AE, Welch SA and Banfield JF (2000) Geomicrobiological controls on light rare earth element, Y and Ba distributions during granite weathering and soil formation. *Journal of Alloys and Compounds* **303–304**, 30–36.
- Taunton,AE, Welch SA and Banfield JF (2000) Microbial controls on phosphate and lanthanide distributions during granite weathering and soil formation. *Chemical Geology* **169**, 371–382
- Taylor, G and Eggleton, R.A (2001) *Regolith Geology and Geomorphology*. Wiley
- Taylor, G and Eggleton, RA. (2001) *Regolith Geology and Geomorphology*. John Wiley and Sons, 375 pp.
- Taylor, J C (1991) Computer Programs for Standardless Quantitative Analysis of Minerals Using the Full Powder Diffraction Profile: *Powder Diffraction* **6**, 2-9.
- Taylor, J C and Clapp, R A (1992) New features and advanced applications of SIROQUANT: a personal computer XRD full profile quantitative analysis software package: *Advances in X-ray Analysis* **35**, 49-55.
- Thiry M and Simon-Coinçon R (1996) Tertiary paleoweathering and silcretes in the southern Paris Basin. *Catena* **26**, 1-26.
- Tilley DB and Eggleton, RA (1996) The natural occurrence of eta-alumina ( $\eta$ -Al<sub>2</sub>O<sub>3</sub>) in bauxite. *Clays and Clay Minerals* **44**, 658-664.
- Tilley DB and Eggleton, RA (2005) Titanite low-temperature alteration and Ti- mobility. *Clays and Clay Minerals* **53**, 100-107.
- USGS Spectroscopy Lab. <http://speclab.cr.usgs.gov/>.
- Veniale F, Delgado A, Marinoni L and Setti M. (2002) Dickite genesis in the ‘varicoloured’ clay-shale formation of the Italian Apennines: an isotopic approach. *Clay Minerals* **37**, 255-266.
- Beck KC (1977) Miocene of the S.E. United States: A model for chemical sedimentation in a perimarine environment. *Sedimentary Geology* **17** *Developments in Sedimentology*, 22.
- Wells M (2005) Murrin Murrin nickel laterite deposit, WA. In Butt, CRM, Robertson IDM, Scott, KM and Cornelius, M. (eds) *Regolith expression of Australian ore systems*, 115-117. CRC LEME.
- White AF and Brantley SL Eds. (1995) *Chemical Weathering Rates of Silicate Minerals. Reviews in Mineralogy Vol 31*. Min. Soc. Amer. 583 pp.
- Wilcock S (1998) Sediment-hosted magnesite deposits. *AGSO Journal of Australian Geology and Geophysics* **17**, 247-251.
- wiles, D B and Young, R A (1981)*Journal of Applied Crystallography* **14**, 149-151.
- Will, Hunag and Parrish (1983)*Journal of Applied Crystallography* **26**, 611-622.
- Wilson MJ (2004) Weathering of primary rock-forming minerals: processes, products and rates. *Clay Minerals* **39**. 233-266.

- Wilson, M.J. (Ed) (1994) *Clay Mineralogy: spectroscopic and chemical determinative methods*. Chapman and Hall.
- Zheng H and Bailey SW (1994) Refinement of the nacrite refinement. *Clays and Clays Minerals* **42**, 46-52.
- Zoltai, T. and Stout, J.H. *Mineralogy: Concepts and Principles*. Burgess, Minneapolis.
- Zussman, J. (Ed.) *Physical Methods in determinative mineralogy*. A.P. London.